

**ANALYSIS OF RESIDUAL ATMOSPHERIC
DELAY IN THE LOW LATITUDE REGIONS
USING NETWORK-BASED GPS POSITIONING**

By

Tajul Ariffin Musa

B. Surv., Universiti Teknologi Malaysia, Malaysia, 1995

M. Sc., Universiti Teknologi Malaysia, Malaysia, 1998

A thesis submitted to The University of New South Wales
in partial fulfilment of the requirements for the Degree of
Doctor of Philosophy

School of Surveying and Spatial Information Systems
The University of New South Wales
Sydney NSW 2052, Australia

January, 2007

PLEASE TYPE

THE UNIVERSITY OF NEW SOUTH WALES
Thesis/Dissertation Sheet

Surname or Family name: MUSA

First name: TAJUL ARIFFIN

Other name/s: -

Abbreviation for degree as given in the University calendar: PhD

School: SURVEYING & SPATIAL INFORMATION SYSTEMS

Faculty: ENGINEERING

Title: ANALYSIS OF RESIDUAL ATMOSPHERIC DELAY IN THE
LOW LATITUDE REGIONS USING NETWORK-BASED GPS
POSITIONING

Abstract 350 words maximum: (PLEASE TYPE)

The atmosphere in low latitude regions is of particular interest to GPS researchers because the propagation of GPS signals becomes significantly delayed compared with other regions of the world. Hence this limits GPS positioning accuracy in equatorial regions. Although the atmospheric delay can be modelled, a residual component will still remain. Reducing, or mitigating the effect of residual atmospheric delay is of great interest, and remains a challenge, especially in equatorial regions.

Analysis of relative positioning accuracy of GPS baselines has confirmed that the residual atmospheric delay is distance-dependent, even in low latitude areas. Residual ionospheric delay is the largest component in terms of both absolute magnitude and variability. However it can be largely eliminated by forming the ionosphere-free combination of measurements made on two frequencies. The residual tropospheric delay is smaller in magnitude but rather problematic due to strong spatio-temporal variations of its wet component. Introducing additional troposphere "scale factors" in the least squares estimation of relative position can reduce the effect of the residual.

In a local GPS network, the distance-dependent errors can be spatially modelled by network-based positioning. The network-based technique generates a network "correction" for user positioning. The strategy is to partition this network correction into dispersive and non-dispersive components. The latter can be smoothed in order to enhance the ionosphere-free combination, and can be of benefit to ambiguity resolution. After this step, both the dispersive and non-dispersive correction components can be used in the final positioning step. Additional investigations are conducted for stochastic modelling of network-based positioning. Based on the least squares residuals, the variance-covariance estimation technique can be adapted to static network-based positioning. Moreover, a two-step procedure can be employed to deal with the temporal correlation in the measurements.

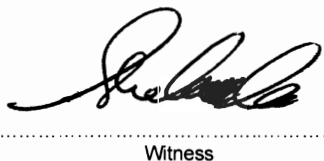
Test results on GPS networks in low latitude and mid-latitude areas have demonstrated that the proposed network-based positioning strategy works reasonably well in resolving the ambiguities, assisting the ambiguity validation process and in computing the user's position. Furthermore, test results of stochastic modelling in various GPS networks suggests that there are improvements in validating the ambiguity resolution results and handling the temporal correlation, although the positioning result do not differ compared to using the simple stochastic model typically used in standard baseline processing.

Declaration relating to disposition of project thesis/dissertation

I hereby grant to the University of New South Wales or its agents the right to archive and to make available my thesis or dissertation in whole or in part in the University libraries in all forms of media, now or here after known, subject to the provisions of the Copyright Act 1968. I retain all property rights, such as patent rights. I also retain the right to use in future works (such as articles or books) all or part of this thesis or dissertation.

I also authorise University Microfilms to use the 350 word abstract of my thesis in Dissertation Abstracts International (this is applicable to doctoral theses only).


Signature


Witness

28/05/08
Date

The University recognises that there may be exceptional circumstances requiring restrictions on copying or conditions on use. Requests for restriction for a period of up to 2 years must be made in writing. Requests for a longer period of restriction may be considered in exceptional circumstances and require the approval of the Dean of Graduate Research.

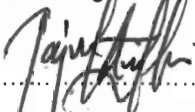
FOR OFFICE USE ONLY

Date of completion of requirements for Award:

THIS SHEET IS TO BE GLUED TO THE INSIDE FRONT COVER OF THE THESIS

ORIGINALITY STATEMENT

'I hereby declare that this submission is my own work and to the best of my knowledge it contains no materials previously published or written by another person, or substantial proportions of material which have been accepted for the award of any other degree or diploma at UNSW or any other educational institution, except where due acknowledgement is made in the thesis. Any contribution made to the research by others, with whom I have worked at UNSW or elsewhere, is explicitly acknowledged in the thesis. I also declare that the intellectual content of this thesis is the product of my own work, except to the extent that assistance from others in the project's design and conception or in style, presentation and linguistic expression is acknowledged.'

Signed 

Date 28/05/08

COPYRIGHT STATEMENT

'I hereby grant the University of New South Wales or its agents the right to archive and to make available my thesis or dissertation in whole or part in the University libraries in all forms of media, now or here after known, subject to the provisions of the Copyright Act 1968. I retain all proprietary rights, such as patent rights. I also retain the right to use in future works (such as articles or books) all or part of this thesis or dissertation.

I also authorise University Microfilms to use the 350 word abstract of my thesis in Dissertation Abstract International (this is applicable to doctoral theses only).

I have either used no substantial portions of copyright material in my thesis or I have obtained permission to use copyright material; where permission has not been granted I have applied/will apply for a partial restriction of the digital copy of my thesis or dissertation.'

Signed 

Date 28/05/08

AUTHENTICITY STATEMENT

'I certify that the Library deposit digital copy is a direct equivalent of the final officially approved version of my thesis. No emendation of content has occurred and if there are any minor variations in formatting, they are the result of the conversion to digital format.'

Signed 

Date 28/05/08

ABSTRACT

The atmosphere in low latitude regions is of particular interest to GPS researchers because the propagation of GPS signals becomes significantly delayed compared with other regions of the world. Hence this limits GPS positioning accuracy in equatorial regions. Although the atmospheric delay can be modelled, a residual component will still remain. Reducing, or mitigating the effect of residual atmospheric delay is of great interest, and remains a challenge, especially in equatorial regions.

Analysis of relative positioning accuracy of GPS baselines has confirmed that the residual atmospheric delay is distance-dependent, even in low latitude areas. Residual ionospheric delay is the largest component in terms of both absolute magnitude and variability. However it can be largely eliminated by forming the ionosphere-free combination of measurements made on two frequencies. The residual tropospheric delay is smaller in magnitude but rather problematic due to strong spatio-temporal variations of its wet component. Introducing additional troposphere “scale factors” in the least squares estimation of relative position can reduce the effect of the residual.

In a local GPS network, the distance-dependent errors can be spatially modelled by network-based positioning. The network-based technique generates a network “correction” for user positioning. The strategy is to partition this network correction into dispersive and non-dispersive components. The latter can be smoothed in order to enhance the ionosphere-free combination, and can be of benefit to ambiguity resolution. After this step, both the dispersive and non-dispersive correction components can be used in the final positioning step. Additional investigations are conducted for stochastic modelling of network-based positioning. Based on the least squares residuals, the variance-covariance estimation technique can be adapted to static network-based positioning. Moreover, a two-step procedure can be employed to deal with the temporal correlation in the measurements.

Test results on GPS networks in low latitude and mid-latitude areas have demonstrated that the proposed network-based positioning strategy works reasonably well in resolving the ambiguities, assisting the ambiguity validation process and in computing the user's position. Furthermore, test results of stochastic modelling in various GPS networks suggests that there are improvements in validating the ambiguity resolution results and handling the temporal correlation, although the positioning result do not differ compared to using the simple stochastic model typically used in standard baseline processing.

ACKNOWLEDGEMENTS

It is with a great deal of pleasure that I acknowledge my heartfelt thanks and gratitude to my supervisors Dr. Samsung Lim and Prof. Chris Rizos, and co-supervisor, Dr. Jinling Wang, for their continuous support, guidance and encouragement throughout the course of this research. I am much indebted to them for shaping my research career. I also like to thank you my employer, Universiti Teknologi Malaysia and the Government of Malaysia who awarded me with a study grant throughout my study period.

I also wish to thank my fellow graduate students, and Satellite Navigation and Positioning (SNAP) group, Dr. Craig Roberts, Dr. Volker Janssen, Dr. Hung Kyu Lee, Dr. Chalemchorn Satirapod, Dr. Binghao Li, Dr. Ravindra Babu, Mr. Xiaodong Jia, Mr. Thomas Yan, Dr. Yufei Wang, Dr. Joel Barnes, Mr. Peter Mumford, Dr. Linlin Ge, Dr. Binghao Li, Dr. Andrew Dempster, Dr. Steve Hewitson, Mr. Jack Wang, Mr. Weidong John, Dr. Yong Li, Mr. Ashgar, for their support in a variety of ways during this study. Special thanks, in particular, goes to Dr. Craig Roberts for his valuable comments and discussions. All other staff in the School of Surveying and Spatial Info. System, I thank you. Sincere thanks are extended to Mr. Baharin Ahmad, Ms. Suhaila Sulong and Malaysian post-graduates in Sydney for their moral support during this study. Not forgetting our friends in all-over Australia, that helps making our stay in this foreign land, a meaningful one.

I'm, indeed, grateful to Department of Surveying & Mapping Malaysia (DSMM), Malaysian Meteorological Service (MMS), Singapore Integrated Multiple Reference Station (SIMRSN), International GNSS Service (IGS), South California Integrated GPS Network (SCIGN), Sydney Network (SYDNET) and Japan GPS Earth Observation Network (GEONET) to support me with their valuable data.

Last but not least, I would like to extend my deepest appreciation to my wife, Adenin Md Nasir, who substituted my absence in caring for my children Aineen Sofea and Arif Emrullah. Finally, I thank my beloved mother, for the constant prayers she offered for family and me.

DEDICATION

To
My Dearest Wife

Adenin

TABLE OF CONTENTS

ABSTRACT	i
ACKNOWLEDGEMENTS	iii
DEDICATION	iv
TABLE OF CONTENTS	v
LIST OF TABLES	ix
LIST OF FIGURES	xi
LIST OF ABBREVIATIONS	xviii
LIST OF SYMBOLS	xxi
CHAPTER 1 INTRODUCTION	1
1.0 Low Latitude Atmosphere – Research Plan	1
1.1 Motivation for Research	5
1.1.1 The Continuously Operating Reference Stations	5
1.1.2 The Local CORS & Network-Based Positioning	6
1.2 Research Statements & Objectives	8
1.3 The Research Scope	10
1.4 Contributions of the Research	11
1.5 Outline of Thesis	11
CHAPTER 2 GPS & THE PROPAGATION OF SIGNALS THROUGH THE EARTH’S ATMOSPHERE	13
2.0 Introduction	13
2.1 GPS Overview	13
2.1.1 The Signals	14
2.1.2 GPS Modernization	16
2.1.3 GPS Receivers	17
2.1.4 GPS Observables and Observation Equations	19
2.1.5 GPS Error Sources	21
2.2 Propagation of GPS Signals Through the Earth’s Atmosphere	25
2.2.1 Atmospheric Layers	25
2.2.2 Ionospheric Delay on GPS	28
2.2.3 Tropospheric Delay on GPS	37
2.3 GPS Positioning	49
2.3.1 Point Positioning	50
2.3.2 Differential & Relative Positioning	52

2.4	Relative Positioning.....	54
2.4.1	Data Differencing	54
2.4.2	Least Squares Estimation for DD Observations	56
2.4.3	Ambiguity Resolution.....	60
CHAPTER 3 LONG-RANGE AMBIGUITY SETUP & ANALYSIS OF DISTANCE-DEPENDENT RESIDUAL ERRORS		66
3.0	Introduction	66
3.1	Effect of Distance-Dependent Errors on GPS Baseline	67
3.1.1	Effect of Ionospheric Delay on GPS Baseline.....	67
3.1.2	Effect of Tropospheric Delay on GPS Baseline	69
3.1.3	Effect of Orbital Error on GPS Baseline	71
3.2	Inter-Frequency Combinations.....	72
3.2.1	Phase Linear Combination.....	72
3.2.2	Geometry-Free to Approximate Ionospheric Delay	75
3.2.3	Ionosphere-Free to Approximate Tropospheric Delay & Orbital Error.....	75
3.3	Setup for Long-range AR	77
3.3.1	Ambiguity Estimation via IF Combination	77
3.3.2	Widelane Ambiguity Estimation	79
3.3.3	Consideration into Quasi IF Algorithm	81
3.4	Residuals Analysis of DD Distance-Dependent Errors.....	82
3.4.1	Test Area.....	82
3.4.2	Results and Discussion	86
3.5	Concluding Remarks	100
CHAPTER 4 LOW LATITUDE TROPOSPHERE: A STUDY USING GPS DATA IN SOUTH-EAST ASIA		102
4.0	Introduction	102
4.1	Study Area and Climate Conditions	103
4.1.1	Coverage Area	103
4.1.2	Local Climate and Weather Conditions.....	104
4.2	Testing A Priori Tropospheric Delay Modelling.....	108
4.2.1	Test Methodology	108
4.2.2	The One-Day Experiment - Results and Discussion	111
4.2.3	The Monsoon Experiment – Results & Discussion.....	116
4.3	Coordinate Repeatabilities During The Monsoon.....	121
4.4	The Monsoon Zenith Path Delay.....	126
4.4.1	Strategies for ZPD Estimation	128

4.4.2	Monsoon ZPD & Sensitivity of ZPD to Network Size.....	130
4.5	Concluding Remarks	139
CHAPTER 5 NETWORK-BASED POSITIONING APPROACH TO MITIGATE DISTANCE-DEPENDENT ERRORS.....		
5.0	Introduction	142
5.1	Concept of Network-Based Positioning.....	143
5.1.1	Background.....	143
5.1.2	Methods of Implementing the Network-Based Positioning	145
5.1.3	Processing for Network-Based Positioning.....	147
5.2	Network-Based Functional Model – Linear Combination Model.....	153
5.2.1	The Basic Model.....	153
5.2.2	The Single-Differenced Model	158
5.2.3	The Double-Differenced Model	159
5.3	Proposed Network-Based Processing.....	160
5.3.1	Proposed Network AR.....	161
5.3.2	Dispersive and Non-Dispersive Corrections	162
5.3.3	Proposed User-Side Processing Strategies	163
5.3.4	Code Development – The Research Approach.....	165
5.4	Tests for Local GPS Networks.....	167
5.4.1	Test Area.....	167
5.4.2	Test Methodology & Data Description.....	169
5.4.3	Results & Discussion.....	172
5.5	Concluding Remarks	188
CHAPTER 6 INVESTIGATION INTO STOCHASTIC MODELLING FOR STATIC NETWORK-BASED GPS POSITIONING.....		
6.0	Introduction	190
6.1	Formulation of the Stochastic Model	191
6.1.1	Quality Indicators	191
6.1.2	VCV Matrix for Network-Based Positioning.....	194
6.2	Test of Stochastic Modelling.....	200
6.2.1	Experimental Data & Methods of Processing	200
6.2.2	Analysis of Test Results	202
6.3	Handling the Temporal Correlations.....	205
6.4	Testing of Temporal Correlation.....	207

6.4.1	Experimental Data, Methods of Processing and Assessments	207
6.4.2	Analysis of Results	212
6.5	Concluding Remarks	217
CHAPTER 7 CONCLUSIONS AND RECOMMENDATIONS.....		219
7.0	Summary & Conclusions.....	219
7.1	Recommendations	224
REFERENCES.....		226
BIBLIOGRAPHY		239
ACADEMIC ACTIVITY.....		240

LIST OF TABLES

Table

2.1	PRN ranging codes characteristics (Hoffman-Wellenhof et al., 2001).....	15
2.2	Current (<i>c</i>), near future (<i>nf</i>) and future (<i>f</i>) GPS carrier and code signal.....	17
2.3	Estimated ionospheric group delay with assumption of 100 TECU (Bassiri & Hajj, 1993).....	36
2.4	Some existing empirically determined values for the refractivity constants.....	37
2.5	Correction terms for the Saastamoinen model (Saastamoinen, 1973).....	43
2.6	Meteorological dependent of zenith total delay correction ($dtrop_{corr}$) (Beutler et al., 1988).....	48
2.7	Estimated C/A code pseudorange budget and RRE based on one sigma error. Adapted from Worley (2006).....	51
2.8	IGS combined product precision and latencies (courtesy of IGS website).....	52
3.1	Linear combinations of carrier phase.....	74
3.2	Stations coordinates (wrt ITRF2000) and baseline length.....	84
3.3	Statistical analyses of DD ionospheric delay residuals related to Figure 3.7.....	88
3.4	Statistical analyses of raw DD tropospheric delay residuals related to Figure 3.10.....	91
3.5	Statistical analyses of DD tropospheric delay residuals related to Figure 3.13.....	94
3.6	Statistical analyses of DD orbital error residuals related to Figure 3.17.....	98
3.7	Statistical analyses of DD orbital error residuals related to Figure 3.19.....	99
4.1	Mean daily solar radiation, evaporation and temperature for July 2003 during the South-West monsoon (courtesy of MMS).....	105
4.2	Mean daily solar radiation, evaporation and temperature for September 2003 during the inter-monsoon (courtesy of MMS).....	106
4.3	Mean daily solar radiation, evaporation and temperature for December 2003 during the North-East monsoon (courtesy of MMS).....	108
4.4	Baseline length, station height and RMS DD IF residuals in Test 1, Test 2 and Test 3. Station KTPK is the reference station with orthometric height of 102.117m. All station orthometric heights were calculated by first obtaining station geoid heights from the EGM96 geoid calculator (via http://earth-info.nga.mil/GandG/wgs84/gravitymod/egm96/intpthel.html).....	114
4.5	Percentile improvements in the RMS DD IF residuals after applying the dry models (Test 2) and total models (Test 3) against having no	

	model applied (Test 1), and the percentile difference between Test 2 and Test 3.	116
4.6	Baseline length, station height and height differences relative to station UTMJ. All station geoid heights were obtained from the EGM96 geoid calculator (via http://earth-info.nga.mil/GandG/wgs84/gravitymod/egm96/intpthel.html).	116
4.7	RMS of coordinate repeatability for July 2003 (South-West Monsoon).	126
4.8	RMS of coordinate repeatability for September 2003 (Inter-Monsoon).	126
4.9	RMS of coordinate repeatability for December 2003 (North-East Monsoon).	126
4.10	Summary of inputs and processing features for ZPD estimation.	131
4.11	Statistics for the absolute ZPD estimate during the South-West monsoon according to Figure 4.21.	134
4.12	Statistics for the absolute ZPD estimate during the North-East monsoon according to Figure 4.22.	134
5.1	SYDNET reference station coordinates.	168
5.2	SIMRSN reference station coordinates.	169
5.3	Statistical values for single epoch AR for the SYDNET test.	181
5.4	Statistical values for single epoch AR for the SIMRSN test.	181
5.5	Statistics of ambiguity validation for the SYDNET test.	184
5.6	Statistics of ambiguity validation for the SIMRSN test.	184
5.7	Position statistics for VILL (SYDNET) with (single-base) and without (network-based) corrections applied compared to the known coordinate.	188
5.8	Position statistics for NYPC (SIMRSN) with (single-base) and without (network-based) corrections compared to the known coordinate.	188
6.1	Stations coordinates and baseline lengths from station FXHS.	201
6.2	Estimated baseline lengths, estimated baseline vectors and standard deviations of the baseline vectors for Methods A & B.	204
6.3	Estimated correlation coefficients for the DD residuals of Data Set 1.	216
6.4	Estimated correlation coefficients for the DD residuals of Data Set 2.	216
6.5	Estimated correlation coefficients for the DD residuals of Data Set 3.	216

LIST OF FIGURES

Figure

1.1	The Earth's imaginary lines (map sourced from: http://www.worldatlas.com).....	1
1.2	Scenery of the protected Tropical Rainforest in Malaysia. Top: The largest (16.75 metre in diameter), the tallest (65 metre) and the oldest (1300years) 'Cengal' trees in Terengganu; Middle: The world's longest canopy walk (500m) located in National Rainforest Park, built 40-50 metres above the ground; Bottom: The 'humid' tropical rainforest in Pahang. (sourced from: http://www.forestry.gov.my and http://www.journeymalaysia.com).....	2
1.3	High TEC values in the low latitude region. "The global ionospheric map (GIM) is generated at the Jet Propulsion Laboratory, California Institute of Technology, using GPS data collected from the global network of the International GPS Service for Geodynamics (Ref.: http://iono.jpl.nasa.gov/index.html)".	4
1.4	The IGS tracking stations (sourced from: http://igs.cb.jpl.nasa.gov/network/netindex.html).....	6
1.5	From single to multiple reference stations and from single-base to network-based positioning.	7
2.1	Left: Unpolarized Electro-Magnetic Radiation (EMR) such as natural light vibrates in all directions but maybe polarized. Polarization can be classified as linear, circular and elliptical (sources http://hyperphysics.phy-astr.gsu.edu). Right: Example of right-handed circularly polarized where the electric vector would appear to be rotating counter-clockwise approaching an observer. In case of GPS, the signal is not perfectly circular polarization (Spilker, 1996a).....	16
2.2	The major components of a generic one-channel GPS receiver (Langley, 1998b).	18
2.3	Overview of GPS error sources.....	21
2.4	Earth's atmospheric layers (Guidry, 2002).	25
2.5	Ionospheric layers and electron density for a site in the mid-latitude regions. The electron density is higher during the daytime compare to the nighttime in mid-latitude site (HAARP, 2003).	26
2.6	The tropospheric and stratospheric layers, and the tropopause. The relations of these layers to temperature, height, and pressure and atmospheric water vapour are illustrated (Mockler, 1995).	27
2.7	Geometry of single layer ionosphere model.	30
2.8	Magnitude of the 1 st order ionospheric phase effect for L1, L2 and future L5 as a function of the satellite zenith angle assuming vertical TEC fixed at 100 TECU, h_m being 350km, and the maximum N_e value of 3×10^{12} electrons.m ⁻³ (Odijk, 2002).	31
2.9	The 11 year solar cycle of sunspot numbers (NASA, 2006). Top: the positions of the spots shows that these bands first form at mid-	

	latitudes, widen, and then move toward the equator as each cycle progresses. Bottom: information on the sizes of sunspots show the year 1960 recorded the highest.....	34
2.10	Two-hourly estimated (red line) and predicted (blue line) mean VTEC values from January 1995 to September 2006 (CODE, 2006). The highest recorded value was about 60TECU in year 2002.....	34
2.11	Regions of the world with high ionospheric activity (Seeber, 1993).....	35
2.12	Geometry of tropospheric delay (Hofmann-Wellenhof et al., 2001).	44
2.13	Navigation Solution.....	51
2.14	Geometry of single-differencing (left) and double-differencing (right).....	55
3.1	Baseline constraints due to the ionospheric delay at different zenith angle and VTEC values (in TECU) on L1, L2 and the future L5 frequency. The highest effect occurs on the future L5 frequency at 70° zenith angle and VTEC of 100TECU. The lowest effect occurs on L1 frequency at 10° zenith angle and VTEC of 50TECU.....	68
3.2	Error in baseline length (ppm) due to ‘absolute troposphere error’.....	70
3.3	Error in station height (cm) due to ‘relative troposphere error’.....	70
3.4	Error in baseline length (in centimetres) due to the effect of satellite orbital error (in metres).	72
3.5	Overview of the setup for long-range AR.....	81
3.6	MASS station distribution and IGS station (NTUS) in Singapore.....	84
3.7	All satellites combination; DD ionospheric delay residuals (scale on L1) for 24hour period for long (top), medium (middle) and short (bottom) baselines.	87
3.8	Statistical plots of DD ionospheric delay residuals related to Figure 3.7.....	88
3.9	Relation of ionospheric delay residuals (scale on L1) and satellite elevation angle for short (red), medium (blue) and long (black) baseline. The satellite pair is 7-10 as viewed from station UTMJ for about 3 hours (4am to 7am) on DoY 208/03.....	89
3.10	All satellites combination; raw DD tropospheric delay residuals for 24hour period, as derived from long (top), medium (middle) and short (bottom) baselines.	90
3.11	Statistical plots of raw DD tropospheric delay residuals related to Figure 3.10.	91
3.12	Relation of raw DD tropospheric delay residuals and satellite elevations for the short (red), medium (blue) and long baseline (black). The satellite pair is 30-26 as view from station UTMJ for about 2.5hour on DoY 208/03.....	92
3.13	All satellite combination; DD tropospheric delay residuals after applying the a priori (total) Saastamoinen Model, for long (top), medium (middle) and short (bottom) baselines.	93
3.14	Statistical plots of DD tropospheric delay residuals related to Figure 3.13.....	93
3.15	The IGS-derived zenith path delay (ZPD) estimates for station NTUS on DoY 208/03.	95
3.16	Relation of DD tropospheric delay residuals (a priori model is applied) and satellite elevation angles for the short (red), medium	

	(blue) and long baseline (black). The satellite pair is 30-26 as viewed from station UTMJ for 2.5hour on DoY 208/03.....	96
3.17	All satellite combination; DD orbital error residuals, i.e. broadcast minus precise orbit, for long (top), medium (middle) and short (bottom) baselines.	97
3.18	Statistical plots of DD orbital error residuals related to Figure 3.17.	98
3.19	All satellite combination; DD orbital error residuals, i.e. ultra-rapid orbit minus precise orbit, for long (top), medium (middle) and short (bottom) baselines.	99
3.20	Statistical plots of DD orbital error residuals related to Figure 3.19.	100
4.1	The study area and existing GPS CORS Networks: Regional network (part of the global IGS network) and the local network (MASS network).	103
4.2	Rainfall over the Malaysian Peninsula during the South-West monsoon in July 2003 and location of weather stations (courtesy of MMS).	105
4.3	Rainfall over the Malaysian peninsula during the inter-monsoon in September 2003 and location of weather stations (courtesy of MMS).	106
4.4	Rainfall over the Malaysian peninsula during the North-East monsoon in December 2003 and location of weather stations (courtesy of MMS).	107
4.5	Testing strategy for a priori troposphere models and analysis of coordinates repeatabilities.	110
4.6	Test 1: DD IF residuals without applying a priori troposphere model.	111
4.7a)	Test 2: DD IF residuals with applying the dry modified Hopfield model.	112
4.7b)	Test 2: DD IF residuals with applying the dry Saastamoinen model.	112
4.8a)	Test 3: DD IF residuals with applying the total modified Hopfield model.	112
4.8b)	Test 3: DD IF residuals with applying the total Saastamoinen model.	113
4.9	RMS DD IF residuals (in metres) vs the baseline length. The RMS values along the horizontal axis indicate the trend of distance-dependence. The RMS values along the vertical axis decrease according to Test 1, Test 2 and Test 3.	115
4.10	RMS DD IF values (in metres) vs height differences. The RMS values along the horizontal axis have no specific trend towards the increment of the height differences. The RMS values along the vertical axis decrease according to Test 1, Test 2 and Test 3.	115
4.11	The (average) RMS DD IF residuals during the period of the South-West monsoon, inter-monsoon and North-East monsoon at each station relative to station UTMJ. The baselines are ordered on the x-axis from the shortest to the longest UTMJ (see also Table 4.6). The line plot refers to Test 1 (y-axis on the right). The bar plot refers to Test 2 and Test 3 (y-axis on the left).	117
4.12	South-West monsoon; percentile improvements in the RMS residuals in Test 2 (dry models) and Test 3 (total models) with respect to Test 1 (no model). All stations define baselines relative to UTMJ.	119

4.13	Inter-monsoon; percentile improvements in the RMS residuals in Test 2 (dry models) and Test 3 (total models) with respect to Test 1 (no model). All stations define baselines relative to UTMJ.....	119
4.14	North-East monsoon; percentile improvements in the RMS residuals in Test 2 (dry models) and Test 3 (total models) with respect to Test 1 (no model). All stations define baselines relative to UTMJ.....	120
4.15	Coordinate repeatabilities for station BEHR during the North-East monsoon without applying the scale factor.....	124
4.16	Coordinate repeatabilities for station BEHR during the North-East monsoon with applying the scale factor.....	124
4.17	Coordinate repeatabilities for station SEGA during the South-West monsoon without applying the scale factor.....	125
4.18	Coordinate repeatabilities for station SEGA during the South-West monsoon with applying the scale factor.....	125
4.19	Estimation of ZPD (time resolution of 6-hour). Site KOUR in the Equatorial region shows the highest, short term variability. Site ZIMM in a mid-latitude region shows a clear annual signal (maximum in summer, minimum in winter). Site MCM4 in Antarctica has the smallest mean ZPD due to the dry Antarctic conditions (Cutler et al., 1998c).....	127
4.20	Strategy 1 (n station approach) vs Strategy 2 (n-1 station approach; reference station UTMJ excluded). The troposphere parameters for all stations were estimated every 4-hours to obtain estimates of absolute ZPD. The IGS-derived absolute ZPD value for station NTUS is plotted (every 2-hours).....	130
4.21	One-week continuous absolute ZPD estimates (every 2-hours) for station NTUS derived from IGS, regional and local networks during the South West monsoon.....	133
4.22	One-week continuous absolute ZPD estimates (every 2-hours) for station NTUS derived from IGS, regional and local networks during the North-East monsoon.....	133
4.23	Difference of absolute ZPD from regional ($\Delta ZPD^{\text{Regional}}$; Equation 4.5) and local ($\Delta ZPD^{\text{Local}}$; Equation 4.6) networks wrt IGS-derived ZPD estimates for station NTUS during the South-West monsoon period.	135
4.24	Difference of absolute ZPD from regional ($\Delta ZPD^{\text{Regional}}$; Equation 4.5) and local ($\Delta ZPD^{\text{Local}}$; Equation 4.6) networks wrt IGS-derived ZPD estimates for station NTUS during the North-East monsoon period.	136
4.25	Mean values for $\Delta ZPD^{\text{Regional}}$ and $\Delta ZPD^{\text{Local}}$ during the South-West and North-East monsoon periods with respect to different cut-off elevation angles.....	136
4.26	RMS values for $\Delta ZPD^{\text{Regional}}$ and $\Delta ZPD^{\text{Local}}$ during the South-West and North-East monsoon periods with respect to different cut-off elevation angles.....	137
4.27	Difference of relative ZPD from regional ($\delta ZPD^{\text{Regional}}$; Equation 4.5) and local ($\delta ZPD^{\text{Local}}$; Equation 4.6) networks for baseline KTPK-NTUS during the South-West monsoon period.	138

4.28	Difference of relative ZPD from regional ($\delta ZPD^{\text{Regional}}$; Equation 4.5) and local ($\delta ZPD^{\text{Local}}$; Equation 4.6) networks for baseline KTPK-NTUS during the North-East monsoon period.....	138
4.29	Mean values for $\delta ZPD^{\text{Regional}}$ and $\delta ZPD^{\text{Local}}$ during the South-West and North-East monsoon period with respect to different cut-off elevation angles.....	139
4.30	RMS values for $\delta ZPD^{\text{Regional}}$ and $\delta ZPD^{\text{Local}}$ during the South-West and North-East monsoon period with respect to different cut-off elevation angles.....	139
5.1	Overview of the network-based positioning technique utilising (at least) three reference stations from a CORS network.....	143
5.2	VRS (left) and FKP (right) methods utilising three reference stations.	145
5.3	Processing for network-based positioning based on the VRS and FKP methods.....	147
5.4	Network-based processing with ‘shifted’ user-side processing.....	153
5.5	Geometric illustration of orbital error in SD measurements; the user station collinear with and located between two reference stations (Wu, 1994).	154
5.6	Representation of the orbital error components (Han, 1997).....	155
5.7	The UNSW (upgraded) GPS baseline processing modules for the proposed network-based positioning technique.....	166
5.8	SYDNET Network: SPWD is the master station; VILL is the user station; UNSW, WFAL and CWAN are the other reference stations.....	167
5.9	SIMRSN Network: LOYA is the master station; NYPC is the user station; SEMB, KEPC and NTUO are the other reference stations.....	168
5.10	Methodology used to assess the performance of solutions using the network-based and single- base positioning techniques.	170
5.11	Number of satellites in view (at 10° elevation angle and above) and available corrections for the station VILL in SYDNET.	171
5.12	Number of satellites in view (at 10° elevation angle and above) and available corrections for the station NYPC in SIMRSN.....	171
5.13	GDOP values for VILL (SYDNET) and NYPC (SIMRSN) during the tests.....	172
5.14	SYDNET, the mid-latitude experiment. Top: the ‘uncorrected’ DD ionospheric delay residuals (dispersive effects) and Bottom: the corresponding dispersive corrections (note the line at zero value indicates that no correction exists for some satellites); for all satellite combinations in the master-to-user station SPWD-VILL. The DoY is 131/05 during the year of low solar activity.	173
5.15	SIMRSN, the equatorial experiment. Top: The ‘uncorrected’ DD ionospheric delay residuals (dispersive effects) and Bottom: The corresponding dispersive corrections (note the line at zero value indicates no correction exists for some satellites); for all satellite combinations in the master-to-user station LOYA-NYPC. The DoY is 166/03 during a year of comparatively high solar activity.....	174
5.16	The SYDNET experiment: The ‘uncorrected’ DD ionospheric delay residuals on L1 and the corresponding dispersive corrections (y-axis on the left) for PRN21-22; the y-axis on the right indicates the satellite elevation angles.	175

5.17	The SIMRSN experiment: The ‘uncorrected’ DD ionospheric delay residuals on L1 with the corresponding dispersive corrections (y-axis on the left) for PRN10-24. The y-axis on the right indicates the satellite elevation angles.	175
5.18	SYDNET, the mid-latitude experiment in DoY 166/03. Top: The ‘uncorrected’ DD IF residuals (dispersive effects); Middle: The original non-dispersive corrections; and Bottom: The original non-dispersive corrections (note the line at zero value indicates no correction exists for some satellites); for all satellite combinations in the master-to-user station SPWD-VILL.....	176
5.19	SIMRSN, the equatorial experiment in DoY 166/03. Top: The ‘uncorrected’ DD IF residuals (dispersive effects); Middle: The original non-dispersive corrections; and Bottom: The original non-dispersive corrections (note the line at zero value indicates no correction exists for some satellites); for all satellite combination in the master-to-user station LOYA-NYPC.....	177
5.20	The SYDNET experiment: The ‘uncorrected’ DD IF residuals with the corresponding original and smooth corrections (y-axis on the left) for PRN21-26; the y-axis on the right indicates the satellite elevation angles.....	178
5.21	The SIMRSN experiment: The ‘uncorrected’ DD IF residuals with the corresponding original and smooth corrections (y-axis on the left) for PRN10-29; the y-axis on the right indicates the satellite elevation angles.....	178
5.22	The SYDNET experiment: The ‘uncorrected’ and ‘corrected’ DD IF residuals for PRN21-26; the y-axis on the right indicates the satellite elevation angles.....	179
5.23	The SIMRSN experiment: The ‘uncorrected’ and ‘corrected’ DD IF residuals for PRN10-29; the y-axis on the right indicates the satellite elevation angles.....	180
5.24	Statistical plots for single epoch AR for the SYDNET test.....	181
5.25	Statistical plots for single epoch AR for the SIMRSN test.....	181
5.26	F-ratio values of single-base and network-based techniques using various elevation cut-off angles for the SIMRSN test.....	182
5.27	F-ratio values of single-base and network-based techniques using various elevation cut-off angles for the SYDNET test.....	183
5.28	DD L1 residuals for SPWD-VILL (SYDNET), red is with correction and blue is without correction applied.....	185
5.29	DD L1 residuals for LOYA-NYPC (SIMRSN), red is with correction and blue is without correction applied.....	186
5.30	Offset of the estimated user positions (compared to the known position) of VILL (SYDNET). The estimated coordinates are obtained with and without correction applied.....	187
5.31	Offset of estimated user positions (compared to the known position) of NYPC (SIMRSN). The estimated coordinates are obtained with and without correction applied.....	187
6.1	Geometric layout of the test network, part of SCIGN network.....	200
6.2	Result of ambiguity validation tests (F-ratio & W-ratio for processing Methods A and B, for baselines FX-CM and FX-CS, DoY 221/00, 222/00 and 227/02.....	203

6.3	Time series of least squares phase residuals (metre) for selected satellite pairs in each session for Methods A and B. The cross-marker (black) and star-marker (red) represents the residual for Methods A and B respectively. The dash-dot line, black and red, represents the residual standard deviations for Methods A and B respectively.	205
6.4	Data Set 1 (SIMRSN): KEPC is a master; NYPC is a user; NTUO, LOYA and SEMB are the reference stations.	208
6.5	Data Set 2 (Part of SCIGN): QHTP is a master; CMP9 is a user; FMTP and GVRS are the reference stations.	208
6.6	Data Set 3 (Part of GEONET): 3008 is a master; 3016 is a user; 3029 and 3030 are the reference stations.	209
6.7	Residual plots for zero-baseline test. Base satellite is PRN01 at 66.4° (average) elevation angle with 10s observation rate.	211
6.8	Autocorrelation plots (for the DD residuals in Figure 6.7) for the zero-baseline test.	212
6.9a	Residual plots of Methods A (blue-star) and B (red-star) for Data Set 1, with 15s representing 1epoch. Base satellite is PRN10 at 46.1° (average) elevation angle.	213
6.9b	Autocorrelation plots (for the DD residuals in Figure 6.9a) for Methods A (blue-line) and B (red-line) for Data Set 1.	213
6.10a	Residual plots of Methods A (blue-star) and B (red-star) for Data Set 2, with 30s representing 1epoch. Base satellite is PRN06 at 61.9° (average) elevation angle.	214
6.10b	Autocorrelation plots (for the DD residuals in Figure 6.10a) for Methods A (blue-line) and B (red-line) for Data Set 2.	214
6.11a	Residual plots of Methods A (blue-star) and B (red-star) for Data Set 3, with 30s representing 1epoch. Base satellite is PRN29 at 56.5° (average) elevation angle.	215
6.11b	Autocorrelation plots (for the DD residuals in Figure 6.11a) for Methods A (blue-line) and B (red-line) for Data Set 3.	215
7.1	Variations of distance-dependent residuals against baseline length.	220

LIST OF ABBREVIATIONS

AF	Ambiguity Function
AFM	Ambiguity Function Method
AR	Ambiguity Resolution
AS	Anti Spoofing
C/A-code	Coarse Acquisition code
CORS	Continuously Operating Reference Stations
DD	Double-Differenced
DGPS	Differential Global Positioning System
DoY	Day of Year
EGM96	Earth Geopotential Model 1996
EMR	Electro-Magnetic Radiation
FKP	Flächenkorrekturparameter or Area Correction Parameters
GAW	Global Atmospheric Watch
GDAS	Global Data Assimilation System
GDOP	Geometric Dilution of Precision
GEONET	GPS Earth Observation Network
GF	Geometry Free
GIM	Global Ionospheric Map
GLONASS	Global Navigation Satellite System
GNSS	Global Navigation Satellite System
GPS	Global Positioning System
IF	Ionosphere Free
IGS	International GNSS Service
ISF	Ionospheric Scale Factor
ITRF	International Terrestrial Reference Frames
LAMBDA	Least Square Ambiguity Decorrelation Adjustment
LC	Linear Combination
LCM	Linear Combination Method
LIM	Linear Interpolation Method

MASS	Malaysian Active Surveying Station
M-code	Military Code
MINQUE	Minimum Norm Quadratic Unbiased Estimation
MMS	Malaysian Meteorological Service
NCEP	National Centres for Environmental Prediction
NL	Narrow Lane
NMEA	National Marine Electronics Association
NSF	Noise Scale Factor
NWM	Numerical Weather Models
NWP	Numerical Weather Prediction
P-code	Precise Code
PLL	Phase Lock Loop
PPP	Precise Point Positioning
PPS	Precise Positioning Service
PRN	Pseudo Random Noise
QIF	Quasi Ionosphere Free
RMS	Root Mean Square
RRE	Residual Range Error
RTCM	Radio Technical Committee for Maritime
RTK	Real-Time Kinematic
RTZD	Relative Tropospheric Zenith Delay
SA	Selective Availability
SCIGN	Southern California Integrated GPS Network
SD	Single-Differenced
SIMRSN	Singapore Integrated Multiple Reference Station
SNR	Signal to Noise Ratio
SPS	Standard Positioning Service
SYDNET	Sydney Network
TEC	Total Electron Content
TECU	Total Electron Content Unit
TMRP	Tropical Meteorological Research Programme
UN	United Nations
UNSW	University of New South Wales
VCV	Variance-Covariance

VRS	Virtual Reference Station
VTEC	Vertical Total Electron Content
WADGPS	Wide Area Differential Global Positioning System
WGS84	World Geodetic System 1984
WL	Wide Lane
WMO	World Meteorological Organisation
WRT	With Relative To
ZPD	Zenith Path Delay

LIST OF SYMBOLS

F	Carrier Frequency
f_{L1}	Primary Frequency
f_{L2}	Secondary Frequency
f_0	Fundamental Frequency
λ	Carrier Wavelength
P	Code Range Observation
p	Geometric Satellite-Receiver Range
c	Speed of EMR
dt_R	Receiver Clock Error
dt^S	Satellite Clock Error
$\bar{\epsilon}$	Other Biases and Errors Contaminating the Code Range Observation
X^S	Satellite Position Vector
X_R	Receiver Position Vector
φ	Carrier Phase Observation
N	Unknown ‘Integer Carrier Phase Ambiguity’
\bar{E}	Other Biases and Errors Contaminating the Carrier Phase Observation
L	Carrier Phase Observation
n	Refractive Index
c	Signal in a Vacuum
v	Speed in the Medium
α	Constant
N_e	Free Electron Density
f	Corresponding Frequency
d_{ion}	First order Ionosphere Path Delay
z	Zenith Angle
R_E	Radius of the Earth
h_m	Height of the Ionosphere Layer
A	Signal Azimuth at the Receiver Location
P	Partial Pressure

T	Absolute Temperature in Kelvin
T'	Absolute Temperature in Celcius
ρ	Density
R	Universal Gas Constant
M	Molar Weight
d_{trop}	Tropospheric Delay
H'	Station Height
$B/\delta R$	Correction Quantities
$\nabla\Delta$	Double-Differencing Operator
σ^2	Variance of the One-Way Carrier Phase Measurement
I	Identity Matrix
W	Weight Matrix
f	Number of Degree of Freedom
r	Number of Receivers
x_c	Coordinates of Float Solutions
δB_{ion}	Baseline Scale Error
B	Baseline Length
dh	Station Height Error
$d_{\text{trop}_{\text{rel}}}$	Relative Troposphere Error
i/j	Integer Numbers
β	Arbitrary Numbers
t	Epoch
θ	Elevation Angle
μ	Along-Track Component
ν	Cross-Track Component
Q	Cofactor Matrix
ρ_x	Correlation Coefficient
τ	Time Lag

1.0 Low Latitude Atmosphere – Research Plan

The Area

The 'low latitude' region can be defined as the area between the Earth's Tropic of Cancer (23.5°N) and Tropic of Capricorn (23.5°S), containing the Equatorial zone (see Figure 1.1). The low latitude region is also known as the equatorial region since the atmospheric conditions are similar to those of the equatorial zone – largely a region without distinctive seasons of the year. This region experiences tropical and sub-tropical climate, is in many ways unique for researchers interested in the Earth's climate and space weather.



Figure 1.1 The Earth's imaginary lines (map sourced from: <http://www.worldatlas.com>).

In the low latitude region the elevation angle to the Sun remains relatively high. The area is therefore exposed to intense sunlight all year round, with the temperature ranging from 20°C to 35°C (except in the desert areas). As a general rule, the warmer the air, the more water vapour it can hold. As the air rises due to temperature difference, condensation occurs and the vapour forms droplets and clouds, to ultimately produce

rain. The low latitude region, especially around the Equator, therefore often gets heavy rainfall. The minimum annual precipitation is normally around 2,000mm and the relative humidity frequently exceeds 70%.

The Rationale

Abundant water and sunlight help trees produce plentiful oxygen that is vital for life on Earth. Many have claimed the tropical rainforests in low latitude region are essentially the Earth's 'lungs'. However, there is not much scientific evidence to support this claim (Broecker, 2006). Figure 1.2 shows typical scenery in the unique rainforest of Malaysia - one of the oldest tropical rainforests in the world.



Figure 1.2 Scenery of the protected Tropical Rainforest in Malaysia. **Top:** The largest (16.75 metre in diameter), the tallest (65 metre) and the oldest (1300years) 'Cengal' trees in Terengganu; **Middle:** The world's longest canopy walk (500m) located in National Rainforest Park, built 40-50 metres above the ground; **Bottom:** The 'humid' tropical rainforest in Pahang. (sourced from: <http://www.forestry.gov.my> and <http://www.journeymalaysia.com>).

The Earth's weather and climate is heavily influenced by the amount of water vapour and other greenhouse gases in the lower part of the (neutral) atmosphere known as the

troposphere. An increase of temperature leads to increased evaporation. The troposphere can sustain large volumes of water vapour, which in turn traps radiant energy. This trapped radiation causes temperatures to increase and hence to create more warming. This is known as the Greenhouse Effect. (The Greenhouse Effect is a natural process of the Earth however human activity contributes to this effect as well).

In 2005, the World Meteorological Organisation and Global Atmospheric Watch (WMO-GAW), a United Nations (UN) organisation, released a report on global greenhouse gases, notably carbon dioxide (CO₂) and nitrous oxide (N₂O) (Ref: <http://www.wmo.int/web/arep/gaw/ghg/ghg-bulletin-en-11-06.pdf>). This report confirmed that greenhouse gases have reached new highs, with CO₂ at 379.1 parts per million (ppm) and N₂O at 319.2 parts per billion (ppb) - these values being higher than those in pre-industrial times. Moreover, WMO-GAW has indicated that from 1990 to 2005 the atmospheric radiation forced by all long-lived greenhouse gases increased by 21.5%. In fact, this is the most worrying fact for many scientists, who have debated global warming, climate changes and increased greenhouse gas emissions for over a decade (see www.davidsuzuki.org).

On the other hand, without water vapour and the other greenhouse gases planet Earth would be much colder. Since the atmosphere in the low latitude region contains large amounts of water vapour it contributes to many meteorological phenomena, such as tropical storms, and the El Niño and La Niña (in the Equatorial Pacific). Therefore serious attention has been focussed on this area. Recently the WMO has established the Tropical Meteorological Research Programme (WMO-TMRP) with the objective to improve our understanding of the physical processes of tropical systems.

In the atmosphere zone above the troposphere, the layer containing free electrons is known as the ionosphere. Here the solar radiation (predominantly ultra-violet radiation) causes ionisation. The ionosphere is important for studying the space weather which is mostly affected by solar phenomena such as solar flares, coronal holes, and coronal mass ejections which cause strong geomagnetic storms on Earth (Coster et al., 2003). The highest total electron content (TEC) values, the strongest large-scale gradients of TEC and the greatest ionospheric disturbances are typically observed at about 30° on

either side of the Earth's magnetic equator (Wanninger, 1993). Figure 1.3 is a plot of the global TEC value during the latest 'solar maximum' year in 2002. In the low latitude region, the ionospheric scintillations generally occur during the period of very high solar activity, causing significant problems for radio astronomers. Ionospheric scintillations can cause unpredictable changes in the amplitude and phase of the radio signals that pass through the ionospheric layer. Even during a 'solar minimum' period, the low latitude region still has significantly larger TEC values compared to other regions.

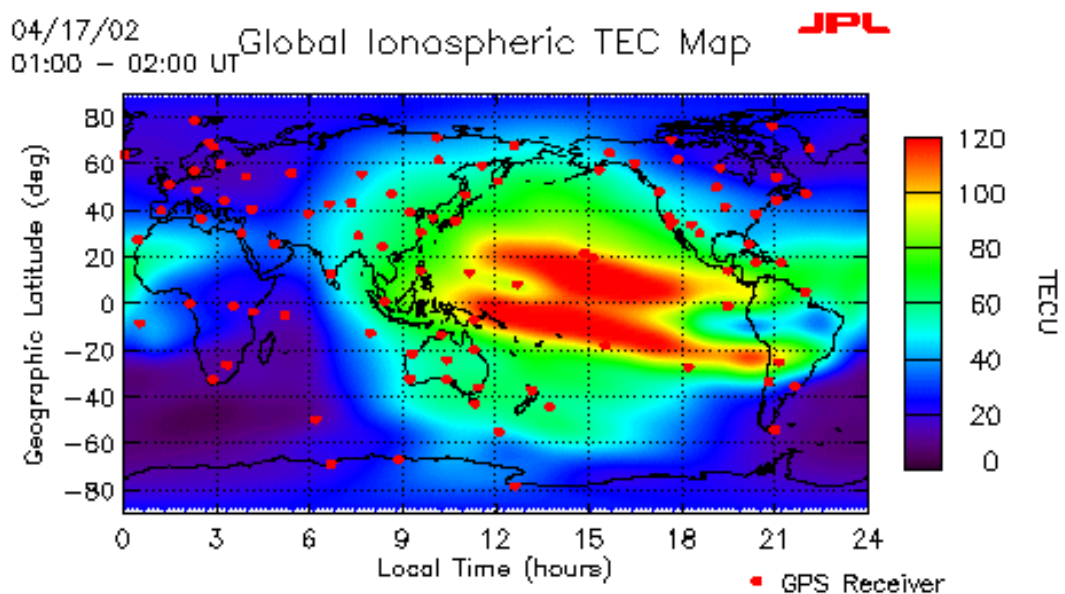


Figure 1.3 High TEC values in the low latitude region. “The Global Ionospheric Map (GIM) is generated at the Jet Propulsion Laboratory, California Institute of Technology, using GPS data collected from the global network of the International GPS Service for Geodynamics (Ref.: <http://iono.jpl.nasa.gov/index.html>)”.

Satellite Positioning Problems

Currently, the United States Global Positioning System (GPS) is the only global satellite-based radio positioning (and timing) system with a full constellation, ensuring at least four (usually more) satellites are visible above the local horizon anywhere on Earth, at any time of the day. The satellites are used for positioning activities in static or kinematic mode, in (near) real-time or post-mission mode, to address a whole range of applications including military and security use, surveying and mapping, earth sciences, land and maritime transportation, aviation, agriculture, tsunami alert, wildlife monitoring, recreational activities, and many more. There is also a growing interest in

the study of the interaction between the GPS signals and the atmosphere for Earth weather and climate and space weather research.

One of the major concerns for GPS users in the low latitude region is the effect of Earth's atmosphere on positioning. This is because of atmospheric propagation delay on the GPS signals due to the ionospheric and the tropospheric layers. In the worse case scenario, strong ionospheric scintillation can cause GPS receivers to lose lock, or receivers are not able to maintain lock for prolonged periods of time (Wanninger, 1993; Leick, 2004). Moreover, the large amount of water vapour also affects the propagation of GPS signals through the troposphere. In GPS surveying and other high accuracy positioning applications, 'double-differencing' is the preferred technique to cancel out the effect of the atmospheric delay and other spatially correlated errors. This differencing technique is less effective in low latitude areas since the *residual* atmospheric delay could complicate the positioning process.

The Challenge

Since the conditions in the atmosphere vary both spatially and temporally, it is important to analyse the quality of positioning results in many places and at different times. In low latitude regions the atmosphere is very active and still little understood from a GPS point of view. Hence understanding the complex physical and chemical processes of the Earth's atmosphere could be improved by intensive research in the low latitude region, providing a challenge for both atmospheric studies and precise positioning activities.

1.1 Motivation for Research

1.1.1 The Continuously Operating Reference Stations

Over the last decade GPS Continuously Operating Reference Stations (CORS) have been deployed around the world to support high accuracy positioning applications. CORS may be operated as an individual station, typically as the base station for GPS baseline surveying. However, in most cases nowadays, CORS are operated as a

permanent *network*, providing opportunities to enhance the functionality of these reference stations in many aspects of operations (see Marel, 1998). A good example is the global network of the International GNSS Service (IGS) and their products (IGS, 2005). Figure 1.4 shows the location of many of the reference stations that make up the IGS network. Note that there are comparatively few IGS stations in the low latitude region. Recently the establishment of a few CORS in the Equatorial region has offered the opportunity to research the atmospheric effects on GPS in this area. These CORS are typically part of independent regional GPS networks with baseline lengths up to hundreds of kilometres. Combined with the IGS stations, the regional network can supply valuable GPS data to be analysed, and therefore contribute to greater understanding of the behaviour of the low latitude atmosphere.

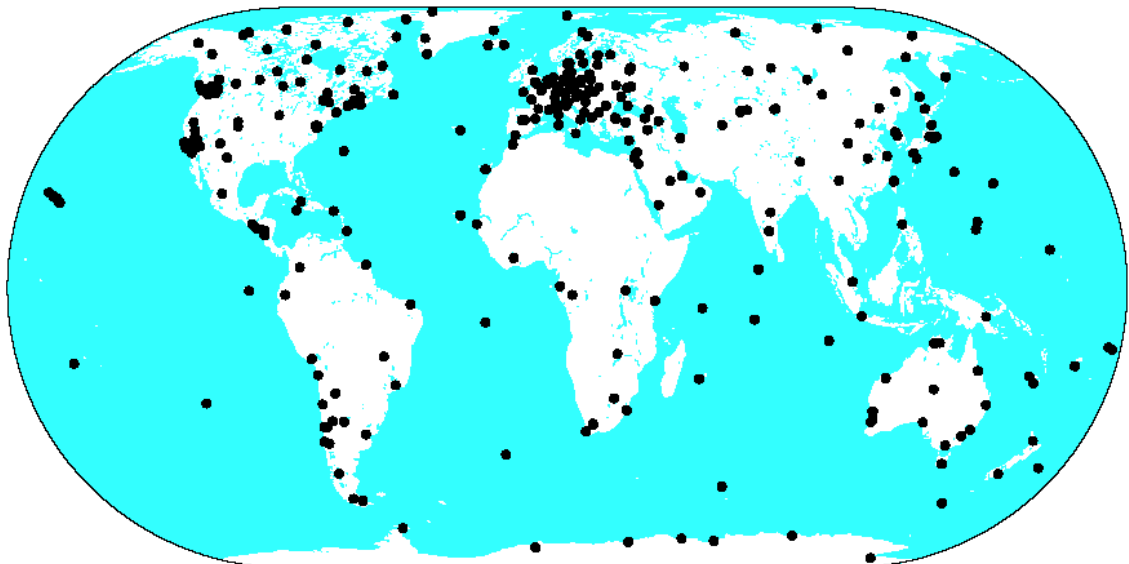


Figure 1.4 The IGS tracking stations (sourced from: <http://igsceb.jpl.nasa.gov/network/netindex.html>).

1.1.2 The Local CORS & Network-Based Positioning

The shortcoming of IGS and regional networks is that their coverage is not dense enough to be sensitive to small-scale errors, and therefore they do not meet the requirements for GPS surveying in the area. At present, many countries have developed their own local GPS networks that extend over tens of kilometres. Carrier phase-based positioning by combining and interpolating (or extrapolating) measurements from a local network of reference stations is often referred to as “network-based positioning”.

Figure 1.5 illustrates the benefits of using the network-based positioning approach.

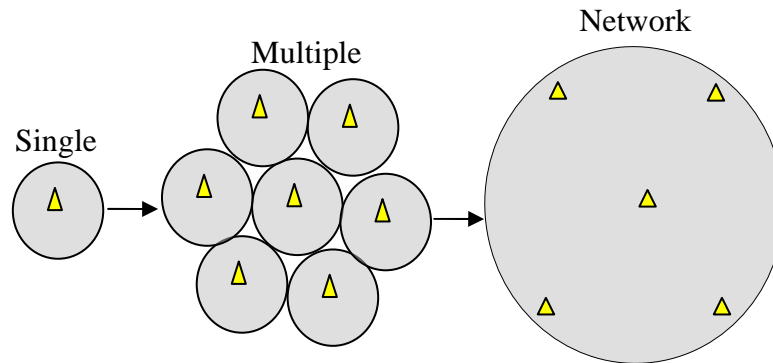


Figure 1.5 From single to multiple reference stations and from single-base to network-based positioning.

The single-base reference station approach provides a coverage of 10km or less for carrier phase-based positioning – related to the effectiveness of cancelling the spatially correlated errors using double-differencing techniques - in particular the atmospheric delay and GPS satellite orbital errors are distance-dependent (i.e. increase with the baseline length) (Beutler et al., 1988; Georgidaou & Kleusberg, 1988). Although a priori models and data differencing mitigate the errors, the *residuals* still distance-dependent. On the other hand, multiple reference stations cover a larger area because network-based positioning can model, to a greater or lesser extent, the *distance-dependent residual errors*.

The concept of carrier phase-based network-based positioning is very similar to so-called ‘wide area’ differential GPS (WADGPS), in a sense that both techniques generate ‘network corrections’ to a user’s measurements. WADGPS provides regional coverage by utilising pseudorange code-based corrections to deliver the metre-level relative accuracy. On the other hand, the network-based positioning is an efficient way of improving long-range ambiguity resolution (AR), when reference station separations are many tens of kilometres, which is a key step for centimetre-level positioning (Han & Rizos, 1996a; Racquet, 1998; Wanninger, 1995; Wübbena et al., 1996). Network-based positioning may be implemented in static, rapid-static and kinematic positioning modes, and in (near) real-time or post mission operational modes.

Although research on network-based positioning algorithms has been underway over the

last decade, and some commercially available network processing products, there is still room for improvements. One can partition the ‘network corrections’ into *dispersive* (ionosphere-related) and *non-dispersive* (troposphere- and orbit-related) components according to their dependency on the GPS signal frequencies. The dispersive and non-dispersive correction components exhibit different variations. By understanding the behaviour of distance-dependent errors (e.g. from residuals analysis), appropriate modelling can improve the quality of the corrections. Moreover, dispersive and/or non-dispersive corrections can be applied to various GPS measurement combinations, and hence benefit the user processing in many ways. This option is not available if ‘lumped’ (i.e. combined dispersive + non-dispersive) corrections are used.

Unlike the case of the functional model for network-based positioning, research on the associated stochastic models is still in its infancy. Even for the single-base reference positioning technique discussions in the research literature on the stochastic properties of GPS measurements are comparatively limited. Such stochastic models could be adopted, as a starting point, to aid in understanding the stochastic properties of network-based positioning. It is also desirable to find out whether applying such sophisticated stochastic models does improve the positioning process, and the quality of the results of network-based positioning.

1.2 Research Statements & Objectives

Atmospheric delay is very important accuracy limiting factor in GPS carrier phase-based positioning and low latitude areas are regions of strong atmospheric conditions. Atmospheric delay is a distance-dependent error in differential carrier phase-based positioning. Although it can be reduced somewhat by applying an a priori model, there remain considerable distance-dependent residual errors. Distance-dependent residual errors can be spatially modelled by carrier phase network-based positioning techniques.

The objectives of this research are therefore:

- To analyse the distance-dependent residual errors on GPS baselines in low

- latitude regions,
- To investigate the residual tropospheric delay on GPS baselines in low latitude regions,
 - To develop a processing strategy for network-based positioning that can account for the distance-dependent residual errors, and
 - To investigate the stochastic modelling for static network-based positioning.

The analysis of distance-dependent residual errors is essential in a sense that it provides the general background to the whole study. Since the distance-dependent residual errors vary spatially and temporally, they have been intensively studied by many investigators (Alves et al., 2006; Chen, 2001; Dai, 2002; Vollath et al., 2003; Wanninger, 1993; Wübenna et al., 1996). Moreover, the analysis will provide the basic knowledge for subsequent attempts to model the distance-dependent residual errors. The analysis for the effect of distance-dependent residual errors on GPS baselines was first conducted with some theoretical experiments. Next, the analysis of time-series of double-differenced residuals on three baselines in a low latitude region was conducted.

The investigation into the effects of regional tropospheric delay on GPS baselines was conducted using a network of CORS in South-East Asia. Since these CORS produce dual-frequency measurements, the linear combination of L1 and L2 can produce the ‘Ionosphere-Free’ (IF) observables. By using the precise GPS orbits during processing, the residuals of the IF combination are assumed to be dominated by the tropospheric delay. The investigation includes a performance analysis of a priori troposphere models and the effect of residual tropospheric delay on GPS station coordinates during the monsoon and inter-monsoon seasons. Additionally, the estimation of troposphere zenith path delay (ZPD) is conducted using the regional and local GPS network during the monsoon period.

A processing strategy for network-based positioning is proposed that uses the IF measurement combination and an existing network-based algorithm known as Linear Combination Method (LCM). The ‘smooth’ non-dispersive network correction is used to improve the residuals of the IF combination, and therefore indirect ambiguity for GPS L1 and/or L2 measurements can be resolved via various inter-frequency combinations such as the widelane and the narrowlane observables. Once the indirect

L1 ambiguity is resolved it can be removed from the original (double-differenced) L1 measurements. Finally, the dispersive and non-dispersive corrections can be applied in the positioning step. Data from CORS networks in mid-latitude and low-latitude areas were tested. The proposed processing strategy was tested in post-mission mode, but could be considered a ‘simulated’ real-time kinematic (RTK) mode.

The investigation into stochastic modelling for static network-based positioning was conducted by the variance-covariance estimation technique known as Minimum Norm Quadratic Unbiased Estimation (MINQUE). MINQUE uses the least squares residuals as the indicator with the assumption that it contains sufficient information to reflect the presence of the (residual) biases and measurement noises. In addition, the stochastic model can be applied in a two-stage process to transform the measurements into a set of new observables which should be free of temporal correlation. Tests were conducted using various GPS CORS networks.

1.3 The Research Scope

The experiments in this research were conducted using data from several CORS networks. The main reason for using such a data source is to assume that the station-dependent errors, such as hardware-related errors, multipath, and measurement noises, are at a minimum. This assumption is reasonable because CORS usually have a good positioning environment, geodetic-quality receivers are used, the antennas are robust against multipath, and an open sky view is guaranteed.

Although the main focus is the low latitude region, GPS data from mid-latitude sites were also tested.

Since the tests of network-based positioning are conducted in a simulated RTK mode, problems could occur if the user receiver does not remain stationary for a sufficient period of time for initialising the RTK process. The main reason is that the assumption of minimal station-dependent errors is no longer true. The station-dependent errors influence AR, even though distance-dependent errors can be reduced by the network-

based positioning technique.

1.4 Contributions of the Research

The contributions of this research can be summarised as follows:

- 1) Analysis of distance-dependent residual errors in a low-latitude region has been carried out.
- 2) A comprehensive analysis of the regional tropospheric delay has been carried out in the South-East Asia area.
- 3) A new processing strategy for user network-based positioning has been developed based on the residuals after the IF measurements and network-based algorithm are applied.
- 4) A ‘realistic’ stochastic model has been adapted to the static network-based positioning.

1.5 Outline of Thesis

This chapter provides a background on the low latitude atmosphere, and argues why the Equatorial area should be a focus for Earth’s atmospheric study in order to enhance the GPS positioning quality. Motivation, objectives, and the contributing factors for this research work are outlined.

Chapter 2 reviews some of the important concepts and topics that are frequently referred to and discussed in this research. There are four major issues: 1) background information about the GPS signals and mathematical modelling of the satellite-receiver ranges, 2) GPS signal propagation through the atmosphere, and its effect in general, and appropriate mathematical models to deal with it, 3) techniques of GPS positioning, and

4) details about relevant processing aspects of relative GPS positioning.

Chapter 3 discusses the effect and the residual analysis of distance-dependent errors on GPS baselines, and introduces the concept of long range AR. The basis for long range AR is explained via various GPS artificial measurements.

Chapter 4 presents some case studies of the effect of regional tropospheric delay in the South-East Asia area on GPS positioning. The performance of a priori tropospheric models and the precision of station coordinates are addressed using GPS data collected during monsoon and inter-monsoon seasons. Issues such as the estimation of ZPD using regional and ‘local’ GPS CORS network data during the monsoon season are discussed as well.

Chapter 5 presents background to network-based positioning, and the conventional network-based algorithm that is used in the study, followed by a new proposal for a network-based processing strategy. Tests were conducted for two CORS networks, one located in a mid-latitude region and the other in a low latitude region.

Chapter 6 presents background to the quality indicators that are often used in the ‘realistic’ stochastic model. The mathematical background of variance-covariance estimation by MINQUE is highlighted and adapted to the network-based positioning technique. The extension of the conventional stochastic model into a two-stage process is discussed in order to permit the handling of the temporal correlation of GPS measurements.

Chapter 7 summarises the research findings, draws some conclusions, and suggests recommendations for future research.

Chapter 2

GPS & THE PROPAGATION OF SIGNALS THROUGH THE EARTH'S ATMOSPHERE

2.0 Introduction

This chapter reviews some of the important concepts and topics frequently referred to and discussed in this thesis. There are four major sections in this chapter. The first part highlights some background information concerning the GPS signals, including the mathematical modelling relating the satellite-receiver range to these signals. The second part discusses propagation of GPS signals through the atmosphere. The effects of the Earth's ionosphere and troposphere on the propagation of GPS signals, and the mathematical models, are discussed in this section. Thirdly, discussions focus on GPS positioning techniques such as point positioning and relative positioning. Finally, details concerning the relative positioning technique, and relevant processing aspects such as parameter estimation and ambiguity resolution, are addressed.

2.1 GPS Overview

The Navigation System with Timing And Ranging (NAVSTAR) GPS is a satellite-space-based radio positioning and precise time transfer system that has been developed, maintained and operated by the United States (US) Department of Defense (DoD). The system nominally consists of 24 satellites in almost circular orbital planes, with altitudes above the Earth's surface of about 20200km. The satellites continuously transmit their signals to users on or above the Earth, permitting users to determine the position of their GPS receivers anywhere on land and sea, in the air or in Earth orbit, at any time and in all weather conditions.

2.1.1 The Signals

The current GPS satellites transmit continuously two carrier frequencies in the L-band, the subset of ultra-high frequency (UHF) band. The two carrier frequencies are called L1 ($f_{L1}=1575.42\text{MHz}$), the primary frequency, and L2 ($f_{L2}=1227.6\text{MHz}$), the secondary frequency. Actually, the GPS satellites transmit additional radio frequency signals at frequencies referred to as L3: associated with Nuclear Detonation Detection Systems; and L4: reserved for other DoD purposes (Misra & Enge, 2004).

The L1 is modulated by two Pseudo-Random-Noise (PRN) ranging codes, one for civil users, and the other for DoD authorized users. The L2 is modulated by only one PRN code for DoD authorized users. The two PRN ranging codes are known as the Coarse Acquisition or Clear Access (C/A) code available on L1 only, and Precise (P/Y) code available on L1 and L2. These two codes have the characteristic as below:

C/A-code. Each C/A-code has a sequence of 1,023 binary digits (also called chips, bits, codes or pulse) which is repeated every millisecond. The C/A-code is broadcast at one-tenth of fundamental frequency ($f_0=10.23\text{MHz}$). The duration of each C/A-code chip is about 1microsecond which approximately corresponds to a 300m chip length or wavelength. The C/A-code belongs to the family of Gold codes (Gold, 1967) which has some special characteristics such as to rapidly distinguish the signals received simultaneously from different satellites. The C/A code is the principal civilian ranging signal and the basis for the Standard Positioning Service (SPS).

P-code. The P-code has a long sequence of approximately $2.3457 \cdot 10^{14}$ chips, which is repeated approximately once every 266.4 days. The total P-code length is partitioned into 37 unique one-week segments and becomes one of the satellite identification systems. For example, PRN13 refers to the satellite that transmits the 13th weekly portion of the PRN-code (Leick, 2004). The P-code is broadcast at f_0 and wavelength approximately 30m; ten times the resolution of the C/A-code. Thus, the P-code is more precise than the C/A-code (Misra & Enge, 2004). The P-code provides the Precise Positioning Service (PPS).

Y-code. Under the DoD policy of ‘anti-spoofing’ (AS) since 31 January 1994, the P-code is encrypted by combining it with a secret W-code to become the private Y-code. Therefore, the AS policy denies access to the encrypted version of the P/Y-code by civilian users. Fortunately, advances in civilian receiver technology has enabled the user to counteract the effect of AS to some extent. Such a dual-frequency receiver has the capability to reconstruct the P-code under AS even though the structure of the Y-code is not known (see Hoffmann-WellenhofHoffmann-Wellenhof et al., 2001).

The PRN ranging code characteristics are summarised in Table 2.1. A detailed description on the technical background of the GPS signal can be found in Spilker (1996a) and Ward (1996).

Table 2.1 PRN ranging codes characteristics (Hoffmann-Wellenhof et al., 2001).

Parameter	C/A-code	P-code
Chipping rate	1.023x10 ⁶ bits per second	10.23x10 ⁶ bits per second
Chip length	~300m	~30m
Repetition rate	Millisecond	One week
Code type	37 unique codes	37 one-week segments
Properties	Easy to acquire	More accurate

Also superimposed on the carriers is the navigation message containing information about the satellite clock, satellite orbit parameters, satellite system status and various correction data (more details in Spilker, 1996b). The navigation message is transmitted at a relatively slow rate of 50 bits per seconds. Each bit is 20 milliseconds long. The message is formatted into frames of 1500 bits and it takes 30 seconds to transmit a frame. Each frame is subdivided into five subframes. Each subframe is 6 seconds long and contains 10 words with 30 bits. The total information is packed into 25 frames (Master Frame) and requires 12.5 minutes for transmission (Misra & Enge, 2004).

These three components of a GPS signal (carrier, ranging code and navigation data) are derived coherently from f_0 by the use of onboard atomic oscillators. The signals transmitted by a GPS satellite are (right-handed) circularly polarized waves (Figure 2.1) in order to combat the fading problem associated with Faraday rotation of the plane of polarization due to the Earth's magnetic field (Langley, 1998a).

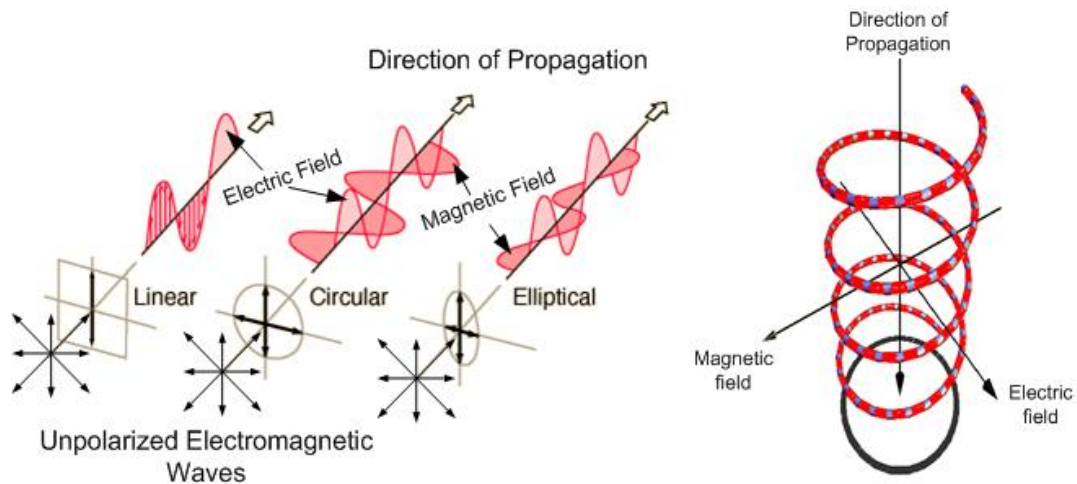


Figure 2.1 Left: Unpolarized Electro-Magnetic Radiation (EMR) such as natural light vibrates in all directions but may be polarized. Polarization can be classified as linear, circular and elliptical (sources <http://hyperphysics.phy-astr.gsu.edu>). **Right:** Example of right-handed circularly polarized where the electric vector would appear to be rotating counter-clockwise approaching an observer. In case of GPS, the signal is not perfect circular polarization (Spilker, 1996a).

2.1.2 GPS Modernization

The GPS signal structure has not changed since the first Block I GPS satellite was launched in February 22, 1978. In January 1999, the U.S. government announced a GPS modernization effort to extend the capabilities of GPS. The first step of GPS modernization can be considered to have been implemented on midnight GMT on May 1, 2000 when Selective Availability (SA) was deactivated. SA was a technique intended to reduce the accuracy of the single-receiver GPS positioning result by altering (or "dithering") the GPS satellite clock signals or more correctly falsifying the satellite clock error parameters broadcast in the navigation message. Since SA has been deactivated, the accuracy of the L1-only SPS has dramatically improved (see for example http://www.ngs.noaa.gov/FGCS/info/sans_SA).

GPS modernization includes the introduction of a new civilian code on L2 (known as 'L2C') and a new Military (M) code in addition to the existing P/Y-codes on both L1 and L2 (Fontana et al., 2001). These new signals are transmitted by all Block IIR-M satellites, the first of which was successfully launched on September 2005. The follow-

on satellite series after the 8 Block IIR-M satellites are the 16 Block IIF series. These satellite generations will have the same capabilities as the Block IIR-M, but will include a third frequency known as 'L5' at 1176.45MHz. These satellites are planned for launch in 2007/08. The L5 frequency will have two PRN ranging codes modulated onto it: the in-phase code (denoted as the I5-code), and the quadrature code (denoted as the Q5-code). The L2C and the L5 are expected to be fully operational (with 24 transmitting satellites) in approximately 2015. Details of the L2C and L5 signal structure can be found in the revised version of ICD-GPS-200C (2003) and ICD-GPS-705 (2002).

The last component of GPS modernization is the addition of another civilian signal on L1 known as 'L1C' (Hudnut, 2005). This signal is designed for the next generation GPS Block III series, which are planned to be launched beginning in the year 2013. The GPS modernization effort will make the system more robust for many GPS applications. Table 2.2 summarizes the details of the carrier frequencies and codes of GPS signals, now and in the future.

Table 2.2 Current (*c*), near future (*nf*) and future (*f*) GPS carrier and code signal.

Carrier Frequency\ Code	Carrier Frequency (MHz)	Carrier Wavelength (cm)
L1(<i>c</i>): C/A & P/Y(<i>c</i>), M(<i>nf</i>), L1C(<i>f</i>)	$f_{L1}=154x f_0$	$\lambda_{L1}=19.03$
L2(<i>c</i>): P/Y(<i>c</i>), L2C(<i>c</i>) & M(<i>nf</i>)	$f_{L2}=120x f_0$	$\lambda_{L2}=24.42$
L5(<i>nf</i>): I5 & Q5(<i>nf</i>)	$f_{L5}=115x f_0$	$\lambda_{L5}=25.48$

2.1.3 GPS Receivers

A GPS receiver consists of a number of electrical blocks (Figure 2.2). The major electrical components include the antenna and preamplifier, a radio frequency end section, a signal tracker block (code and carrier), a command entry and display board, and a power supply. The operation of the receiver is controlled by a micro-processor. Most of the receivers come with data storage and facilities to download the GPS data to a computer.

Basically, the functions of a GPS receiver are (Misra & Enge, 2004):

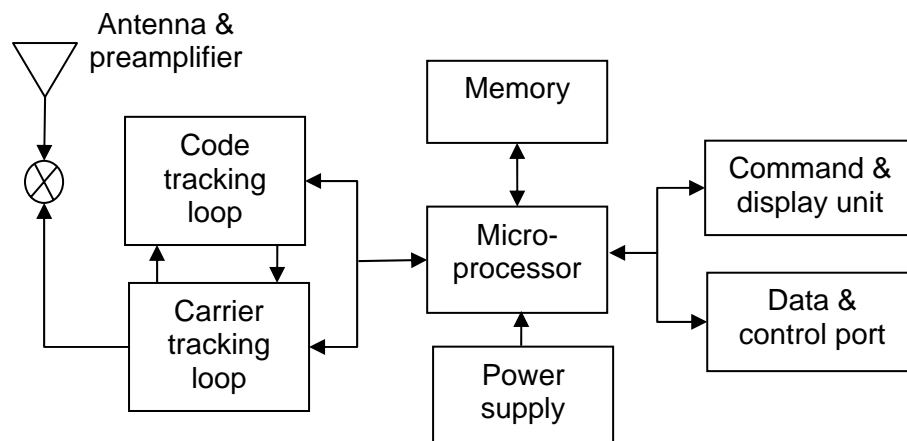


Figure 2.2 The major components of a generic one-channel GPS receiver (Langley, 1998b).

- to capture the radio frequency signals transmitted by the GPS satellites,
- to separate the signals from satellites in view,
- to perform measurements of the signal transit time (and Doppler shift),
- to decode the navigation message in order to determine the satellite position, velocity, and clock parameters,
- to estimate the user position, velocity, and time.

There are broad ranges of GPS receivers to satisfy the user position requirements. Generally, based on the user applications, the receiver can be classified into three categories:

- 1) for recreational applications - such as in hiking and orienteering, and usually is satisfied with metre-level accuracy in absolute positioning available from L1-only receiver design,
- 2) for navigation applications - used in marine, air and land navigation, which require metre to decimetre-level accuracy in absolute/differential positioning. Single frequency (L1-only) receivers are often used for this application,
- 3) for surveying and mapping applications - demand from decimetre to millimetre-level accuracy in relative positioning and would require code and carrier phase measurements at both L1 and L2 frequencies and advanced positioning algorithms inside the receiver.

Additionally, there are few manufacturers of equipment dedicated solely to the extraction of accurate time from the GPS signal (Lewis, 1996). Detail on technical background of the GPS receiver operation can be found in Dierendonck (1996) and Misra & Enge (2004).

2.1.4 GPS Observables and Observation Equations

The GPS transmitted radio signals carry information that is processed by a suitably designed GPS receiver. Of particular interest are the two range-type measurements derived from the code range and the carrier phase observations.

The Code Range

The GPS receiver at the time of reception of the satellite signal compares this signal (and the information modulated on it) with a reference carrier signal and PRN code generated using the receiver's local oscillator. The receiver-generated PRN code must be shifted (or delayed) to align with the received satellite signal in order to measure the signal travel time from satellite to receiver. The measured travel time is multiplied by the speed of EMR to obtain the code range corresponding to the receiver-satellite range. The alignment of the two codes (satellite-generated and local receiver-generated) can be measured to about 0.1% of the chip length, equivalent to 0.3m and 0.03m precision for C/A and P-code respectively (Hoffmann-Wellenhof et al., 2001).

The simplified mathematical model for the code range observation is (in length units of metre):

$$P = p + c(dt^S - dt_R) + \bar{e} \quad (2.1)$$

where P is the code range observation (m); p is the geometric satellite-receiver range (m); c is speed of EMR in metre per second (ms^{-1}); dt_R is receiver clock error (s) wrt to 'true' time; dt^S is satellite clock error (s) wrt to 'true' time; and \bar{e} are other biases and errors contaminating the code range observation (m). The geometric range p can be expressed as:

$$p = |X_R - X^S| \quad (2.2)$$

where X^S is the satellite position vector at signal transmit time (wrt 'true' time); and X_R is receiver position vector at signal reception time (wrt 'true' time). The definitions of 'true' time and clock errors are further discussed in Section 2.1.5. Because of these clock errors, the code range is also often referred to as the 'pseudorange'. Equation 2.1 is valid for both C/A code and P-code observations.

The Carrier Phase Range

A carrier phase observation is obtained from the measured carrier beat phase; that is, the reference carrier phase generated in the receiver minus the incoming carrier phase from a GPS satellite (from this point on, the carrier beat phase will be referred to simply as the carrier phase). The receiver only measures the fractional part of the carrier phase (it is, after all, just a sine wave). The receiver keeps track of the complete cycles of the phase by setting an integer counter when the signal is first acquired, and then counting the whole cycles as the observations are continued.

The phase can be measured to better than 0.01 cycles precision, which corresponds to millimetre precision (Hoffmann-Wellenhof et al., 2001), far more precise than using the code. However, the receiver cannot measure the integer number of the full carrier cycles in the geometric range between the satellite and receiver. Hence, the carrier phase is 'ambiguous' by an unknown integer number of cycles. This phase ambiguity is time-constant as long as the receiver does not lose lock during the continuous tracking of the satellite signal. If loss-of-lock occurs, the receiver cycle counter will reset (or reinitialize), which causes a 'jump' in the accumulated carrier phase observation. This event is known as a 'cycle slip'.

Ignoring the small deviation in satellite and receiver frequency from the fundamental frequency, the simplified mathematical expression for the carrier phase observation can be written as (in units of cycles):

$$\varphi = \frac{f}{c} p + f(dt^S - dt_R) + N + \frac{f}{c} \bar{E} \quad (2.3)$$

where ϕ is the carrier phase observation (cycle); f is the frequency of the carrier wave (cycle.s⁻¹); N is the unknown 'integer carrier phase ambiguity' (cycle); \bar{E} are the other biases and errors that contaminate the carrier phase observation (m). The other terms are the same as in Equation 2.1. The carrier phase observations can also be expressed in metric units:

$$L = p + c(dt^S - dt_R) + \lambda N + \bar{E} \quad (2.4)$$

where L is the carrier phase observation (m) and λ is the wavelength of corresponding carrier phase (m) expressed by c/f . The above equations are valid for carrier phase observations on either the L1 or L2 frequencies. It should be noted that the carrier phase range is affected by the same clock error terms as the pseudoranges.

2.1.5 GPS Error Sources

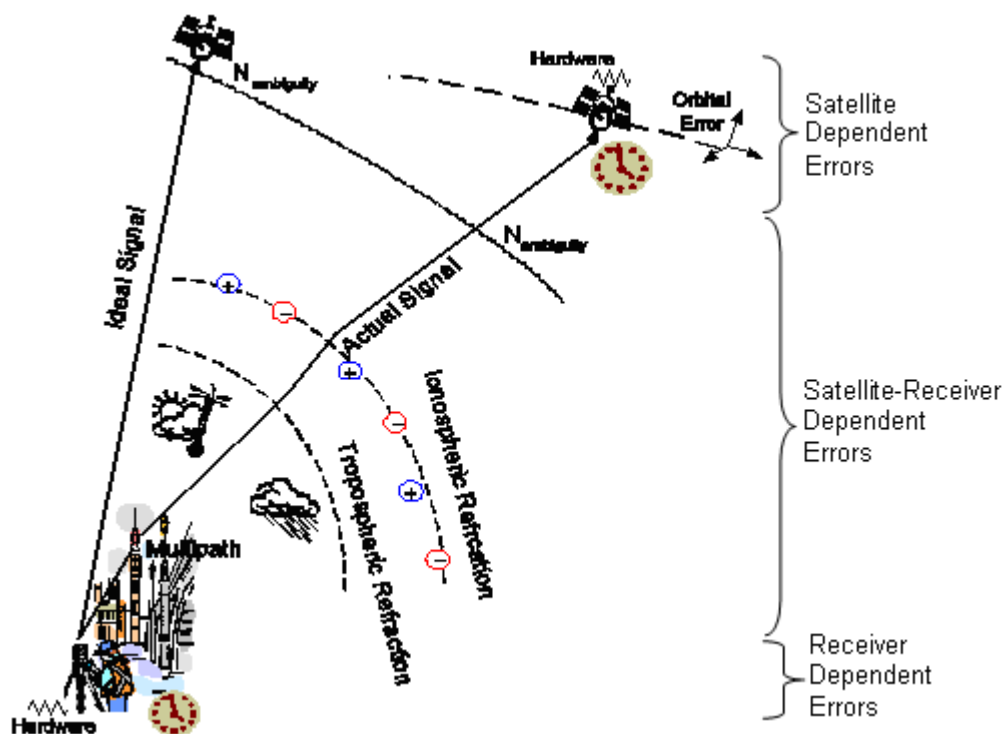


Figure 2.3 Overview of GPS error sources.

The GPS range measurements are affected by both, biases and noise. A bias tends to persist over a period of time, but the noise, generally, refers to quickly varying error that averages out to zero over a short time interval (Misra & Enge, 2004). In GPS

positioning they are therefore treated as errors. The identified GPS errors that bias the ranges may be categorised as (Figure 2.3): i) satellite dependent errors/effects, ii) satellite-receiver dependent errors/effects, and iii) receiver dependent errors/effects.

i) Satellite Dependent Errors

Orbital error. The orbital error is usually decomposed into components along three orthogonal directions: along-track, cross-track and radial (see Misra & Enge, 2004; Bauersima, 1983; Beutler et al, 1988). The orbital error can be considered to be the imperfect modelling of the predicted satellite trajectory (position and velocity) at some reference time, leading to it being different to the 'true' orbit. One example of the means by which the orbital error can be quantified is by comparing the satellite position derived from the broadcast orbit (in navigation message) with the one that is precisely determined by the IGS. The quality of the satellite orbit determination process is mainly dependent on such effects as reference system and tracking station coordinate uncertainties (e.g. due to earth or ocean tidal loading), and perturbation force mismodelling of gravitational effects, relativistic effects, solar radiation pressure, etc. It must be emphasised that the orbital error does not affect the measured range directly, but they affect the correctness of the geometric range, and therefore impact on the quality of the estimated receiver position when the satellite position is constrained (as is usual for most positioning and navigation applications). More details concerning GPS satellite orbits and the modelling approach can be found in such texts as Beutler et al. (1998a) and Hoffmann-Wellenhof et al. (2001).

Satellite clock error. The 'satellite clock error' is a synchronisation offset of the stable atomic clock (cesium or rubidium) installed on each satellite compared with a definition of 'true' time, e.g, the GPS time [The GPS time is given by its composite clock or "paper" clock on the basis of measurements from a set of cesium and rubidium frequency standards in use at the GPS monitor stations and aboard the satellites (detail via <http://tycho.usno.navy.mil/gpstt.html>)]. The offset (its magnitude and temporal variability) is dependent on the stability of the individual satellite clocks (and is expressed as an offset at a reference time, plus the predicted clock drift and drift rate), and other external effects such as relativity (Misra & Enge, 2004).

Satellite hardware errors. These errors have several sources: the electronic-specific effects that cause signal travel time delay between the satellite signal generator and the satellite transmitter; satellite antenna phase offsets and orientation (the difference between the GPS satellites centre of mass and phase centre of its transmitter); and the effect of phase wind-up (a rotation of the satellite antenna around its vertical axis). Blewitt (1998) points out that in the past the phase wind-up effect occurred when the satellite began to spin due to some malfunction. Further reading, and details on modelling, of these hardware errors can be found in Kouba & Heroux, (2001) and Witchayangkoon (2000).

ii) Satellite-Receiver Dependent Errors and Phase Ambiguity Bias

Atmospheric delay / Propagation errors. The GPS signals travelling from the satellite to the receiver propagate through the Earth's atmosphere. The atmosphere consists of charged particles, neutral atoms, molecules, gases, etc., and changes the velocity (speed and direction) of the GPS signals. In other words the signals are refracted. A change in signal speed changes the signal transit time. Consequently, the 'measured' range between the satellite and the receiver is different from its 'line-of-sight' geometric range. This effect is often addressed as atmospheric refraction or atmospheric delay, and is mostly due to the Earth's ionosphere and troposphere. Further discussions on the atmospheric layers and their effects are found in Section 2.2.

Phase ambiguity bias. Because the receiver cannot measure the number of complete carrier frequency cycles between the satellite and the receiver, the measured phase (and hence the phase range) is biased by the initial unknown number of integer cycles or the 'ambiguity parameter'. The unknown ambiguity parameter can be estimated along with other parameters of interest during position determination via least squares estimation. However, the estimation provides only the real value of the ambiguity. The process to 'resolving' the ambiguity to its likeliest integer value is known as the 'ambiguity resolution' (see Section 2.4.3).

Multipath (Imaging & Scattering). The GPS signals may travel along a straight path to the receiver antenna (apart from small bending effects due to atmospheric refraction). However, because of reflections from nearby objects such as buildings, metallic structures, ground or water surfaces, etc.; the signals may travel along more than one

path (referred to as multipath) to reach the receiver antenna. The multipath effect is in many respects systematic in nature, but it may also be considered a largely random effect as well (Hoffmann-Wellenhof et al., 2001), affecting both code and phase measurements. Other effects that are often categorised as multipath are 'imaging' and 'scattering' (Langley, 1998a). Imaging is caused by the reflecting object producing an image to confuse the GPS signal from the original one. Scattering is due to the signal scattering around the surface of the installed antenna, causing interference with the direct signal.

iii) Receiver Dependent Errors

Receiver clock error. The inexpensive receiver clock (usually a low-cost crystal quartz oscillator), as in the case of the satellite clock, has to be synchronised with GPS time if accurate range is to be derived from the signal travel time based on the difference between time of transmission (as measured by the satellite clock) and time of reception (measured by the receiver clock). Thus, the synchronisation offset with respect to GPS time for the receiver clock is referred to as the 'receiver clock error'.

Receiver coordinate uncertainties. This affects the range modelling in the same way as does orbital error. Any uncertainties in the a priori receiver coordinates will affect the geometric range from receiver to satellite. Even though the receiver coordinates may be precisely known, one must consider several effects, such as the solid earth tides, ocean loading effects, plate tectonic movement, etc., which vary with time. Typically receiver coordinates are expressed in a terrestrial reference frame such as the 'GPS datum' World Geodetic System 84 (WGS-84). Assuming user known coordinates are referred to the International Terrestrial Reference System (via one of its International Terrestrial Reference Frames such as ITRF2000) and continuously monitored, this is no longer a critical issue (Merrigan et al., 2002).

Receiver hardware errors & measurement noise. These include receiver antenna phase centre offset (and variations). GPS measurements are referred to the antenna phase centre, which should coincide with the electrical centre. However, there may be a constant offset, and this offset may vary with different signal frequency, strength and direction (Leick, 2004). The measurement process in the receiver can be made to a certain level of precision. The receiver itself is not a perfect device, hence small effects

due to thermal noise, tracking loop noise and other electronic-specific effects will remain. Even in the absence of any signal, the receiver and antenna will detect a certain noise power (Langley, 1998b). Ibid (1998b) demonstrated that for a geodetic quality receiver, the C/A code noise is about 0.04m RMS (Root Mean Square). Thus, the noise level in the carrier phase measurements can be expected to be much less due to its smaller wavelength. Measurement noise is also frequency dependent. Furthermore, in practice the signals' noise will be dominated by the effects of multipath.

2.2 Propagation of GPS Signals Through the Earth's Atmosphere

2.2.1 Atmospheric Layers

The Earth's atmosphere consists of charged particles, neutral atoms, molecules and gases, which can be divided into several layers (Figure 2.4). Some of these layers act as a natural shield to protect the Earth from solar radiation, comets, etc.

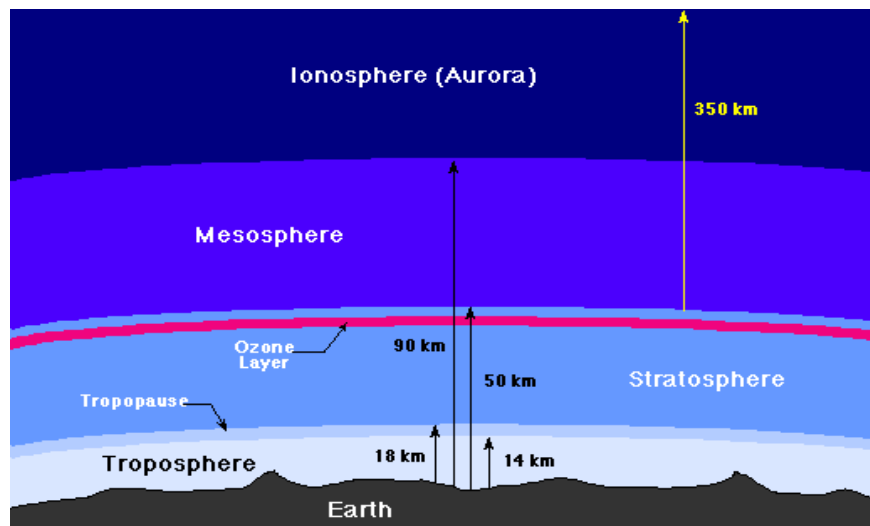


Figure 2.4 Earth's atmospheric layers (Guidry, 2002).

The major influence of the atmosphere layers on GPS signals originates from the ionosphere and the neutral atmosphere layer (troposphere, stratosphere and part of the mesosphere). As previously mentioned, the satellites signals are refracted by the atmospheric layers. In GPS positioning, the effects from the atmospheric refraction or

atmospheric delay are considered to be 'noise', and need to be somehow accounted for in the observations. However, in the case of atmospheric physics the effect is considered to be a 'signal', and its study can improve our understanding of the Earth's atmosphere.

The Ionospheric Layer

The ionosphere is that part of the Earth's atmosphere where solar radiation (predominately by ultra-violet radiation) results in ionisation. The ionospheric layer starts at about 50km and extends to a thousand kilometres or so above the Earth's surface in height. The ionosphere is divided into several layers; D, E, F1 and F2, based on the level of ionisation (Figure 2.5).

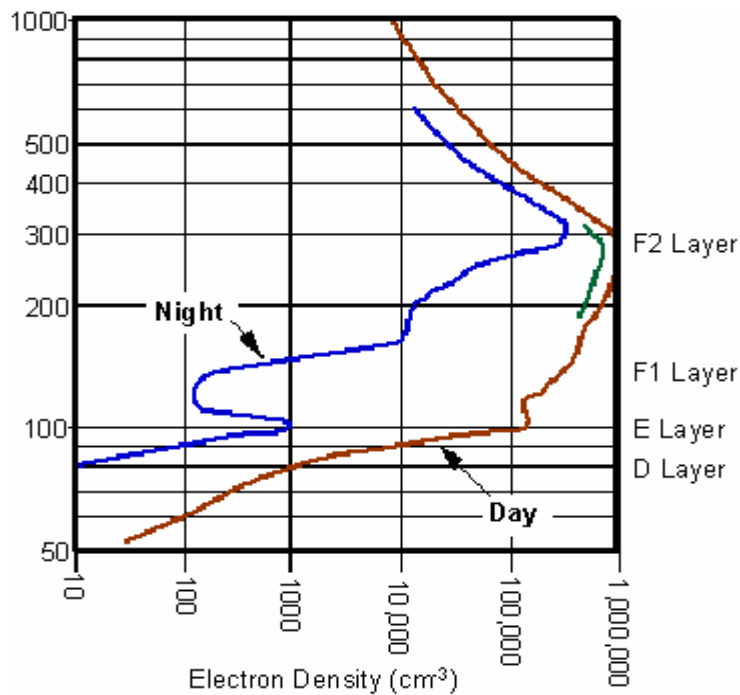


Figure 2.5 Ionospheric layers and electron density for a site in the mid-latitude regions. The electron density is higher during the daytime compare to the nighttime in mid-latitude sites (HAARP, 2003).

In the F2 layer the electron concentrations reach their highest values, with its maximum usually at a height of 350-400km. The electron density is less in the E layer and rapidly decreases below the D layer and above the F2 layer. Figure 2.5 shows the electron density (in mid-latitude site) is higher during the daytime and lesser in the nighttime.

Factors that influence the variability of the ionospheric electron density will be discussed later.

The Neutral Atmosphere Layer

The neutral atmosphere reaches almost 80km in altitude and consists of the stratosphere, troposphere, and part of mesosphere (Figure 2.4). The stratosphere and troposphere are separated by the tropopause (Figure 2.6). The most dense and lowest layer of the Earth's neutral atmosphere is the troposphere. Extending from the surface to the stratosphere at an approximately 13km altitude, it is within the troposphere where almost all weather occurs.

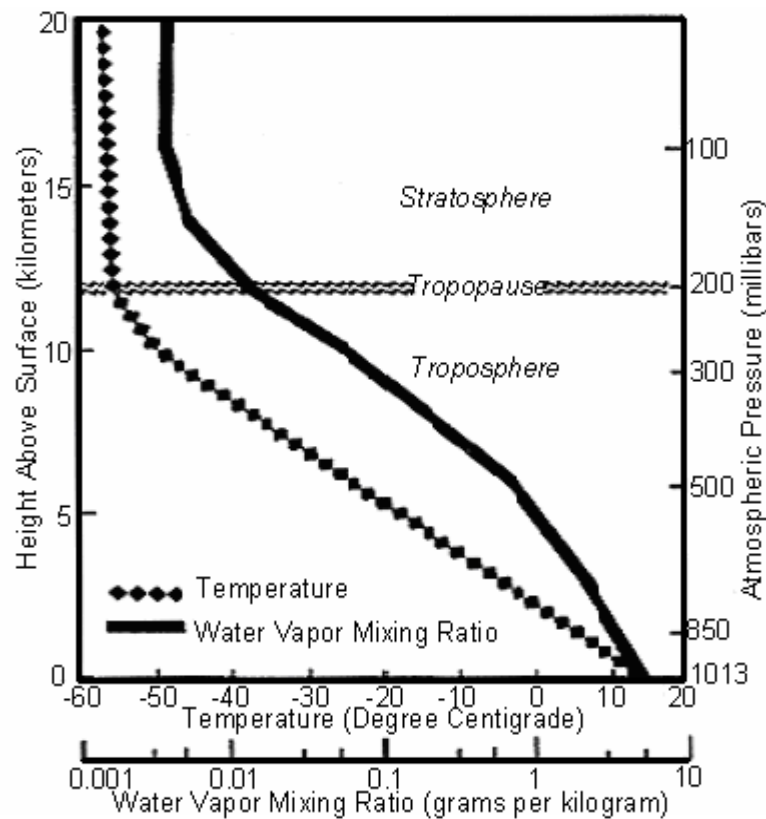


Figure 2.6 The tropospheric and stratospheric layers, and the tropopause. The relations of these layers to temperature, height, and pressure and atmospheric water vapour are illustrated (Mockler, 1995).

The troposphere is composed of a mixture of several neutral dry gases, primarily nitrogen and oxygen, and traces of others including pollutants. The dry gases are dominant in the troposphere with slow variations and are easy to model using the ideal gas law and a hydrostatic model. The troposphere also contains a variable amount of

water vapour, which varies depending on the temperature and pressure of the air. Figure 2.6 shows the water vapour mixing ratio and relationship with temperature, pressure, and height above the surface. As can be seen, the water vapour content is significant between 12km altitude and the surface. The water vapour content increases with increasing temperature and pressure, but decreases as the elevation increases. As the troposphere is the densest layer, it has the greatest influence on the propagation of the GPS signals amongst the neutral atmosphere layer (Hoffmann-Wellenhof et al., 2001).

2.2.2 Ionospheric Delay on GPS

Ionospheric Refractive Index

The refractive index (n) of a medium is defined as the ratio of the speed of propagation of the signal in a vacuum (c) to the speed in the medium (v) (Misra & Enge, 2004):

$$n = \frac{c}{v} \quad (2.5)$$

The value of n is equal to unity for radio signals that travel through the vacuum. The ionosphere is a dispersive medium to a radio wave – the refractive index is inversely proportional to the frequency of the signal (Langley, 1998a). The ionospheric refractive index, can, to first order, be approximated by the Appleton-Hartree formula (Kleusberg, 1998):

$$n = 1 \pm \frac{\alpha N_e}{f^2} \quad (2.6)$$

where α is a constant (see also Equation 2.10), N_e is the free electron density (electrons.m⁻³), and f is the corresponding frequency (Hz). Equation 2.6 denotes a group refractive index if $n > 1$, indicating the wave is *delayed*; and a phase refractive index if $n < 1$, indicating the wave is *advanced*. Hence, phase and group velocity can now be distinguished. Due to modulation with PRN codes, the GPS signal can be considered as the superposition of a group, or packet, of waves which is delayed ('group delay') by the ionosphere. Meanwhile the GPS carrier phase, the 'unmodulated' wave, is advanced ('phase delay'). Finally, Equation 2.6 indicates that the ionospheric refractive index is different for L1 and L2 signals.

First Order Ionospheric Delay Modelling

The integration of Equation 2.6 along the path (S) of the signal through the ionosphere yields the electromagnetic path lengths for the code (p_{code}) and phase (p_{phase}) (Langley, 1998a):

$$p_{\text{code}} = \int_S \left(1 + \frac{\alpha N_e}{f^2} \right) dS = p + \text{dion} \quad (2.7)$$

$$p_{\text{phase}} = \int_S \left(1 - \frac{\alpha N_e}{f^2} \right) dS = p - \text{dion} \quad (2.8)$$

where p is the geometric range (m), and dion is the first order ionospheric path delay (m):

$$\text{dion} = \frac{\alpha}{f^2} \text{TEC} \quad (2.9)$$

with TEC is the integrated electron density along the signal path. The TEC is often expressed in terms of the TEC unit (TECU) where $1 \text{ TECU} = 10^{16} \text{ electrons.m}^{-2}$. Equation 2.9 indicates that the higher the frequency, the less the delay. The constant α is given by (Rothacher & Mervart, 1996):

$$\alpha = 40.3e10^{16} \text{ ms}^{-2} \text{TECU}^{-1} \quad (2.10)$$

It should be noted that due to the assumptions in Equation 2.6, higher order ionospheric effects are neglected in the derivation of Equations 2.7-2.9. Derivation of an expression that takes into account higher order ionospheric delay effects can be found in Bassiri & Hajj (1993). Their study found that the effect of the first order delay is far larger (about three orders of magnitude) than the higher order delay (see also Table 2.3). In addition, the derivation of Equations 2.6-2.9 assumes that the signal travels through the ionosphere in a 'linear' manner (in fact there is an ionospheric bending effect). Odijk (2002) calculated the ionospheric bending effect under worst case ionosphere conditions and concluded that the effect is at the millimetre level. Hence higher order ionospheric delay, and the bending effect, will not be considered any further in this thesis.

Single Layer Ionospheric Delay Modelling

It is a common practice in GPS ionosphere modelling to represent the ionosphere as an infinitesimally thin single layer at a fixed altitude above the Earth's surface (Figure 2.7). The modelling considers the zenith angle (z) at the height of receiver location and takes into account the zenith angle (z'), as 'seen' from the intersection point of the signal path with the ionosphere layer at height h_m .

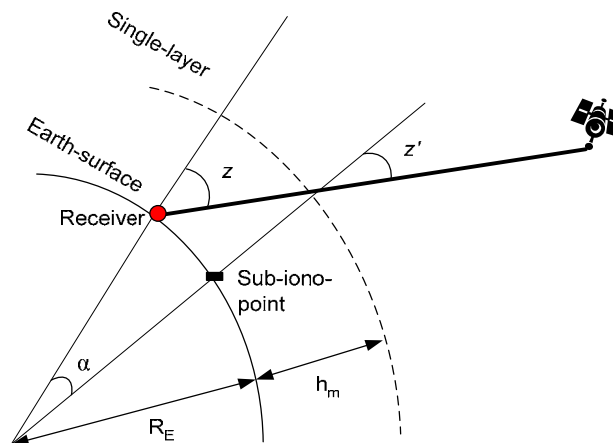


Figure 2.7 Geometry of single layer ionosphere model.

The delay effect is different for a satellite at a different zenith angle. For example, the satellite signal near the observer's horizon will travel through more of the ionosphere layer than a signal at the zenith. Thus, a low elevation satellite will experience a greater ionospheric delay. Odijk (2002) simulates the first order ionospheric phase delay as a function of satellite elevation angle. The results are shown in Figure 2.8, which indicates that the effect on L1 signals ranges from 16m in the zenith and grows to about 50m at the horizon. Larger effects can be observed on L2 (as well as on the future L5 signal).

For modelling purposes it is therefore necessary to introduce a 'mapping function' in order to project the vertical ionospheric delay into the slant ionospheric delay (and vice versa). The simplest mapping function is represented by the cosine of zenith angle z :

$$f(z) = \frac{1}{\cos z} \quad (2.11)$$

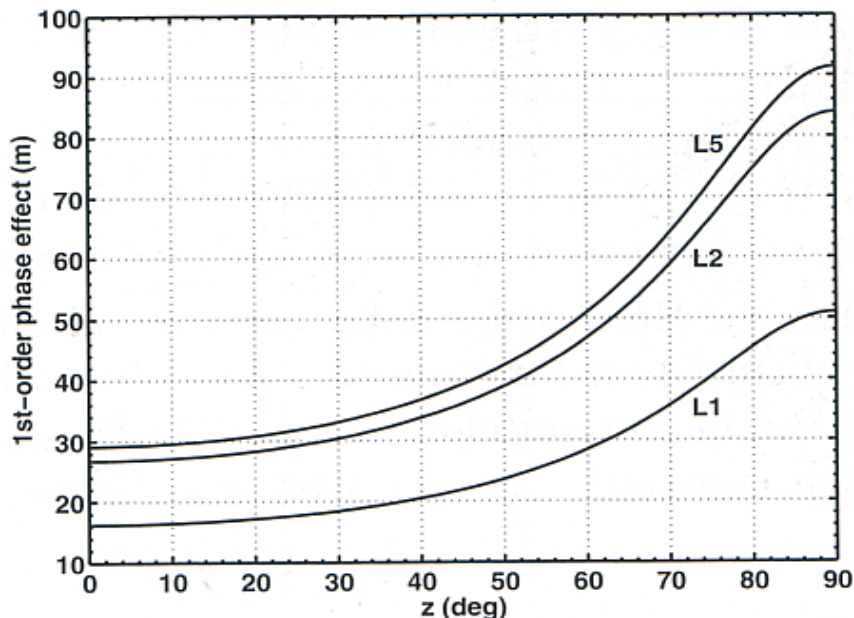


Figure 2.8 Magnitude of the 1st order ionospheric phase effect for L1, L2 and future L5 as a function of the satellite zenith angle assuming vertical TEC fixed at 100 TECU, h_m being 350km, and the maximum Ne value of 3×10^{12} electrons.m⁻³ (Odijk, 2002).

Other mapping functions for ionospheric delay are used, for example as described by Klobuchar (1996):

$$f(E) = 1 + 16 \left(0.53 - \frac{E}{\pi} \right)^3 \quad (2.12)$$

where $E=90^\circ-z$ is the satellite elevation as seen from the receiver. Considering the single layer ionosphere model and associated mapping function, say Equation 2.11, dion in Equation 2.9 is conveniently expressed as:

$$\text{dion} = \frac{1}{\cos z} \cdot \frac{\alpha}{f^2} \text{VTEC} \quad (2.13)$$

where

$$z' = \sin^{-1} \left[\frac{R_E}{R_E + h_m} \sin z \right] \quad (2.14)$$

VTEC is the vertical TEC; R_E is the radius of the Earth (usually taken as being 6371km); z' and z were previously defined; and h_m is the height of the ionosphere layer above the Earth's surface. The value of h_m is not defined precisely, and a value of between 300km to 400km is often used. A modified single layer mapping function is suggested by CODE (2006), by replacing $\sin(z)$ with $\sin(\alpha z)$ in Equation 2.14, where α is the angle between the receiver and the sub-ionosphere point (SIP) (consult Figure 2.7). From Equations 2.13 and 2.9, the VTEC can also be mapped into the (slant) TEC (and vice versa):

$$\frac{\text{VTEC}}{\text{TEC}} = \cos z' \quad (2.15)$$

The distance of the SIP having the same coordinates as the signal piercing point at the ionosphere layer can be derived as (Kleusberg, 1998):

$$\eta = z' - z \quad (2.16)$$

and the SIP latitude (φ_{SIP}) and longitude (λ_{SIP}) can be written as (Ibid, 1998):

$$\varphi_{\text{SIP}} = \sin^{-1} [\cos \eta \sin \varphi' + \sin \eta \cos \varphi \cos A'] \quad (2.17)$$

$$\lambda_{\text{SIP}} = \lambda' + \left[\frac{\sin \eta \sin A'}{\cos \varphi} \right] \quad (2.18)$$

where φ' and λ' are the latitude and longitude of the receiver, and A' is the signal azimuth at the receiver location.

The Variability of TEC

The TEC is highly variable, in both a temporal and spatial sense. The magnitude of the TEC varies on the season and the time of day the observation is made. However, the major factors are the level of solar activity and the geomagnetic location of the receiver.

The following comments can be made on the variability of TEC according to the above factors:

Seasonal variation - Typically, the electron density levels are higher in winter than in summer Kleusberg (1998). Since the Sun's radiation is higher in the summer, this is somewhat of an unexpected result. Ibid (1998) calculated the ionosphere vertical refractivity profiles during the winter and summer seasons at a northern latitude area using the International Reference Ionosphere (IRI) model. He claimed the ionospheric refractivity in winter is about 10 times higher than in summer.

Time of day – In mid-latitude areas the TEC is largest during daytime (typically after local noon) and at its minimum at nighttime until dawn (Langley, 1998a; see also Figure 2.5). In equatorial regions however, the situation is reversed. Wanninger (1993) shows a clear variation of Equatorial TEC occurring between sunset and midnight, and occasionally continues until dawn. Daytime TEC values in mid-latitude areas during a solar maximum on average can reach up to 40 TECU, and decrease during nighttime. However, in equatorial regions this value can be exceeded by a factor of two or more (Langley, 1998a).

Solar Activity – The solar activity is usually characterised by the sunspot number. Detailed observations of sunspots have been carried out by the Royal Greenwich Observatory since 1874, and can be represented in the so-called “butterfly diagram” (Figure 2.9). Note that the maximum sunspot number occurs in an 11 year cycle. The last solar maximum occurred during the years 2000/03. The maximum influence can be viewed as the evolution of the TEC (Figure 2.10), as shown on the Global Ionosphere Map (GIM) (CODE, 2006).

Geomagnetic location – The Earth's magnetic field influences particle motion in the Earth's orbit and traps charged particles such as free electrons. The geomagnetic field is strongest at low latitudes. Thus, higher electron densities can be expected in this area. Figure 2.11 indicates the geomagnetic boundaries relevant to ionospheric effects. The ionosphere is most active in a band extending up to approximately 30° on either side of the geomagnetic equator – where the highest TEC gradients and TEC values are

observed. In the auroral/polar regions, variable and irregular TEC can be observed. In mid-latitude areas the TEC gradient and TEC values are the lowest (Wanninger, 1993).

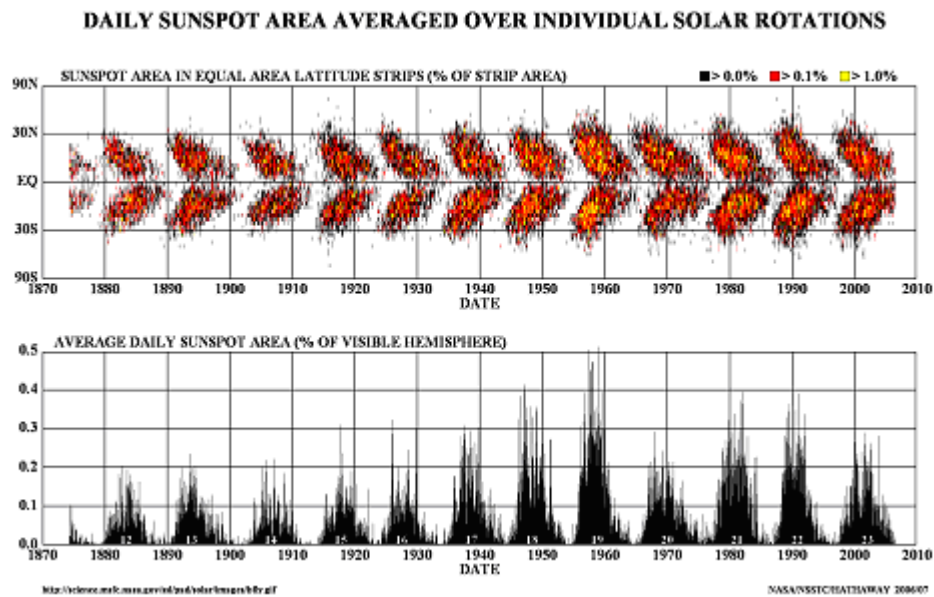


Figure 2.9 The 11 year solar cycle of sunspot numbers (NASA, 2006). **Top:** the positions of the spots shows that these bands first form at mid-latitudes, widen, and then move toward the equator as each cycle progresses. **Bottom:** information on the sizes of sunspots show the year 1960 recorded the highest.

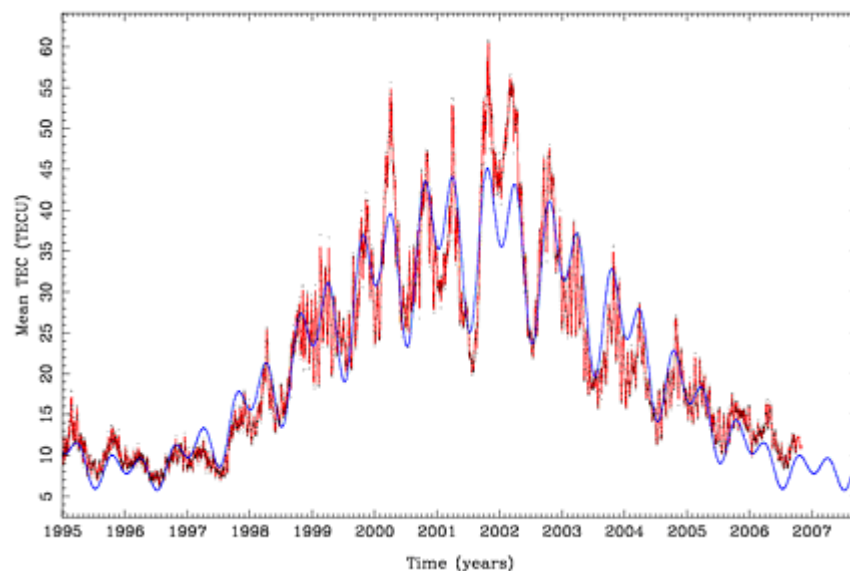


Figure 2.10 Two-hourly estimated (red line) and predicted (blue line) mean VTEC values from January 1995 to September 2006 (CODE, 2006). The highest recorded value was about 60TECU in year 2002.

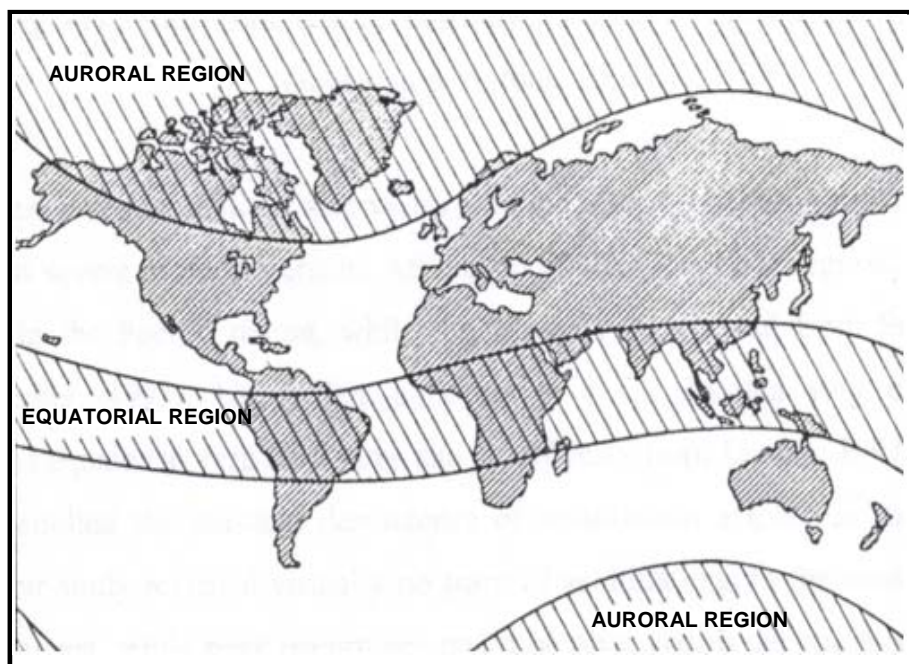


Figure 2.11 Regions of the world with high ionospheric activity (Seeber, 1993).

Warnant (2002) claims that typical values of 20 TECU at all latitudes in periods of low solar activity; 100 TECU is a value for the equatorial region and a ‘maximum’ value for mid-latitudes during periods of high solar activity; and 200 TECU encountered only in the equatorial region during very high solar activity. Zain et al. (2002) report on TEC variations in South-East Asia and quote a variation of between 20%-25% during geomagnetic storms. The ionospheric scintillations, which can cause the received signal amplitude and phase to fluctuate rapidly with time, mainly occur in geomagnetic equator and auroral/polar region (Wanninger, 1993; Langley, 1998a). In mid-latitudes scintillations are rarely observed, but Medium-Scale Travelling Ionospheric Disturbances (MSTIDs) occur frequently, mainly in daytime in the winter months during periods of high solar activity (Wanninger, 1999).

Estimation of Ionospheric Delay

The effect of the first order ionospheric delay on GPS signals can be calculated by inserting the corresponding frequencies, and the value from Equation 2.10 into Equation 2.9. For every 1 TECU, the magnitude of the delay to the L1 and L2 signals (phase and group delay) are $4.48 \times 10^{-16} (\lambda_{L1})^2 = 0.162\text{m}$ and $4.48 \times 10^{-16} (\lambda_{L2})^2 = 0.267\text{m}$ respectively. Thus, for high realistic TEC conditions, say 60 TECU as in Figure 2.10, the delay on L1 is 9.7m and 16.02m for L2!

Hence the effect of ionospheric delay is very severe on GPS navigation applications, for which single frequency (L1-only) receivers are often used. In this case, one option is to apply an ionospheric model to reduce the effect on the observations. The most commonly used model is the simple empirical ionospheric model by Klobuchar (1986), based on 8 parameters broadcast in the GPS navigation message. The parameters are used to approximate the Global VTEC, and therefore enable the calculation of the ionospheric delay effect. The model performance removes approximately 50%-60% RMS of the ionosphere effect, depending on the area coverage where the parameters are determined (Langley, 1998a). Hoffmann-Wellenhof et al. (2001) explain systematically the calculation steps for the Klobuchar model.

Fortunately, due to the dispersive nature of the ionosphere, the ionospheric delay can be directly measured if dual frequency receivers are used. The relationship of the first order ionospheric delay to L1, L2 and TEC can be written as (Rothacher & Mervart, 1996):

$$\text{dion}_{L1} = \frac{f_{L2}^2}{f_{L1}^2} \text{dion}_{L2} \quad (2.19)$$

Thus the delay can be scaled to the desired frequency, and subsequently the effects can be eliminated from the measurements (see also Chapter 3). A study by Bassiri & Hajj (1993) claims this elimination (of first order delay effect) can result in residual range error (RRE) at the zero level. Table 2.3 summarises their study results. Note the effects of higher order delays are also given.

Table 2.3 Estimated ionospheric group delay with assumption of 100 TECU (Bassiri & Hajj, 1993).

Ionospheric Delay	Delay to L1 (m)	Delay to L2 (m)	RRE (m)
First Order	16.223	26.718	0.0
Second Order	~0.016	~0.033	~-0.011
Third Order	~0.009	~0.002	~-0.007

2.2.3 Tropospheric Delay on GPS

Refractivity of Air

For radio frequencies up to about 30GHz, the troposphere is a non-dispersive medium; i.e., the refraction is independent of the frequency of the signals passing through it (Leick, 2004; Langley, 1998a). The refractive index of the atmospheric gases is close to unity: $n \approx 1.0003$ at sea level (Misra & Enge, 2004). Thus, it is often more convenient to express the refractive index in terms of refractivity, $N=10^6(n-1)$ (Leick, 2004). The refractivity of a parcel of air is dependent on the ambient atmosphere conditions, which can be separated according to whether they are dry gases or water vapour (Thayer, 1974):

$$N = K_1 \left(\frac{P_{\text{dry}}}{T} \right) Z_{\text{dry}}^{-1} + \left[K_2 \left(\frac{e}{T} \right) + K_3 \left(\frac{e}{T^2} \right) \right] Z_{\text{wet}}^{-1} \quad (2.20)$$

where P_{dry} is the partial pressure of dry air in millibars (mb); T is the absolute temperature in Kelvin (K); Z_{dry}^{-1} and Z_{wet}^{-1} are the inverse compressibility factors to account for dry air constituents and water vapour respectively; e is the partial pressure of water vapour (mb); and K_1 , K_2 , and K_3 are the refractivity (empirically-derived) constants. These constants have been determined by direct measurements made by microwave cavities and certainly cannot fully describe the local situation (Hoffmann-Wellenhof et al., 2001). Some of the commonly used sets of refractivity constants are listed in Table 2.4 (found in Bevis et al., 1994; Langley, 1998a).

Table 2.4 Some existing empirically determined values for the refractivity constants.

Constants	Smith & Weintraub (1953)	Thayer (1974)	Hasegawa & Stokesbury (1975)	Bevis et al. (1994)
K_1 (K mb ⁻¹)	77.61±0.01	77.60±0.014	77.60±0.032	77.60±0.05
K_2 (K mb ⁻¹)	72±9	64.8±0.08	69.40±0.15	70.4±2.2
K_3 (10 ⁵ K ² mb ⁻¹)	3.75±0.03	3.776±0.004	3.701±0.003	3.739±0.012

The inverse compressibility factors for the dry and wet components are given by (Owens, 1967):

$$Z_{\text{dry}}^{-1} = 1 + p_{\text{dry}} \left[57.97e^{-8} \left(1 + \frac{0.52}{T} \right) - 9.4611e^{-4} \frac{T'}{T} \right]$$

$$Z_{\text{wet}}^{-1} = 1 + 1650 \frac{e}{T^3} (1 - 0.01317T' + 1.75e^{-4}T'^2 + 1.44e^{-6}T'^3) \quad (2.21)$$

where T' is temperature in Celsius ($^{\circ}\text{C}$). These factors only correct for small departures of the moist atmosphere from an ideal gas. Alternatively, the pressure (P) and density (p) for the dry (p_{dry}) and wet air (p_{wet}) can be related by the gas law (Spilker, 1996c):

$$P_{\text{dry}} = p_{\text{dry}} \frac{R}{M_{\text{dry}}} TZ_{\text{dry}}, \quad P_{\text{wet}} = e = p_{\text{wet}} \frac{R}{M_{\text{wet}}} TZ_{\text{wet}} \quad (2.22)$$

where R is the universal gas constant ($8.31434\text{Jmol}^{-1}\text{K}^{-1}$); M_{dry} is the molar weight of dry air (28.9644kg/kmol); and M_{wet} is the molar weight of wet air (18.0152kg/mol). Substituting Equation 2.21 into 2.20:

$$N = K_1 \frac{Rp_{\text{dry}}}{M_{\text{dry}}} + K_2 \frac{Rp_{\text{wet}}}{M_{\text{wet}}} + K_3 \frac{e}{T^2} Z_{\text{wet}}^{-1}$$

$$= K_1 \frac{Rp_{\text{total}}}{M_{\text{dry}}} + \left(K_2 - K_1 \frac{M_{\text{wet}}}{M_{\text{dry}}} \right) \frac{e}{T} Z_{\text{wet}}^{-1} + K_3 \frac{e}{T^2} Z_{\text{wet}}^{-1} \quad (2.23)$$

where p_{total} is the total mass density of air given by:

$$p_{\text{total}} = p_{\text{dry}} + p_{\text{wet}} \quad (2.24)$$

As can be noticed, the first term of Equation 2.23 is dependent only on the total mass density of air; the second and third terms are more complex and are contaminated by the fractional water vapour content. Thus, the refractivity for the dry and wet components can be written as follows:

$$\begin{aligned}
 N_{\text{dry}} &= K_1 \frac{R_{p_{\text{total}}}}{M_{\text{dry}}} \\
 N_{\text{wet}} &= \left(K_2 - K_1 \frac{M_{\text{wet}}}{M_{\text{dry}}} \right) \frac{e}{T} Z_{\text{wet}}^{-1} + K_3 \frac{e}{T^2} Z_{\text{wet}}^{-1}
 \end{aligned}
 \tag{2.25}$$

According to Businger et al. (1996), the term dry should be replaced by the hydrostatic component of refractivity because there is a contribution from the hidden water vapour. Nevertheless, it is convenient to address them as dry and wet components, as is frequently done in the GPS literature.

Tropospheric Path Delay Modelling

The effect of the neutral atmosphere is denoted as tropospheric refraction, tropospheric path delay or simply tropospheric delay (Hoffmann-Wellenhof et al., 2001). The tropospheric delay to a GPS signal can be approximated as (Ibid, 2001; Rothacher & Mervart, 1996):

$$dt_{\text{trop}} = \int_S (n - 1) dS = 10^{-6} \int_S N dS
 \tag{2.26}$$

where n is the troposphere refractive index and N is the refractivity as previously described. The integration in Equation 2.26 is performed along the path (S) of the GPS signal through the atmosphere. The symbol dt_{trop} is the difference between the length of the curved path and the geometric range, which is equivalent to the total delay due to the gradient in the refraction index of the troposphere. This is not entirely true since the above integration neglects the bending effect of the troposphere (the signal is assumed to be coming from the zenith direction). According to Spilker (1996c) the bending effect reaches 3mm for elevation $E \geq 20^\circ$; 2cm for $E = 10^\circ$ and 17cm at $E = 5^\circ$. Duan et al. (1996) mentioned the bending effect becomes important for low elevation satellites ($\sim 5^\circ$). The bending effect can be reduced by setting a higher elevation cut-off angle, typically around 15° which is a common practise in GPS positioning. Correction for this effect is also given by Saastamoinen (1972; 1973), and further discussed in Spilker (1996c).

Interestingly, Equation 2.25 shows that the refractivity can be divided into a dry and wet component. The total tropospheric delay in Equation 2.26 can therefore be expressed as (Hoffmann-Wellenhof et al., 2001):

$$\begin{aligned} dtrop &= 10^{-6} \int N_{dry} dS + 10^{-6} \int N_{wet} dS \\ &= dtrop_{dry} + dtrop_{wet} \end{aligned} \quad (2.27)$$

Since the integration in Equations 2.26-2.27 is assumed to be in the zenith direction, $dtrop$ represents the total zenith tropospheric delay, or simply as zenith path delay (ZPD). As a consequence, $dtrop_{dry}$ and $dtrop_{wet}$ refer to the zenith dry delay and the zenith wet delay respectively. Recently, developments in tropospheric delay modelling further distinguish between the azimuthally symmetric delay and asymmetric components (Schuler, 2001):

$$dtrop = dtrop_{dry, symm} + dtrop_{dry, asymm} + dtrop_{wet, symm} + dtrop_{wet, asymm} \quad (2.28)$$

where $dtrop_{\dots, symm}$ is the tropospheric delay term under the assumption of symmetry in azimuth, and $dtrop_{\dots, asymm}$ is the tropospheric correction term taking the asymmetric effect into account. The asymmetric components can be determined by the application of a horizontal tropospheric gradient model. A study by Meindl et al. (2003) covering 308 days of data from permanent stations of the IGS has concluded that the repeatability of the horizontal coordinate components can be improved by a factor of 1.5 (from 1.5mm to 1mm), although the improvement in the height component is less pronounced (from 4.1mm to 3.6mm), after introducing horizontal gradients.

As mentioned in Section 2.2.1, the troposphere is influenced by the meteorological conditions (temperature, pressure and water vapour), and the variations of these parameters as a function of receiver altitude (see also Figure 2.6). Thus, the elevation of the satellite as observed from the receiver is an important factor in modelling the delay. At the zenith, the total tropospheric delay is the smallest but it gradually increases to its maximum effect at the horizon. To emphasise this elevation dependence it is necessary to write the total delay in Equation 2.27 as a product of mapping function:

$$dtrop = f(z)[dtrop_{dry} + dtrop_{wet}] \quad (2.29)$$

where $f(z)$ is the mapping function (can be similar to Equation 2.11). Further discussion concerning the troposphere mapping function will be given after the next section.

A priori Tropospheric Delay Modelling

In contrast to the ionospheric delay, the tropospheric delay is frequency independent, and the phase and group velocities of the signal when propagating through the non-ionised troposphere are exactly the same (Misra & Enge, 2004). Accordingly the tropospheric delay cannot be measured directly by observing multi-frequency signals, and the measurements from code and carrier phase experience the common delay. Therefore tropospheric delay modelling is important to estimate the delay and reduce the effect on GPS signals (and ultimately on positioning results).

Over the last few decades a number of (a priori) tropospheric models have been developed. The basis of these models is the integration of the refractivity derived in Equation 2.23, and mapping the result to arbitrary elevation angles using a mapping function. The models include; Hopfield, Black & Eisner, Davis, Atshuler & Kalaghan, and so on. Review of these models can be found in Spilker (1996c), Schuler (2001) and Hofmann-Wellenhof et al. (2001). Here, two models that are widely used in GPS positioning, are detailed, namely the Saastamoinen and the Modified Hopfield model.

Saastamoinen Total Delay Model

Saastamoinen (1972) developed a total delay tropospheric model based on the empirical value associated with the ideal gas law. The model estimates the total tropospheric delay as a function of the elevation angle for radio frequency signal at elevation angles $E \geq 10^\circ$. For station height at sea level, the (total) Saastamoinen model is given as:

$$dtrop_{corr} = \frac{0.002277}{\cos(Z)} \left[P_0 + \left(\frac{1255}{T_0} + 0.005 \right) e_0 - 1.156 \tan^2(Z) \right] \quad (2.30)$$

where $dtrop_{corr}$ is the total tropospheric delay correction in metres; P_0 is (at the user's antenna) surface pressure (mb); T_0 is surface temperature (K); e_0 is surface partial

pressure of water vapour (mb); and Z is the apparent zenith angle which can be determined from true zenith angle z of the satellite by the formula $Z = z - \Delta z$ where

$$\Delta z = \frac{16'' \tan(z)}{T_0} \left(P_0 + \frac{4800}{T_0} e_0 \right) - 0'' .07 (\tan^3(z) + \tan(z) \left(\frac{P_0}{1000} \right)) \quad (2.31)$$

is the angle of refraction. The values for pressure, temperature and humidity (to calculate e_0) can be measured, but practically the values were derived from standard atmospheric model (see discussion in “Tropospheric Delay Effect and Current Modelling Trends”).

The refined version of Equation 2.30 (the so-called ‘standard formula’) is given as (Saastamoinen, 1973):

$$\text{dtrop}_{\text{corr}} = \frac{0.002277(1+D)}{\cos(Z)} \left[P_0 + \left(\frac{1255}{T_0} + 0.005 \right) e_0 - B \tan^2(Z) \right] + \delta R \quad (2.32)$$

where $D = 0.0026 \cos(2\phi) + 0.00028H'$ is the correction for local latitude ϕ and station height H' above sea level in kilometre; B and δR are correction quantities obtained/interpolated from Table 2.5. Noted that the Saastamoinen model already includes the function $\cos(z)$ as the mapping function.

Davis et al. (1985) shows the derivation of dry delay correction ($\text{dtrop}_{\text{dry}}$) from the total Saastamoinen model. Their final formulation for the dry correction is equivalent to:

$$\text{dtrop}_{\text{dry}} = \frac{0.0022768 \pm 0.0000005 p_0}{(1-D)} \quad (2.33)$$

As can be seen in Equation 2.33, the dry Saastamoinen model is quite simple. The meteorological data it relies on is only the surface pressure, which is easy to measure. Elgered et al. (1991) state that a surface pressure with accuracy of 0.3mb or better permits the calculation of the zenith dry delay to better than 1mm accuracy. Hence the

dry component is easier to handle, and can be modelled more precisely than the wet component.

Table 2.5 Correction terms for the Saastamoinen model (Saastamoinen, 1973).

	Apparent zenith angle	Station height above sea level							
		0.0km	0.5km	1.0km	1.5km	2.0km	3.0km	4.0km	5.0km
$\delta R(m)$	60°00'	0.003	0.003	0.002	0.002	0.002	0.002	0.001	0.001
	66°00'	0.006	0.006	0.005	0.005	0.004	0.003	0.003	0.002
	70°00'	0.012	0.011	0.010	0.009	0.008	0.006	0.005	0.004
	73°00'	0.020	0.018	0.017	0.015	0.013	0.011	0.009	0.007
	75°00'	0.031	0.028	0.025	0.023	0.021	0.017	0.014	0.011
	76°00'	0.039	0.035	0.032	0.029	0.026	0.021	0.017	0.014
	77°00'	0.050	0.045	0.041	0.037	0.033	0.027	0.022	0.018
	78°00'	0.065	0.059	0.054	0.049	0.044	0.036	0.030	0.024
	78°30'	0.075	0.068	0.062	0.056	0.051	0.042	0.034	0.028
	79°00'	0.087	0.079	0.072	0.065	0.059	0.049	0.040	0.033
	79°30'	0.102	0.093	0.085	0.077	0.070	0.058	0.047	0.039
	79°45'	0.111	0.101	0.092	0.083	0.076	0.063	0.052	0.043
	80°00'	0.121	0.110	0.100	0.091	0.083	0.068	0.056	0.047
B (mb)		1.156	1.079	1.006	0.938	0.874	0.757	0.654	0.563

Modified Hopfield Model

Hopfield (1969) developed a dual quartic zenith model based on empirically-determined values for dry and wet refractivity as a function of station height (h) above the Earth's surface, given as:

$$N_{\text{dry}}(h) = N_{\text{dry},0} \left[\frac{h_{\text{dry}} - h}{h_{\text{dry}}} \right]^4, \quad N_{\text{wet}}(r) = N_{\text{wet},0} \left[\frac{h_{\text{wet}} - h}{h_{\text{wet}}} \right]^4 \quad (2.34)$$

Based on a fit of global radiosonde data, Hopfield derived an effective height of the dry atmosphere layer as $h_{\text{dry}} = [40136 + 148.72(T - 273.16)]\text{m}$, by taking into account the temperature T (K) of the troposphere. The mean height value for the wet atmosphere layer (h_{wet}) is estimated at 12km, though not correct in all cases. Hopfield claimed the values ranging from 10 to 14 even 16km, and the RRE (from dtrop) have an RMS of ~2% between these values. Specific values for h_{dry} and h_{wet} cannot be determined due to their dependence on location and temperature. The values for $N_{\text{dry},0}$ and $N_{\text{wet},0}$ are taken from Equation 2.25 with the following assumption (Schuler, 2001):

$$\begin{aligned}
 N_{\text{dry},0} &= K_1 \frac{R p_{\text{total}}}{M_{\text{dry}}} \approx K_1 \frac{p}{T} \\
 N_{\text{wet},0} &= \left(K_2 - K_1 \frac{M_{\text{wet}}}{M_{\text{dry}}} \right) \frac{e}{T} Z_{\text{wet}}^{-1} + K_3 \frac{e}{T^2} Z_{\text{wet}}^{-1} \approx K_2 \frac{e}{T} + K_3 \frac{e}{T^2}
 \end{aligned}
 \tag{2.35}$$

The modified version of refractivity formula in Equation 2.34 is derived by introducing lengths of position vectors (r) instead of heights, and become the basis of Modified Hopfield model (Hoffmann-Wellenhof et al., 2001):

$$N_{\text{dry}}(r) = N_{\text{dry},0} \left[\frac{r_{\text{dry}} - r}{r_{\text{dry}} - R_E} \right]^4, \quad N_{\text{wet}}(r) = N_{\text{wet},0} \left[\frac{r_{\text{wet}} - r}{r_{\text{wet}} - R_E} \right]^4
 \tag{2.36}$$

where $r_{\text{dry/wet}} = R_E + h_{\text{dry/wet}}$; $r = R_E + h$ and R_E is the Earth radius value in metres. The geometrical basis of the modelling is shown in Figure 2.12 (for the dry layer case).

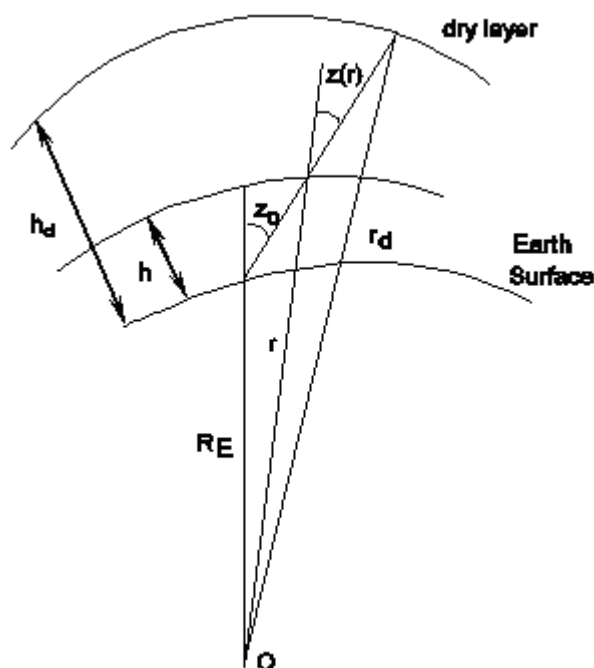


Figure 2.12 Geometry of tropospheric delay (Hofmann-Wellenhof et al., 2001).

Using the analogy as in Equation 2.27, by inserting the mapping function as in Equation 2.11 (assuming the dry and wet mapping functions are the same), one obtains the total corrections as:

$$dtrop_{corr} = 10^{-6} \int_{r=R_E}^{r=r_{dry}} \frac{N_{dry}(r)}{\cos z(r)} dr + 10^{-6} \int_{r=R_E}^{r=r_{wet}} \frac{N_{wet}(r)}{\cos z(r)} dr \quad (2.37)$$

where $z(r)$ is a variable that needs to be resolved. The relationship between receiver zenith angle (z_0) in Figure 2.12 and the zenith angle $z(r)$ at height h is given by:

$$\frac{R_E}{r} = \frac{\sin z(r)}{\sin z_0} \quad (2.38)$$

Rearranging $z(r)$ and applying the trigonometric identity to the above equation:

$$\cos z(r) = \frac{1}{r} \left(r^2 - R_E^2 \sin^2 z_0 \right)^{\frac{1}{2}} \quad (2.39)$$

Inserting Equation 2.39 and 2.36 into Equation 2.37:

$$dtrop_{corr} = \frac{10^{-6} N_{dry,0}}{(r_{dry} - R_E)^4} \int_{r=R_E}^{r=r_{dry}} \frac{r(r_{dry} - r)^4}{\left(r^2 - R_E^2 \sin^2 z_0 \right)^{\frac{1}{2}}} dr + \frac{10^{-6} N_{wet,0}}{(r_{wet} - R_E)^4} \int_{r=R_E}^{r=r_{wet}} \frac{r(r_{wet} - r)^4}{\left(r^2 - R_E^2 \sin^2 z_0 \right)^{\frac{1}{2}}} dr \quad (2.40)$$

The integration in Equation 2.40 can be approximated by adopting an expansion series as further explained in Hoffmann-Wellenhof et al. (2001):

$$dtrop_i(E) = 10^{-12} N_{i,0} \left[\sum_{k=1}^9 \frac{\alpha_{k,i}}{k} r_i^k \right] \quad (2.41)$$

and

$$\begin{aligned} r_i &= \left[(R_E + h_i)^2 - (R_E \cos E)^2 \right]^{\frac{1}{2}} - R_E \sin E \\ \alpha_{1,i} &= 1, \quad \alpha_{2,i} = 4a_i, \quad \alpha_{3,i} = 6a_i^2 + 4b_i \\ \alpha_{4,i} &= 4a_i(a_i^2 + 3b_i), \quad \alpha_{5,i} = a_i^4 + 12a_i^2b_i + 6b_i^2 \\ \alpha_{6,i} &= 4a_ib_i(a_i^2 + 3b_i), \quad \alpha_{7,i} = b_i^2(6a_i^2 + 4b_i) \\ \alpha_{8,i} &= 4a_ib_i^3, \quad \alpha_{9,i} = b_i^4 \end{aligned} \quad (2.42)$$

where

$$a_i = \frac{\sin E}{h_i}, \quad b_i = \frac{\cos^2 E}{2h_i R_E} \quad (2.43)$$

and the elevation angle E is used instead of the zenith angle z_0 in Equations 2.41-2.43; and replacing the subscript $i = \text{dry}$ to get the correction for the dry delay; or $i = \text{wet}$ to get the correction for the wet delay. In this fashion the total tropospheric delay correction at any elevation angle E is just the sum of the dry and wet delay correction terms, analogous to Equation 2.40. It is obvious that the dry delay from this model needs two pieces of meteorological information, i.e. pressure p and temperature T (see Equation 2.35), as opposed to the Saastamoinen dry model where only p is needed (see Equation 2.33). For the wet delay model the uncertainties very much depend on the partial water vapour e and temperature T (also in Equation 2.35).

Troposphere Mapping Function

Due to the critical altitude dependency, the troposphere mapping function is an important component and is subject to its own modelling. A mathematical explanation of some of the most common mapping functions can be found in Schuler (2001) and Spilker (1996c). As mentioned earlier, setting higher satellite elevation cut-off angles reduces the effect of the tropospheric delay. Other benefits are the elimination of the tropospheric bending effect, as well as lower systematic errors due to an imperfect mapping function. On the other hand, the inclusion of low elevation satellites provides data redundancy, and improves the satellite geometry, implying an increase in the precision of the estimated station coordinates. Sunil et al. (1997) reported more than 70% improvement in the estimated station height when elevation cut-off angles of 3° to 5° are used in the GPS data processing.

The mapping function can be further divided into dry (f_{dry}) and wet (f_{wet}) components. Thus, Equation 2.29 can be written as:

$$dtrop = dtrop_{\text{dry}} f_{\text{dry}}(z) + dtrop_{\text{wet}} f_{\text{wet}}(z) \quad (2.44)$$

Tropospheric mapping functions may also utilise meteorological information. Mendes & Langley (1994) provide a comprehensive analysis of fifteen mapping functions and found almost all mapping functions are very effective at elevation angles above 15°. They also recommend that for elevation angles less than 10°, that the Niell, Herring and Ifadis mapping functions should be used. Ifadis (2000) developed a mapping function called IF-NEW and tested results from 80° to 1° elevation angles at a cold temperate station. He claimed the IF-NEW results in dry delay residuals ranging from 0.003m (at 80° elevation angle) to -0.382m (at 1° elevation angle) for the stations tested. Niell (2000) developed a mapping function that can be used to calculate the tropospheric delay at elevations down to 3° but stated that the results will not be so accurate in the equatorial region (due to the high water vapour content in the troposphere).

Rocken et al. (2001) suggested that for low elevation observations (less than 5°), the mapping function should be a location- and time-specific function that can be derived from:

- a) mapping the International Reference Atmosphere with added water vapour climatology;
- b) the same as (a) with the added use of surface meteorological data, i.e. temperature, pressure and humidity; and
- c) use of the numerical analysis model of the National Centres for Environmental Prediction (NCEP) - National Center for Atmospheric Research.

They reported ~50% improvements for dry mapping and lower improvements for wet mapping in comparison to the Niell mapping function for low elevation angle observations.

Tropospheric Delay Effect and Current Modelling Trends

Janes et al. (1989) claim that about 90% of the total delay is due to the dry components. The dry delay can effectively be modelled to reduce its contribution down to 1% due to a small variation in the dry gases in the atmosphere (Spilker, 1996c). The problem lies in modelling the wet component, i.e. the other 10% of the total delay. The wet delay is approximately proportional to the amount of water vapour in the atmosphere. Due to

strong variations in the distribution of water vapour in space and time, the wet delay is less predictable and therefore much more difficult to model.

If it could be assumed that tropospheric modelling was ideal, the limitations now are the input of meteorological information, especially the accuracy of water vapour data. Beutler et al. (1988) consider the impact of 1% errors in temperature, pressure and humidity on the estimated zenith total delay correction. These are given in Table 2.6, based on calculations using the Saasatmoinen model. Inspection of Table 2.6 indicates that the errors range from the centimetre to the sub-centimetre level. Too small to detect, this error will be magnified into the estimated station height by approximately three times (further discussed in Chapter 3). For example, a 4mm error in relative humidity will produce a 1cm error in station height.

Table 2.6 Meteorological dependent of zenith total delay correction ($dtrop_{corr}$) (Beutler et al., 1988).

Temperature (T)	Pressure (P)	Humidity (H)	$\left \frac{\partial dtrop_{corr}}{\partial T} \right $	$\left \frac{\partial dtrop_{corr}}{\partial p} \right $	$\left \frac{\partial dtrop_{corr}}{\partial H} \right $
°C	mb	%	mm/°C	mm/mb	mm/1%
0	1000	100	5	2	0.6
30	1000	100	27	2	4
0	1000	50	3	2	0.6
30	1000	50	14	2	4

High precision instrumentation such as ground-based water vapour radiometers are not able to provide measurements to that level of accuracy (i.e., the 1% level in Table 2.6) (Rothacher & Mervart, 1996; Tregoning et al., 1998). Moreover it may not entirely represent the conditions at the site (meteorological measurement usually made near to the site). Nowadays it is a rare practice to measure meteorological parameters when using GPS. Even so, the precision of such instruments does require a proper calibration. One remedy is to use a ‘standard’ atmosphere model; with reference pressure (1013.25mb), temperature (18°C) and relative humidity (50%) at sea level. These values can be used in the a priori tropospheric model with appropriate standard atmosphere equations (see these equations in Rothacher & Mervart, 1996).

Current trends in modelling the tropospheric delay effect are to combine GPS data and numerical weather models (NWM). This combination already shows promising results for both the GPS positioning and meteorological communities, as reported by many researchers, for example: Rocken et al. (2001); Schuler (2001); Pacione & Vespe (2003); Vollath et al. (2003); (Niell, 2003); Eresmaa & Jarvinen (2006). Careful GPS data processing provides precise estimates of ZPD. Since the dry model is easy to predict from Equation 2.33 or Equation 2.41, or other related dry models, the residual relates to the wet delay (which is related to the water vapour content in the atmosphere). Thus, Equation 2.27 can be written as:

$$dtrop_{wet} = dtrop - dtrop_{dry} \quad (2.45)$$

which serves as the basis of a GPS water vapour sensor. However, to obtain accurate results for the dry component modelling, pressure and temperature values are needed (depending on the model used), which are not often available at GPS receivers. Hence the NWM is a possible remedy. As NWMs become more mature and accurate, the model will provide 'interpolated' meteorological information to support GPS positioning. It also can support the calculation of the so-called 3-D weather fields, which allow accurate derivation of the mapping function (Rocken et al., 2001), as well as the estimation of tropospheric horizontal gradients (Schuler, 2001). Some NWMs are the Global Data Assimilation System (GDAS; NCEP United States National Oceanic and Atmospheric Administration) and the 3D-Var assimilation system (Gustafsson et al., 2001). Skone & Hoyle (2005) have demonstrated the used of an array of GPS reference stations to recover estimates of the wet delay which is important to model the vertical and horizontal structure of water vapor over a local area. Their study implements the so-called 4-D tomographic water vapor model and found that this network technique provides a very promising opportunity to study weather conditions.

2.3 GPS Positioning

GPS range observations can be processed, in post- or (near) real-time mode, to obtain the location of static (i.e. stationary) or kinematic (i.e. moving) receiver. To do so,

Equations 2.1 and 2.4 are now revised by considering the error sources as discussed in Section 2.1.5 and the atmosphere effects in Section 2.2. The range as observed from a satellite to a receiver can be written for C/A code measurements on the L1 frequency ($P_{C/A}$); P code measurements on the L1 frequency (P_{L1}); P code measurements on the L2 frequency (P_{L2}); carrier phase on the L1 frequency (L_{L1}); and carrier phase on the L2 frequency (L_{L2}) (all in metric units):

$$P_{C/A} = p + c(dt^S - dt_R) + dion_{C/A} + dtrop + (dH^S + dH_R)_{C/A} + dmp_{C/A} + e_{C/A} \quad (2.46)$$

$$P_{L1} = p + c(dt^S - dt_R) + dion_{P1} + dtrop + (dH^S + dH_R)_{P1} + dmp_{P1} + e_{P1} \quad (2.47)$$

$$P_{L2} = p + c(dt^S - dt_R) + dion_{P2} + dtrop + (dH^S + dH_R)_{P2} + dmp_{P2} + e_{P2} \quad (2.48)$$

$$L_{L1} = p + c(dt^S - dt_R) - dion_{L1} + dtrop + (dH^S + dH_R)_{L1} + dmp_{L1} + \lambda_{L1} N_{L1} + E_{L1} \quad (2.49)$$

$$L_{L2} = p + c(dt^S - dt_R) - dion_{L2} + dtrop + (dH^S + dH_R)_{L2} + dmp_{L2} + \lambda_{L2} N_{L2} + E_{L2} \quad (2.50)$$

where the terms \bar{e} and \bar{E} in Equations 2.1 and 2.4 have been expanded to include the ionospheric delay ($dion_*$), tropospheric delay ($dtrop$), satellite hardware delay (dH^S_*), receiver hardware delay (dH_R_*), multipath effect (dmp_*), pseudorange measurement noise (e_*), carrier phase measurement noise (E_*), and other terms which have been previously included in Equations 2.1, 2.3 and 2.4. The symbol (*) denotes the terms that are frequency-dependent, which is indicated by the given subscripts in the above equations.

2.3.1 Point Positioning

GPS point positioning outputs the coordinates of a single receiver (latitude, longitude and height) wrt the WGS-84 datum, using range observations defined in Equations 2.46 - 2.50. There are two forms of point positioning: pseudorange-based navigation solution and precise point positioning.

Navigation Solution

Point positioning utilising C/A code pseudoranges (Equation 2.46) is referred to simply as the GPS 'navigation solution'. Such a navigation solution relies on the satellite coordinates and the satellite clock correction information broadcast in the navigation message. The largest contribution to the bias in the range in Equation 2.46 originates

from the receiver clock errors. Note that a 1microsecond error in time used to calculate range will bias the range by approximately 300m (given $c \sim 3 \times 10^8 \text{m.s}^{-1}$). Neglecting other error terms in Equation 2.46, and assuming a single-epoch solution leads to four unknown parameters of interest, namely the receiver clock error (dt_R) and the receiver coordinates (e.g., latitude, longitude, height). Thus, four simultaneous pseudoranges from four satellites in view (Figure 2.13) enables the unknown parameters to be determined 'instantaneously'. In practice more than four pseudorange observations are often measured and the least squares estimation outputs the optimal (unique) navigation solution. This positioning mode is easy to implement and suitable for real-time applications that can be addressed with vertical and horizontal accuracies as given in Table 2.7 (the calculations in Table 2.7 are discussed in Langley (1999) and Wormley (2006)).

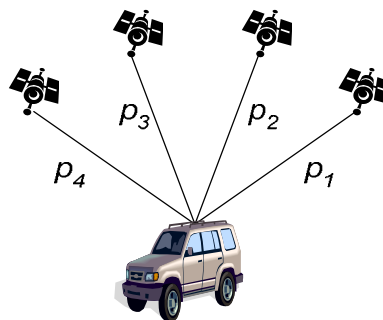


Figure 2.13 Navigation Solution.

Table 2.7 Estimated C/A code pseudorange budget and RRE based on one sigma error. Adapted from Wormley (2006).

Error source	RMS RRE (m)	Random (m)	Total (m)
Orbital (nav. message)	2.1	0.0	2.1
Satellite clock (nav. message)	2.0	0.7	2.1
Ionosphere (corrected)	4.0	0.5	4.0
Troposphere (corrected)	0.5	0.5	0.7
Multipath	1.0	1.0	1.4
Hardware & Measurement error	0.5	0.2	0.5
-----	-----	-----	-----
UserEquivalent Range Error (UERE) or root sum square of RMS RRE	5.1	1.4	5.3
Vertical Dilution of Precision (VDOP)	2.5		
Horizontal Dilution of Precision (HDOP)	2.0		
-----	-----	-----	-----
Vertical one-sigma errors (m)	13.3		
Horizontal one-sigma errors (m)	10.6		

Precise Point Positioning

Precise point positioning (PPP) relies on the precise information of the satellite orbit and clock. This technique is becoming increasingly popular now that the IGS produce accurate predicted satellite orbit and satellite clock errors (Kouba & Heroux, 2001). Current levels of accuracy (and latency) of IGS orbits and satellite clock products are given in Table 2.8 (Access of IGS products can be via <http://igsceb.jpl.nasa.gov/components/usage.html>). One can use these IGS products, together with the observations defined in Equations 2.47-2.50, as the basis for PPP.

Table 2.8 IGS combined product precision and latencies (courtesy of IGS website).

Product		Accuracy	Latency	Updates	Sample Interval
Ultra-Rapid (predicted half)	Orbit	~10 cm	real time	Four times daily	15 min
	Sat. Clocks	~5 ns			
Ultra-Rapid (observed half)	Orbit	<5 cm	3 hours	Four times daily	15 min
	Sat. Clocks	~0.2 ns			
Rapid	Orbit	<5 cm	17 hours	daily	15 min
	Sat. Clocks	0.1 ns			5 min
Final	Orbit	<5 cm	~13 days	weekly	15 min
	Sat. Clocks	<0.1 ns			5 min

PPP algorithms have been developed over a number of years, for example, in the BERNESE package (Rothacher & Mervart, 1996). Nevertheless PPP algorithms are more complicated than standard navigation solutions because of the need to model as many of the GPS errors as possible, in order to ensure high accuracy positioning results. PPP requires the estimation of parameters such as station coordinates, tropospheric parameters, receiver clock error and carrier phase ambiguities. In addition the dual-frequency relationship is used to eliminate the effect of ionospheric delay (to first order). Clearly the process requires more observations, and perhaps extra time, to generate the results compared to the standard navigation solution. Currently, positioning solutions (in static or kinematic mode) using PPP are reported with decimetre level accuracy (Gao & Chen, 2004; Kouba & Heroux, 2001).

2.3.2 Differential & Relative Positioning

The terms of 'differential' and 'relative' are synonymous. However, the differential and relative positioning techniques are different in many ways. Differential GPS (DGPS)

technique is based on the use of two or more receivers, where one (stationary/static) reference or base receiver is located at a known point (e.g. from previous survey) and the position of the user receiver (mostly moving/kinematic) is to be determined (Hoffmann-Wellenhof et al., 2001). In DGPS, the position of the user receiver is determined on the basis of applying the position corrections or range (code or phase) corrections as they can be calculated with the use of the known position of the reference station (Ibid, 2001; Misra & Enge, 2004). Generally, DGPS utilises code pseudorange as the major measurements to obtain metre level but may apply the phase smoothed code ranges for sub-metre accuracy. Higher accuracy can be achieved by taking the carrier phase as the major measurements after solving the carrier phase ambiguities.

Whilst the DGPS technique is designed to solve the user's position, the relative positioning technique is used to determine the baseline vectors or baseline components relating the reference and user stations. In relative positioning, the simultaneous measurements (in contrast to DGPS) at both reference and user station are directly combined (Hoffmann-Wellenhof et al., 2001; Leick, 2004). In fact, GPS relative positioning cancels many of the systematic errors affecting simultaneous observations made from the reference station and user receiver. Relative positioning may utilise carrier phase and/or code measurements but in the past the term 'relative' was referred to carrier phase measurements, and 'differential' was referred to code measurements. Highest accuracies are achieved in the (static) relative positioning technique with observed carrier phases (Ibid, 2001). Further discussions on relative positioning technique can be found in Section 2.4.

Both the DGPS and relative positioning technique can be conducted in static and/or kinematic mode. The positioning result can be post-processed or can be obtained while the receiver is still on site. The latter requires the use of radio links (or other communications links) to transfer the corrections i.e. for the DGPS technique, or measurements i.e. for the relative positioning technique, between the two stations. This leads to the Real-Time Kinematic (RTK) technique. In fact, the result of RTK can only be achieved in near real-time due to the transmission delay (as well as the delay in data processing). Further discussions on the relative positioning are given in the next section.

2.4 Relative Positioning

2.4.1 Data Differencing

“Linear biases can be accounted for either by reducing the number of observations so that the biases cancel, or by adding an equal number of unknowns to model the biases. Both approaches give identical results” (Lindlohr & Wells, 1985). The former approach is uses a technique based on ‘data differencing’. Various GPS data differencing options are available, such as differencing between satellites, between receivers, between epochs, between frequencies, and even between code and phase observables (see Teunissen & Kleusberg, 1998). The differencing of data between receivers and between satellites, observed on the same frequencies, is the most crucial operation. In the following, the code and phase differencing are described for the case of P-code measurements on the L1 and L2 signals.

Single-Differencing

The between-receiver differencing of two GPS observations (l) from receivers A and B, observing the same satellite (i), on the same frequency (f), and at the same epoch (t) is defined as:

$$l_{f,AB}^i(t) = l_{f,A}^i(t) - l_{f,B}^i(t) \quad (2.51)$$

This is known as single-differenced (SD), and the geometry is illustrated in Figure 2.14. Applying Equation 2.51 to Equations 2.47-2.50, the SD observations are obtained as follows:

$$\Delta P_1 = \Delta p - c\Delta t_R + \Delta d_{ionP1} + \Delta dtrop + \Delta(dH_R)_{P1} + \Delta dmp_{P1} + \Delta e_{P1} \quad (2.52)$$

$$\Delta P_2 = \Delta p - c\Delta t_R + \Delta d_{ionP2} + \Delta dtrop + \Delta(dH_R)_{P2} + \Delta dmp_{P2} + \Delta e_{P2} \quad (2.53)$$

$$\Delta L_1 = \Delta p - c\Delta t_R - \Delta d_{ionL1} + \Delta dtrop + \Delta(dH_R)_{L1} + \Delta dmp_{L1} + \lambda_{L1}\Delta N_{L1} + \Delta E_{L1} \quad (2.54)$$

$$\Delta L_2 = \Delta p - c\Delta t_R - \Delta d_{ionL2} + \Delta dtrop + \Delta(dH_R)_{L2} + \Delta dmp_{L2} + \lambda_{L2}\Delta N_{L2} + \Delta E_{L2} \quad (2.55)$$

where Δ is a differencing operator; and the other terms were previously defined. Some assumptions are made, such as that observations at individual receivers are simultaneous

and between receivers the clock drifts are properly synchronised or accounted for. The common satellite dependent errors (superscript S in Equations 2.47-2.50) as observed from stations A and B were cancelled, which include the satellite clock error and satellite hardware delays. Moreover, the atmospheric delay terms are now considerably reduced when the receiver distance is short because atmospheric conditions are strongly correlated. The receiver clock error is still unknown in Equations 2.52-2.55, as well as the remaining receiver's hardware delays.

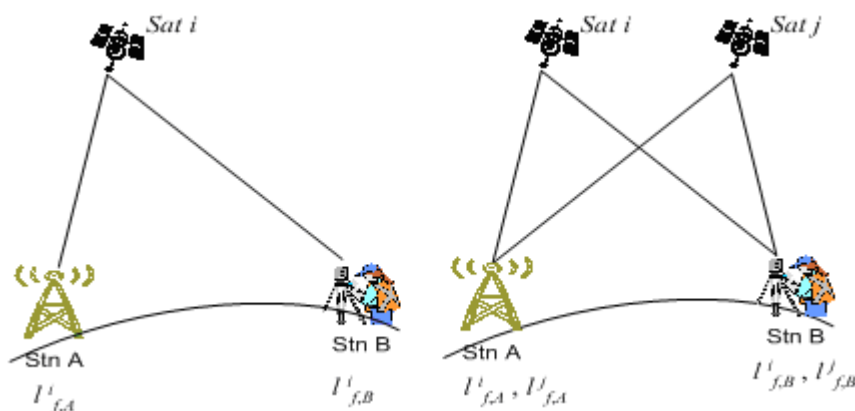


Figure 2.14 Geometry of single-differencing (left) and double-differencing (right).

Double-Differencing

If another set of SDs exist, say on satellite j , a double-differencing procedure can be followed that is equivalent to differencing between receivers (i.e., A and B) and between satellites (i.e., i and j), and at the same epoch (t):

$$I_{f,AB}^{ij}(t) = I_{f,AB}^i(t) - I_{f,AB}^j(t) \quad (2.56)$$

This is known as double-differenced (DD), and the geometry is illustrated in Figure 2.14. Applying Equation 2.56 to Equations 2.52-2.55, the DD observations are obtained as follows:

$$\Delta \nabla P_1 = \Delta \nabla p + \Delta \nabla \text{dion}_{P1} + \Delta \nabla \text{dtrop} + \Delta \nabla \text{dmp}_{P1} + \Delta \nabla e_{P1} \quad (2.57)$$

$$\Delta \nabla P_2 = \Delta \nabla p + \Delta \nabla \text{dion}_{P2} + \Delta \nabla \text{dtrop} + \Delta \nabla \text{dmp}_{P2} + \Delta \nabla e_{P2} \quad (2.58)$$

$$\Delta \nabla L_1 = \Delta \nabla p - \Delta \nabla \text{dion}_{L1} + \Delta \nabla \text{dtrop} + \Delta \nabla \text{dmp}_{L1} + \lambda_{L1} \Delta \nabla N_{L1} + \Delta \nabla E_{L1} \quad (2.59)$$

$$\Delta\nabla L_2 = \Delta\nabla p - \Delta\nabla \text{dion}_{L_2} + \Delta\nabla \text{dtrop} + \Delta\nabla \text{dmp}_{L_2} + \lambda_{L_2} \Delta\nabla N_{L_2} + \Delta\nabla E_{L_2} \quad (2.60)$$

where $\Delta\nabla$ is a double-differencing operator; and the other terms were previously defined. The common receiver dependent errors (subscript R in Equations 2.52-2.55) as observed from stations A and B were cancelled, which include the receiver clock error and receiver hardware delays. A point worth mentioning is that although the receiver clock error has been cancelled to first order, the residual effects of clock error due to satellite motion and Earth's rotation still affect the computation of range term. Rothacher & Mervart (1996) show that if the residual clock error is kept below 1microsecond, the range error is smaller than 1mm. Blewitt (1997) discussed various approaches to dealing with this problem in GPS geodetic software.

The effects of unmodelled atmospheric errors, multipath and random errors are generally increased slightly by double-differencing as compared to single-differencing (Ibid, 1997). On the other hand, the motivation of double-differencing is to cancel the receiver's clock error, which would create much larger errors. Overall, the simplified mathematical model of the DD observation is the reason it is very popular within data processing software. However, differencing (i.e., SD or DD) also eliminates information from the observations.

2.4.2 Least Squares Estimation for DD Observations

The least squares technique is often employed to estimate the parameters of interest embedded within the DDs. To review this technique it is necessary to describe the mathematical model and estimation procedure in matrix form (bold notation). Consider Equation 2.56 with observations at some epoch i with two receivers tracking k satellites (Hoffmann-Wellenhof et al., 2001):

$$\mathbf{DD}_{(i)} = \mathbf{C} \mathbf{SD}_{(i)} \quad (2.61)$$

where \mathbf{SD} are the single-differenced observations; \mathbf{DD} are the double-differenced observations; and \mathbf{C} is the double-differencing operator given by (for a fixed satellite as reference satellite):

$$\mathbf{C}^{k-1,k} = \begin{bmatrix} 1 & -1 & 0 & \dots & 0 \\ 1 & 0 & -1 & \dots & 0 \\ \dots & \dots & \dots & \ddots & \vdots \\ 1 & 0 & 0 & \dots & -1 \end{bmatrix} \quad (2.62)$$

Applying the error propagation law, the ‘a priori’ variance-covariance (VCV) matrix for the double-differenced observations is (Ibid, 2001):

$$\mathbf{VCV}(\mathbf{DD})_{(i)} = \mathbf{C} \cdot \mathbf{VCV}(\mathbf{SD})_{(i)} \cdot \mathbf{C}^T \quad (2.63)$$

where

$$\mathbf{VCV}(\mathbf{SD}) = 2\sigma^2\mathbf{I} \quad (2.64)$$

and σ^2 is the variance of the one-way carrier phase measurements with expectation value zero, under the assumption that the phase errors show a random behaviour and follow the normal distribution. The matrix \mathbf{I} is the identity matrix. Numerically, Equation 2.63 is given by:

$$\mathbf{VCV}(\mathbf{DD})_{(i)} = \sigma^2 \begin{pmatrix} 4 & 2 & \dots & 2 \\ 2 & 4 & \dots & 2 \\ \dots & \dots & \dots & \dots \\ 2 & 2 & \dots & 4 \end{pmatrix} \quad (2.65)$$

It is important to note that the VCV matrix of the double-differenced observations in Equation 2.65 implies that they are mathematically correlated, with same variance and statistically independent in time and space. In standard least squares theory, a set of linearised double-differenced observables can be written in the form as (Blewitt, 1998):

$$\mathbf{z} = \mathbf{Ax} + \mathbf{v} \quad (2.66)$$

where \mathbf{z} is the column vector of observed-minus-computed observables, \mathbf{A} is the design matrix, \mathbf{x} is the column vector of the unknown parameters, and \mathbf{v} is a column vector of errors. Let assume the expectation (E) of \mathbf{v} is zero, and,

$$E(\mathbf{v}\mathbf{v}^T) = \mathbf{VCV} \equiv \mathbf{W}^{-1} \quad (2.67)$$

where \mathbf{W} is the weight matrix as calculated from the inverse of VCV matrix of the DD observables. The least squares estimator of the unknown parameter \mathbf{x} is:

$$\hat{\mathbf{x}} = (\mathbf{A}^T \mathbf{W} \mathbf{A})^{-1} \mathbf{A}^T \mathbf{W} \mathbf{z} \quad (2.68)$$

To solve Equation 2.68, approximate values of the unknown parameters are needed. Equation 2.68 is dependent on the design matrix \mathbf{A} , \mathbf{VCV} and the set of observations \mathbf{z} . The estimated observables and the least squares residuals can be computed as:

$$\hat{\mathbf{z}} = \mathbf{A} \hat{\mathbf{x}} \quad (2.69)$$

$$\hat{\mathbf{v}} = \mathbf{z} - \hat{\mathbf{z}} \quad (2.70)$$

It is usual after computing the least squares residual to also compute the quantity $\hat{\sigma}^2$, the unit variance (e.g., Cross, 1983):

$$\hat{\sigma}^2 = \frac{\hat{\mathbf{v}}^T \mathbf{W} \hat{\mathbf{v}}}{f} \quad (2.71)$$

where f is the number of degrees of freedom. Equation 2.68 has the following statistical properties:

$$E(\hat{\mathbf{x}}) = E(\mathbf{x}) = \mathbf{x} \quad (2.72)$$

$$E(\hat{\mathbf{x}}\hat{\mathbf{x}}^T) = \hat{\sigma}^2 (\mathbf{A}^T \mathbf{W} \mathbf{A})^{-1} \equiv \mathbf{VCV}_{\hat{\mathbf{x}}} \quad (2.73)$$

Thus $\mathbf{VCV}_{\hat{\mathbf{x}}}$ (i.e. VCV matrix of the parameters) is dependent only on \mathbf{A} and \mathbf{VCV} . It can be noticed that once the functional and stochastic models have been specified, one is already in a position to know the precision of the least squares result. It also implies that if one is not satisfied with this precision, it can be changed by changing \mathbf{A} and/or \mathbf{VCV} (Teunissen et al., 1998).

The estimated parameters in Equation 2.68 may include the three baseline components (dx , dy , dz) or baseline vector between the two receivers and the unknown DD ambiguities (one may also consider estimating parameters to model the residual tropospheric delay). Therefore, the estimation process in Equation 2.68 requires a sufficient set of linearly independent DD observations. The number of linearly independent observations (ld) is given by:

$$ld = i(r-1)(k-1) \quad (2.74)$$

where r is number of receivers, and the other values have been previously defined. Assuming reference station A and user station B observe the L1 carrier phase on the same $k = 4$ satellites, at the same epoch $i = 1$; there are $(r-1)(k-1)$ DD ambiguities and 3 additional unknown coordinates of the user station B. In total, there are 6 unknown values to be estimated but only 3 linear independent observations, which obviously lead to an under-determined system. Even if extra DD L1 observations are available at this epoch, or DD L2 carrier phase measurements are included, the system is still under-determined because more unknowns are added; i.e. the specific DD ambiguities that are unique to L1 and L2 frequencies.

Obviously no single epoch solution is available for carrier phase observations in the above case. The possible solution is to track the k satellites at least on two consecutive epochs (provided the DD ambiguities remain constant, i.e., there are no cycle slips). Even so, poor estimation of ambiguity parameters in Equation 2.68 can be expected if the two (or extended to few other epochs) are close together in time due to slow changing of the receiver-satellite geometry. Consequently, this matter is further complicated by the unmodelled systematic errors and noise in the carrier phase observations. Teunissen & Kleusberg (1998) suggest four strategies to overcome the above problem. These four strategies can be combined or used on a stand alone basis. They can be characterised as follows:

Using long observational time spans - the GPS satellites are about 20200km from the Earth's surface and there is little change in receiver-satellite geometry over tens of seconds. Long observational time spans therefore ensure that the receiver-satellite geometry has changed sufficiently. It is only the distribution of the satellites in the sky

and the availability of observations at multi-frequencies that add strength to the geometry in such a case (Leick, 2004). Long observational time spans also provide a better estimate of the (real) ambiguity, not far from its integer value.

Using an antenna swap technique – using this technique, one does not have to wait for the change in the satellite-receiver geometry in the estimation of the ambiguity parameters. This technique works best if the two antennas are located close to each other. Assuming that four or more satellites were observed, the antenna swap technique solves the above problem by moving the stationary antenna A to the initial position of the moving antenna B while, at the same time, moving the mobile antenna from its initial position to the position of the stationary antenna. The antennas remain connected to their respective receivers and a carrier tracking is maintained throughout by both receivers. The result of the above procedure is sufficient to precisely determine the (short) baseline vector of A and B, and the calculation of the ambiguity can be performed in a very short time. Further reading on this technique can be found in Hoffmann-Wellenhof et al. (2001), Leick (2004) and Misra & Enge (2004).

Starting from known baseline – using two sites with known coordinates (i.e. from previous survey), the receivers can be placed at a known baseline vector. As a result, less parameters of interest need to be estimated. Thus, this condition gives an advantage to the estimation of the ambiguity parameters in a very short time.

Using integer ambiguity fixing – this is performed using the optimised algorithms which include the integer estimators. The basic inputs of the technique require the (sets of) estimated real-valued ambiguity and the stochastic properties from the estimate to conduct search for the best likely integer. The idea behind the present technique is therefore to find a way of removing the unknown ambiguities from the system of carrier phase observation equations. This technique is further discussed in the next section.

2.4.3 Ambiguity Resolution

‘Ambiguity resolution’ is the process that takes the estimated ‘float’ (real-valued) ambiguity parameters and converts them to the likeliest integer values. If the process is successful this process will strengthen the carrier phase mathematical model (in the float

solution), as well as transforming the carrier phase observations into high accuracy range measurements. The ambiguity in this case is often called the 'fixed' ambiguity, and parameters estimated from the 'fixed' or 'resolved' ambiguity observations are referred to as the fixed (or ambiguity-fixed) solution.

Successful ambiguity resolution is, however, a challenge. Rizos (1997) suggests several steps in the ambiguity resolution which is discussed as the following (in the context of DD ambiguities):

a) Defining the a priori values of the ambiguity parameters

A process to estimate the DD 'float' ambiguity plus its variance-covariance information. One way is to estimate them from Equation 2.68 by separating the ambiguity component from the baseline components. The real-valued ambiguity term can be denoted as $\hat{\mathbf{x}}_N$ and the corresponding variance-covariance as $\mathbf{VCV}_{\hat{\mathbf{x}}_N}$. From the previous discussion the quality of $\hat{\mathbf{x}}_N$, which is stochastically described in $\mathbf{VCV}_{\hat{\mathbf{x}}_N}$, is very much dependent on the baseline length, the magnitude of the unmodelled systematic errors (residual atmospheric and orbital error), multipath and measurement noise, and the receiver-satellite geometry during the observations.

b) Use a search algorithm to identify the likely integer value (ambiguity candidates)

Say, for n observed satellites from two receivers, the corresponding (float) DD ambiguities need to be resolved is n-1. However, the correct integer ambiguities lies amongst the many possible combinations or candidates of integer ambiguity sets which in total can be calculated as (Landau & Euler, 1992):

$$\text{Total Candidates} = (2W + 1)^{n-1} \quad (2.75)$$

where W is the one-side search window for each ambiguity parameter. In the case of the large variances of the estimated float ambiguities (i.e., far from the integer value), the total candidates should increase and the process to determine the correct ambiguities becomes difficult. For example, should the position come out of the estimation good to 2m the search window has to be at least ± 10 cycles (in L1 cycle). Thus, if six satellites are observed, applying Equation 2.75 leads to $21^5 = 4,084$,

101 different combinations need to be examined. A search procedure needs to be conducted for this purpose. The search may be conducted to give the likely ambiguities directly, or in such a way that is not to obtain the ambiguity value explicitly, or merely define candidate ambiguity sets that must be searched. In addition, the search may be applied to one epoch of data or take into account the data from the whole observation session. Basically, there are three search techniques that can be characterized as the following:

- i) *Search in the measurement domain* – the basis of this search is to combine the carrier phase and pseudorange measurements. It takes advantage of the fact that, the combination allows direct estimation of the float DD ambiguity from each satellite pair at single epoch due to the inclusion of pseudorange measurement. Interestingly, if all observations in Equations 2.57-2.60 are available, they can be combined in certain ways to produce observations that are independent of geometry and the ionosphere effect. As the integer ambiguity does not change (assuming no cycle slips), in principle, the uncertainty in the estimate can be reduced by averaging over a sequence of estimates and rounding-off to the nearest integer (Misra & Enge, 2004). The technique, however, very much depends upon the accuracy of the pseudorange and suffers from pseudorange multipath. In practise, this technique may require long periods of ‘clean data’. Ibid (2004) show that in the case of the short baseline of 150m with relatively clean antenna environment, over tens of seconds were needed to reduce the integer estimation error to one-half cycle and later to approach the right integer ambiguity. Despite these problems this technique appears to be the simplest of the ambiguity search techniques, and is useful on its own, or in combination with another search procedure.

- ii) *Search in the coordinate domain* – the so-called ambiguity function method (AFM) is an example of this class of search technique. The geometric condition of the search procedure in this method is based on cubic search volume in which the estimated coordinates of the user station is placed into the centre of a cube. The method creates a grid point over the search cube, and each grid point represents a candidate for a final solution. All the trial

points are tested, and compared between the largest to second largest 'Ambiguity Function' (AF) value. The correct user position is that which makes the AF value maximum. Ambiguities values are not explicitly obtained as the maximum AF is considered to occur at the lines-of-ambiguities (i.e. the correct ambiguities). This method is computationally intensive if the search volume is large. However, the technique is insensitive to cycle slips since the AF does not depend on the ambiguities. This property defines the uniqueness of this method compared to other solution methods. Further reading and mathematical function of the AF can be found in Leick (2004), Hoffmann-Wellenhof et al. (2001) and Han & Rizos (1996b).

- iii) *Search in the ambiguity domain* – This is a sophisticated procedure that uses the float ambiguities and the corresponding stochastic properties as described in (a) to define the effective mathematical search space (a hyper-ellipsoid, ellipsoid or cube), which is assumed to contain the correct DD integer ambiguity value. The search for the likeliest ambiguity set is performed using the theory of integer least squares estimation, which requires the minimisation of the quadratic form of the residuals (Teunissen, 1994). The performance in this procedure is evaluated by the capability to discriminate a correct ambiguity set from all other candidate sets, a process that can be handled through some validation and rejection criteria and reducing the ambiguity search space for computational efficiency. Several fast ambiguity search algorithms of this class are available (see, e.g., Kim & Langley, 2000), and the most popular is considered to be the Least Square Ambiguity Decorrelation Adjustment (LAMBDA) method (Teunissen, 1994). Jonge & Tiberius (1996) and Jonge et al. (1996) provide a comprehensive mathematical description and computational aspects of the LAMBDA method. A simplified mathematical explanation of the method can also be found in Joosten & Tiberius (2002), Leick (2004) and Misra & Enge (2004).

c) Assurance criteria to the best set of integer values

The search in the ambiguity domain can output one or more integer ambiguity sets, and the set that results in the minimum quadratic form of the integer least squares

residuals will be considered as the ‘best’ or optimal solution. To assure this is the case, a criteria is added to test whether the best integer ambiguity set is statistically better than the second best set (Wang, 1999). This test procedure is often called the ‘validation’, ‘discrimination’ or ‘ratio’ test. Several test statistics have been developed. Verhagen (2004) has studied the theoretical assessment of these statistical tests and noted that further research to improve the test is needed. However, the so-called F-ratio test (Frei & Beutler, 1990) is often used in practice and appears to work satisfactorily. Practical implementation of F-ratio test is described in Landau & Euler (1992).

d) Applying the ‘fixed’ ambiguity to the new solution (‘fixed solution’)

Once the selected set of integer ambiguities (\mathbf{N}) is assured in step (c), they can be removed from Equations 2.59-2.60 by converting the ambiguous ranges to unambiguous ranges (of millimetre precision). If one seeks the determination of the baseline component, a short calculation can be performed by modifying Equation 2.68, and constraining \mathbf{N} :

$$\tilde{\mathbf{x}} = \hat{\mathbf{x}}_C - \mathbf{VCV}_{\hat{\mathbf{x}}_C \hat{\mathbf{x}}_N} \mathbf{VCV}_{\hat{\mathbf{x}}_N} (\hat{\mathbf{x}}_N - \mathbf{N}) \quad (2.76)$$

where $\hat{\mathbf{x}}_C$ are coordinates of the float solution; $\mathbf{VCV}_{\hat{\mathbf{x}}_C \hat{\mathbf{x}}_N}$ is the off-diagonal term in Equation 2.73 that relates the coordinates and the ambiguity terms of the float solution; and the other terms have been previously defined. The solution of $\tilde{\mathbf{x}}$ in Equation 2.76 is now regarded as the ‘fixed solution’.

Following the discussion in this section, a few strategies can be identified to increase the reliability of the ambiguity resolution process:

Short baseline - in order to justify the simplified DD model where the atmospheric delay (and orbital error) is assumed to be eliminated in the data differencing process.

Use of dual-frequency data – useful to form some linear combinations of observables that do not contain the ionospheric effect, have longer wavelength (easier to resolve the ambiguities), and to ‘bootstrap’ a set of DD ambiguities.

Use of precise pseudorange data – use of P-code measurements rather than C/A code measurements, in order to have more precise pseudoranges which assist the ambiguity search.

Use of good a priori information – for example, by introducing the baseline length to reduce the unknowns to the ambiguity terms only. This is very useful for permanent reference station processing where the precise coordinates of the stations have been previously determined.

Improve ambiguity resolution and validation algorithm – to increase the performance of the search in the ambiguity domain and to find better stochastic assurance criteria (i.e. ratio test statistic) of the best ambiguity set with respect to the second best.

LONG-RANGE AMBIGUITY SETUP & ANALYSIS OF DISTANCE-DEPENDENT RESIDUAL ERRORS

3.0 Introduction

Relative positioning by long-range carrier phase measurements is prone to distance-dependent errors. Combined with station-dependent errors such as hardware-related errors, multipath, and measurement noises, distance-dependent errors complicate the ambiguity resolution (AR) for carrier phase ranges and affect the accuracy of other parameters of interest. Due to distance-dependent errors, the inter-receiver distance or “baseline length” must be in the so-called “effective range” so that the errors associated with each receiver can become highly correlated and therefore a differencing technique can efficiently mitigate these errors. One may also consider extending the period of observation sessions, a priori atmospheric modelling, utilising the dual-frequency measurement relationship, implementing the use of more precise satellite orbit information, etc. Although major components of the distance-dependent errors can be modelled, or to a large extent cancelled out by differencing, the residual (or unmodelled) components will remain and cannot be ignored.

There are several questions that arise concerning the residuals of distance-dependent errors. For example, what is their effect to a GPS baseline? What is their magnitude (and variation), and is there a relationship with different baseline length? What is the effective baseline length for differencing (with other modelling techniques) in order to mitigate residual errors? Which category of these errors most severely affects the positioning process, and which is most difficult to reduce? Although the systematic behaviour of these errors can be modelled, dealing with these problems is not easy due to their spatial and temporal variations as pointed out in Chapter 2. Moreover, the GPS

measurements are contaminated by station-dependent errors. With some reasonable assumptions and constraints, however, the above questions can be answered.

This chapter provides the background on the effect of distance-dependent errors on a GPS baseline and the residual analysis of these errors in double-differenced form. Firstly, the theoretical aspects on the effect of distance-dependent errors on a GPS baseline will be addressed. Secondly, a linear combination of phase measurements is discussed to deal with the long-baseline case. Thirdly, a particular setup for long-range AR is derived, followed by a residual analysis of the distance-dependent errors. The residual analysis has been attempted for the data in the equatorial region, the region of the world where the most severe effects of atmospheric delay can be observed.

3.1 Effect of Distance-Dependent Errors on GPS Baseline

The most disturbing influence in long-range positioning has been recognized as the effect of distance-dependent errors: ionospheric delay, tropospheric delay and orbit errors (Beutler et al., 1988; Georgidaou & Kleusberg, 1988). If the baseline is long enough to decorrelate these errors, the differencing process becomes far less efficient. In this case, the (residuals) distance-dependent errors will remain and hence will complicate the positioning process such as the AR. One may also be interested to know the effect of distance-dependent errors on a GPS baseline. Based on a single-differenced observation and geometrical analysis, Beutler et al. (1988) provides an excellent mathematical basis to understand this problem. In this section, their formulation has been tested with various parameters to demonstrate the effect of distance-dependent errors on GPS baselines.

3.1.1 Effect of Ionospheric Delay on a GPS Baseline

The effect of ionospheric delay on the baseline can be derived from the geometry of a single-layer (Figure 2.7) and Equation 2.13. The ionospheric delay induces a scale error to the baseline, which can be written as:

$$\frac{\delta B_{\text{ion}}}{B} = -\frac{1}{R_E \cos z} \frac{40.3}{f^2} \text{VTEC} \quad (3.1)$$

where δB_{ion} is the baseline scale error due to ionospheric delay in parts per million (ppm), B is the baseline length (km), and the rest of terms have been previously defined. The formula indicates that the ionospheric delay is proportional to the baseline length. Based on the realistic TECU values in Figure 2.10, the mean VTEC is more likely in the range of 50 to 60TECU during periods of high solar activity, but can increase further to about 100TECU in the equatorial region. Figure 3.1 shows the simulation results of the formulation in Equation 3.1, assuming the VTEC value to be 50 and 100TECU. The calculations vary with zenith angles on L1, L2 and the future (GPS modernized and Galileo) L5 frequencies. For the L1 frequency, the maximum baseline length is shorter due to the ionospheric delay, by between 7ppm and 3.8ppm at zenith angle of 70° and VTEC value of 100TECU. The effect becomes higher in the case of L2, which clearly indicates that the lower the frequency, the larger the error. The same can be expected for the future L5 frequency.

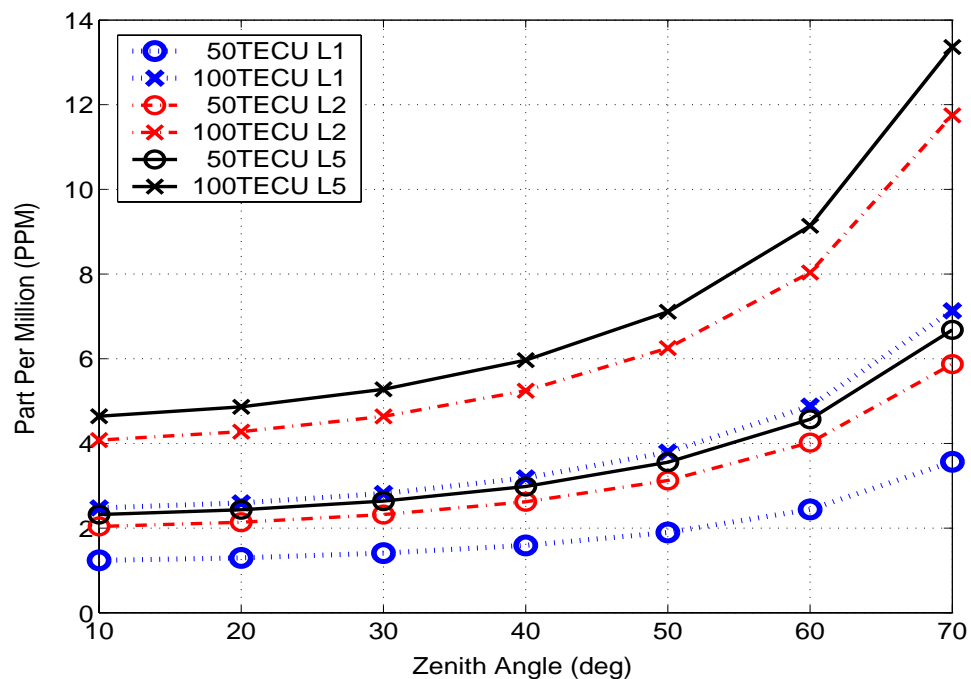


Figure 3.1 Baseline constraints due to the ionospheric delay at different zenith angle and VTEC values (in TECU) on L1, L2 and the future L5 frequency. The highest effect occurs on the future L5 frequency at 70° zenith angle and VTEC of 100TECU. The lowest effect occurs on L1 frequency at 10° zenith angle and VTEC of 50TECU.

3.1.2 Effect of Tropospheric Delay on a GPS Baseline

Consider two receivers located at the same altitude with identical meteorological conditions (temperature, pressure and humidity). The use of an a priori tropospheric model (e.g. from Equation 2.30) should result in an identical correction, and therefore it can be assumed that both receivers have a ‘common’ tropospheric delay (at both ends of the baseline). However, the tropospheric model is a function of the mapping function (e.g. in Equation 2.29) and both receivers view satellites at different zenith angles, that are dependent on the baseline length. The error introduced on the estimated baseline length by neglecting this common tropospheric delay, as a function of zenith angle, is defined as ‘absolute troposphere error’ (Beutler et al., 1988; Rothacher & Mervart, 1996). The effect of absolute troposphere error on the estimated baseline length is given as:

$$\frac{\delta B_{\text{trop}}}{B} = \frac{dtrop_{\text{abs}}}{R_E \cos Z} \quad (3.2)$$

where δB_{trop} is baseline scale error (ppm), $dtrop_{\text{abs}}$ (mm) is the absolute troposphere error, and the rest of the terms have been previously defined.

Now, consider two receivers located nearby to each other (few km) but at different altitudes (e.g. mountainous area vs mean sea level). In this situation the meteorological condition at the two receivers would be much different. In this case, any unmodelled error due to the tropospheric delay at one of the endpoints of a baseline relative to the other endpoint, is defined as ‘relative troposphere error’ (Beutler et al., 1988; Rothacher & Mervart, 1996). The relative troposphere error, therefore, is more prominent to the estimated station height rather than to the estimated baseline length. The effect of the relative troposphere error to the estimated station height, as a function of zenith angle, can be calculated as:

$$dh = \frac{dtrop_{\text{rel}}}{\cos Z} \quad (3.3)$$

where dh is the station height error (cm), $dtrop_{rel}$ is the relative troposphere error (cm), and the other terms have been previously defined.

To simulate both Equations 3.2 and 3.3, the unmodelled tropospheric delay (say, after applying the a priori model) is assumed to be in the range of 1cm to 10cm for zenith angles from 0° to 70° . Applying these values to Equations 3.2 and 3.3 gives the results as shown in Figures 3.2 and 3.3, respectively.

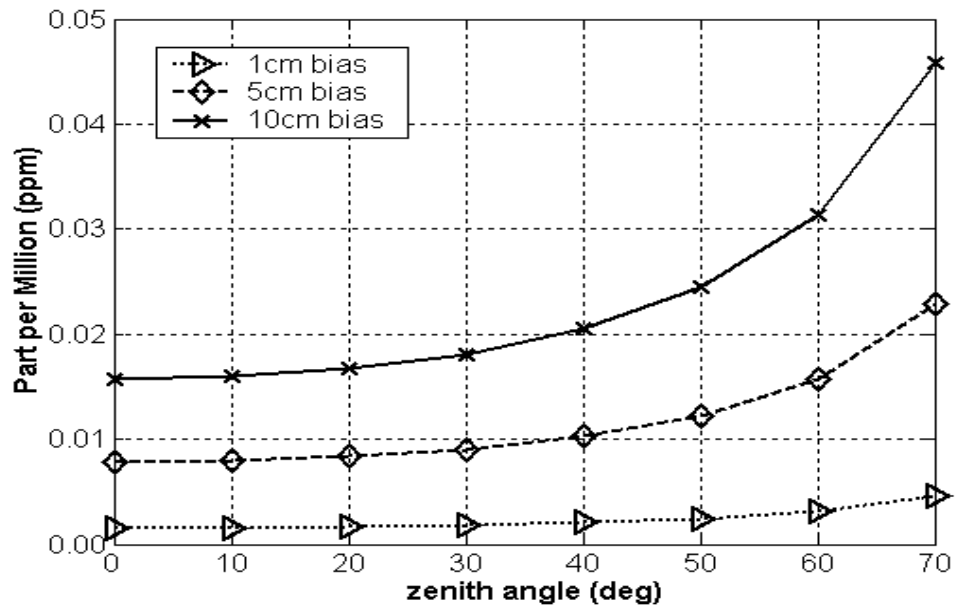


Figure 3.2 Error in baseline length (ppm) due to ‘absolute troposphere error’.

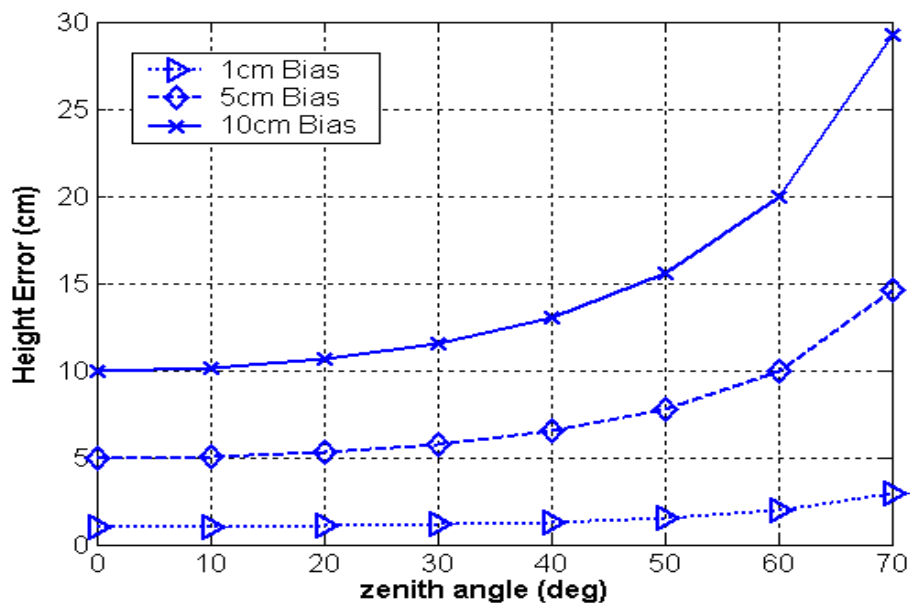


Figure 3.3 Error in station height (cm) due to ‘relative troposphere error’.

A few remarks can be made about the effect of tropospheric delay (absolute and relative):

- a) Absolute troposphere error is distance-dependent; the maximum effect of 10cm error for near horizon signals results in about 0.05ppm scale error for the estimated baseline.
- b) Relative troposphere error is induced by station height differences; the maximum effect for near horizon signals is about three times the error, amplified by the mapping function.
- c) Relative troposphere error is of more serious concern than absolute troposphere error.

3.1.3 Effect of Orbital Error on GPS Baseline

Satellite orbital error as discussed in Chapter 2 is quantified in three orbit components: along-track, cross-track and radial error. The radial component is the principal source of orbital error in the range measurement (Misra & Enge, 2004), and can be approximated as (Beutler, et al, 1988):

$$\delta B_{\text{orbit}} = B \frac{\delta r}{p} \quad (3.4)$$

where δB_{orbit} is the baseline scale error (m) due to orbital error, δr is the orbital radial error (m), p is a geometric range $\sim 20,200\text{km}$, and B is the baseline length (km). The broadcast GPS orbits are much improved nowadays, with the accuracy typically better than 2m in RMS for all orbital components (IGS, 2005). Considering the RMS value is in the range of 1m - 5m and the baseline length ranges from 100km - 500km, the baseline scale error is calculated using Equation 3.4. Figure 3.4 summarises the results which show that the maximum orbital error of 5m produces only a 12.5cm error in the 500km baseline length (i.e., 0.25ppm). Hence, orbital error is not a serious residual bias compared to the effects of the atmosphere.

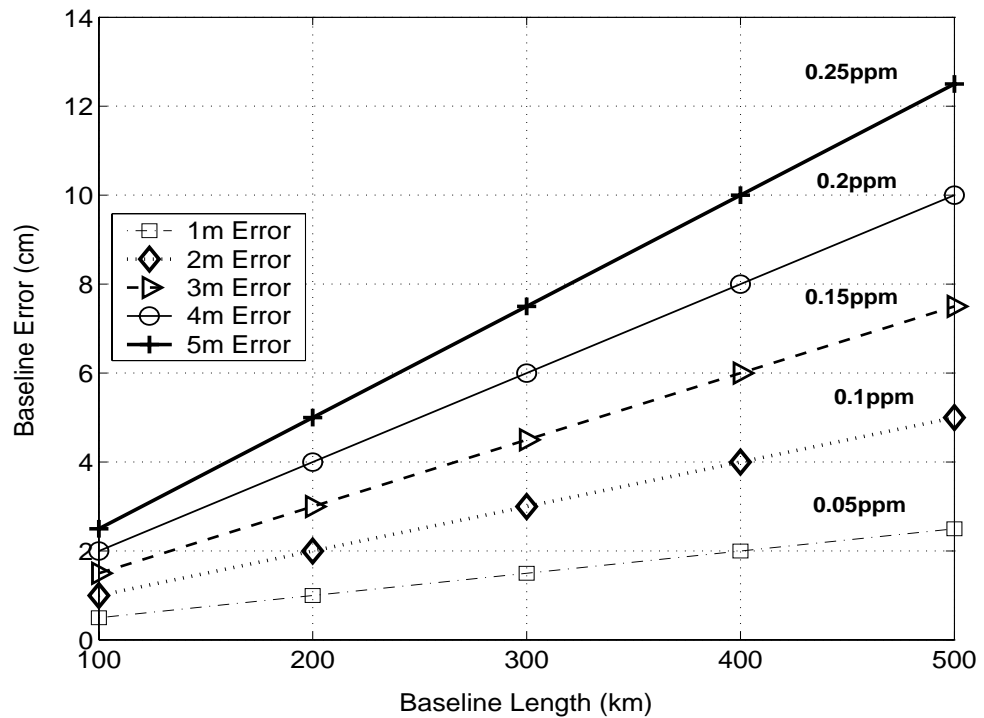


Figure 3.4 Error in baseline length (in centimetres) due to the effect of satellite orbital error (in metres).

3.2 Inter-Frequency Combinations

In the case where dual-frequency GPS data are available, inter-frequency combinations can be constructed from the original carrier phase (or code) observations by forming a linear combination. Advantages of certain linear combinations include assisting the AR, cycle slip detection and repair, multipath studies and smoothing of the code pseudorange. However, the main advantage from linear combinations is to estimate, and subsequently eliminate (at least to the first order), the effect of ionospheric delay.

3.2.1 Phase Linear Combination

A general form of the linear combination can be expressed as (in units of length) (Collins, 1999):

$$LC = \alpha L1 + \beta L2 \quad (3.5)$$

where LC is the carrier phase linear combination (m), α and β are arbitrary numbers. Assume that the original ‘un-differenced’ carrier phase observations in Equations 2.49 and 2.50 contain station-dependent errors that can be neglected (i.e., multipath, hardware delay, measurement noise). Applying Equation 3.5 to these equations leads to:

$$\begin{aligned} LC &= p(\alpha + \beta) + dtrop(\alpha + \beta) + [\alpha\lambda_{L1}N_{L1} + \beta\lambda_{L2}N_{L2}] - [\alpha dion_{L1} + \beta dion_{L2}] \\ &= p(\alpha + \beta) + dtrop(\alpha + \beta) + [\alpha\lambda_{L1}N_{L1} + \beta\lambda_{L2}N_{L2}] - dion_{L1}(\alpha + \frac{f_{L1}^2}{f_{L2}^2}\beta) \\ &= p + dtrop + \lambda_{LC}N_{LC} + dion_{LC} \end{aligned} \quad (3.6)$$

where Equation 2.19 is used to scale the ionospheric delay on L1 frequency. Thus, the following two equations must be satisfied in order to constrain the geometric range in LC and to preserve the integer ambiguity value.

$$\alpha + \beta = 1 \quad (3.7)$$

$$\alpha = i \frac{\lambda_{LC}}{\lambda_{L1}}, \quad \beta = j \frac{\lambda_{LC}}{\lambda_{L2}} \quad (3.8)$$

where i and j are integer numbers and λ_{LC} is the wavelength of the LC (see Equation 3.11). Interestingly, α and β converts L1 and L2 into cycles before combining them i.e., by applying Equation 3.8 to Equation 3.5. The linear combination in cycle units is given by:

$$\frac{LC}{\lambda_{LC}} = \varphi_{LC} = i\varphi_{L1} + j\varphi_{L2} \quad (3.9)$$

where φ_{LC} is the phase linear combination in units of cycles. Equation 3.9 has the following properties (Xu, 2003; Hoffmann-Wellenhof et al., 2001; Rizos, 1997; Abidin, 1993):

The cycle ambiguity:

$$N_{LC} = N_{i,j} = iN_{L1} + jN_{L2} \quad (3.10)$$

The effective wavelength:

$$\lambda_{LC} = \lambda_{i,j} = \frac{\lambda_{L1}\lambda_{L2}}{i\lambda_{L2} + j\lambda_{L1}} \quad (3.11)$$

The ionospheric delay of LC ($dion_{LC}$) relative to $dion_{L1}$:

$$dion_{LC} = (isf)dion_{L1} \quad (3.12)$$

where, $isf = \frac{\lambda_{L1}}{\lambda_{L2}} \frac{(i\lambda_{L1} + j\lambda_{L2})}{(i\lambda_{L2} + j\lambda_{L1})}$

The noise of LC (σ_{LC}) relative to L1 (assuming equal noise to L1 and L2):

$$\sigma_{LC} = (nsf)\sigma_{L1} \quad (3.13)$$

where, $nsf = \frac{\lambda_{L2}(i^2 + j^2)^{\frac{1}{2}}}{i\lambda_{L2} + j\lambda_{L1}}$

Various inter-frequency combinations can be formed via Equation 3.5 or 3.9, but some useful combinations for this study are listed in Table 3.1. Calculations to extract the value of i and j (and the value of α and β) in Table 3.1 can be found in Collins (1999). The linear combination is also applied to data differencing. Next, the linear combinations used to approximate the atmospheric delay and orbital error are discussed in the context of double-differencing (DD).

Table 3.1 Linear combinations of carrier phase.

Phase Combination	i	j	α	β	λ_{LC} (m)	Ambiguity	isf	nsf
First Carrier(L1)	1	0	1	0	0.190	N_{L1}	1.00	1.00
Second Carrier (L2)	0	1	0	1	0.244	N_{L2}	1.65	1.28
Wide-Lane(WL)	1	-1	4.529	-3.529	0.862	$N_i - N_j$	-1.28	6.41
Narrow-Lane (NL)	1	1	0.562	0.438	0.107	$N_i + N_j$	1.28	0.80
Ionosphere-Free (IF)	77	-60	2.546	-1.546	0.006	$77N_i - 60N_j$	0.00	3.23
Geometry-Free (GF)	-	-	1	-1	-	$\lambda_{L1}N_{L1} - \lambda_{L2}N_{L2}$	-0.65	1.63

3.2.2 Geometry-Free to Approximate Ionospheric Delay

Consider the value of $\alpha = 1$ and $\beta = -1$. Inserting these values into Equations 3.5-3.6 gives:

$$\begin{aligned}\Delta\nabla L_{GF} &= \Delta\nabla L1 - \Delta\nabla L2 \\ &= \lambda_{L1}\Delta\nabla N_{L1} - \lambda_{L2}\Delta\nabla N_{L2} + \Delta\nabla\text{dion}_{L1} - \Delta\nabla\text{dion}_{L2}\end{aligned}\quad (3.14)$$

In contrast to Equation 3.7, the value of $\alpha+\beta = 0$ and it follows that there are no constraints on the geometric range in Equation 3.14. Therefore, Equation 3.14 is also known as the ‘DD Geometry-Free’ (GF) combination. Using the ionospheric delay relationship of Equation 2.19, the above equation can be rewritten as:

$$\begin{aligned}\Delta\nabla L1 - \Delta\nabla L2 &= \lambda_{L1}\Delta\nabla N_{L1} - \lambda_{L2}\Delta\nabla N_{L2} + \Delta\nabla\text{dion}_{L1} \\ &\quad - \frac{f_{L1}}{f_{L2}}\Delta\nabla\text{dion}_{L1}\end{aligned}\quad (3.15)$$

Rearranging Equation 3.15 and applying the value for the L1 and L2 frequencies:

$$\Delta\nabla\text{dion}_{L1} = 1.5457(\Delta\nabla L1 - \Delta\nabla L2 + \lambda_{L2}\Delta\nabla N_{L2} - \lambda_{L1}\Delta\nabla N_{L1})\quad (3.16)$$

Therefore, if $\Delta\nabla N_{L1}$ and $\Delta\nabla N_{L2}$ can be resolved to their integer values, Equation 3.16 is a good approximation for the DD ionospheric delay on L1 (the same can be derived for DD L2).

3.2.3 Ionosphere-Free to Approximate Tropospheric Delay & Orbital Error

Consider Equation 3.9 (in DD form) and expressing the DD ionospheric delay on L1 frequency, which can be written as (in cycles):

$$i\Delta\nabla\phi_{L1} + j\Delta\nabla\phi_{L2} = \left[\frac{i}{\lambda_{L1}} + \frac{j}{\lambda_{L2}} \right] (\Delta\nabla p + \Delta\nabla dtrop) + [i\Delta\nabla N_{L1} + j\Delta\nabla N_{L2}] - \Delta\nabla dion_{L1} \left[\frac{i}{\lambda_{L1}} + \frac{f_{L1}^2}{f_{L2}^2} \frac{j}{\lambda_{L2}} \right] \quad (3.17)$$

In order to eliminate the last term on the right hand side of Equation 3.17 and at the same time preserving the integer ambiguity, the value of i and j can be chosen as 77 and -60 respectively (Table 3.1). Applying these values to the above equation leads to (in cycles):

$$\Delta\nabla\phi_{77,-60} = \lambda_{77,60}\Delta\nabla p + \lambda_{77,60}\Delta\nabla O + \lambda_{77,60}\Delta\nabla dtrop + \Delta\nabla N_{77,-60} \quad (3.18)$$

or (in units of length):

$$\Delta\nabla L_{77,-60} = \Delta\nabla p + \Delta\nabla O + \Delta\nabla dtrop + \lambda_{77,60}\Delta\nabla N_{77,-60} \quad (3.19)$$

where Equation 3.19 (or 3.18) is known as the ‘DD Ionosphere-Free’ (IF) combination, $\lambda_{77,-60}$ is the wavelength of IF, and $\Delta\nabla N_{77,-60}$ is the DD IF ambiguity. Note that the DD orbital error ($\Delta\nabla O$) is introduced for the first time, as extracted from the geometric range $\Delta\nabla p$. As discussed in Chapter 2, the IF combination eliminates the first order effect of ionospheric delay and the effect of the higher order ionospheric delay is further reduced (see Table 2.3).

If it can be assumed that the precise orbit (‘true orbit’) is used, the orbital error can be removed from Equation 3.19 (or 3.18) and the equation rearranged so that:

$$\Delta\nabla dtrop = \Delta\nabla L_{77,-60} - (\Delta\nabla p + \lambda_{77,60}\Delta\nabla N_{77,-60}) \quad (3.20)$$

which represents the DD tropospheric delay or (in zenith direction) relative tropospheric zenith delay (RTZD) (Brunner & Tregoning; 1994; Zhang & Lachapelle, 2001). This is of course not entirely true because Equation 3.20 is contaminated by station-dependent errors. Even though these station-dependent errors can be reduced (see Section 3.4), in practice it is almost impossible to resolve $\Delta\nabla N_{77,-60}$ directly using Equation 3.19 (or

3.18) due to the very short IF wavelength of 6mm (see Table 3.1)! This problem will be addressed in the next section.

Orbital error, according to the definition in Section 2.1.5, can be quantified by taking the difference of Equation 3.19 (or 3.18); one is derived from broadcast (or other orbit sources), and the other is derived from the IGS precise orbit (considered here the ‘true orbit’). Thus:

$$\Delta\nabla O_{\text{broadcast}} = \Delta\nabla_{L77,-60(\text{broadcast})} - \Delta\nabla_{L77,-60(\text{precise orbit})} \quad (3.21)$$

is a good approximation of the error due to imperfect orbit modelling in the broadcast orbit. Note that the above equation does not require the determination of the ambiguity value as it has been cancelled out.

3.3 Setup for Long-range AR

In order to use Equations 3.16 and 3.20 (next section), the DD ambiguities (i.e. $\Delta\nabla N_{L1}$, $\Delta\nabla N_{L2}$ and $\Delta\nabla N_{77,-60}$) need to be resolved to their integer values. As pointed out in Chapter 2, the process of AR requires a good estimate of the ‘float ambiguity’. For a long-baseline, the idea is to use the knowledge of the inter-frequency combinations, especially where the ionospheric delay can largely be eliminated. As in the previous discussion, station-dependent errors are ignored to simplify the discussion.

3.3.1 Ambiguity Estimation via IF Combination

The DD IF ambiguity as it appears in Equations 3.19-3.20 can be written as (see Table 3.1):

$$\Delta\nabla N_{77,-60} = 77 \Delta\nabla N_{L1} - 60 \Delta\nabla N_{L2} \quad (3.22)$$

Although $\Delta\nabla N_{77,-60}$ is an integer, direct AR using Equation 3.19 (or Equation 3.18) is almost impossible due to the very short wavelength (as previously mentioned). An

indirect technique can be used to fix the ambiguities $\Delta\nabla N_{L1}$, $\Delta\nabla N_{L2}$ and $\Delta\nabla N_{77,-60}$ in this case. Consider the widelane ambiguity (N_{WL}) in Table 3.1, and expressing it in DD form:

$$\Delta\nabla N_{WL} = \Delta\nabla N_{L1} - \Delta\nabla N_{L2} \quad (3.23)$$

Rearranging and applying Equation 3.23 to Equation 3.22 produces another expression for $\Delta\nabla N_{77,-60}$:

$$\begin{aligned} \Delta\nabla N_{77,-60} &= 77 \Delta\nabla N_{L1} - 60(\Delta\nabla N_{L1} - \Delta\nabla N_{WL}) \\ &= 77\Delta\nabla N_{L1} - 60\Delta\nabla N_{L1} + 60(\Delta\nabla N_{L1} - \Delta\nabla N_{L2}) \\ &= 17\Delta\nabla N_{L1} + 60\Delta\nabla N_{WL} \end{aligned} \quad (3.24)$$

Applying Equation 3.24 to Equation 3.19 produces:

$$\begin{aligned} \Delta\nabla L_{77,-60} &= \Delta\nabla p + \Delta\nabla O + \Delta\nabla dtrop + 17\lambda_{77,60}\Delta\nabla N_{L1} \\ &\quad + 60\lambda_{77,60}\Delta\nabla N_{WL} \end{aligned} \quad (3.25)$$

If $\Delta\nabla N_{WL}$ can be resolved to its integer value, Equation 3.25 can be used to estimate the float $\Delta\nabla N_{L1}$ value (and the float-ambiguity generated position) under an IF ‘environment’. This can be followed by a search technique in the ambiguity domain such as the LAMBDA method (Teunissen, 1994) to resolve $\Delta\nabla N_{L1}$. However, the wavelength of $\Delta\nabla N_{L1}$ in this case is only 0.107m (see Table 3.1, narrowlane). Obviously, other related errors in Equation 3.25 need to be minimised, for example, by using the IGS orbit information and the application of an a priori tropospheric model. Because the a priori tropospheric model does not represent the wet delay well (see Chapter 2), the remaining residuals will affect the estimation process in Equation 3.25. Residual tropospheric delay can be compensated for by introducing troposphere scale factors into the parameter estimation process (Rothacher & Mervart, 1996; Dodson et al., 1996), as will be discussed further in Chapter 4.

Thus, if $\Delta\nabla N_{L1}$ can be resolved to its integer values, $\Delta\nabla N_{L2}$ can be derived from Equation 3.23 using the previously determined $\Delta\nabla N_{WL}$. Therefore, the integer

ambiguity for IF can be resolved from Equation 3.22. Next, the widelane ambiguity estimation is explained.

3.3.2 Widelane Ambiguity Estimation

Typical Approach

The DD widelane carrier phase combination can be derived from Equation 3.17 by inserting the corresponding values $i = 1$ and $j = -1$ (in cycles):

$$\Delta\nabla\varphi_{WL} = \Delta\nabla\varphi_{L1} - \Delta\nabla\varphi_{L2} = \left[\frac{1}{\lambda_{L1}} - \frac{1}{\lambda_{L2}} \right] (\Delta\nabla p + \Delta\nabla O + \Delta\nabla dtrop) + [\Delta\nabla N_{L1} - \Delta\nabla N_{L2}] - \Delta\nabla dion_{L1} \left[\frac{1}{\lambda_{L1}} - \frac{f_{L1}^2}{f_{L2}^2} \frac{1}{\lambda_{L2}} \right] \quad (3.26)$$

Note that $\Delta\nabla O$ is added to the above equation. Multiplying Equation 3.26 by the corresponding widelane wavelength λ_{WL} gives (in metric units),

$$\Delta\nabla L_{WL} = \Delta\nabla p + \Delta\nabla dO + \Delta\nabla dtrop + \lambda_{WL} \Delta\nabla N_{WL} + \frac{77}{60} \Delta\nabla dion_{L1} \quad (3.27)$$

This combination produces a longer wavelength of 0.862m (see Table 3.1) that gives significant advantage to the AR. Thus, if the ionospheric delay is about 1 cycle of L1, the effect on the widelane is only 0.3636 cycle (less than half of the widelane cycle). Benefits can be found if an a priori ionospheric model is applied (e.g. the Klobuchar model, or a global ionosphere model from the IGS). The functional model and statistical properties of Equation 3.27 are used in the parameter estimation (see Section 2.4.2) to obtain the float DD widelane ambiguity and the corresponding user's position (generally known as a 'float solution'). A search algorithm can be employed to resolve the integer ambiguities in the case of an extended observation session. The coordinates of the fixed solution are not suitable for high precision positioning due to the high noise in the widelane combination (see Table 3.1). However, it can be used to derive approximate coordinates.

Code Narrowlane Approach

The typical approach described in the previous section took advantage of its long wavelength in order to resolve the widelane ambiguity. However, the widelane combination in Equation 3.27 is still contaminated by the ionospheric delay. If precise P_{L1} and P_{L2} are available, a code narrowlane combination can be formed in the same way as for the phase combination using Equation 3.5. According to the value of $\alpha = 0.562$ and $\beta = 0.438$ (see Table 3.1), the DD code narrowlane ($\Delta\nabla P_{NL}$), in metres, can be written as:

$$\begin{aligned} \Delta\nabla P_{NL} &= 0.562 \Delta\nabla P_{L1} + 0.438 \Delta\nabla P_{L2} \\ &= \frac{f_1}{f_1 + f_2} \Delta\nabla P_{L1} + \frac{f_2}{f_1 + f_2} \Delta\nabla P_{L2} \\ &= \Delta\nabla p + \Delta\nabla dO + \Delta\nabla dtrop + \frac{77}{60} \Delta\nabla dion_{L1} \end{aligned} \quad (3.28)$$

Taking the difference of Equations 3.27 and 3.28 yields:

$$\Delta\nabla N_{WL} = \frac{\Delta\nabla L_{WL} - \Delta\nabla P_{NL}}{\lambda_{WL}} \quad (3.29)$$

Equation 3.29 indicates that this combination is both GF and IF, and therefore independent of the baseline length. Moreover, it directly provides an estimate of the float widelane ambiguity at each epoch for each satellite. Typically, the code multipath reduces the quality of the estimated ambiguity because of its long wavelength (~30m). Thus, since the beginning of an operation or when a new satellite signal is acquired, a sequential approach can be implemented to smooth the code pseudoranges (see, e.g. Hoffmann-Wellenhof et al., 2001), which may improve the estimate of the float ambiguities. A simple least squares filter (that is, the arithmetic mean of the float ambiguities) can be used in the analysis (see Allison, 1991). After accumulation of some epochs (i.e., without signal interruption), and providing that the mean of the station-dependent errors is zero, the ambiguities will converge to their integer values. If and only if the sum squared of residuals has magnitudes <0.5 widelane, then the ambiguities can be set to integers simply by rounding-off to the nearest integer values. If necessary this can be augmented by an integer search procedure.

Figure 3.5 gives the overview of the setup for the long-range AR as discussed here and in the previous sub-sections.

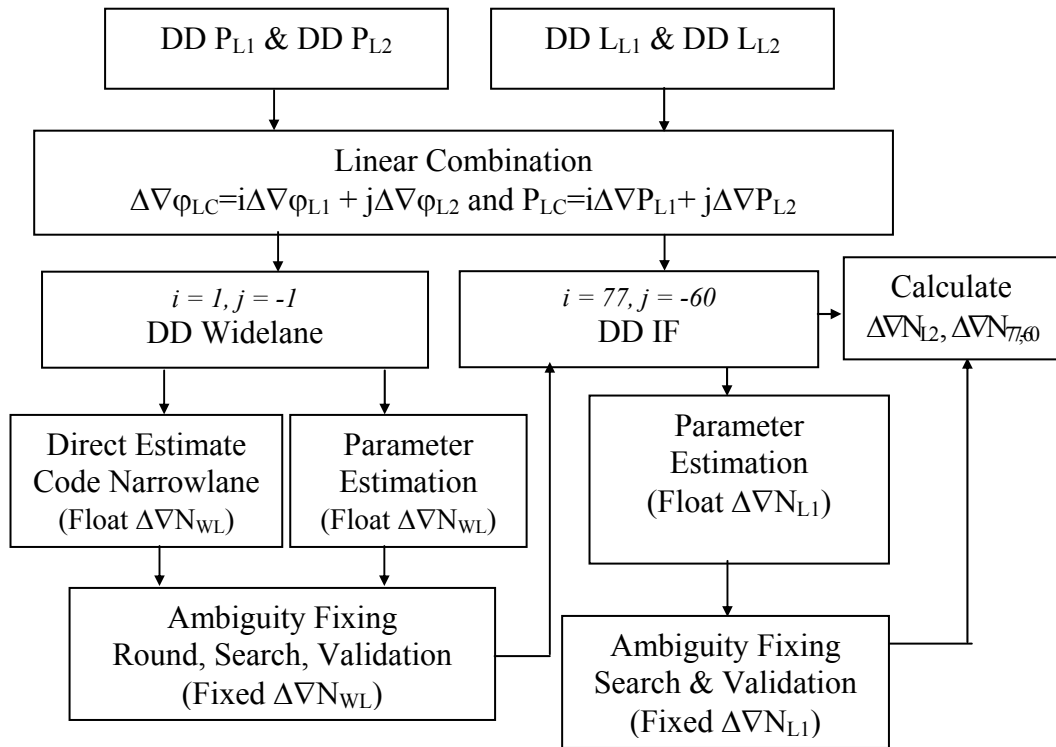


Figure 3.5 Overview of the setup for long-range AR.

3.3.3 Consideration into Quasi IF Algorithm

The setup for long-range AR in Figure 3.5 has been implemented in Chapter 5. In the early analysis of the distance-dependent errors (the current chapter and in the next chapter), the BERNESE software has been used to undertake the huge data analysis task. One of the techniques for long-range (up to thousands of kilometres) AR used in this software is the so-called ‘Quasi Ionosphere Free’ (QIF) technique. The QIF technique processes dual-frequency carrier phase observations and tries to resolve L1 and L2 ambiguities in the same run, as opposed to the technique described in sub-sections 3.3.1 and 3.3.2.

The basis of the QIF algorithm can be explained as follows:

- a) The starting point of QIF is to estimate the float ambiguities of DD L1 and DD L2 during the initial parameter estimation.

- b) These float values are introduced as errors into the DD IF (Equation 3.19), and according to Equation 3.25 the errors can be expressed in the form of narrowlane cycles.
- c) The relationship between DD widelane, DD L1 and DD L2 ambiguities (Equation 3.23) is used to conduct searches for the likeliest integer values for the DD L1 and DD L2.
- d) For each pair of error integers DD L1 and DD L2 from (c), a test is conducted by taking the difference between the error integer and the float (real-valued) ambiguity value.
- e) The smallest value from the test in (d) is then accepted as the correct integer value.

Further details of the QIF can be found in Rothacher & Mervart (1996) and Mervart (1995).

3.4 Residuals Analysis of DD Distance-Dependent Errors

Any errors that remain after the DD process (after applying the a priori models) generally can be addressed as ‘residual errors’. The unmodelled station- and distance-dependent errors reflect these residuals. However, station-dependent errors would be at a minimum level if the positioning environment is reasonably good, e.g. geodetic quality receivers are used, antennas are robust against multipath, and an open sky view is guaranteed. Applying such constraints, together with accurate receiver coordinates, the DD residuals can be assumed to be dominated by the distance-dependent errors.

3.4.1 Test Area

Justification

The test area is in South-East Asia: Malaysia and Singapore. Located within the region of the world’s highest ionospheric activity (see Figure 2.11), severe effects of ionospheric delay on positioning results can be expected in this equatorial region. Moreover, one must also expect strong tropospheric delay within this area as the climate in these countries is defined as ‘tropical rainforest’ with high temperature, high

humidity and abundant rainfall all year round. Detailed descriptions of the local climate in this area are given in Chapter 4. Clearly, this is a challenging area for GPS positioning, but very important to the Earth atmospheric studies.

Related Research

Research on the effect of distance-dependent errors and GPS meteorology in this area has been infrequent until the year 2000. The absence of basic infrastructure such as a continuously operating GPS network is the main reason. With the establishment of continuously operating reference station (CORS) networks such as the Malaysian Active Surveying Stations (MASS) and the Singapore Integrated Multiple Reference Stations (SIMRSN), research on atmospheric effects in this area is expanding. Many papers deal with the use of GPS for monitoring TEC values (see, e.g., Ho et al., 2002; Wan Salwa et al., 2002; Zain et al., 2002). All these studies indicate a strong behaviour of the ionosphere in this area. Janssen (2003) studied the area during the maximum solar year using GPS on baselines ranging in length from 20km to 63km. He used the GPS network-based approach with mixed-mode (single- and dual-frequency) receivers for positioning purposes. He found the results are rather disappointing because his network technique could not appropriately model the strong ionospheric spatial and temporal variabilities within this region.

However, to the best of the author's knowledge, there are no other research reports dealing with the tropospheric problems for GPS positioning in this area. Due to the climatic conditions in the Malaysia-Singapore area, the tropospheric effect on GPS positioning cannot be neglected. Roberts (2002), in his case study of a low-cost volcano monitoring system in Indonesia, where the tropical rainforest climate is also present, studied the tropospheric effect. He used low-cost single-frequency receivers over short baselines (<10km) and experienced positioning problems due to the ionospheric effect. He also pointed out that the tropospheric effect is another serious problem because of the climatic conditions and the mountainous topography of the area.

Data Description

In this chapter, the residuals analysis of distance-dependent errors is performed using the data recorded by four CORS stations: three of them belong to MASS (SEGA, UTMJ and BEHR), and the fourth station is an IGS station (NTUS). The locations of SEGA,

UTMJ, BEHR and NTUS are shown in Figure 3.6. All MASS stations are tied to the International Reference Frame (ITRF) at epoch 2000 (Abdul et al., 2000). Surface meteorological measurements for these stations were not available at the time when the data was collected for this study. Each station is equipped with a dual-frequency receiver and a choke-ring antenna, and their locations chosen so that the effect of multipath is minimal. Other site information such as coordinate of station, type of antenna, etc; can be obtained from the MASS website <http://www.geodesi.jupem.gov.my/mass/mass.htm> and the IGS website <http://igs.cb.jpl.nasa.gov/network/site/ntus.html>. The test data is selected (randomly) for day of year (DoY) 208/03. In fact, this day is in the high solar radiation period (Figure 2.10). The data covers 24 hours, with 30 second measurement interval, from 0:00UT to 24:00UT or 8:00am (27/7/03) to 8:00am (28/7/03) local time, and at least 6 satellites were observed at each epoch. Twenty four hours of the data should be sufficient for the purpose of this test. The baselines are classified as ‘short’ (25km), ‘medium’ (143km) and ‘long’ (339km), and station UTMJ is selected as the base station.

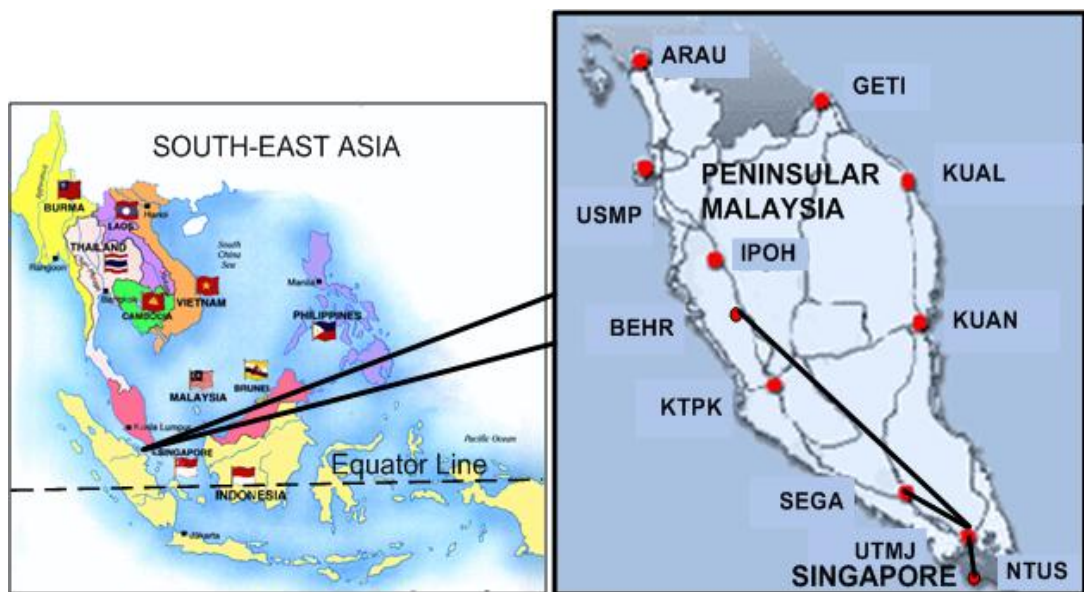


Figure 3.6 MASS station distribution and IGS station (NTUS) in Singapore.

Table 3.2 Stations coordinates (wrt ITRF2000) and baseline length.

Stn UTMJ to:	Latitude	Longitude	Ellipsoidal Hgt. (m)	Baseline Length (km)
BEHR	3° 45' 55"	101° 31' 01"	68.690	339
SEGA	2° 29' 11"	102° 43' 55"	25.232	143
NTUS	1° 20' 45"	103° 40' 48"	75.423	25
UTMJ	1° 33' 57"	103° 38' 22"	80.421	0

Processing Techniques

As the baseline lengths in this test are up to 339km, AR is not an easy task even with static receivers and precise site coordinates. Further modelling, estimation and elimination of the related distance- and station-dependent errors may ensure the success of AR. The BERNESE software is employed as it is capable of geodetic-quality GPS data processing. The software includes the options for modelling the the satellite radiation pressure, the troposphere (or estimating a scale factor), the ionosphere (QIF), the satellite orbit (or estimating the parameters) the receiver/satellite antenna phase centre variations; sophisticated cycle slip screening, and so on (see Rothacher & Mervart, 1996). Moreover, the technique used here utilises the precise orbit downloaded from the IGS, an a priori troposphere model (Saastamoinen model) is applied and the tropospheric delay residuals are estimated by introducing the estimated troposphere scale factor parameters (1 parameter every 6 hours). All the data were masked at the 15° cut-off elevation angle and the known coordinates (Table 3.2) were used as a priori values. The QIF technique (Section 3.3.3) was used for AR. The resolved (DD) L1 and L2 ambiguities were stored for the next processing steps, which included:

i) Extraction of Residuals DD Ionospheric Delay (on L1)

This step utilises the DD GF linear combination by introducing the fixed ambiguities of L1 and L2. The residuals of the DD GF represent the ionospheric delay, which can be further scaled to L1 (or L2) frequencies (Equation 3.16). Knowing these delays on L1, the effect on the other linear combinations can be derived through the ionosphere scale factor in Table 3.1.

ii) Extraction of Residuals of Raw DD Tropospheric Delay

This step makes use of the DD IF linear combination by introducing the fixed ambiguities of L1 and L2. The raw observation data, however, are processed without applying the a priori tropospheric model. The residuals from this step are a good approximate of the residuals of the raw DD tropospheric delay (see Equation 3.20).

iii) Extraction of Residuals DD Tropospheric Delay (a priori model applied)

This step is identical to step (ii). However, the a priori troposphere model is applied to the raw data. Here the (total) Saastamoinen model is applied and a

standard meteorological model is utilised (see Section 2.2.3 – Tropospheric Delay Effect and Current Modelling Trends). Thus, any residuals from this run can be referred as the DD tropospheric delay residuals (sub-section 3.2.3).

iv) Extraction of Residuals DD Orbit Errors

This step requires two step processing: first the processing of the DD IF linear combination makes use of the precise orbit (the ‘true orbit’), and the second processing utilises the broadcast orbit. According to Equation 3.21, the difference of the DD IF residuals from these two runs will indicate the effects of DD orbit errors (i.e. broadcast minus precise orbit). Because it is planned to use the ultra-rapid IGS orbits in future work, tests were also performed to analyse the residuals of the ultra-rapid minus precise orbits.

3.4.2 Results and Discussion

a) Residuals of DD Ionospheric Delay

Figure 3.7 show that the DD ionospheric delay residuals as being quite large between midnight to 4 hours after midnight. This confirms the discussion in the previous chapter (see sub-section 2.2.2, the variability of TEC) that TEC is very active during the nighttime in the Equatorial area. It can be noticed that large residuals also occurred after 14:00 hour local time. This suggests that the behaviour of the Equatorial ionosphere is hard to predict. As expected, the plots show the long and medium baselines suffer more (larger ionospheric delay residuals) than the short baseline. Obviously the residuals are distance-dependent.

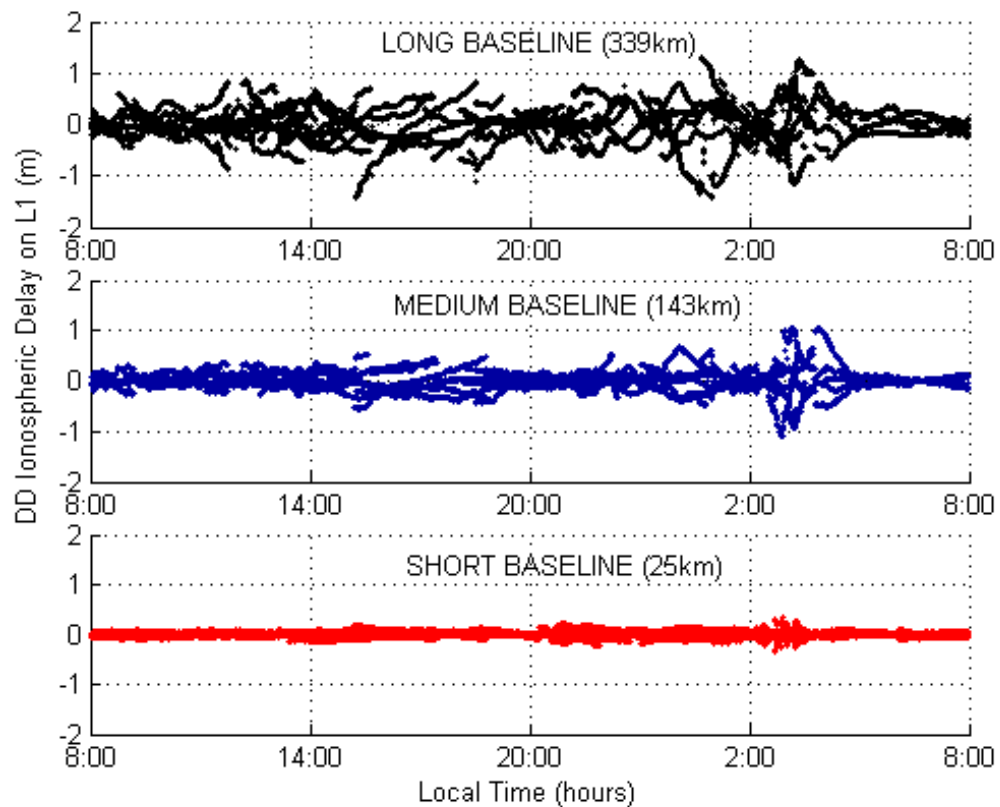


Figure 3.7 All satellites combination; DD ionospheric delay residuals (scale on L1) for 24hour period for long (top), medium (middle) and short (bottom) baselines.

Inspecting Figure 3.8 and the corresponding statistical Table 3.3, it can be seen that the residuals reach over $\pm 130\text{cm}$ for the long baseline, $\pm 100\text{cm}$ for the medium baseline, and $\pm 30\text{cm}$ for the short baseline. This is equivalent to 6.3cycles, 5.3cycles and 1.6cycles of L1; 8.8cycles, 6.7cycles and 2.0 cycles of L2; 2.5cycles, 2cycles and 0.57cycles of widelane; for the long, medium and short baselines respectively (using the isf in Table 3.1). This situation prevents direct AR using L1, L2, or even the widelane combination. The IF combination and long observation sessions are the reason for successful AR during this time period. In the case of the short baseline, the probabilities are higher compared to the others. However, Table 3.3 indicates that the variations can reach up to 6cm. These conditions, plus other effects such as tropospheric delay, orbital and station-dependent errors, easily complicate the direct AR process using L1 or L2 measurements alone. Practically speaking, fast and (near) real-time AR is not possible for these baselines, and is prone to failure even for the case of a short baseline.

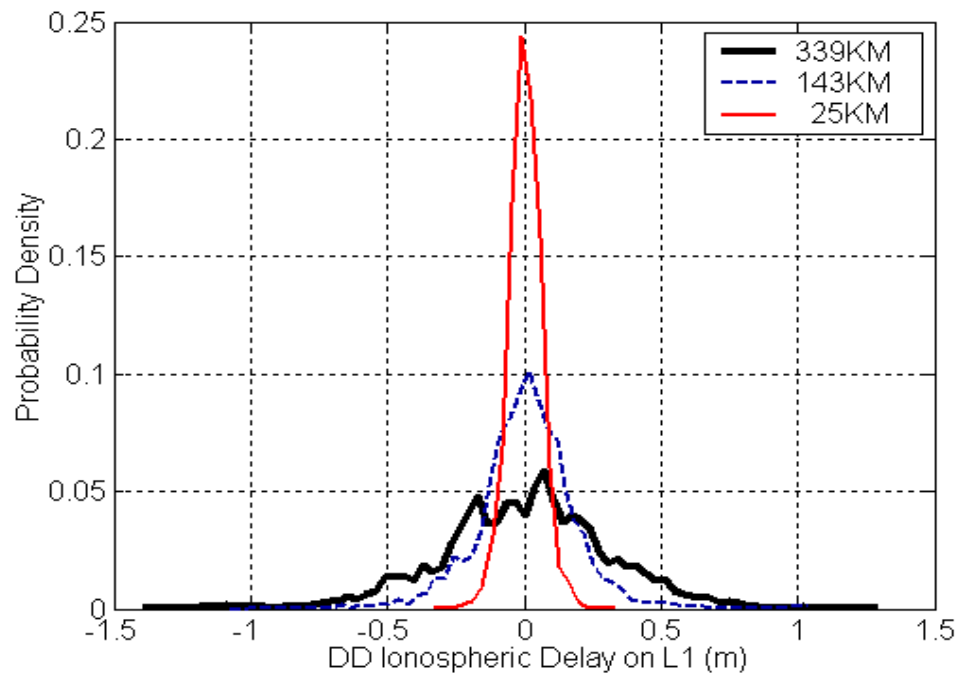


Figure 3.8 Statistical plots of DD ionospheric delay residuals related to Figure 3.7.

Table 3.3 Statistical analyses of DD ionospheric delay residuals related to Figure 3.7.

Baseline	Statistical (DD Ionospheric Delay on L1) (cm)			
	Min	Max	Mean	Stdv
Long	-141.83	131.21	0.06	32.98
Medium	-109.16	105.47	1.07	19.10
Short	-34.30	35.12	0.07	5.95

Although there are residuals smaller than 1cycle (L1), the probability is small and generally is only possible for a few satellite pairs at high elevation angles. Figure 3.9 are subsets of Figure 3.7 for the period 4:00am to 7:00am, are randomly selected for satellites (PRN number) 7 and 10. The figure clearly shows the magnitude of the residual delay is stronger at low elevation angles. The figure also indicates the ionospheric delay residual is difficult to predict; the variation of the medium baseline is slightly higher than the long baseline during the first 1.5 hour period. However, for the 24 hour data analyses, the variation is much higher in the long baseline case, as seen in Table 3.3.

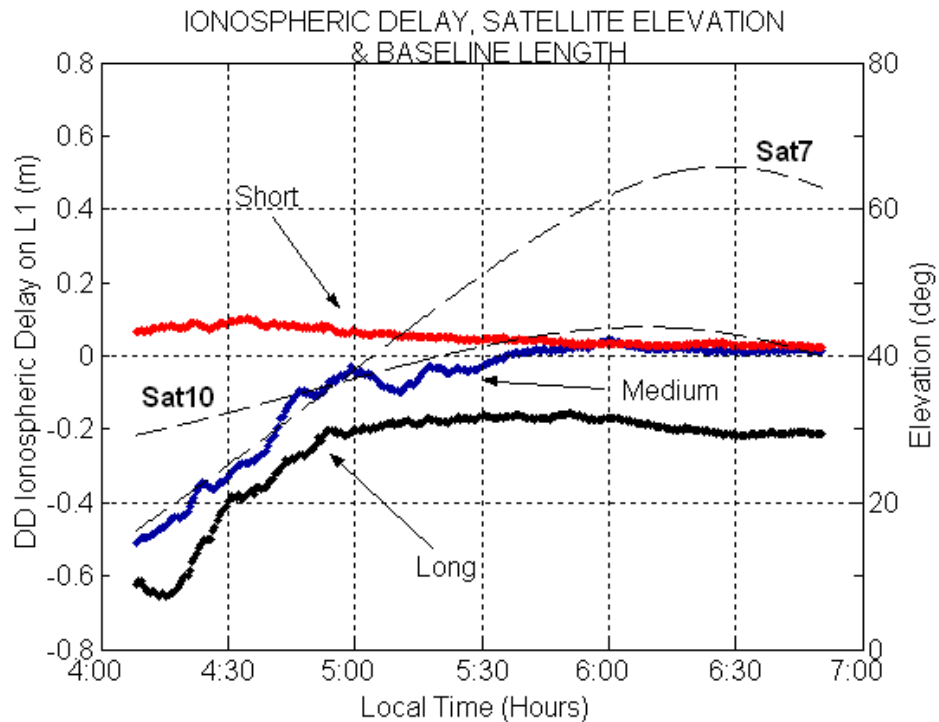


Figure 3.9 Relation of ionospheric delay residuals (scale on L1) and satellite elevation angle for short (red), medium (blue) and long (black) baseline. The satellite pair is 7-10 as viewed from station UTMJ for about 3 hours (4am to 7am) on DoY 208/03.

If a single-frequency receiver is used in this area, the residual analysis suggests that one can only deal with a ‘very short’ baseline (much less than 25km) and an extended span of observations. The use of IGS or broadcast ionosphere models could compensate the effect of the ionosphere. However, these global models have less station coverage in this area and several studies suggest that the model only improves around 50% (of the total effect) (MacDonald, 2002). Nevertheless, the finding in this study supports the work of Wanninger (1993) who experienced difficulties in fixing ambiguities for a 10km baseline in the Equatorial area during the solar maximum year. Similarly frustrating results were reported by Janssen (2003) and Roberts (2002), who used a network of mixed-mode receivers in the Equatorial area when analysing baselines less than 20km in length.

b) Residuals of DD Tropospheric Delay – No A Priori Model

Figure 3.10 show the raw (DD) tropospheric delay residuals (i.e. no a priori tropospheric model applied). As expected, the large magnitude (and variations) of the

residuals are present, especially for long and medium length baselines. Clearly the residuals are distance-dependent.

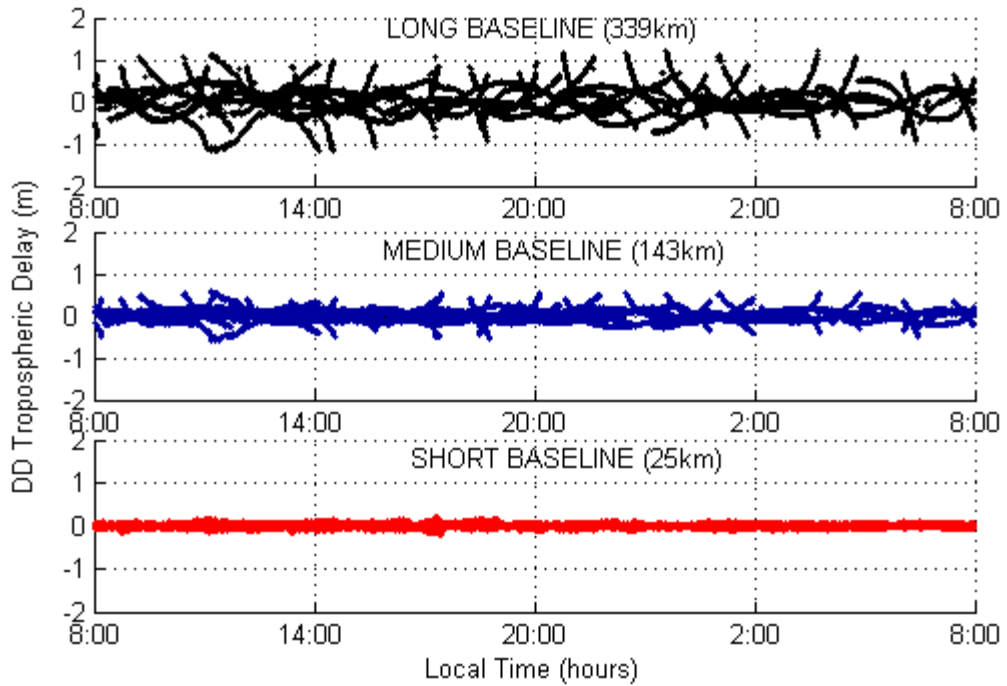


Figure 3.10 All satellites combination; raw DD tropospheric delay residuals for 24hour period, as derived from long (top), medium (middle) and short (bottom) baselines.

Figure 3.11 and the corresponding statistical results in Table 3.4 show that the magnitude and variations of the residuals are less than, but almost similar in pattern to, the case of the ionospheric delay residuals discussed earlier. Therefore the same problem can be expected to arise from the residuals of the raw tropospheric delay.

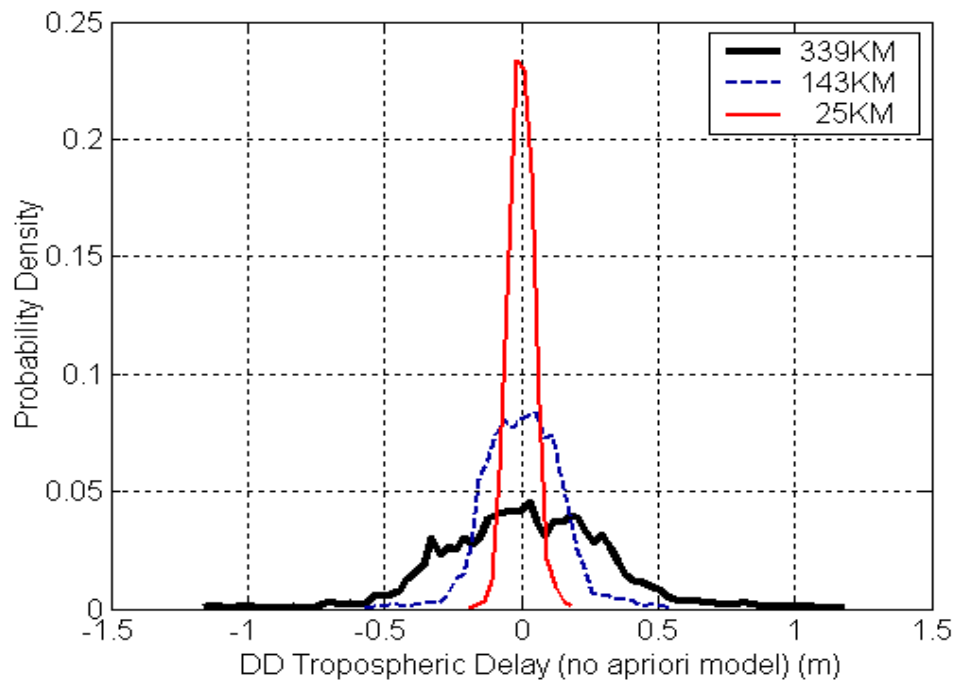


Figure 3.11 Statistical plots of raw DD tropospheric delay residuals related to Figure 3.10.

Table 3.4 Statistical analyses of raw DD tropospheric delay residuals related to Figure 3.10.

Baseline	Statistical (No A Priori Model) (cm)			
	Min	Max	Mean	Stdv
Long	-117.16	119.98	1.81	30.53
Medium	-58.18	57.36	0.85	14.10
Short	-20.62	19.64	0.05	4.59

Figure 3.12 shows the relationship between the raw tropospheric delay residuals and the satellite elevation angle with respect to different baseline lengths. The plots indicate that the magnitude of the residuals is very much dependent on the elevation of the satellites. The variations of the residuals during the first 1hour are the smallest and are similar for all the baselines. The residuals however increase in magnitude when the elevation of satellite 26 decreases. The variations during this 2.5hour period are 2cm, 4cm and 9cm for the short, medium and long baselines respectively.

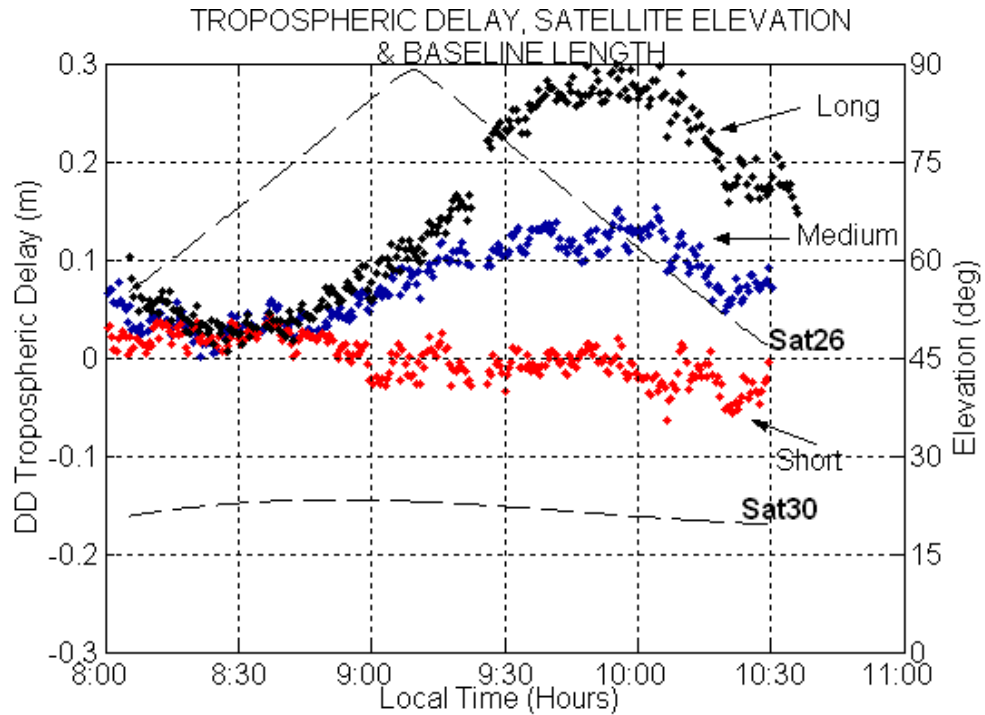


Figure 3.12 Relation of raw DD tropospheric delay residuals and satellite elevations for the short (red), medium (blue) and long baseline (black). The satellite pair is 30-26 as view from station UTMJ for about 2.5hour on DoY 208/03.

c) Residuals of DD Tropospheric Delay - A priori Model Applied

Figure 3.13 shows the DD tropospheric delay residuals with the a priori (total) Saastamoinen model applied. One can clearly notice the effectiveness of this model in reducing the tropospheric delay by comparing this figure to Figure 3.10. In total, the reduction in the residuals is about 80%, 60% and 20% for the long, medium and short baselines respectively.

Inspecting Figure 3.14 and the corresponding Table 3.5, variations of residual tropospheric delay for all baselines during the 24hour are mostly 5cm, whereas the maximum and the minimum values are about ± 21 cm. If the variations of 5cm could be used in Figure 3.3, it can be expected the station height errors due to the relative troposphere error will reach 15cm at 70° zenith angle (relatively low elevation satellite).

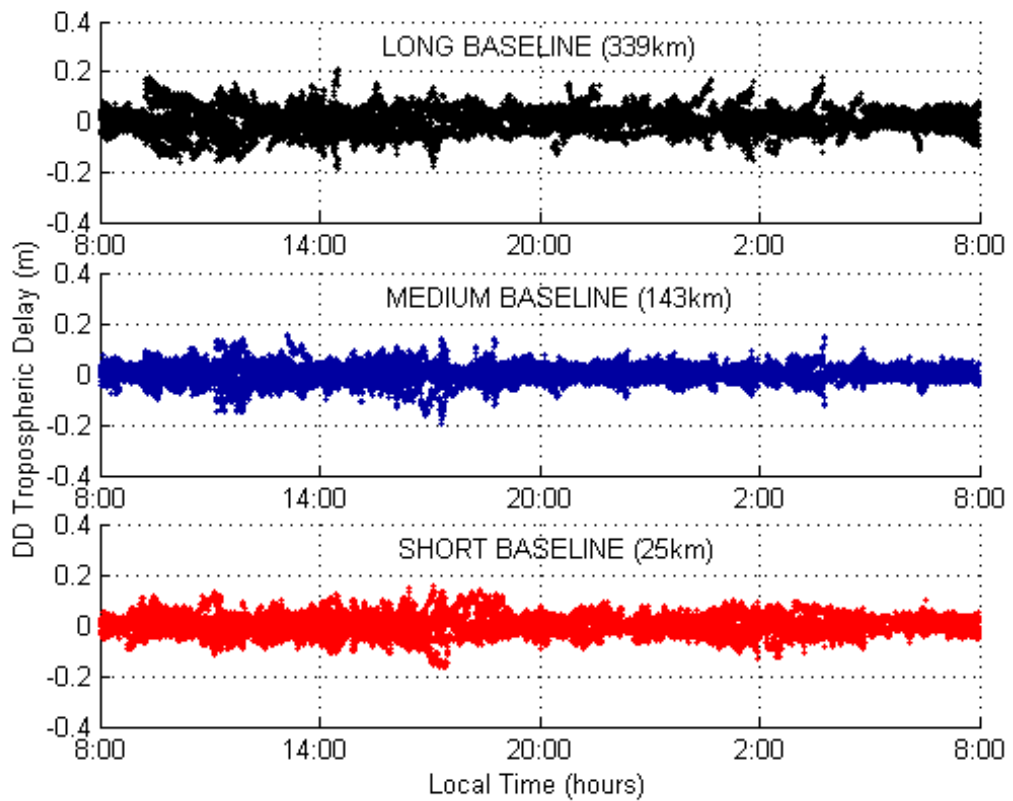


Figure 3.13 All satellite combination; DD tropospheric delay residuals after applying the a priori (total) Saastamoinen Model, for long (top), medium (middle) and short (bottom) baselines.

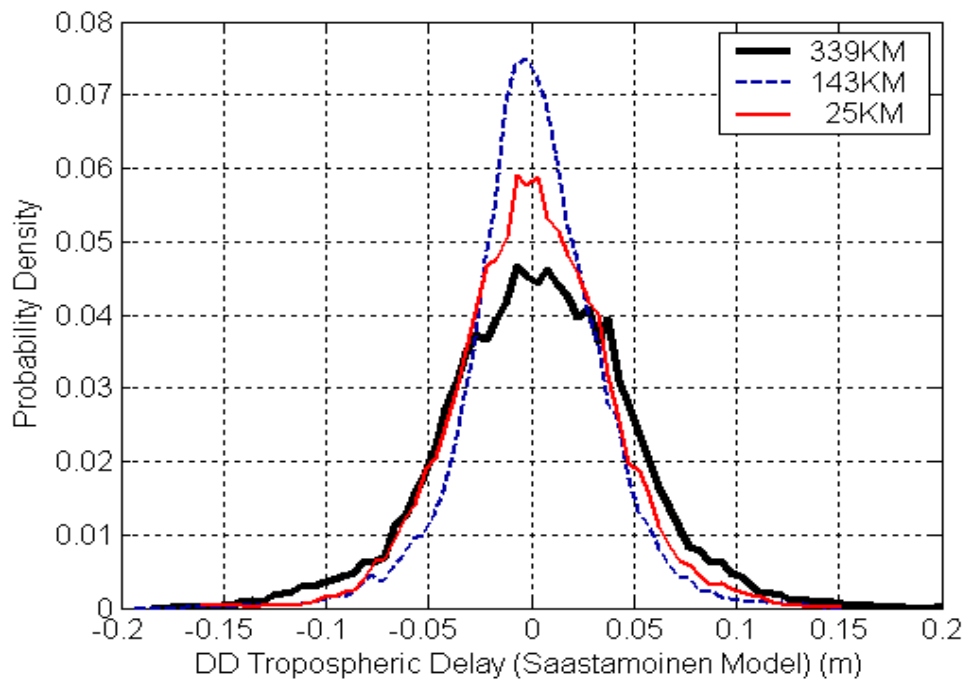


Figure 3.14 Statistical plots of DD tropospheric delay residuals related to Figure 3.13.

Table 3.5 Statistical analyses of DD tropospheric delay residuals related to Figure 3.13.

Baseline	Statistical (Saastamoinen Model) (cm)			
	Min	Max	Mean	Stdv
Long	-18.84	20.90	0.35	4.54
Medium	-19.53	15.49	0.10	3.29
Short	-16.32	15.43	0.07	3.66

Interestingly, residuals for the short baseline do not much improve compared to the other baselines, and the probability of having smaller residuals is less compared to the medium baseline. Moreover, the distance dependency is not obvious. Checking the station coordinates, the (orthometric) height difference between UTMJ-NTUS is only ~5m (see Table 4.6 in Chapter 4). Thus, the height difference is not likely to be a factor that explains this result. Another explanation could be the difference in the meteorological conditions at the two sites during the observations. This is not rare for tropical rainforest areas, where large magnitude and short-term variations of wet delay (mostly due to water vapour in the atmosphere) can be observed. In addition, the sites are exposed to the ocean (see Figure 3.6). Unfortunately, unavailability of meteorological information limits the further investigation of this problem.

Since station NTUS belongs to the IGS station network, the only possibility for analysing this problem is to use the independent check of the IGS-derived ZPD for this station (see definition in Section 2.3.3: troposphere path delay modelling). At best, some indications of the meteorological conditions for the site NTUS can be assessed because the ZPD variations can be related to the water vapour content of the atmosphere. Figure 3.15 shows the IGS-derived ZPD for NTUS for every 2hours from 9:00am 27/7/2003 – 7:00am 28/7/2003 local time. The figure shows that the ZPD started to increase from 9:00am to 5:00pm local time, and dropped sharply with the onset of nighttime. By inspecting the residuals plots for the short baseline UTMJ-NTUS in Figure 3.13 (also in local time), there is a similar trend to the IGS-derived ZPD estimates. Thus, it could be used to infer that short variations of water vapour in the atmosphere at NTUS did occur during this period. If this is the case, it also highlights another difficulty in handling tropospheric delay residuals. The residuals are distance-dependent and are very much influenced by the site's meteorological conditions due to their different altitude, but also

affected by weather conditions, which could be significantly different at the two sites (i.e. UTMJ and NTUS).

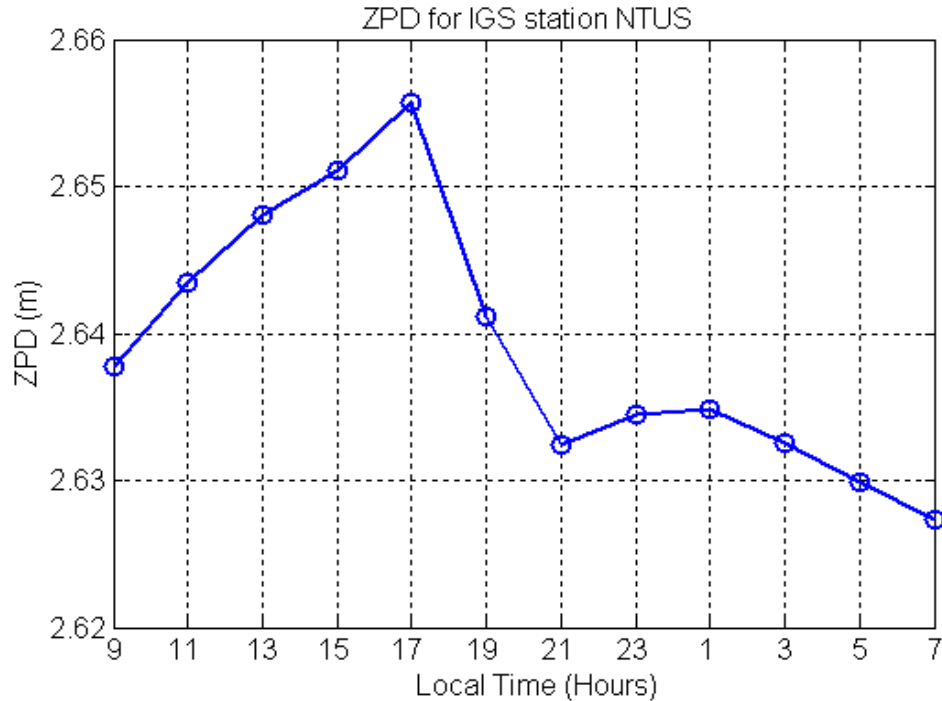


Figure 3.15 The IGS-derived zenith path delay (ZPD) estimates for station NTUS on DoY 208/03.

Figure 3.16 shows the relationship between the tropospheric delay residuals and the satellite elevation angle with respect to different baseline lengths. One can also examine the result in this figure, which is comparable to Figure 3.12 (i.e. no a priori model is applied). Here, the tropospheric delay residuals, as in the case of Figure 3.12, still show a dependence on satellite elevation angle. The variations during the 2.5hours period are 1.8cm, 1.7cm and 2.5cm for short, medium and long baselines respectively. Nevertheless, these plots also show the advantage of applying the a priori (total) Saastamoinen model.

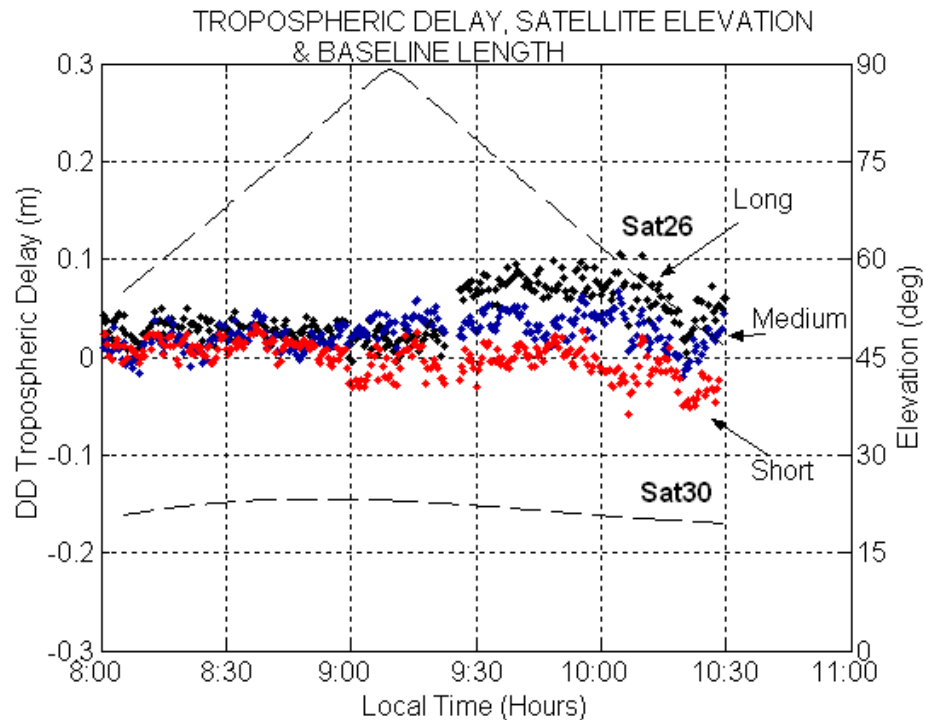


Figure 3.16 Relation of DD tropospheric delay residuals (a priori model is applied) and satellite elevation angles for the short (red), medium (blue) and long baseline (black). The satellite pair is 30-26 as viewed from station UTMJ for 2.5hour on DoY 208/03.

d) DD Orbital Error (Broadcast – Precise Orbit)

Figure 3.17 shows the residuals of (DD) orbital error, from subtracting the geometric range (of DD IF) between the broadcast orbit and the IGS precise orbit ('true orbit'). The plots show that the effect of the orbital error is distance-dependent. In the case of long and medium baselines, it can be noted that there are large variations during the period 14:00-20:00 (6:00-12:00UT). Maximum and minimum residuals in Table 3.6 are more than $\pm 10\text{cm}$ for the long baseline, and less than $\pm 6\text{cm}$ for the medium baseline.

The trends also show large residuals are repeated (step jumps) every 2-3hour over the 24hr period. It is not clear what is the cause of these variations. One of the explanations could be that the broadcast orbit uploads a new message, when the old 'predicted' orbit becomes less reliable. It should be noted that the ephemeris parameters are precisely fit to the GPS satellite orbits and are valid only for a time interval 4 to 6 hours (Wiederholt & Kaplan, 1996) depending on the time since the last GPS Master Control Station upload, based on the assumed once-per-day update schedule. The ephemeris parameters broadcast by a satellite currently change every two hours (Misra & Enge, 2004).

Reoccurring large residuals every 2-3 hours has been found by Racquet (1998) when analysing a baseline (~460km) in the southern part of Norway. Thus, the trend is not particularly limited to the Equatorial region.

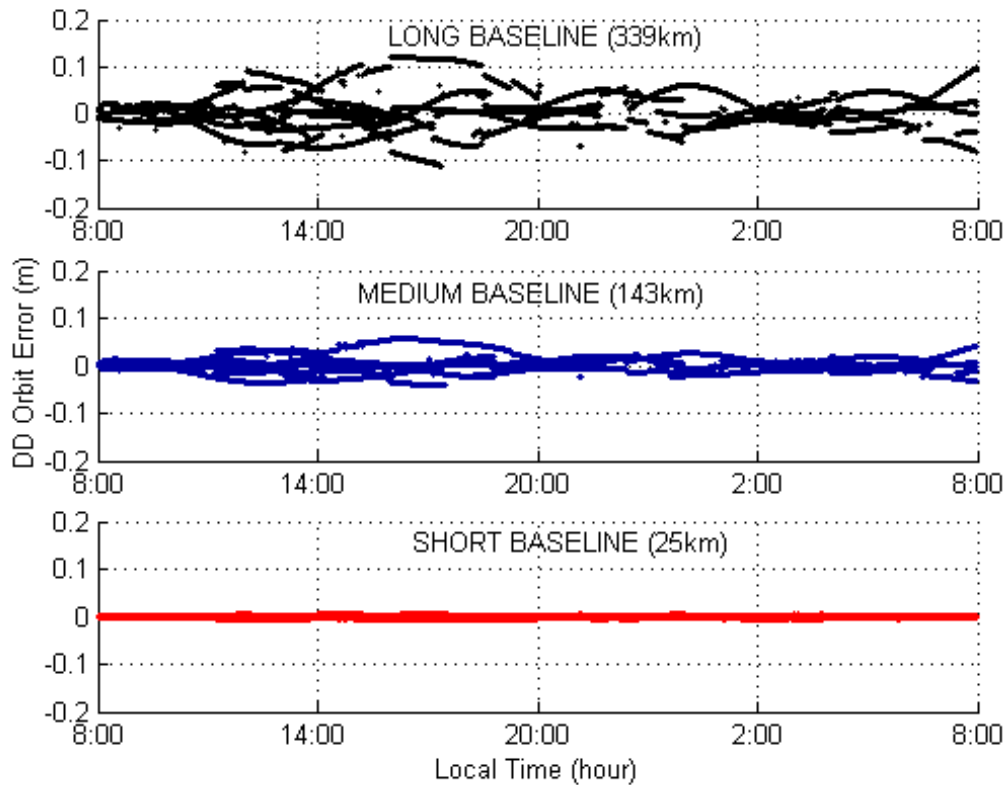


Figure 3.17 All satellite combination; DD orbital error residuals, i.e. broadcast minus precise orbit, for long (top), medium (middle) and short (bottom) baselines.

In the case of the short baseline, the residuals in Figure 3.17 are less noticeable. The statistical analysis in Table 3.6 confirms the magnitude and variation of the residuals during this test period are less than 1cm. Figure 3.18 suggests smaller residuals (much less than 5cm) frequently occur for this baseline compared to the other two. Nevertheless, a further reduction of the residuals for this short baseline should assist AR (see Section 3.3.1), for example, by using the real-time IGS ultra rapid orbit.

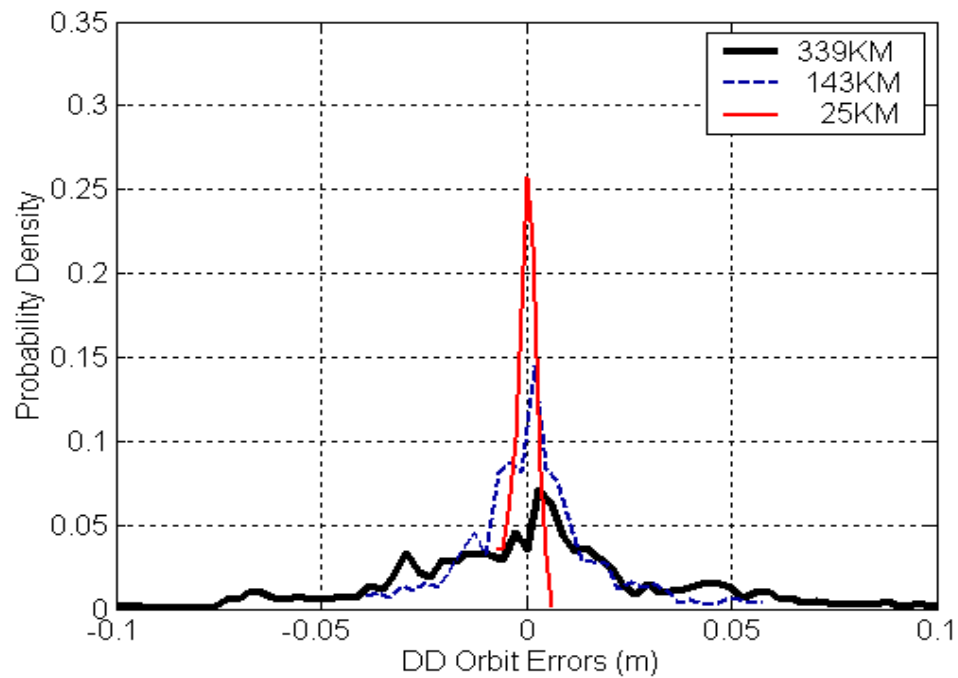


Figure 3.18 Statistical plots of DD orbital error residuals related to Figure 3.17.

Table 3.6 Statistical analyses of DD orbital error residuals related to Figure 3.17.

Baseline	Statistical (Broadcast - Precise Orbit) (cm)			
	Min	Max	Mean	Stdv
Long	-11.26	12.19	0.29	3.70
Medium	-4.06	5.91	0.15	1.63
Short	-0.79	0.71	0.03	0.27

e) DD Orbital Error (Ultra-Rapid – Precise Orbit)

Figure 3.19 shows the (DD) orbital error residuals, by subtracting the geometric range (of DD IF) of the ultra-rapid (predicted half, see Table 2.8) and the precise orbit (‘true orbit’). As can be noticed, the orbital error residuals in this case are very small, with variations less than 0.6cm for all the baselines tested over the 24 hours. Some variations can be detected for the period 22:00-4:00 (14:00-20:00UT). Similar to the broadcast orbit, these large variations could be caused by the less precise satellite positions towards the end of the prediction time.

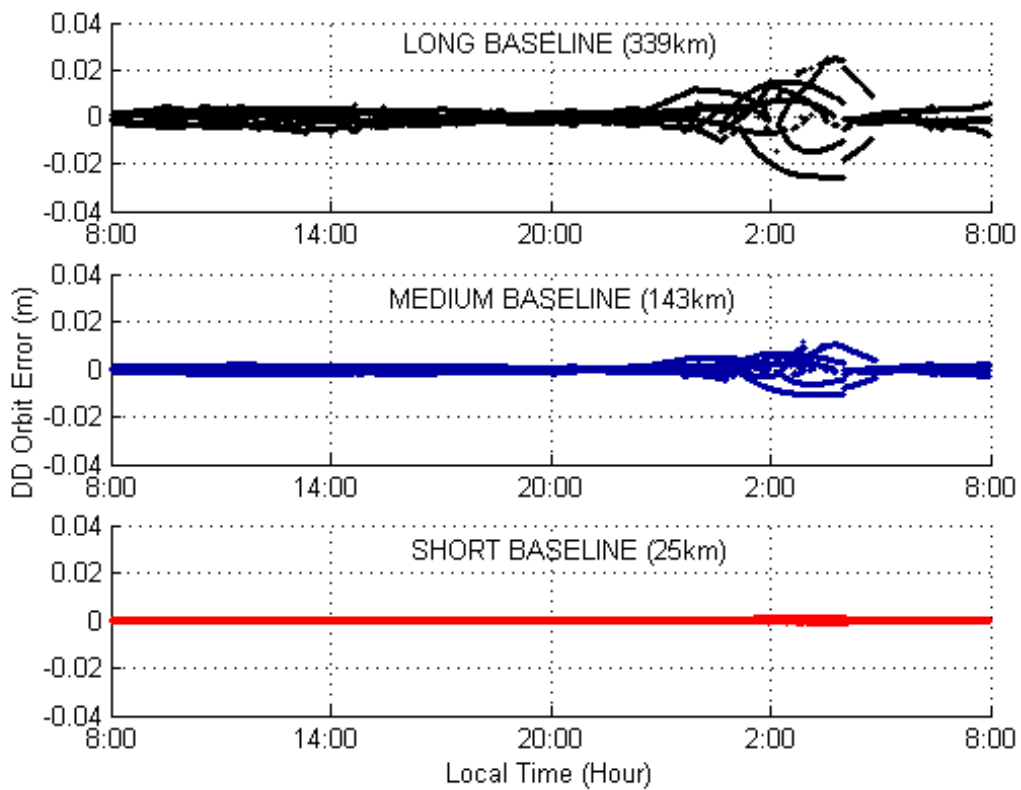


Figure 3.19 All satellite combination; DD orbital error residuals, i.e. ultra-rapid orbit minus precise orbit, for long (top), medium (middle) and short (bottom) baselines.

Figure 3.20 and Table 3.7 clearly show that the residuals of orbital errors from the ultra-rapid orbit are much less significant compared to the previous analysis with the broadcast orbit. In the case of the short baseline, the variations are only 0.03cm during the whole 24hour period. Therefore the ultra-precise orbit clearly has more advantage than the broadcast one, for example in the process of AR.

Table 3.7 Statistical analyses of DD orbital error residuals related to Figure 3.19.

Baseline	Statistical (Ultra - Precise Orbit) (cm)			
	Min	Max	Mean	Stdv
Long	-2.56	2.49	0.01	0.51
Medium	-1.07	1.11	0.00	0.23
Short	-0.12	0.15	0.00	0.03

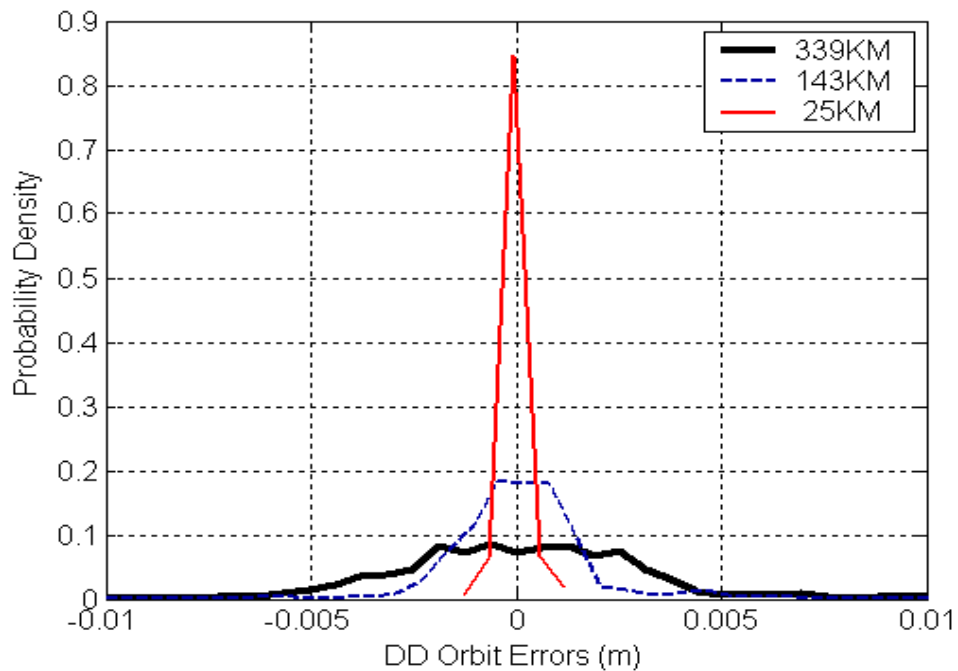


Figure 3.20 Statistical plots of DD orbital error residuals related to Figure 3.19.

3.5 Concluding Remarks

Long-range carrier phase-based positioning is influenced by distance-dependent errors such as ionospheric delay, tropospheric delay and orbital error. A theoretical assessment of these errors shows that the ionospheric delay shortens the estimated baseline length, whereas the tropospheric delay significantly impacts on the estimation of the relative receiver height. The orbital errors introduce a baseline scale error, but the effect is much less significant compared to the ionospheric delay.

The baseline analyses in the equatorial region described here suggest that this is a challenging region for high-accuracy GPS positioning due to the severe effect of distance-dependent errors. Although a differencing technique reduces the distance-dependent errors, it is shown that the residual errors are still large, and are proportional to the baseline length. These residuals easily prevent any success for carrier phase AR and, thus, deteriorate the positioning results. The largest residuals are due to the effect of the ionosphere and therefore limit the baseline length (much less than 25km in this case). However, the effect can practically be eliminated via the IF combination. The

residuals of orbital errors have a similar effect but are smaller in magnitude. Furthermore, the effect can be reduced by using better quality orbits such as the IGS precise or ultra-rapid orbits.

The most problematic component in this class of distance-dependent errors is the tropospheric delay. The delay cannot be eliminated by observing multi-frequency signals, but can be compensated through differencing and/or applying an a priori tropospheric model. It is shown that the 'raw' tropospheric delay can be compensated by up to 80% (in the case of a long baseline) with the application of an a priori Saastamoinen model. However, the variations after double-differencing still reach up to a value of ~4cm even if the baseline is short. Thus, further attention should be given to the troposphere in order to achieve high accuracy carrier phase-based positioning in the equatorial region.

LOW LATITUDE TROPOSPHERE: A STUDY USING GPS DATA IN SOUTH-EAST ASIA

4.0 Introduction

Hot and wet conditions in the equatorial (or low latitude) region can degrade satellite positioning accuracy. Such degradation is associated with the tropospheric effect, attributable predominantly to the wet component (proportional to the water vapour content of the troposphere). Despite efforts to better understand the nature of the signal delay in the low latitude troposphere, further efforts are needed to improve models and methodologies to account for the tropospheric delay in GPS signals. As the water vapour content is very high in this region, it is of special interest for meteorologists to study the tropospheric effect. Such knowledge is vital for understanding global climate, whereas a short term variation of the water vapour content is useful for local weather forecasting.

South-East Asia is the focus of this study as the aim is to investigate the residual effects of the regional tropospheric delay in low latitude regions. GPS data processing and analyses have been conducted to investigate the tropospheric delay effects. The study has been performed during the periods of the North-East and South-West monsoon in the focus area, when the largest variations in the magnitude of the tropospheric delay could be expected. The a priori troposphere models were tested during this monsoon period, and station coordinate repeatabilities in the GPS network were analysed in order to quantify the impact of the tropospheric delay on GPS positioning. In addition, the variations of the zenith tropospheric delay estimated from a local and a regional GPS network were compared to the results obtained from the global IGS network.

4.1 Study Area and Climate Conditions

4.1.1 Coverage Area

The study focused on the Malaysian Peninsula and Singapore, latitude range 1°N to 7°N and longitude range 100°E to 105°E . While the previous analyses in Section 3.4.1 have made use of several stations of the Malaysian Active Surveying Stations (MASS) network, the present study includes additional stations. In this study, the IGS station in Singapore (NTUS) and the MASS stations together are considered a local network. Figure 4.1 shows other IGS stations surrounding the focus area, PIMO in the Philippines, BAKO in West Java (Indonesia) and IISC in Bangalore (India). All the IGS stations are included in this study and treated as a regional network. Hence, the general study area covers the whole region of South-East-Asia.

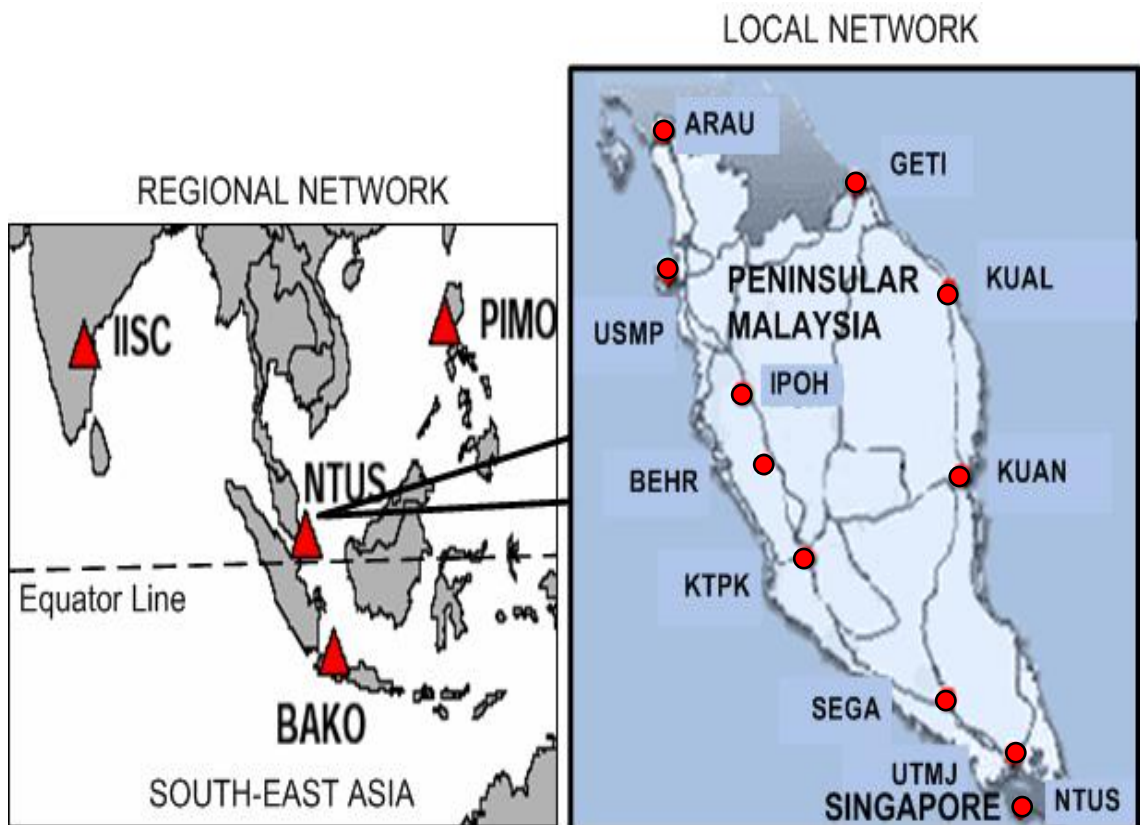


Figure 4.1 The study area and existing GPS CORS Networks: Regional network (part of the global IGS network) and the local network (MASS network).

4.1.2 Local Climate and Weather Conditions

The atmosphere in the study area is in many ways unique. Located in the equatorial region, the declination of the sun remains relatively high and no distinctive season of the year based on received solar energy can be discerned. The climate conditions are always hot, yet almost uniform in temperature and atmospheric pressure. In addition, the climate of the focus area is classified as ‘tropical rainforest’ due to the high humidity and abundant rainfall almost all year round. Moreover, the area is exposed to the influence of the ocean. This has a distinctive impact on the atmosphere of this area, allowing it to hold even more water vapour than in other area. Furthermore, there are significant short periodic variations of water vapour content due to this climate conditions.

The area has two main seasons, the North-East monsoon (November to early March) and the South-West monsoon (early May to August). The two monsoons bring heavy rain, which sometimes leads to extensive flooding in the eastern part of the Malaysian Peninsula especially during the North-East monsoon. In general, the mean monthly rainfall in this area indicates drier weather conditions from May to early July and wetter conditions from November to January. Figures 4.2-4.4 and Tables 4.1-4.3 summarise the local weather conditions for the months July, September and December in 2003, as reported by the Malaysian Meteorological Service (MMS).

Figures 4.2-4.4 show the average amount of rainfall during the period of the two monsoons as well as the inter-monsoon period. Tables 4.1-4.3 provide the mean daily values of solar radiation, evaporation and temperature during these months. The weather stations in these tables are those that are near the MASS stations used in this study. As can be noticed from the reports, there are no distinct wet or dry periods. However, the rainfall distribution in the area is very much influenced by the monsoon seasons. To summarise, the climate and weather conditions in this area reflect the strong influence of the atmospheric water vapour.

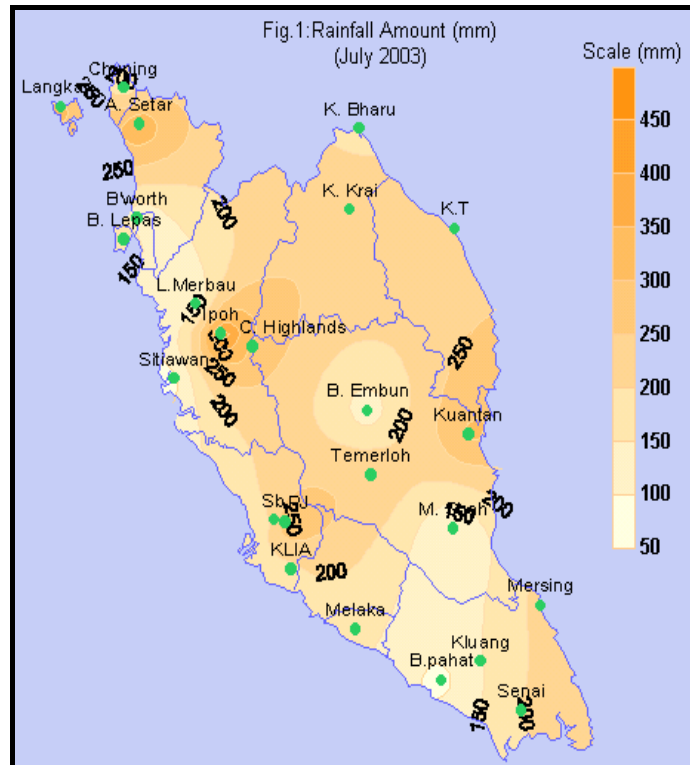


Figure 4.2 Rainfall over the Malaysian Peninsula during the South-West monsoon in July 2003 and location of weather stations (courtesy of MMS).

Table 4.1 Mean daily solar radiation, evaporation and temperature for July 2003 during the South-West monsoon (courtesy of MMS).

Weather Station	Near to MASS station:	S. Radiation (MJ/m ²)	Evaporation (mm)	Temperature (°C)
Chuping	ARAU	12.48 (-3.14)	3.4 (+0.2)	27.0 (0.1)
K.Bharu	GETI	17.82 (-0.07)	3.7 (-0.8)	27.5 (0.2)
B.Lepas	USMP	16.97 (-0.23)	3.5 (-0.2)	27.9 (0.7)
K.T	KUAL	14.99 (-2.70)	3.8 (-0.4)	26.8 (-0.1)
Kuantan	KUAN	16.02 (-0.92)	4.2 (+0.2)	27.0 (0.3)
Kluang	SEGA	14.11 (-1.32)	2.5 (-0.2)	26.3 (0.2)
Sb PJ	KTPK	14.23 (-1.46)	4.0 (-0.4)	27.5 (0.1)
Senai	UTMJ	13.75 (-0.99)	3.5 (+0.2)	25.8 (-0.2)

Note: 1. Max Temp Kluang 35.3°C, Min Temp Senai 21.1°C
 2. Mega Joule per square metre (MJ/m²)
 3. Value in bracket refers to deviation from long-term average

South-West Monsoon, July 2003

‘July is the month of South-West monsoon ... In the month of July 2003, the country received average to above average of rainfall. In many places, a few occurrences of moderate to heavy rainfall contributed significantly to the total monthly rainfall amounts. Despite the wet conditions, some places experienced short dry spells during the month and

a few isolated places recorded average rainfall ... Kuala Krai and Kuantan have recorded the highest daily rainfall for July with 118.5mm since 1985 and 141.4mm since 1951 respectively ... The recorded temperatures were generally higher than the long-term average. In general the country recorded lower than average daily solar radiation and lower than average rates of evaporation ...' (MMS, 2003).

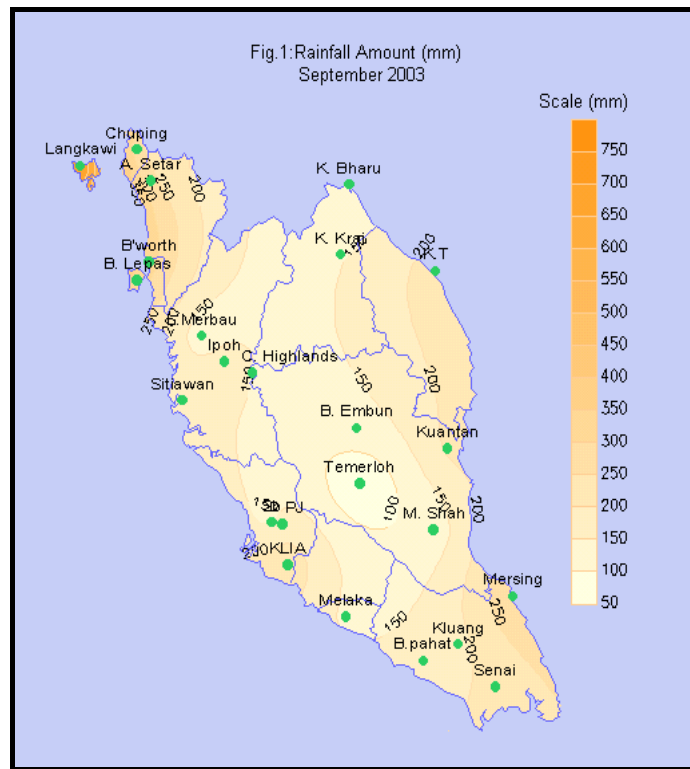


Figure 4.3 Rainfall over the Malaysian peninsula during the inter-monsoon in September 2003 and location of weather stations (courtesy of MMS).

Table 4.2 Mean daily solar radiation, evaporation and temperature for September 2003 during the inter-monsoon (courtesy of MMS).

Weather Station	Near to MASS station:	S. Radiation (MJ/m ²)	Evaporation (mm)	Temperature (°C)
Chuping	ARAU	16.78 (-0.43)	3.0 (-0.1)	26.5 (+0.0)
K.Bharu	GETI	19.39 (+0.88)	5.0 (+0.6)	27.5 (+0.6)
B.Lepas	USMP	16.61 (+0.00)	3.3 (-0.1)	27.7(+1.0)
K.T	KUAL	15.42 (-2.42)	4.1 (-0.1)	26.7(-0.1)
Kuantan	KUAN	18.11 (+1.13)	4.6 (+0.5)	27.2(+0.7)
Kluang	SEGA	14.80 (-0.89)	2.7(-0.1)	26.1(+0.2)
Sb PJ	KTPK	14.69 (-0.96)	4.4 (+0.2)	27.8(+1.0)
Senai	UTMJ	14.71(+1.20)	3.3 (+0.1)	25.6(-0.2)

Note: 1. Max Temp Subang 34.9°C, Min Temp Senai 21.1°C
 2. Mega Joule per square metre (MJ/m²)
 3. Value in bracket refers to deviation from long-term average

Inter-monsoon, September 2003

‘Climatologically, September is the beginning of the inter-monsoon period. In general, the country received average to below average rainfall during this month. In many places, moderate to heavy rainfall for a few days contributed significantly to the total monthly rainfall ... As for the monthly total rainfall over Peninsula Malaysia, Pulau Langkawi recorded the highest rainfall of 709mm and Temerloh recorded the lowest rainfall of 54mm ... The temperatures were warmer than the long-term average of the month’ (MMS, 2003).

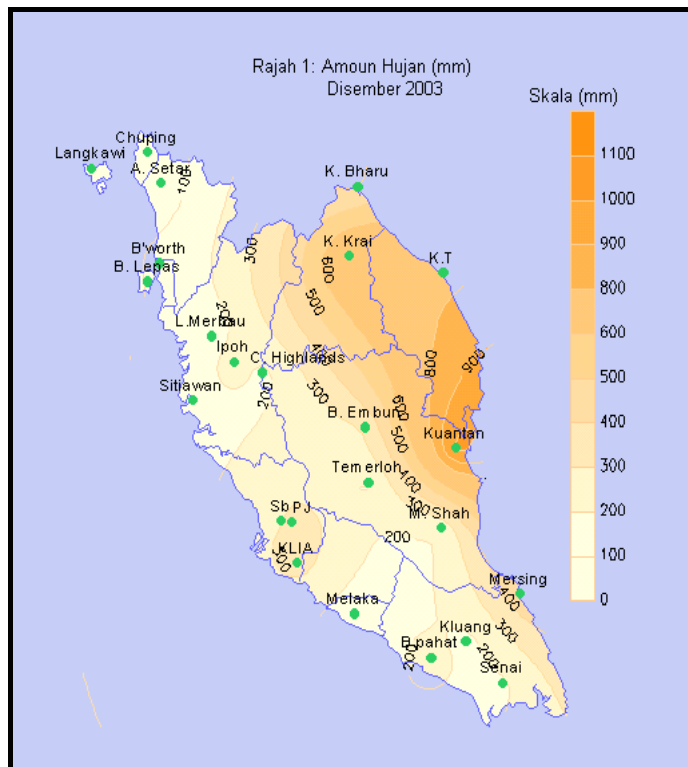


Figure 4.4 Rainfall over the Malaysian peninsula during the North-East monsoon in December 2003 and location of weather stations (courtesy of MMS).

North-East monsoon, December 2003

‘December is the second month of the North-East monsoon and is expected to be wet, particularly over the southern part of the east coast of Peninsular Malaysia. For total monthly rainfall over Peninsular Malaysia, Kuantan recorded the highest rainfall of 1031.9mm while Pulau Langkawi recorded the lowest (12.0mm).... most places in Peninsular Malaysia in this December received average rainfall while a few places were either below/much below or above normal.... For highest daily rainfall, over Peninsular Malaysia, Kuala Terengganu recorded the highest (297.0mm).... Temperature, solar radiation and evaporation varied from below to above average’ (MMS, 2003).

Table 4.3 Mean daily solar radiation, evaporation and temperature for December 2003 during the North-East monsoon (courtesy of MMS).

Weather Station	Near to MASS station:	S. Radiation (MJ/m ²)	Evaporation (mm)	Temperature (°C)
Chuping	ARAU	12.48 (-3.14)	3.7 (+0.3)	26.5 (+0.2)
K.Bharu	GETI	11.31(-2.18)	3.3 (-0.3)	27.2 (+0.9)
B.Lepas	USMP	17.03 (-0.15)	4.5 (+0.3)	27.6 (+0.6)
K.T	KUAL	14.53 (+0.93)	3.5 (-0.2)	25.9 (-0.4)
Kuantan	KUAN	15.12 (+3.23)	3.2 (+0.4)	25.3 (+0.4)
Kluang	SEGA	13.20 (-1.15)	2.7 (+0.0)	25.7 (+0.4)
Sb PJ	KTPK	10.57(-3.53)	3.8 (+0.1)	27.2 (+0.9)
Senai	UTMJ	13.04 (-1.32)	3.0 (-0.1)	25.4 (-0.1)

Note: 1. Max Temp Subang 34.2°C, Min Temp K.T. 21.4°C
 2. Mega Joule per square metre (MJ/m²)
 3. Value in bracket refers to deviation from long-term average

4.2 Testing A Priori Tropospheric Delay Modelling

4.2.1 Test Methodology

Delay in GPS signals due to the non-dispersive nature of the tropospheric layer cannot be measured directly from GPS observations. The tropospheric delay can be partly compensated for by the a priori tropospheric model, however a residual effect remains in the GPS observables. Nevertheless, the residual tropospheric delay can be estimated from the IF measurements (some assumptions applied; see sub-section 3.2.3, Equation 3.20 and Section 3.4).

Prior analyses in Chapter 3 have indicated that the residual tropospheric delay is very significant in this study area. The previous result (see sub-sections 3.4.2 (b) & (c)) remains valid but does not illustrate the overall effect from the residual tropospheric delay. The question also arises as to the performance of the a priori models in the study area. Further experiments are required using more baselines and longer term data analysis. In particular, the performance of the dry and the total a priori tropospheric delay models need to be investigated. For these subsequent investigations, two commonly used a priori tropospheric models were selected; namely the Saastamoinen and modified Hopfield.

Two experiments were conducted as follows:

- a) **One-day experiment** – with almost all MASS stations included (see section 4.2.2);
- b) **Monsoon experiment** – three month data analysis with selected MASS stations and the IGS station NTUS in Singapore (see section 4.2.3).

The BERNese software has been employed (as well as for all other experiments in this chapter). The QIF strategy (see section 3.3.3) has been implemented for the process of ambiguity resolution. In the first run, all the data from experiments (a) and (b) were processed in order to resolve the DD L1 and DD L2 ambiguities. These ambiguities will be introduced while processing the IF measurements in the subsequent run. Next, the processing of the ‘fixed’ DD IF measurements for each baseline was conducted in three test schemes:

- Test 1:** Processing without applying the a priori tropospheric model. The residuals from this test were stored and treated as the ‘raw’ DD IF residuals.
- Test 2:** Processing with applying the dry delay tropospheric models from Saastamoinen (Equation 2.33) and modified Hopfield (see Equations 2.41-2.43). The DD IF residuals from both models were stored separately. The percentile improvements of these DD IF residuals with respect to Test 1 were computed.
- Test 3:** Processing with applying the total delay tropospheric models from Saastamoinen (Equation 2.30) and modified Hopfield (see Equations 2.41-2.43). The DD IF residuals from both models were stored separately. The percentile improvements of these DD IF residuals with respect to Test 1 were computed.

Since the total delay model contains both dry and wet model components, the design of the above test schemes also enables the isolation of the performance of the wet delay modelling. This can be done by comparing the percentile improvements between Test 3 and Test 2. The proposed processing schemes in this section are summarised in Figure 4.5.

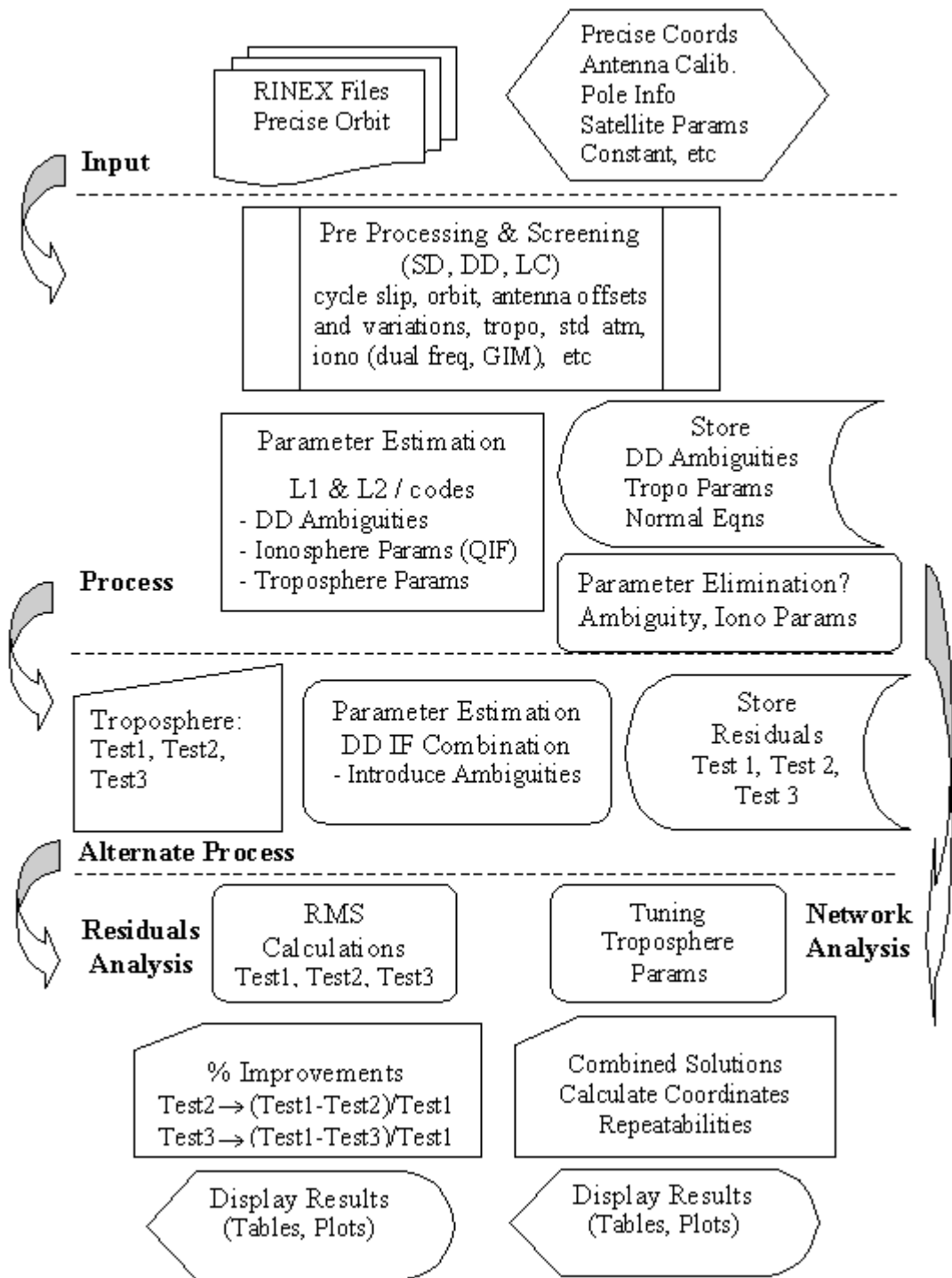


Figure 4.5 Testing strategy for a priori troposphere models and analysis of coordinates repeatabilities.

4.2.2 The One-Day Experiment - Results and Discussion

The experiment was conducted on DoY 29/2003, during the North-East monsoon. Datasets from all MASS stations (see Figure 4.1) were employed, giving wide coverage over the Malaysian Peninsula. However, station IPOH was excluded due to bad data observations, and no data was recorded by station BEHR on this day. Station KTPK was selected as reference because of its central location within the MASS network. In total, there were seven baselines. The 24 hour datasets (from 8:00 am local time), at 30s intervals, were processed at 15° cut-off elevation.

For the selected baseline KTPK-ARAU (the longest baseline in this experiment; see Table 4.4), the time series of the DD IF residuals (for all satellite combinations) is shown in Figure 4.6 (Test 1; no model), Figures 4.7a&b (Test 2; dry models) and Figures 4.8a&b (Test 3; total models). Some comments can be made based on these figures.

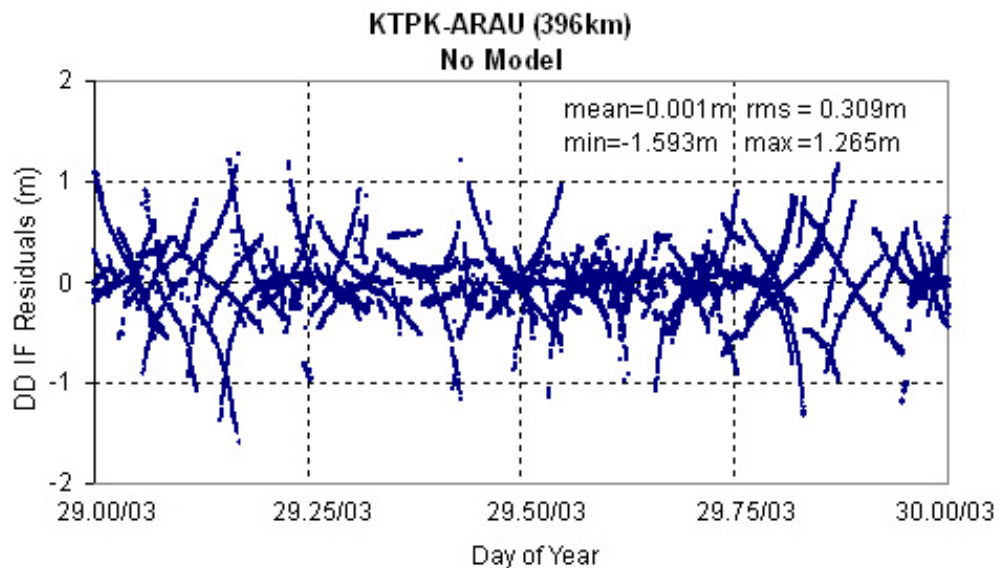


Figure 4.6 Test 1: DD IF residuals without applying a priori troposphere model.

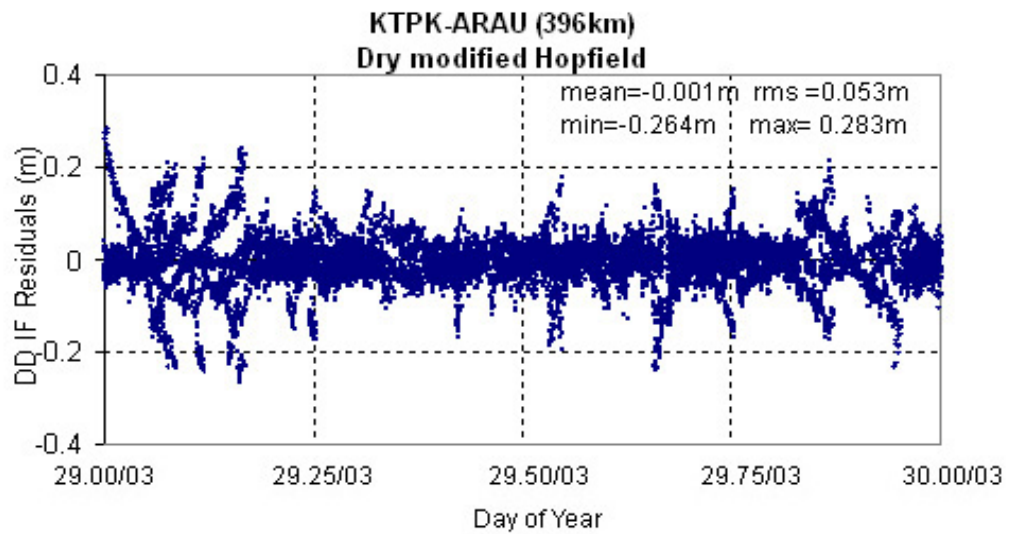


Figure 4.7 a) Test 2: DD IF residuals with applying the dry modified Hopfield model.

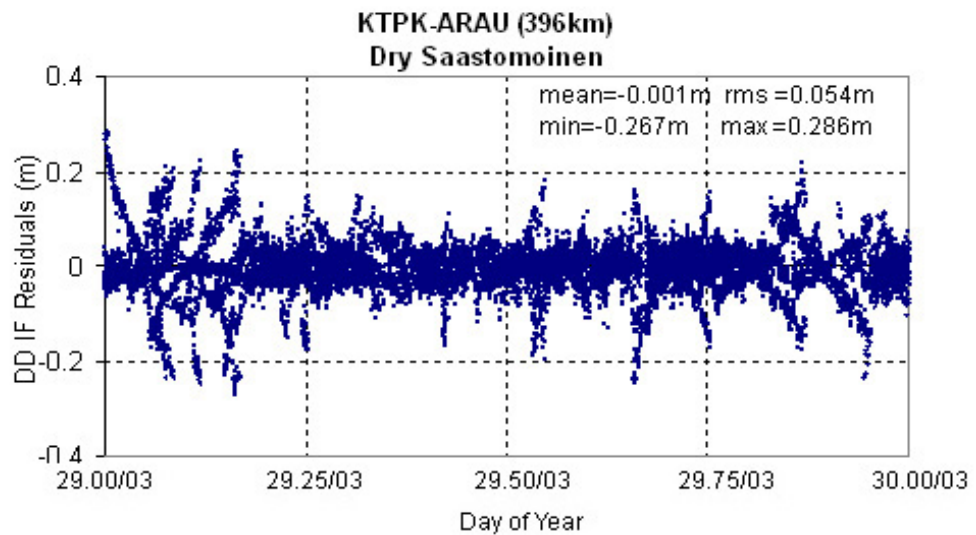


Figure 4.7 b) Test 2: DD IF residuals with applying the dry Saastomoinen model.

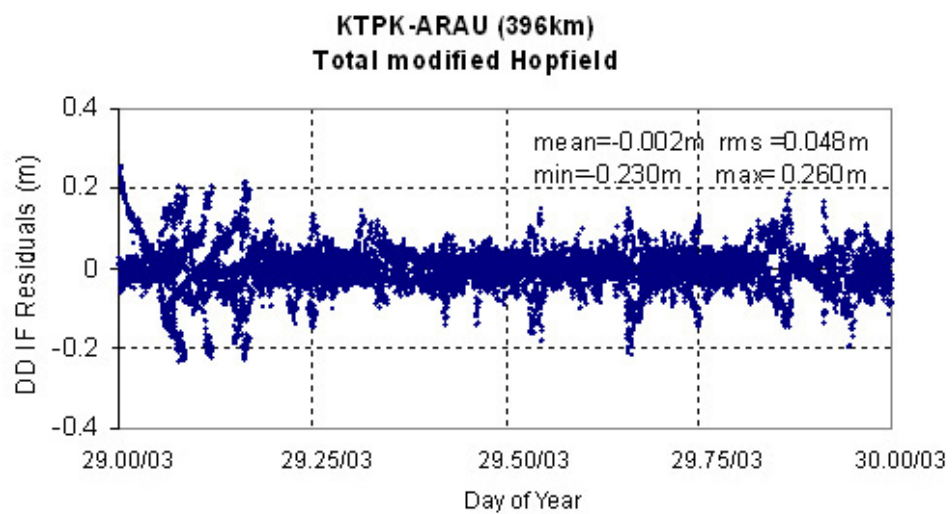


Figure 4.8 a) Test 3: DD IF residuals with applying the total modified Hopfield model.

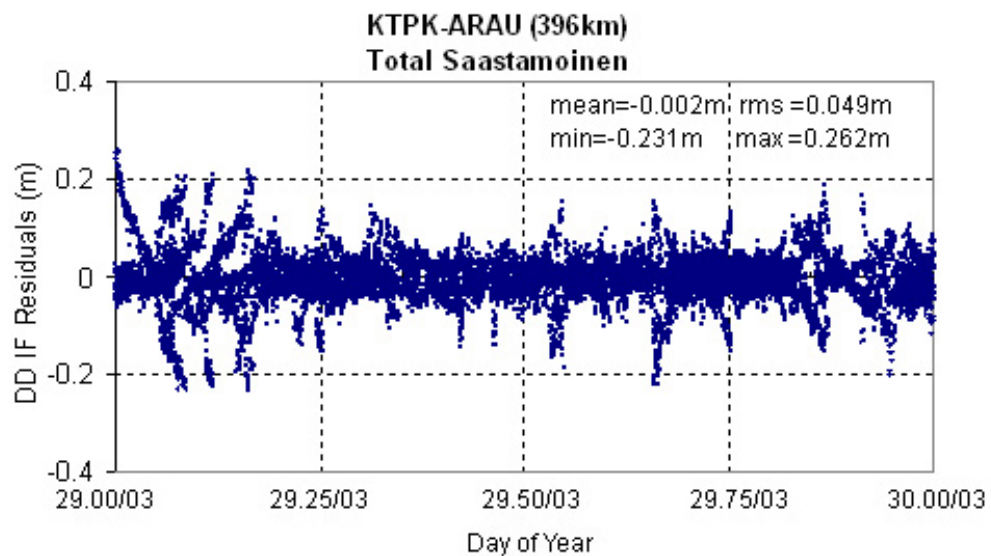


Figure 4.8 b) Test 3: DD IF residuals with applying the total Saastamoinen model.

Firstly, the DD IF residuals in Test 1 (Figure 4.6) have the largest magnitude, compared to Test 2 (Figure 4.7) or Test 3 (Figure 4.8). These outcomes were as expected because no model was applied in Test 1. The result indicates the two models were able to reduce the size of the residuals to some extent. Secondly, no significant residual differences between the two dry models in Test 2 can be noticed (see Figure 4.7 (a) and (b)). This is also true with the two total models in Test 3 (see Figure 4.8 (a) and (b)). At this point, one can only assume that the performance of the Saastamoinen and modified Hopfield models were almost at the same level, for this length baselines under these weather conditions. Thirdly, only a slight reduction can be noticed between the dry and total Saastamoinen models (see Figure 4.7 (b) and Figure 4.8 (b)), which is also true between the dry and total modified Hopfield models (see Figure 4.7 (a) and Figure 4.8 (a)). These results give the early impression that both models have the same difficulty in modelling the wet delay component of the troposphere.

Table 4.4 summarises the numerical results for all the baselines in terms of RMS DD IF residuals. By inspecting these RMS values it can be seen that the other baselines show a similar pattern as in Test 1. Further analyses were conducted by plotting these RMS residuals against the baseline length (Figure 4.9), and against the station (orthometric) height differences (Figure 4.10). From Figure 4.9, the RMS residuals in each test show an overall increase as the inter-station distance increases. This result agrees with the

finding in section 3.4.2 (b) & (c), that the residual tropospheric delay did show the trend of distance-dependence. However, no clear relation between these RMS values and the station height differences can be found in Figure 4.10, which appears to be in disagreement with the fact that the (residual) tropospheric delay increases with the elevation. This outcome is understandable due to the relatively small inter-station heights within the MASS network (less than 0.1km; see Table 4.4).

Table 4.4 Baseline length, station height and RMS DD IF residuals in Test 1, Test 2 and Test 3. Station KTPK is the reference station with orthometric height of 102.117m. All station orthometric heights were calculated by first obtaining station geoid heights from the EGM96 geoid calculator (via <http://earth-info.nga.mil/GandG/wgs84/gravitymod/egm96/intpthel.html>).

Stn KTPK to:	Baseline Length (km)	Ortho. Height Diff. (km)	RMS of DD IF				
			No Model (Test 1) (m)	Dry Model (Test 2)		Total Model (Test 3)	
				SAAS (m)	M.HOPF (m)	SAAS (m)	M.HOPF (m)
ARAU	396	-0.069	0.310	0.054	0.053	0.049	0.048
GETI	341	-0.094	0.373	0.057	0.056	0.049	0.048
USMP	288	-0.070	0.267	0.048	0.048	0.045	0.044
KUAL	285	-0.045	0.254	0.040	0.040	0.034	0.034
UTMJ	278	-0.028	0.221	0.053	0.052	0.047	0.047
KUAN	196	-0.078	0.127	0.027	0.027	0.025	0.025
SEGA	136	-0.079	0.104	0.028	0.028	0.025	0.025

Further assessments in Table 4.5 provide the percentile improvements in the RMS residuals for Test 2 and Test 3 with respect to Test 1. From the table, Test 2 the percentile improvement varies from 73%-85% for each baseline. The percentile improvements increase to about 1%-3% more in Test 3. On average, the two dry models in Test 2 show almost the same percentile improvements: dry Saastamoinen – 80.2%; dry modified Hopfield – 80.36%. This is also true in the case of the two total models in Test 3: total Saastamoinen – 82.26%; total modified Hopfield – 82.26%. In spite of this, only ~2% improvements between the total and dry models were noted. So far, the one-day experiment covering the Malaysian Peninsula has shown that both the Saastamoinen and modified Hopfield models were essentially at the same level of performance. Nevertheless, both models experienced the same difficulty in modelling the wet component of the troposphere.

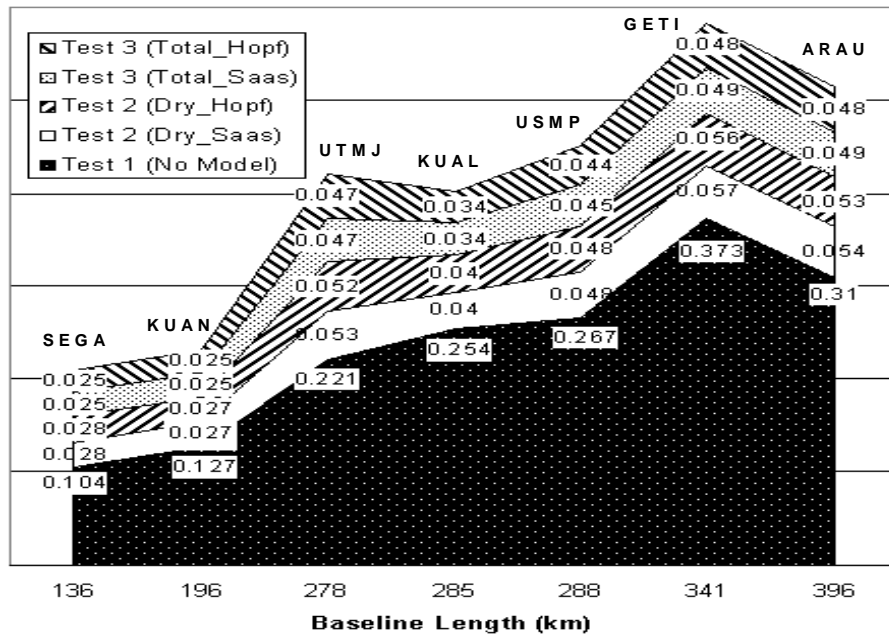


Figure 4.9 RMS DD IF residuals (in metres) vs the baseline length according to Table 4.4. The RMS values along the horizontal axis indicate the trend of distance-dependence. The RMS values along the vertical axis decrease according to Test 1, Test 2 and Test 3.

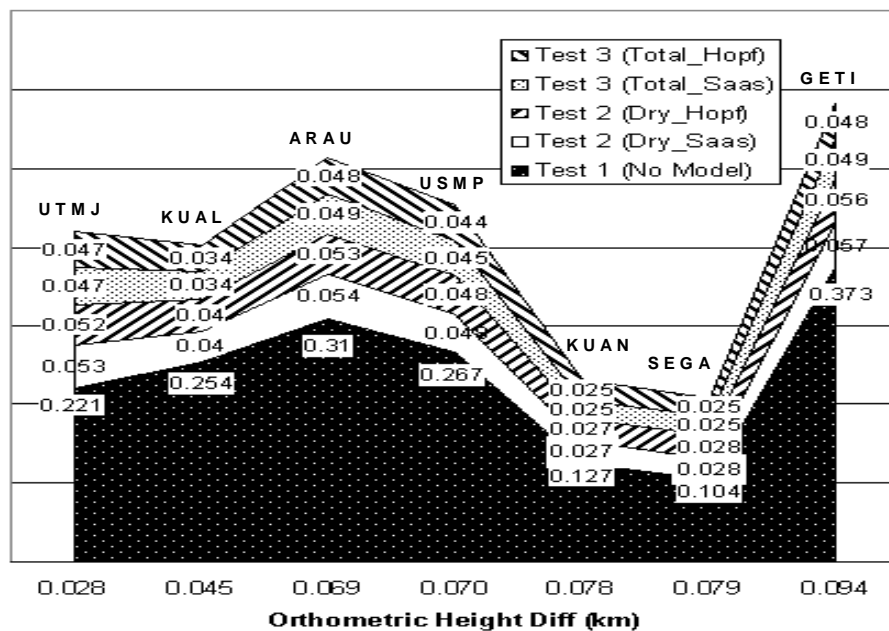


Figure 4.10 RMS DD IF values (in metres) vs height differences according to Table 4.4. The RMS values along the horizontal axis have no specific trend towards the increment of the height differences. The RMS values along the vertical axis decrease according to Test 1, Test 2 and Test 3.

Table 4.5 Percentile improvements in the RMS DD IF residuals after applying the dry models (Test 2) and total models (Test 3) against having no model applied (Test 1), and the percentile difference between Test 2 and Test 3.

Stn KTPK to:	Dry Models (Test 2) (%)		Total Models (Test 3) (%)		Total – Dry (Test 3- Test 2) (%)	
	SAAS	M.HOPF	SAAS	M.HOPF	SAAS	M.HOPF
ARAU	82.6	82.9	84.2	84.5	1.6	1.6
GETI	84.7	85.0	86.9	87.1	2.2	2.1
USMP	82.0	82.0	83.1	83.5	1.1	1.5
KUAL	84.3	84.3	86.6	86.6	2.3	2.3
UTMJ	76.0	76.5	78.7	78.7	2.7	2.2
KUAN	78.7	78.7	80.3	80.3	1.6	1.6
SEGA	73.1	73.1	76.0	76.0	2.9	2.9
Average	80.20	80.36	82.26	82.39	2.06	2.03

4.2.3 The Monsoon Experiment – Results & Discussion

The monsoon experiments were conducted in the months of July, September, and December 2003. According to the meteorological reports in section 4.1.2, these months were the months of the South-West monsoon, inter-monsoon and North-East monsoon in the Malaysian Peninsula. In this experiment, data from five GPS stations were used; UTMJ, NTUS, SEGA, BEHR and KUAN (see Figure 4.1). Station UTMJ was selected as the reference. Table 4.6 shows the baseline UTMJ-BEHR is the longest, and baseline UTMJ-NTUS is the shortest. The information on the station height is also given in Table 4.6. It can be noted that all station (orthometric) heights are less than 0.08km, and station height differences relative to UTMJ were less than 0.06km.

Table 4.6 Baseline length, station height and height differences relative to station UTMJ. All station geoid heights were obtained from the EGM96 geoid calculator (via <http://earth-info.nga.mil/GandG/wgs84/gravitymod/egm96/intpthel.html>).

Station	Distance to UTMJ km	Ellip. Height (h) m	Geoid Height (N) M	Ortho. Height (H=h-N) m	Ortho. Height Diff to UTMJ M
UTMJ	0	80.421	6.77	73.651	0.000
NTUS	25	75.427	7.09	68.333	5.318
SEGA	143	25.232	1.89	23.342	50.309
KUAN	253	25.415	1.70	23.715	49.936
BEHR	339	68.690	-3.65	72.340	1.311

Early data screening shows that none of the stations in this experiment can provide a full month's data. Some daily data were not recorded, or only small amounts of data on some days were stored. However, most stations recorded more than 15 days of the full 24hour observations (at 30s intervals) in each month, except for only 9 days for station KUAN and 10 days for station SEGA during the month of December. Only the full 24hour datasets were considered in this experiment. All datasets were processed using Test 1 (no models), Test 2 (dry models) and Test 3 (total models) scenarios. The daily RMS DD IF residuals from each baseline were computed. To make the analysis easier, the RMS residuals were averaged on a monthly basis, as presented in Figure 4.11. Some general remarks can be made to the results shown in Figure 4.11.

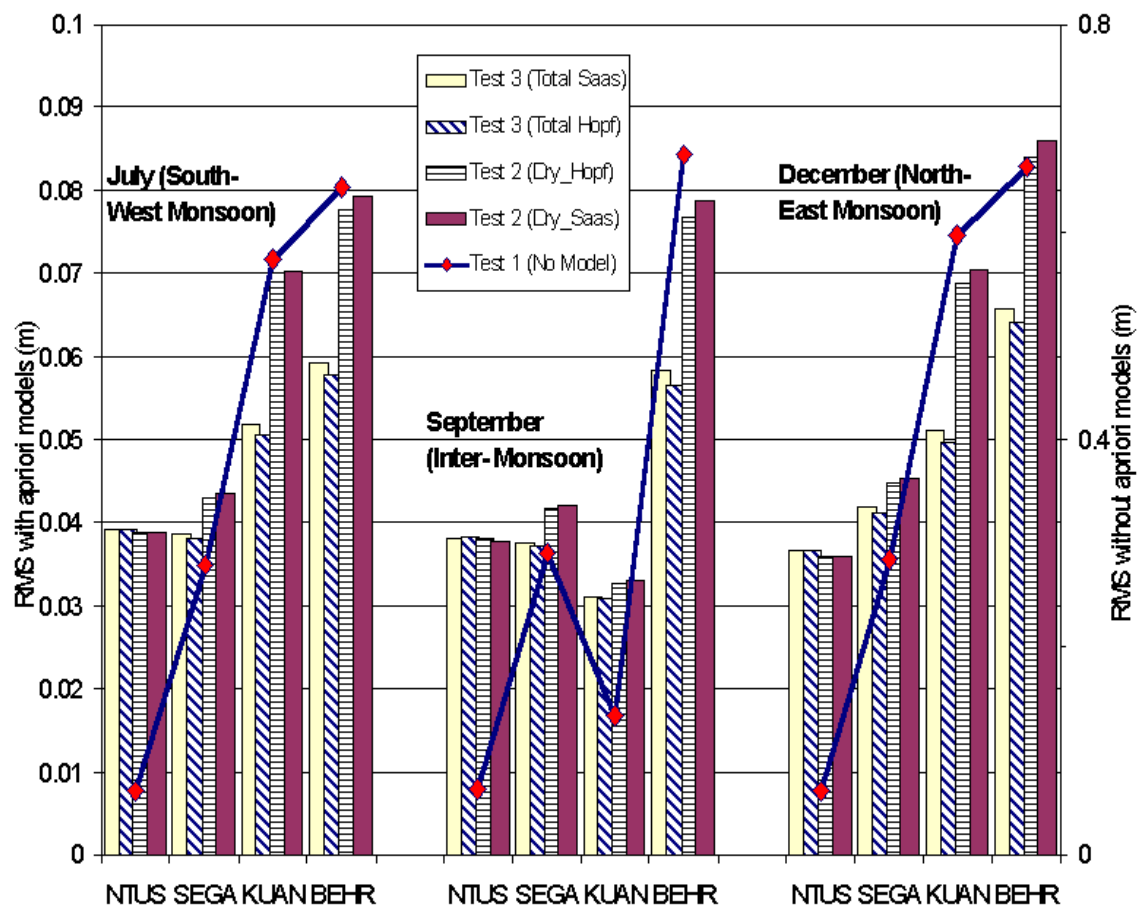


Figure 4.11 The (average) RMS DD IF residuals during the period of the South-West monsoon, inter-monsoon and North-East monsoon at each station relative to station UTMJ. The baselines are ordered on the horizontal axis from the shortest to the longest UTMJ (see also Table 4.6). The line plot refers to Test 1 (vertical axis on the right).

The bar plot refers to Test 2 and Test 3 (y-axis on the left).

Firstly, one can notice that the monthly results of Test 1, Test 2 and Test 3 have shown the trends of distance-dependence. Surprisingly, the long baseline UTMJ-KUAN did not follow this trend during September. These results could be associated with the dry conditions during the inter-monsoon period in September, as reported in Section 4.1.2. Additionally, the evaporation (as part of the water cycle; evaporation, condensation and precipitation) occurs largely during the inter-monsoon period. Consequently, the other baselines in September also indicate more or less a reduced amount of RMS residuals in contrast to July (South-West monsoon) and December (North-East monsoon). The weather station near site KUAN also recorded amongst the highest mean daily solar radiation, evaporation and temperature (see Table 4.2) but low total rainfall during September (see Figure 4.3). These conditions indicate that there is less water vapour in the vicinity of station KUAN. As a result it may affect the GPS signals less during the inter-monsoon period. In contrast, large RMS residuals for station KUAN are obvious during the two monsoon periods.

Secondly, one can clearly see the monthly RMS residuals in Test 2 and Test 3 are much smaller compared to Test 1. As in the previous experiment, this outcome is to be expected since no model was applied in Test 1. Hence, the ability of both the Saastamoinen and modified Hopfield models to mitigate the tropospheric delay in this area is clear. Finally, Figure 4.11 reveals that the longer the baseline, the greater the separation between the RMS residuals in Test 1 and Test 2. This is also true between Test 1 and Test 3. This result implies that the larger the delays the better the performance of the a priori models. In spite of this, the RMS residuals for the shortest (UTMJ-NTUS) and the longest (UTMJ-BEHR) baselines are still in the range of 4cm to 9cm.

Further analyses can be performed using the percentile improvements diagrams, Figures 4.12-4.14, for the months of July, September and December respectively.

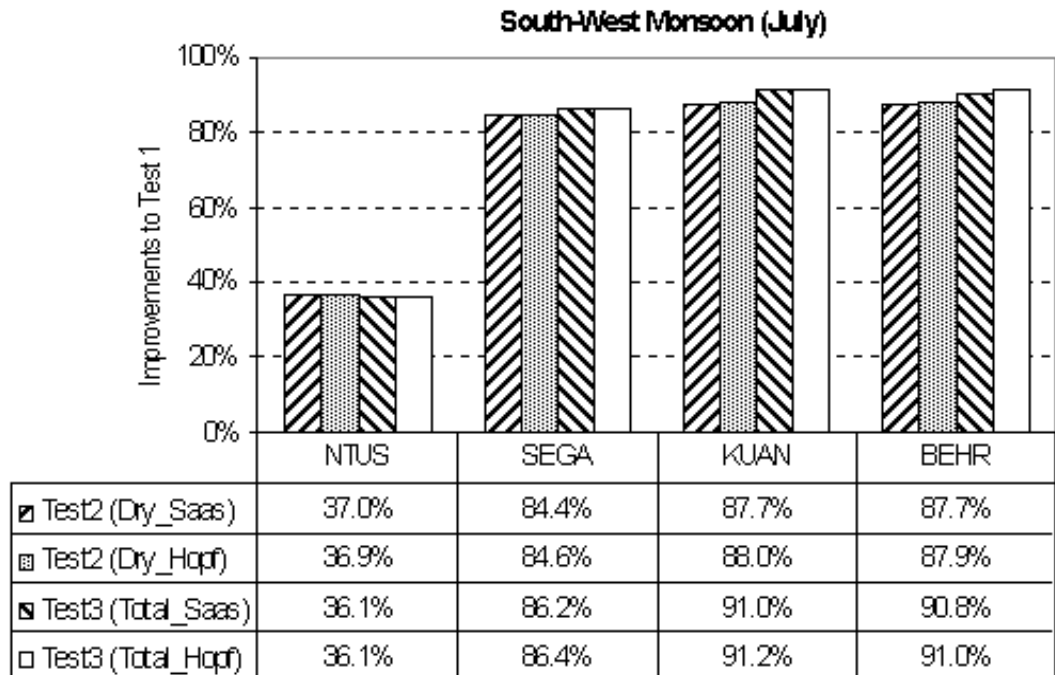


Figure 4.12 South-West monsoon; percentile improvements in the RMS residuals in Test 2 (dry models) and Test 3 (total models) with respect to Test 1 (no model). All stations define baselines relative to UTMJ.

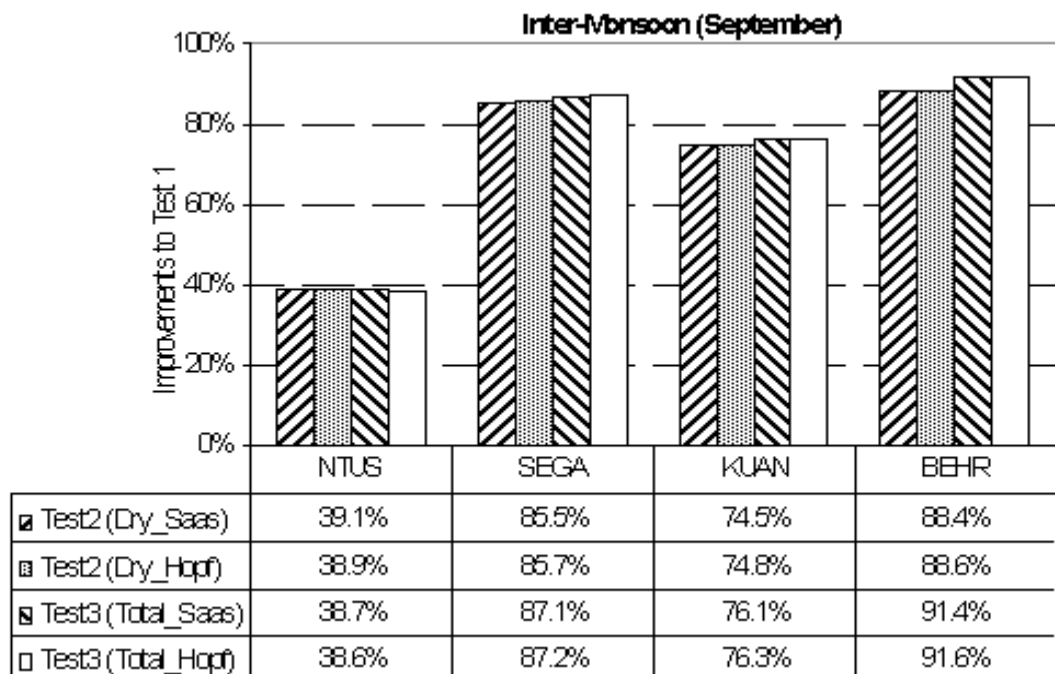


Figure 4.13 Inter-monsoon; percentile improvements in the RMS residuals in Test 2 (dry models) and Test 3 (total models) with respect to Test 1 (no model). All stations define baselines relative to UTMJ.

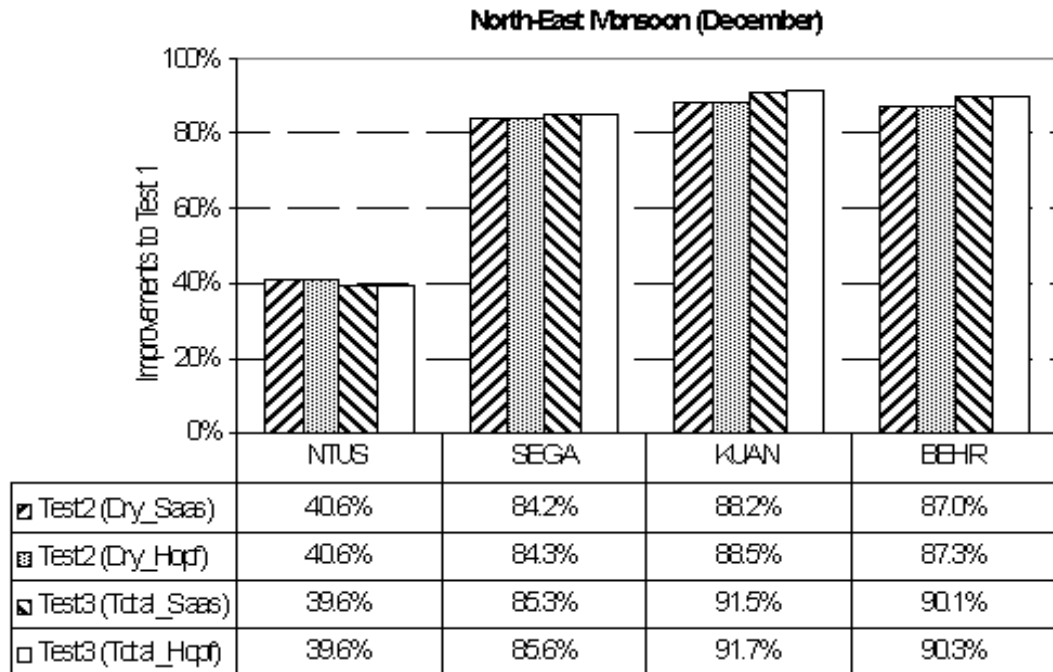


Figure 4.14 North-East monsoon; percentile improvements in the RMS residuals in Test 2 (dry models) and Test 3 (total models) with respect to Test 1 (no model). All stations define baselines relative to UTMJ.

As can be noted in Figures 4.12-4.14, the two dry models in Test 2 both show almost identical percentile improvements. This is also true for the two total models in Test 3. The modified Hopfield has demonstrated a slightly better result ($\sim 0.2\%$) except for the short baseline UTMJ-NTUS in Test 2 during the South-West and inter-monsoon periods. The overall results show that the total models (Test 3) have about 4% percentile improvements over the dry models (Test 2). These results were not much different to those reported in section 4.2.2. On the other hand, neither model performed well in modelling the wet delay component of the troposphere in this area.

Figures 4.12-4.14 indicate that the short baseline UTMJ-NTUS has the lowest percentile improvements ($<41\%$) in spite of significant residual tropospheric delay. There is no obvious explanation for this, but it is believed that both a priori tropospheric models have a certain (minimum) limit to model the delay. In this case (short baseline length of 25km and height difference of 0.005km), it almost reaches the limit. The total models (Test 3) also indicate slightly worse results compared to the dry models (Test 2) for this baseline. Therefore, questions still remain whether to choose between the dry or total delay models when the baseline is short and the height difference is small.

Questions may also arise concerning the performance of the other a priori models in this area. Hoffmann-Wellenhof et al. (2001) suggest that one reason why so many a priori models have been developed is because of the challenge in modelling the wet delay. Unlike in the case of the dry delay, the problem of wet delay modelling remains a considerable subject of interest. Thus, it can be assumed that if other models were applied in this area, a similar conclusion could be drawn as for the previously two tested models. In the next section the effect from the residual tropospheric delay on the station coordinates during the monsoon period will be investigated.

4.3 Coordinate Repeatabilities During The Monsoon

The a priori troposphere model cannot effectively remove the wet delay, and leaves the residuals unmodelled. High accuracy GPS positioning still requires the residuals to be reduced by an appropriate modelling. Duan et al. (1996) and Zhang & Lachapelle (2001) mention that the tropospheric delay residuals can be modelled as a function of elevation angle and associated mapping function. Chen et al. (2000) proposed a conventional Kalman filter to estimate residual tropospheric delay, and Hu et al. (2005) applied an adaptive Kalman filter as an extension to this work.

In post-processing techniques, the residual delay is often accounted for by introducing additional unknown (estimable) parameters in the least square estimation process. For example, a ‘scale factor’ for every station per session can be estimated. The estimation of the scale factor (or ‘troposphere parameter’ as it is sometimes known) tends to average the residual tropospheric delay and thus improves the results. Considering the a priori troposphere correction (for example in Equation 2.30) and the troposphere parameters, the total tropospheric delay correction for a GPS signal can be written as (Rothacher & Mervart, 1996):

$$dtrop_{P_{corr,total}} = dtrop_{P_{corr,apr}} f_{apr}(z) + \alpha(t)f(z) \quad (4.1)$$

where,

$dtrop_{P_{corr,total}}$ = total tropospheric delay correction

$dtrop_{P_{corr,apr}}$ = a priori correction from a specified model.

z	= zenith distance from GPS satellite to the receiver
$f_{\text{apr}}(z)$	= mapping function for the a priori model
$f(z)$	= mapping function for the troposphere parameter. It can be the same as (or different from) $f_{\text{apr}}(z)$
$\alpha(t)$	= time dependent troposphere parameter for the station

However, the scale factor is only a constant offset to the a priori model and does not account for the time varying nature of the atmosphere. Alternatively, a time-varying polynomial scale factor can be introduced to estimate several troposphere parameters per session such as (Chang & Tseng, 1999):

$$\alpha = \alpha_0 + \alpha_1(t_i - t_0) + \alpha_2(t_i - t_0)^2 + \dots + \alpha_n(t_i - t_0)^n \quad (4.2)$$

The polynomial model is then correlated through time via the connection between a start epoch (t_0) and the current measurement epoch (t_i). Further processing strategies for the scale factor parameter estimation are discussed in the next section. Another viable approach is to use a stochastic estimation approach using a first-order Gauss-Markov or random walk process via the Kalman filter technique (Dodson et al., 1996). The mathematical overview and comparison between the least squares and the Kalman filter approach for estimating the troposphere parameter were discussed by Beutler et al. (1998b).

The BERNESE software provides strategies for combining the baseline results (individual solution) from each session into a network (combined) solution. This is possible using the combination of individual sets of normal equations (saved in the previous run). Hence, estimates for each individual solution can be compared with the combined solution and an analysis of coordinate repeatabilities can be made. The strategy is also useful for detecting outliers. As a result, suspect individual station solutions can be pre-eliminated. In addition, handling the troposphere parameters, such as reducing the numbers of parameters or tuning the stochastic elements of the parameters, is simplified. Further details and a description of the step-by-step strategies for the network solution can be found in Rothacher & Mervart (1996). The process is described also in Figure 4.5.

To study the effect of the tropospheric delay residuals on the estimated station coordinates, all the data from the monsoon experiments (section 4.2.3) are further processed by applying the estimated tropospheric scale factor. In this section, the troposphere parameters for all stations were estimated every 2hours per station and per session (one session equivalent to 24hour data). The total Saastamoinen a priori model was used, the cut-off elevation was set at 15° and the mapping function in Equation 2.11 was used. After excluding some individual solutions during the outlier detection process, the coordinate repeatabilities of each station's North, East and Up components were noted.

Figures 4.15 and 4.16 show the coordinate repeatabilities for the station SEGA during the South-West monsoon, with and without the estimation of the scale factor respectively. Since both figures were selected for the same number of days, direct comparison can be made. Figures 4.17 and 4.18 are the equivalent scenarios for station BEHR during the North-East monsoon. Note that there is a very significant improvement, especially in the station Up component, after the scale factor was applied.

Tables 4.7, 4.8 and 4.9 summarise the RMS values of the coordinate repeatabilities (of individual coordinate residuals with respect to a combined solution) for all the stations during the South-West monsoon, inter-monsoon and the North-East monsoon periods. Results from these tables indicate that the scale factor can improve the precision of the coordinate. The RMS repeatabilities are improved by a few millimetres in the North and East direction for all cases. The RMS of the Up components show improvement by 12mm to 36mm, except for the station NTUS which degrades a little to 0.3mm during the South-West monsoon and 5.3mm during the North-East monsoon periods. The RMS repeatabilities during the two monsoon periods (Tables 4.7 and 4.9) were not as good as the results during the inter-monsoon period (Table 4.8) when no scale factor is applied. After applying the scale factor, their differences are minimal, at the level of only a few millimetres.

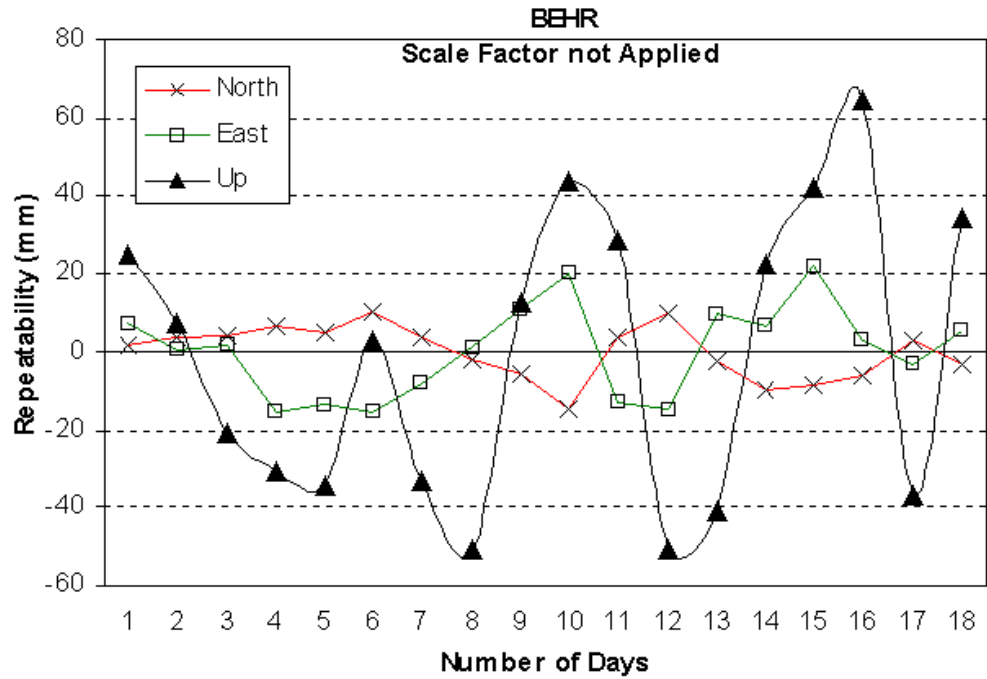


Figure 4.15 Coordinate repeatabilities for station BEHR during the North-East monsoon without applying the scale factor.

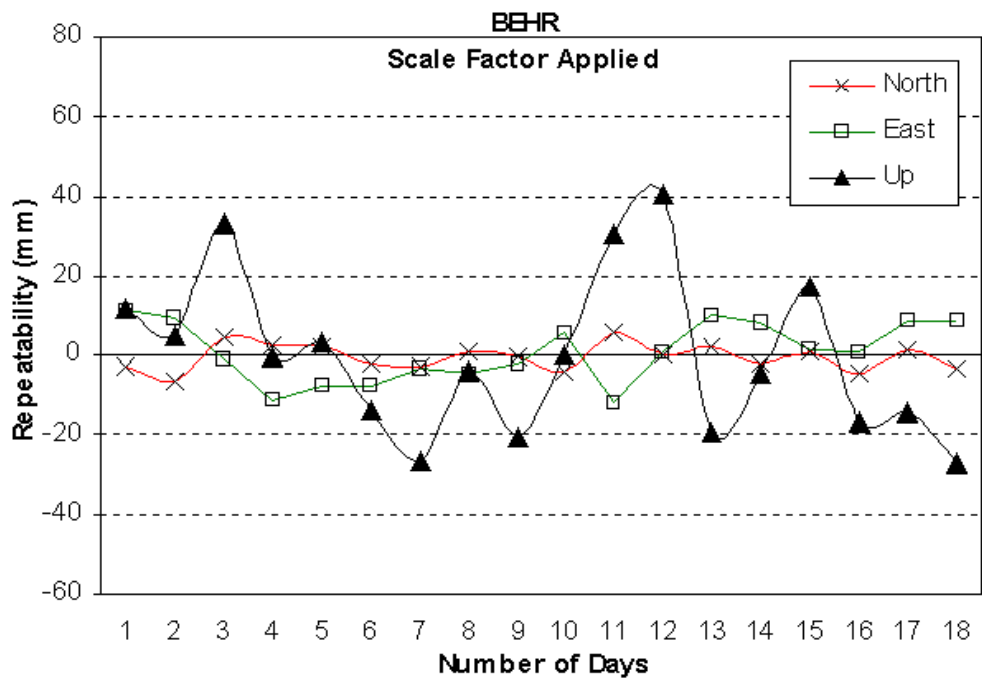


Figure 4.16 Coordinate repeatabilities for station BEHR during the North-East monsoon with applying the scale factor.

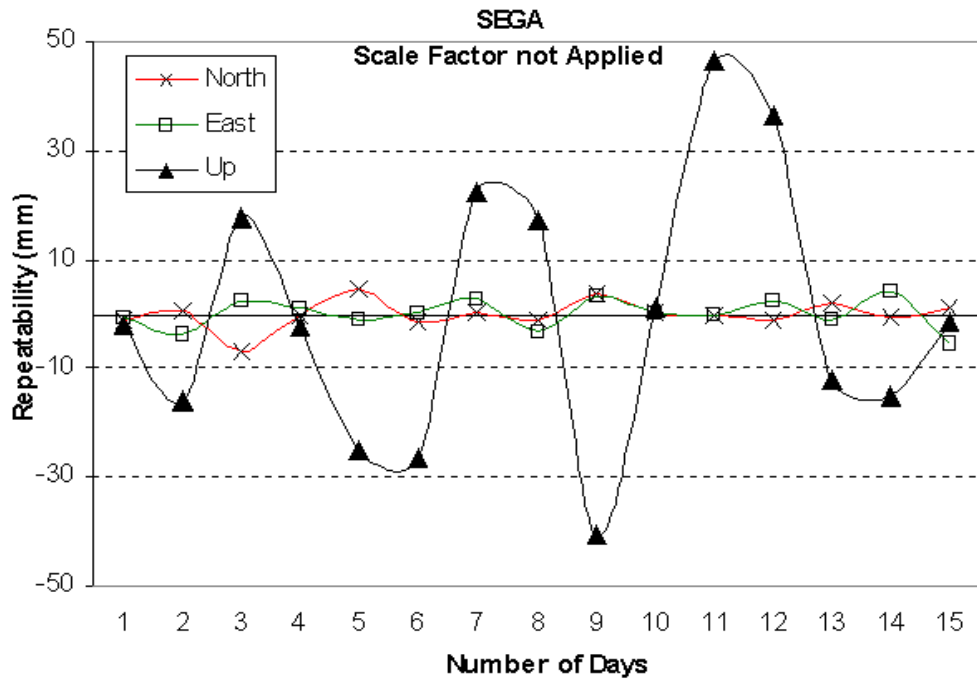


Figure 4.17 Coordinate repeatabilities for station SEGA during the South-West monsoon without applying the scale factor.

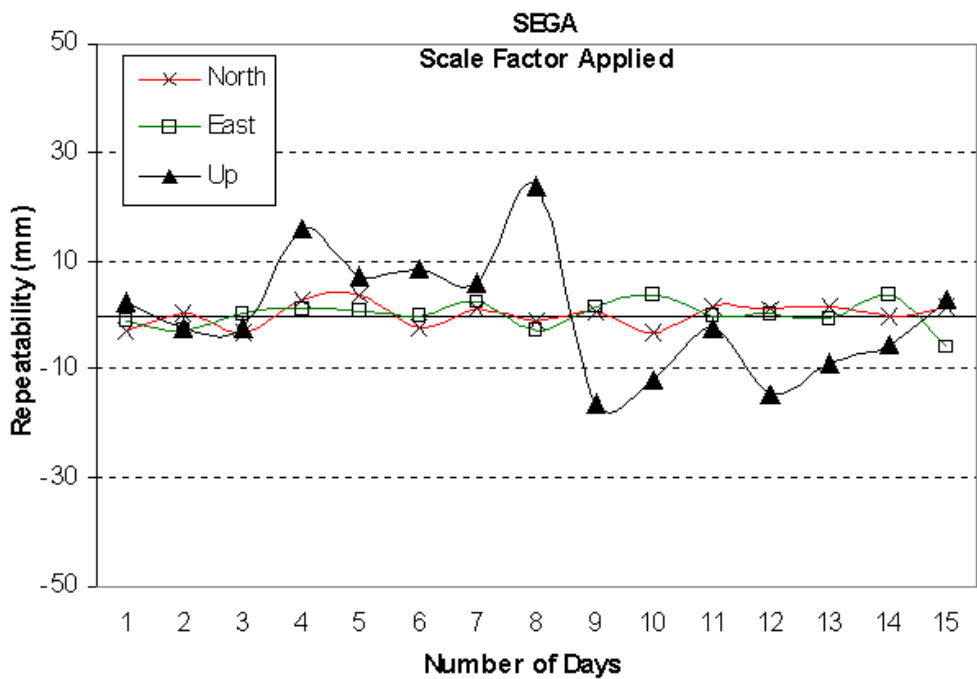


Figure 4.18 Coordinate repeatabilities for station SEGA during the South-West monsoon with applying the scale factor.

Table 4.7 RMS of coordinate repeatability for July 2003 (South-West Monsoon).

STN	No Scale Factor			Scale Factor Applied		
	N (mm)	E (mm)	Up (mm)	N (mm)	E (mm)	Up (mm)
NTUS	4.6	3.6	17.1	4.4	3.5	17.3
SEGA	2.6	2.8	24.2	2.2	2.5	11.1
KUAN	5.0	1.9	47.8	3.8	1.4	12.2
BEHR	5.0	5.1	44.5	2.9	3.9	18.2

Table 4.8 RMS of coordinate repeatability for September 2003 (Inter-Monsoon).

STN	No Scale Factor			Scale Factor Applied		
	N (mm)	E (mm)	Up (mm)	N (mm)	E (mm)	Up (mm)
NTUS	4.2	3.7	15.8	3.8	2.5	14.0
SEGA	2.2	2.7	24.6	2.7	2.5	11.3
KUAN	3.6	1.8	34.0	2.9	1.7	9.8
BEHR	4.8	5.7	30.6	2.8	4.5	18.7

Table 4.9 RMS of coordinate repeatability for December 2003 (North-East Monsoon).

STN	No Scale Factor			Scale Factor Applied		
	N (mm)	E (mm)	Up (mm)	N (mm)	E (mm)	Up (mm)
NTUS	3.3	4.3	10.4	3.0	3.6	15.7
SEGA	3.9	3.2	46.5	2.8	2.5	13.1
KUAN	7.8	4.2	27.2	3.7	1.1	5.6
BEHR	6.9	11.8	36.9	3.3	7.4	20.7

4.4 The Monsoon Zenith Path Delay

Equation 4.1 in another sense is the estimate of the sum of the dry and wet delay in the zenith direction, denoted as (total) tropospheric zenith delay, zenith total delay (ZTD) or simply as tropospheric zenith path delay (ZPD) (see also section 2.2.3: Troposphere Path Delay Modelling). The (zenith) dry delay dominates the ZPD, and has typical magnitude of about 2.3m at mean sea level (Businger et al., 1996) but varies less than 1% over a few hours (Spilker, 1996c). The wet component of the troposphere is a function of the water vapour content along the signal path (Langley, 1998a). The (zenith) wet delay can be less than 10mm in arid regions and as large as 400mm in humid regions (Businger et al., 1996). Unlike the dry delay, the wet delay is highly variable both spatially and temporally. The ZPD gives insight into the atmospheric conditions above the GPS site. Figure 4.19 shows the example of ZPD estimated from

three different IGS sites; KOUR in the equatorial (and coastal); ZIMM at a mid-latitude sites; and MCM4 in the Antarctica.

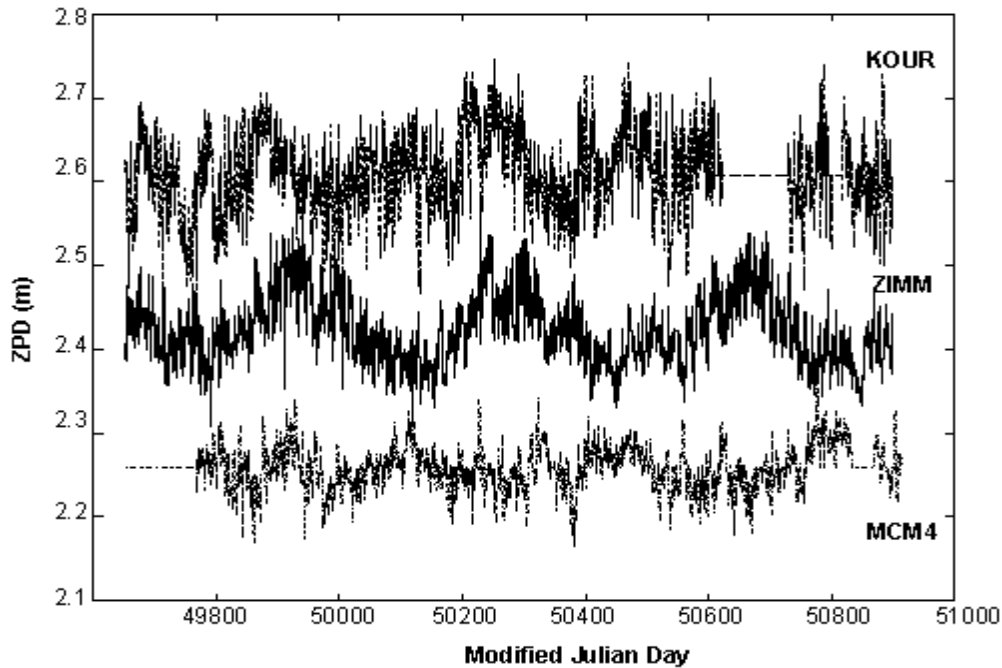


Figure 4.19 Estimation of ZPD (time resolution of 6-hour). Site KOUR in the equatorial region shows the highest, short term variability. Site ZIMM in a mid-latitude region shows a clear annual signal (maximum in summer, minimum in winter). Site MCM4 in Antarctica has the smallest mean ZPD due to the dry Antarctic conditions (Beutler et al., 1998c).

Knowing the precise ZPD value and the surface pressure to an accuracy of 0.3mb (or better) can remove the dry delay (Elgered et al., 1991), thus retaining the wet delay. This relation leads to the potential use of GPS in meteorological research (Bevis et.al, 1992), which is now being extensively conducted (see also section 2.2.3: Tropospheric Delay Effect and Current Modelling Trends). However, after the elimination of the ionospheric delay and orbital errors, the estimated ZPD can still be contaminated by unmodelled errors which are most likely dominated by station-dependent errors (hardware-based errors, multipath and imaging, and measurement noises). The focus is now to investigate the ZPD estimation using the MASS network. As a starting point, strategies for ZPD estimation will be discussed.

4.4.1 Strategies for ZPD Estimation

A relative ZPD (site minus reference) is important for GPS positioning. However, an accurate estimate of absolute ZPD (site specific) is crucial for meteorological applications. Two strategies are recommended in the BERNESE software for the estimation of ZPD (via Equations 4.1-4.2) (Rothacher & Mervart, 1996):

Strategy 1: Estimate for all n stations in a regional or global size network.

Strategy 2: Estimate for all stations except the reference station (n-1) in the case of small network or short baseline.

Rocken et al. (1993) claim that Strategy 1 must be used for baselines longer than 500km to obtain a precise estimate of absolute ZPD. He also found that Strategy 2 can provide good estimates of absolute ZPD (to a secondary station) for baselines less than 50km. However, precise meteorological data from radiometer and barometer instruments is needed at the reference station. Duan et al. (1996) state in the case of small networks, the differential (zenith) delay is sensitive only to the relative ZPD, not to the absolute ZPD. The problem arises because receivers at each end of a short baseline observe satellites at a similar elevation angle. This can be explained by considering the two receivers i and j observing the single satellite:

$$\delta ZPD = ZPD_i f(\theta_i) - ZPD_j f(\theta_j) \quad (4.3)$$

where ZPD is the absolute ZPD for station i or j, $f(\theta)$ is the mapping function and θ is the elevation angle. Thus, as the two receivers are getting closer:

$$\delta ZPD \rightarrow (ZPD_i - ZPD_j) f(\theta_i), \text{ as } \theta_j \rightarrow \theta_i \quad (4.4)$$

The problem of using Strategy 1 or Strategy 2 in GPS processing has been identified by Brunner & McCluskey (1991). They studied these approaches using the simulation of small networks (baseline <11km), medium networks (baseline <112km) and large networks (baseline <1110km). Their study concluded:

- a) Strategy 1 always yields correct results for all parameters (ZPD, baseline, position, etc), except for very small networks where relative ZPD values are correct but the absolute ZPD can be in error.
- b) Strategy 2 always gives incorrect ZPD values and station height estimation, as well as incorrect latitudes, baseline length and ambiguity values, except for small networks with baselines shorter than 50km when the strategy gives errors which are negligibly small.

To study which strategies are better for use with the MASS network, the 24hour datasets in section 3.4.1 were further analysed. These four stations were sufficient for this purpose since there are long (339km), medium (143km) and short (25km) baselines. IGS station NTUS is included to verify the results from Strategy 1 and Strategy 2 since it can provide high quality absolute ZPD estimates from IGS analyses (via <ftp://garner.ucsd.edu/pub/troposphere/>). The data was processed with 15° cut-off elevation, the total Saastamoinen model was used, and the mapping function in Equation 2.11 was applied. In both strategies, the troposphere parameters were only estimated every 4-hours for a 24hour period to reduce the computational load. The absolute ZPD estimated using Strategy 1 and Strategy 2, and the IGS-derived value (for station NTUS) are given in Figure 4.20.

Some comments can be made:

- a) Strategy 1 provides reasonable values for absolute ZPD in the equatorial region. The difference from the IGS-derived estimates for station NTUS is less than 10cm.
- b) Strategy 2 provides unreasonable values for absolute ZPD in equatorial region. The difference from the IGS-derived estimates for station NTUS is more than 20cm.
- c) The a priori values for stations BEHR, SEGA and NTUS are 2.383m, 2.380m and 2.399m respectively. The offset of this value to Strategy 1 is about 20cm, most likely because of the poorly modelled wet delay (residual tropospheric delay).

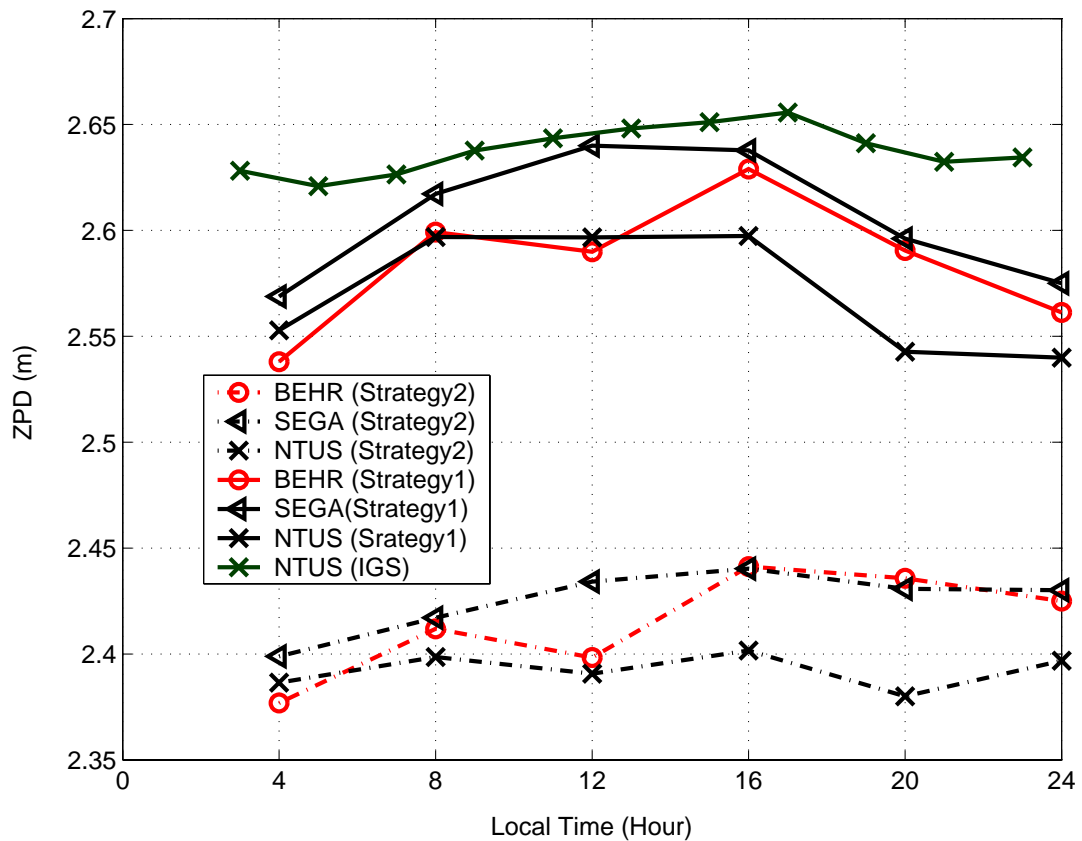


Figure 4.20 Strategy 1 (n station approach) vs Strategy 2 (n-1 station approach; reference station UTMJ excluded). The troposphere parameters for all stations were estimated every 4-hours to obtain estimates of absolute ZPD. The IGS-derived absolute ZPD value for station NTUS is plotted (every 2-hours).

4.4.2 Monsoon ZPD & Sensitivity of ZPD to Network Size

In the case of the MASS network, it is not so clear whether this size of network can provide precise estimates of the ZPD. Nevertheless, the IGS stations surrounding the MASS network in South-East Asia can be utilised to provide enough satellite elevation in the ZPD estimation (since their distance from MASS is more than 1000km). This section reports on analyses of the ZPD values during the two monsoon periods. For the above reasons, two networks were tested:

- The 'regional network' - here the IGS and the MASS stations, as in Figure 4.1.
- The 'local network' - here the MASS stations. However, the IGS station NTUS is also considered part of the local network due to its close proximity to the MASS network.

One-week datasets were selected during each monsoon period; DoY 204-210 (July 23-29 2003; South-West monsoon) and DoY 323-329 (November 9-25 2003; North-East monsoon). Station KTPK was selected as the reference. Three MASS stations were excluded: IPOH (due to bad observation data), KUAN and SEGA (their distance from the reference is less than 200km). All IGS datasets were downloaded from <ftp://garner.ucsd.edu/pub>. Table 4.10 summarises important inputs and characteristics of the estimation of the ZPD from both networks.

Table 4.10 Summary of inputs and processing features for ZPD estimation.

Measurements	'Fixed' DD L1 & DD L2 via DD IF
Orbit Type	Precise/Final IGS orbit
Ambiguity Technique	Quasi-Ionosphere Free (QIF)
Cut-off Elevation	20°, 15° and 10°
A Priori Trop. Model	Total Saastamoinen with standard atmosphere
Troposphere Parameter	Strategy 1 (n approach)
Number of Troposphere Params	Every 2hour for 24hour period; per station
Mapping Function	Cosine function
Apriori Station Coords	Precise ITRF at epoch J2000 (network provider)

Since IGS analysis centres are assumed to provide the most 'probable' values of absolute ZPD for station NTUS, sensitivity analysis of the absolute ZPD estimation to the size of the different networks can be assessed. This is possible because station NTUS is common to the IGS, as well as the regional and local networks. Further explanation is given in Equations 4.5-4.6:

$$\Delta ZPD^{\text{Regional}} = ZPD_{\text{NTUS}}^{\text{IGS}} - ZPD_{\text{NTUS}}^{\text{Regional}} \quad (4.5)$$

$$\Delta ZPD^{\text{Local}} = ZPD_{\text{NTUS}}^{\text{IGS}} - ZPD_{\text{NTUS}}^{\text{Local}} \quad (4.6)$$

where the symbol Δ is the difference of the absolute ZPD; all superscripts define the network category and all subscripts identify the station. It is also important that the time estimate of the absolute ZPD from the local and regional networks should be aligned with the IGS estimate (BERNESE provide this utility).

On the other hand, sensitivity analysis of the relative ZPD to different networks can also be conducted. This is possible because Strategy 1 (see section 4.4.1) can provide the

absolute ZPD estimate for all stations, including the reference station (station KTPK). In this case, all stations are common to the regional and local networks. This can be explained by the following Equations 4.7-4.8 (by considering the two stations KTPK and NTUS):

$$\delta ZPD^{\text{Regional}} = ZPD_{\text{Reference}}^{\text{Regional}} - ZPD_{\text{NTUS}}^{\text{Regional}} \quad (4.7)$$

$$\delta ZPD^{\text{Local}} = ZPD_{\text{Reference}}^{\text{Local}} - ZPD_{\text{NTUS}}^{\text{Local}} \quad (4.8)$$

where the symbol δ denotes the difference of relative ZPD; all superscripts define the network category and all subscripts are the station name.

Figures 4.21-4.22 and the corresponding statistical Tables 4.11-4.12 show the results of the two week analyses for station NTUS during the South-West and North-East monsoon periods. As can be noted, both the regional and local networks show the same trend with the IGS ZPD estimate. The (mean) absolute ZPD from all networks during the South-West monsoon are about 2.6m, but become larger than 2.64m during the North-East monsoon. In any case, the mean offsets to the (constant) a priori model are larger than 0.2m. This value is the usual value in humid regions, as claimed by Businger, et al. (1996), which is associated with the wet delay that cannot be effectively modelled by the total Saastamoinen model. The short term variations of these absolute ZPD values during both weeks can be clearly noticed. The variations from both the regional and local networks are found to be larger than the IGS estimates, particularly during the North-East monsoon period.

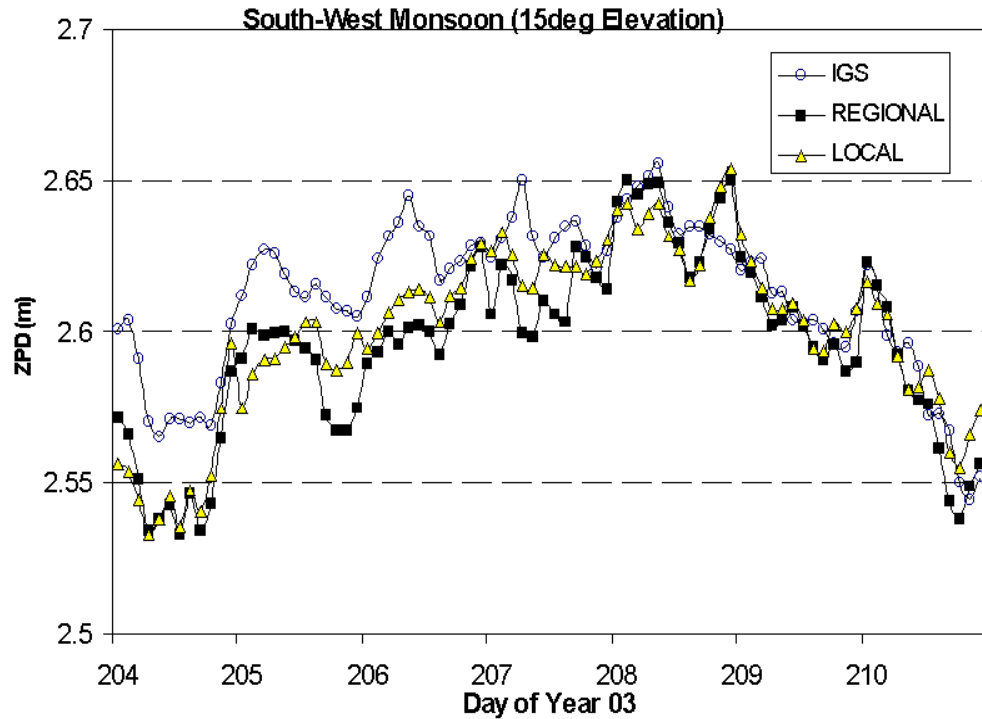


Figure 4.21 One-week continuous absolute ZPD estimates (every 2-hours) for station NTUS derived from IGS, regional and local networks during the South West monsoon.

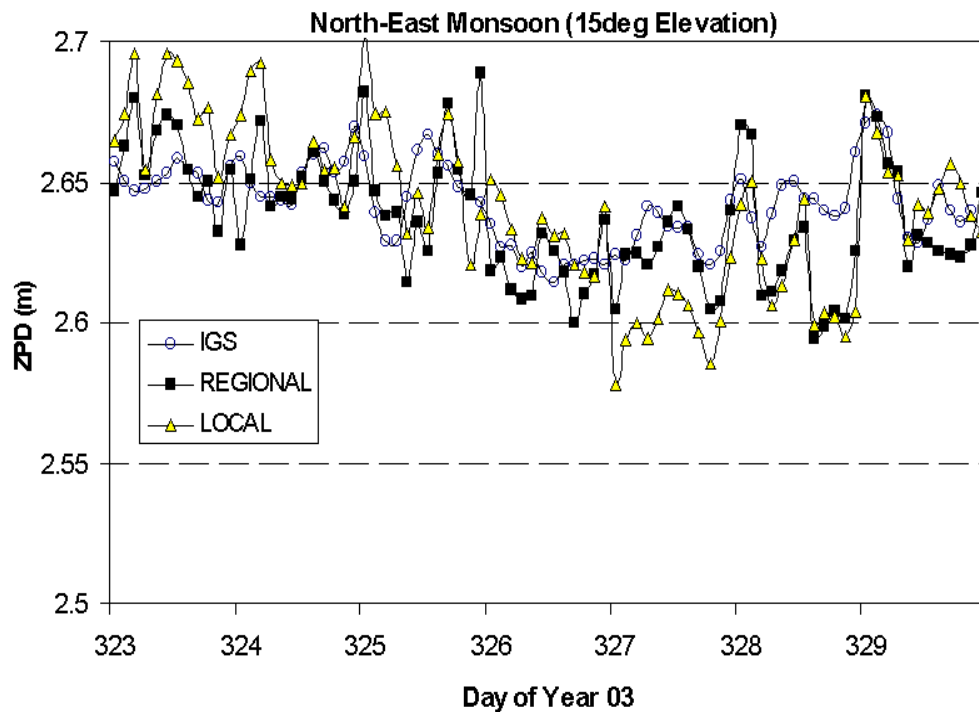


Figure 4.22 One-week continuous absolute ZPD estimates (every 2-hours) for station NTUS derived from IGS, regional and local networks during the North-East monsoon.

Table 4.11 Statistics for the absolute ZPD estimate during the South-West monsoon according to Figure 4.21.

Network	Mean	RMS	Max	Min
IGS	2.612	0.025	2.656	2.544
Regional	2.596	0.030	2.650	2.533
Local	2.601	0.029	2.654	2.533

Note: A priori model value for NTUS is constant at 2.380m

Table 4.12 Statistics for the absolute ZPD estimate during the North-East monsoon according to Figure 4.22.

Network	Mean	RMS	Max	Min
IGS	2.643	0.014	2.674	2.615
Regional	2.637	0.023	2.689	2.595
Local	2.642	0.030	2.701	2.578

Note: A priori model value for NTUS is constant at 2.380m

Figures 4.23-4.24 show the results of $\Delta ZPD^{\text{Regional}}$ and $\Delta ZPD^{\text{Local}}$ (difference of absolute ZPD; see also Equations 4.5-4.6). As can be seen, both $\Delta ZPD^{\text{Regional}}$ and $\Delta ZPD^{\text{Local}}$ are in the range of $\pm 0.05\text{m}$. This is true for both the monsoon periods. Figures 4.25-4.26 provide the statistics (mean and RMS values) of $\Delta ZPD^{\text{Regional}}$ and $\Delta ZPD^{\text{Local}}$ for the 10° , 15° and 20° cut-off elevations. From Figure 4.25, the largest mean (0.027m) was found during the North-East monsoon period in the case of $\Delta ZPD^{\text{Local}}$ with 10° cut-off elevation. Figure 4.26 indicates that the variations in $\Delta ZPD^{\text{Regional}}$ are less than $\Delta ZPD^{\text{Local}}$. This is true for all the cases, except for the South-West monsoon period analysis with 20° cut-off elevation (same variations). These results imply the regional network can provide better precision (wrt IGS) for the absolute ZPD estimation as compared to the local network.

The results at 10° cut-off elevation show no improvement, and are even worse for the North-East monsoon period. Theoretically, the inclusion of low elevation angle observations should provide data redundancy, improve the satellite geometry, and decorrelate the estimates of the absolute ZPD and station heights. A reasonable explanation to this may be associated with the simple cosine mapping function that has

been used. Niell (1996) claimed the cosine function produced an error greater than 1cm at an elevation angle of 10° (see also section 2.2.3: Troposphere Mapping Function). These results indicate accurate absolute ZPD estimates are not easy to achieve. Rocken, et al. (1995) described a ‘rule’: 6.5cm of GPS wet signal delay is approximately 1cm of precipitable water (the depth of water that would result if all atmosphere water vapour in a vertical column of air is condensed to liquid). Thus, accurate absolute ZPD is important for GPS meteorology.

It is worth also mentioning that the IGS absolute ZPD is derived from a combination of IGS analysis centres with different mapping functions, elevation angles as low as 3° , and different selections of reference stations and network configurations. IGS provides high quality estimates of absolute ZPD every 2-hours. Gendt (1998) points out that the consistency between the analysis centres and IGS mean value is at the 4mm level. However, the quality is not as good by a factor of 1.5 to 2 for sites in the equatorial region.

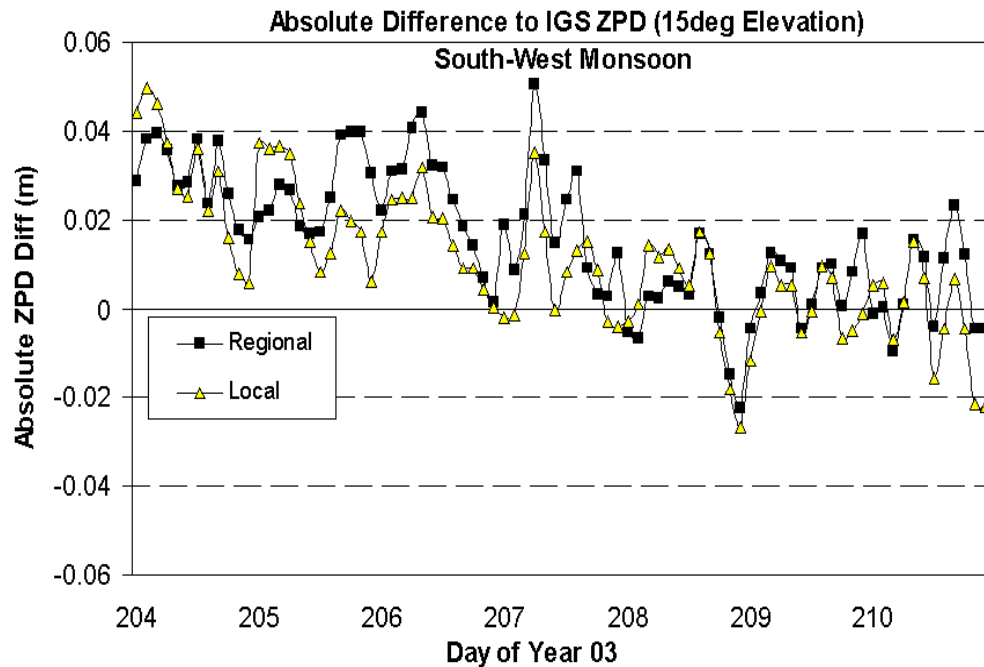


Figure 4.23 Difference of absolute ZPD from regional ($\Delta ZPD^{\text{Regional}}$; Equation 4.5) and local ($\Delta ZPD^{\text{Local}}$; Equation 4.6) networks wrt IGS-derived ZPD estimates for station NTUS during the South-West monsoon period.

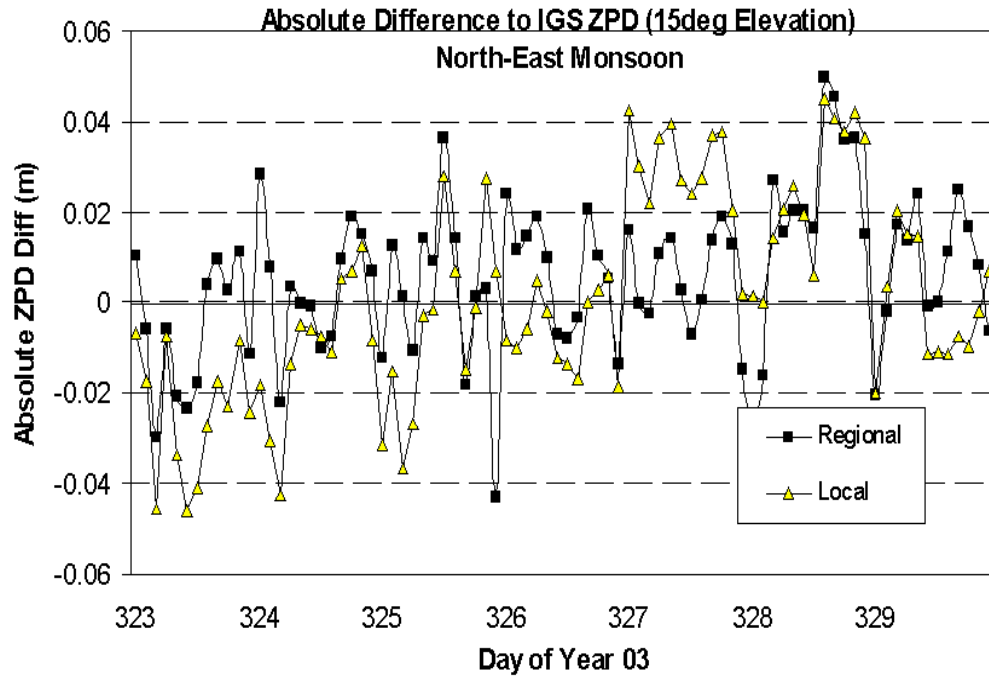


Figure 4.24 Difference of absolute ZPD from regional ($\Delta ZPD^{\text{Regional}}$; Equation 4.5) and local ($\Delta ZPD^{\text{Local}}$; Equation 4.6) networks wrt IGS-derived ZPD estimates for station NTUS during the North-East monsoon period.

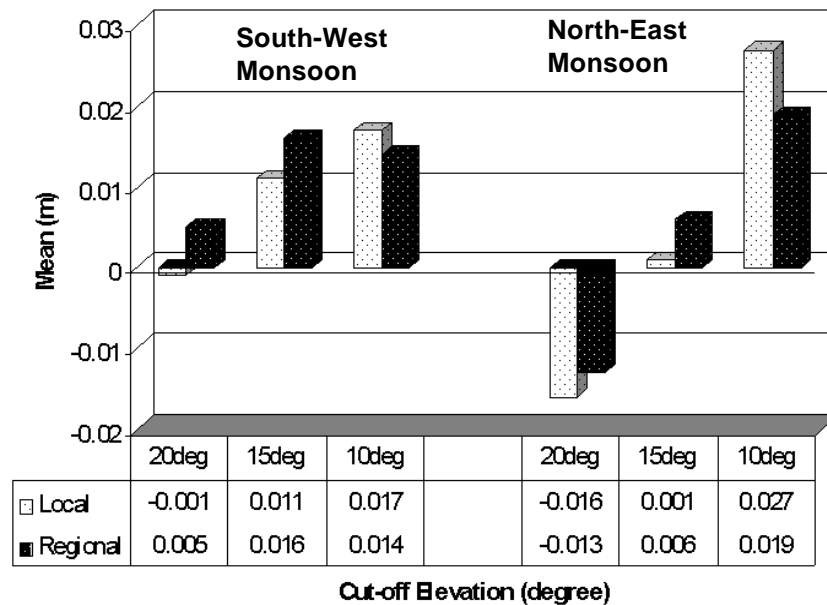


Figure 4.25 Mean values for $\Delta ZPD^{\text{Regional}}$ and $\Delta ZPD^{\text{Local}}$ during the South-West and North-East monsoon periods with respect to different cut-off elevation angles.

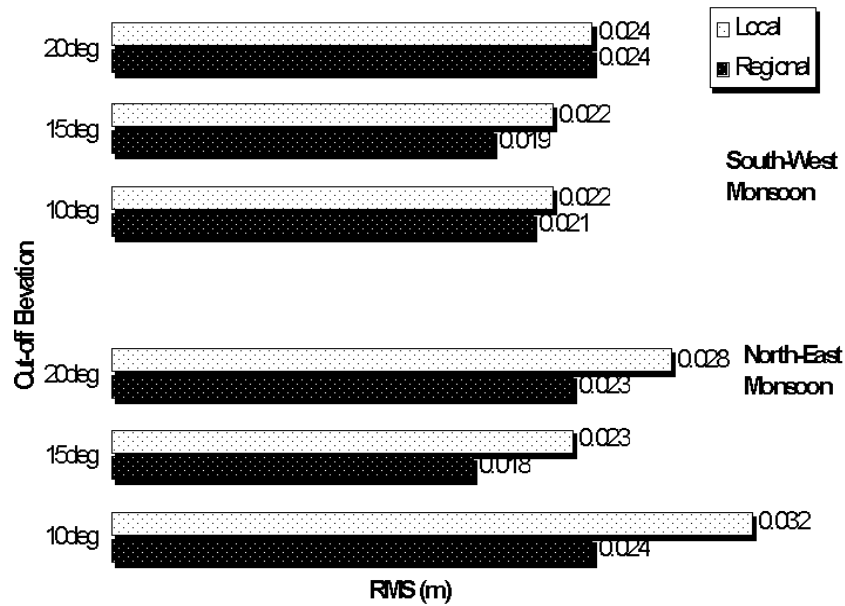


Figure 4.26 RMS values for $\Delta ZPD^{\text{Regional}}$ and $\Delta ZPD^{\text{Local}}$ during the South-West and North-East monsoon periods with respect to different cut-off elevation angles.

Figures 4.27-4.28 show the results of $\delta ZPD^{\text{Regional}}$ and $\delta ZPD^{\text{Local}}$ (difference of relative ZPD; see also Equations 4.7-4.8) using the 15° cut-off elevation. As can be seen from these figures, there is almost no difference between $\delta ZPD^{\text{Regional}}$ and $\delta ZPD^{\text{Local}}$. This is also true for both the monsoon periods and for the other cut-off elevation angles. Figures 4.29-4.30 provide the statistics (mean and RMS values) of $\delta ZPD^{\text{Regional}}$ and $\delta ZPD^{\text{Local}}$ for the 10°, 15° and 20° cut-off elevations. The mean and variations between $\delta ZPD^{\text{Regional}}$ and $\delta ZPD^{\text{Local}}$ differ by only a few millimetres. This result indicates precise relative ZPD can still be obtained without the need for a regional network. Since the relative ZPD is a major concern for (relative) precise GPS positioning, this result is an advantage for positioning activities for an area the size of the MASS network.

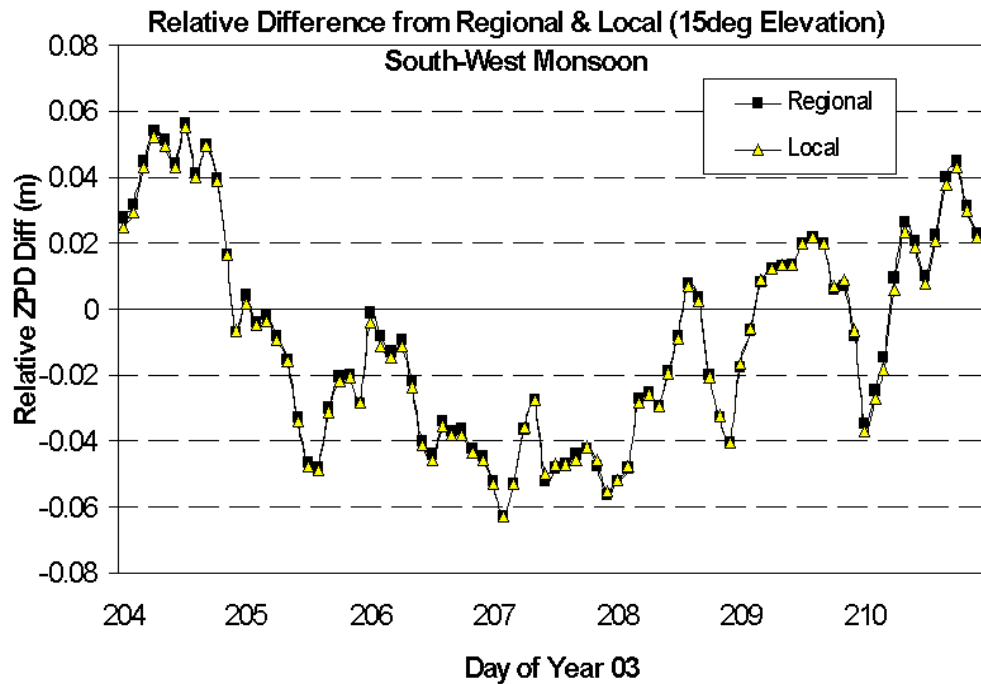


Figure 4.27 Difference of relative ZPD from regional ($\delta ZPD^{Regional}$; Equation 4.5) and local (δZPD^{Local} ; Equation 4.6) networks for baseline KTPK-NTUS during the South-West monsoon period.

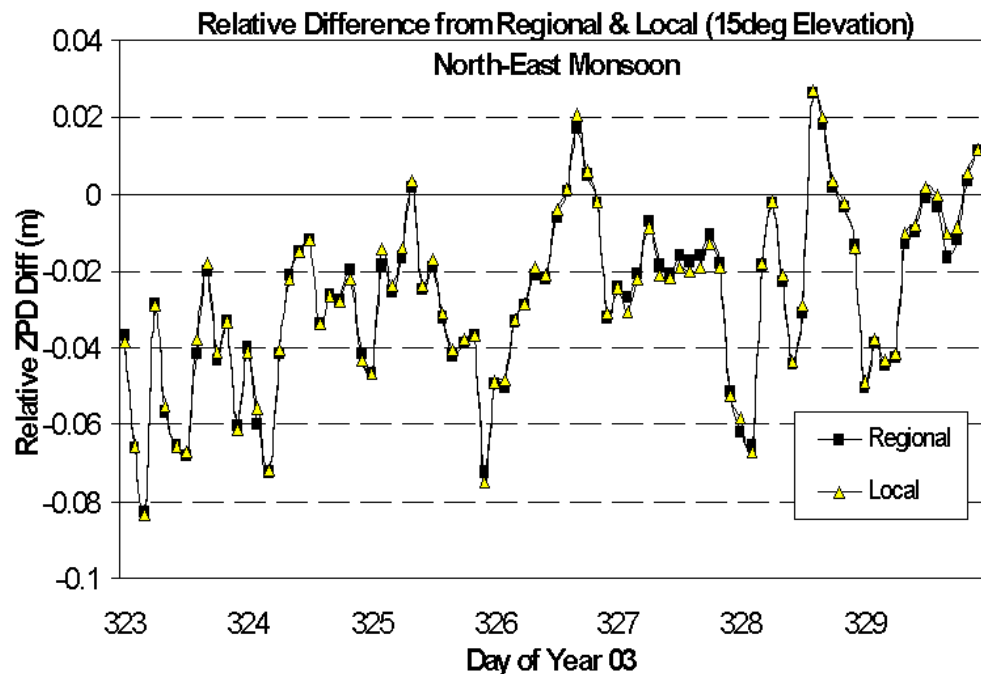


Figure 4.28 Difference of relative ZPD from regional ($\delta ZPD^{Regional}$; Equation 4.5) and local (δZPD^{Local} ; Equation 4.6) networks for baseline KTPK-NTUS during the North-East monsoon period.

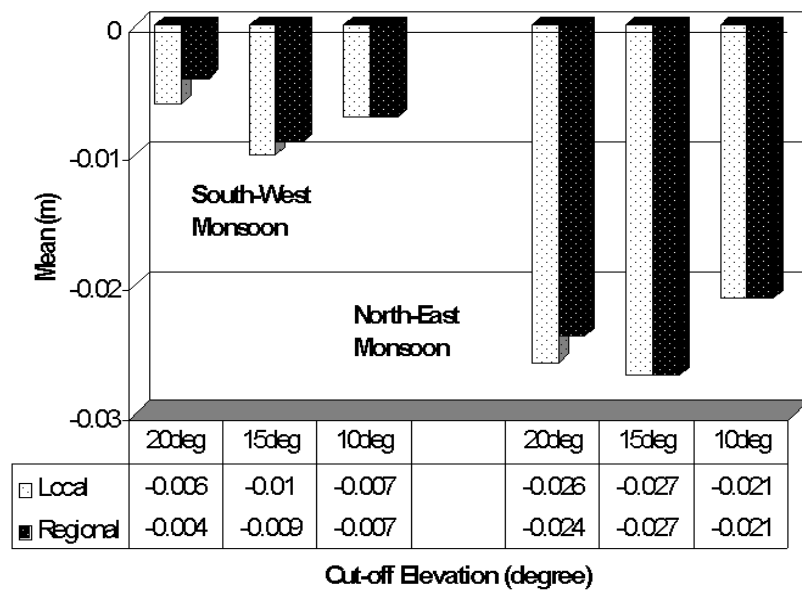


Figure 4.29 Mean values for $\delta ZPD^{Regional}$ and δZPD^{Local} during the South-West and North-East monsoon period with respect to different cut-off elevation angles.

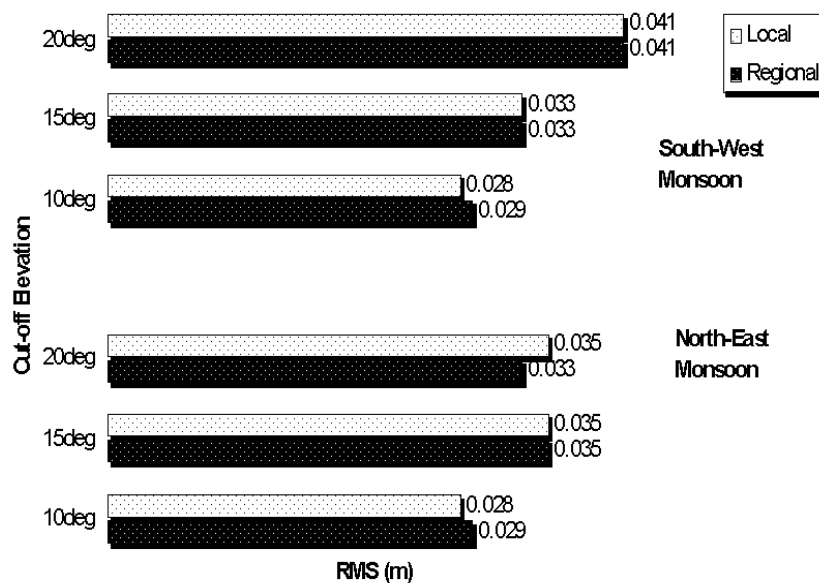


Figure 4.30 RMS values for $\delta ZPD^{Regional}$ and δZPD^{Local} during the South-West and North-East monsoon period with respect to different cut-off elevation angles.

4.5 Concluding Remarks

The present study in the focus area has found:

1. Large residual tropospheric delays are present during the North-East and South-West monsoon periods. The largest occurred during the North-East monsoon which reflects the meteorological reports of hot and wet conditions during this period. Some baselines also show large residuals during the inter-monsoon period as well. These results are expected since the focus area is located in a region where large magnitude and short term variations of the atmospheric water vapour content do occur.
2. Since the (orthometric) height differences between MASS stations are less than 0.1km, no trend relation between height and residual tropospheric delay can be established. However, the residuals are still large due to the strong variability of the meteorological conditions from place to place. Moreover, the residuals show distance-dependence.
3. The dry Saastamoinen and modified Hopfield a priori tropospheric models were able to remove up to 89% of the tropospheric delay. However, no more than 4% improvement over the dry models can be obtained once the total Saastamoinen and modified Hopfield were applied. This indicates that the wet delay is still difficult to handle by either model in the study area. Nevertheless, the Saastamoinen and modified Hopfield models were at about the same level of effectiveness in terms of modelling the tropospheric delay in this area.
4. The residual tropospheric delay can be accounted for by introducing additional (tropospheric) parameters in the least squares estimation process. Improvements in the coordinate repeatabilities were achieved of a few millimetres in the North and East direction, and the height component improved by up to 12-36mm during the two monsoon periods. Thus, the estimation of tropospheric parameters is a mandatory for high precision GPS positioning in this area.
5. The absolute ZPD during the two monsoon periods shows large magnitude and short term variations for sites in this area. The trends in local and regional networks of absolute ZPD estimates agree with the values derived by the IGS. The study shows that a better accuracy of absolute ZPD can be achieved from the regional network. Nevertheless, it was discovered that the high quality

absolute ZPD (wrt IGS) were difficult to obtain, most likely due to the use of a simple mapping function. A more sophisticated mapping function should be used to provide better absolute ZPD and to support GPS meteorology applications.

6. No significant differences were found in the estimation of relative ZPD between the regional or local networks. This is an advantage for positioning activities in this area since the relative tropospheric delay is of major concern in positioning. Hence, there is no urgent need to include the regional network for GPS positioning in this area. This also implies that further attempts to model the residual tropospheric delay for positioning purposes will be adequate by using the local network.

NETWORK-BASED POSITIONING APPROACH TO MITIGATE DISTANCE-DEPENDENT ERRORS

5.0 Introduction

Permanent GPS networks of regional scale have been established in many places around the world to support carrier phase positioning applications. Carrier phase-based positioning by combining and interpolating measurements from a network of reference stations is often referred to as “network-based positioning”. In this technique, ‘network corrections’ must be created in order to model the GPS systematic errors due to the effect of atmospheric delay and orbital error. The effect of the correction term is to reduce the distance-dependent errors for the user and to therefore improve the carrier phase ambiguity resolution (AR) - a key step for centimetre-level positioning.

The network corrections can be partitioned into dispersive (ionosphere-related) and non-dispersive (troposphere- and orbit-related) components according to their dependency on GPS signal frequency. In this research, a simple smoothing function is applied to the non-dispersive corrections. Then the smoothed non-dispersive corrections can be applied to the Ionosphere Free (IF) combination in order to reduce the residual tropospheric delay (and orbital error). Therefore these may be considered “improved IF measurements” which can be of benefit to the process of indirect L1 ambiguity resolution via various linear combinations. Once the indirect L1 ambiguity is resolved, it can be removed from the original double-differenced (DD) L1 measurements. Finally, the dispersive and non-dispersive corrections can be applied to the positioning step. To investigate this proposition, real data from two GPS networks located in different geographical areas were tested.

5.1 Concept of Network-Based Positioning

5.1.1 Background

The concept and technique of (differential) carrier phase network-based positioning was first introduced by Wanninger (1995). The technique utilises at least three reference stations from a local, continuously operating reference station network (CORS) (Figure 5.1). One of the reference stations can be treated as a ‘master station’, usually the nearest to the roving user station.

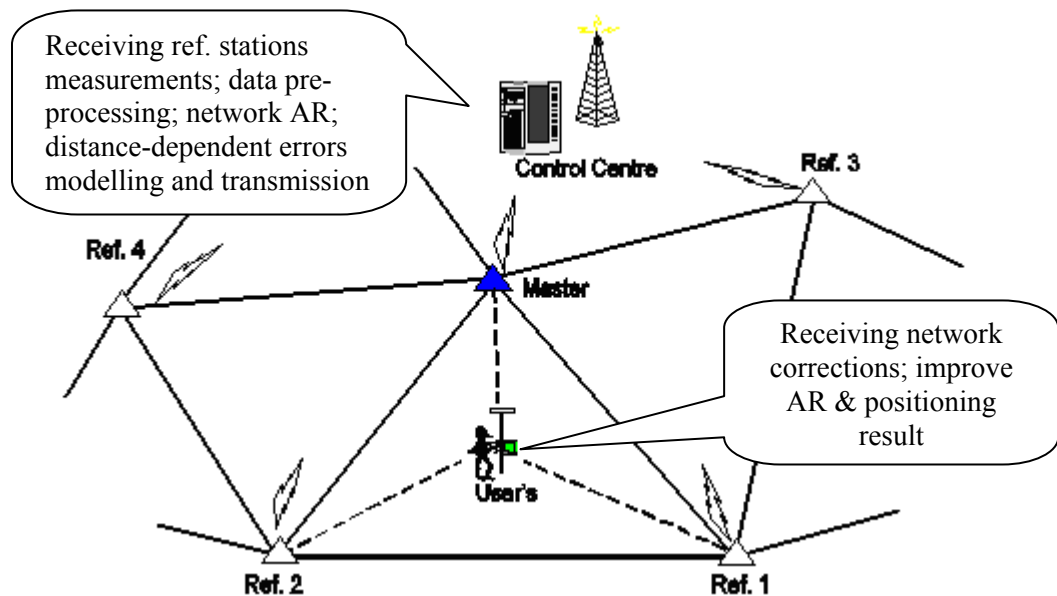


Figure 5.1 Overview of the network-based positioning technique utilising (at least) three reference stations from a CORS network.

The reference stations, through their observations of the individual satellites are able to ‘sense’ the atmospheric delay and orbital error (i.e. the source of distance-dependent errors) within the network on a satellite-by-satellite basis. The measurements from each reference station are sent to a control centre where these measurements are combined. The control centre is responsible for the basic data pre-processing, such as the cycle slip detection and repair, applying an a priori tropospheric model, applying the antenna calibration model, and resolving the network ambiguities (from master to reference stations).

Subsequently, the ‘local’ network corrections can be generated and disseminated to the user for real-time or post-mission processing. By such network modelling (discussed later), the user can process the measurements in such way that they may be considered as coming from a single reference station. A direct result of this network-based technique is the ability to mitigate the distance-dependent errors, and therefore improve the carrier phase AR (including over longer inter-receiver distances) (Fotopoulos & Cannon, 2001).

The following assumptions have been made in implementing the network-based technique (discussed in the context of DD measurements):

- Assumption 1:** Once network carrier phase ambiguities are resolved, the *residuals* contain the (remaining) *correlated* (i.e. still can be modelled) and *uncorrelated* errors within the network.
- Assumption 2:** *Correlated errors* are ionospheric delay, tropospheric delay and orbital error. They have spatial and temporal characteristics (see Chapter 3). The errors can be spatially modelled using the network-based approach.
- Assumption 3:** *Uncorrelated errors* are multipath effect, antenna offset (and variations) and measurement noise. These are station-dependent, and thus cannot be mitigated by the network-based approach. The effects are minimised by calibration (Wanninger & May, 2001; Park et al., 2004), careful site and hardware selection, and the application of special techniques (Wübenna et al., 1996).
- Assumption 4:** Correlated errors can be partitioned into *dispersive* and *non-dispersive* components. *Dispersive error* is related to the ionospheric delay, and is frequency-dependent. *Non-dispersive error* is related to tropospheric delay and orbital error, which is frequency-independent.

The above assumptions can be incorporated into the DD carrier phase measurements (see Equation 2.49 or 2.50) for any satellite pair that can be observed from a master station (m) and reference station (r):

$$\underbrace{\Delta\nabla V_{m,r}}_{\text{Residuals}} = \underbrace{\Delta\nabla L_{m,r}}_{\text{Measurements}} - \underbrace{(\Delta\nabla p_{m,r} + \lambda_{L1}\Delta\nabla N_{m,r})}_{\text{Estimated}} + \underbrace{\Delta\nabla d_{ion_{m,r}}}_{\text{Dispersive}} - \underbrace{(\Delta\nabla d_{trop_{m,r}} + \Delta\nabla O_{m,r})}_{\text{Correlated Non-Dispersive}} - \underbrace{(\Delta\nabla m_{p_{m,r}} + \Delta\nabla E_{m,r})}_{\text{uncorrelated}} \quad (5.1)$$

Note that the orbital error ($\Delta\nabla O$), as introduced in Equation 3.19, and any other uncorrelated errors not listed in Equation 5.1, are assumed to be represented by the measurement noise term.

5.1.2 Methods of Implementing the Network-Based Positioning

Currently there are two popular (commercially available) implementations of network-based positioning: Virtual Reference Station (VRS) and *Flächenkorrekturparameter* (FKP; Area Correction Parameters) or Broadcast Mode (Figure 5.2).

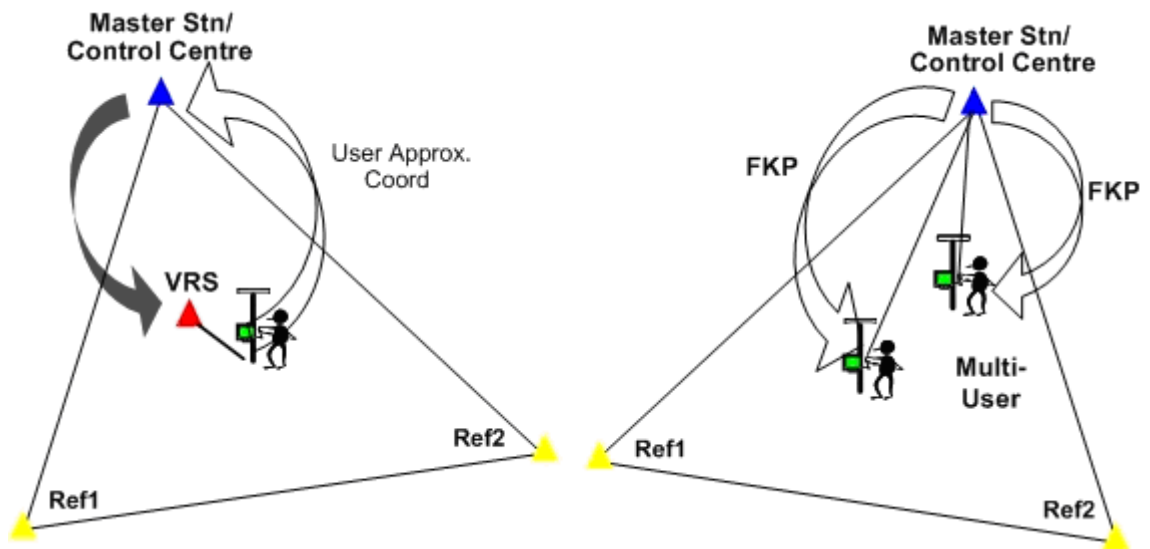


Figure 5.2 VRS (left) and FKP (right) methods utilising three reference stations.

The VRS is a combined method of network modelling and representation of the network corrections for a specific user. In contrast, the FKP can be considered as a method of representing the distance-dependent errors for the entire network, utilising broadcasts to any user within the network.

VRS

The concept of VRS (Lynn & Anil, 1995; Wanninger, 1995) is to simulate data from a local ‘virtual’ reference station located nearby to the user station. This location in fact is the user-approximated position (e.g. from a GPS single-point navigation solution), transmitted to the control centre. The VRS data are generated from the observations at a master station by adding the change of satellite geometric range to the VRS position. This can be explained by taking x^s as satellite position vector, x^r the master station vector and x^v as the VRS station position vector. At epoch t , the geometric range between satellite and master station is:

$$p_r^s(t) = |x^s - x^r| \quad (5.2)$$

and the geometric range between satellite and the VRS is:

$$p_v^s(t) = |x^s - x^v| \quad (5.3)$$

where the change in the geometric range $\Delta p^s = p_v^s(t) - p_r^s(t)$ can be applied to all observables to ‘displace’ the measurements of the GPS master station to the new ‘virtual’ position (Vollath et al., 2000; Hu et al., 2003). The data is corrected using the network corrections as calculated by the network-based algorithm in the processing centre. Next, the ‘corrected’ VRS data is transmitted to the user (near or at the VRS location). The baseline processing software in the user receiver cannot determine whether it has received ‘virtual’ reference data (Wanninger, 2003). Note that two-way communications are needed for the VRS method.

FKP/Broadcast Mode

In this implementation the network-based algorithm estimates so-called ‘network coefficients’, using a geometric model and horizontal coordinates of three or more reference stations, to represent the distance-dependent errors for the entire network (Wübbena et al, 1996; Euler et al., 2001). The network coefficients are transmitted to users for interpolating the network correction (using special receiver firmware in RTK mode) according to their approximate position. The network correction is then ‘reassembled’ with the data from a reference station, which is also transmitted to the

user. As a result, the baseline processing from master-to-user station can be improved. Note that only one-way communication is needed for this method.

Advantages and disadvantages of the two methods were discussed by Landau et al. (2003) and Wübenna et al. (2001b). However, both work satisfactorily to reduce distance-dependent errors (Wübenna et al., 2001a; Vollath et al., 2002).

5.1.3 Processing for Network-Based Positioning

Network-based positioning (based on VRS and FKP) is illustrated in Figure 5.3.

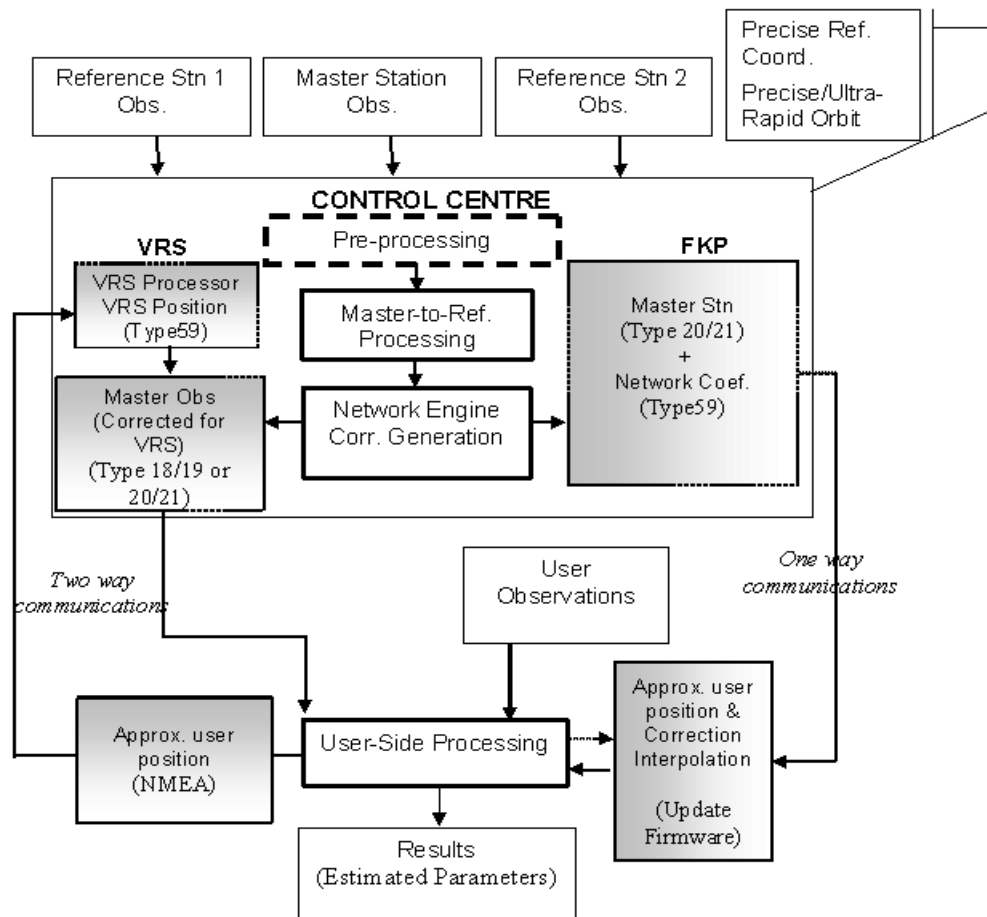


Figure 5.3 Processing for network-based positioning based on the VRS and FKP methods.

Apart from the data pre-processing, there are four common processing steps that can be identified in Figure 5.3:

- i) Master-to-Reference Station Processing;
- ii) Generating Corrections;
- iii) Data Transmission & Format; and
- iv) User-Side Processing.

i) Master-to-Reference Station Processing

Network Ambiguity Resolution

Better modelling of the distance-dependent errors is possible using the residuals of (fixed ambiguity) carrier phase measurements. Therefore, one of the objectives of master-to-reference station data processing is to fix the network ambiguities to their integer values. However, the inter-receiver separations between the master-to-reference stations are quite long (many tens of km) and the distance-dependent residual errors complicate the AR process. Moreover, the network ambiguities need to be resolved as fast as possible in order to support (near) real-time applications.

Fortunately, the process of carrier phase AR in the control centre has several advantages such as using the dual-frequency receiver, utilising the precise pseudorange data and good a priori coordinates of the static reference stations (see Section 2.4.3). Furthermore:

- Station-dependent errors are at a minimum level at the reference stations (see Section 3.4);
- The processing centre (as part of computer network) can download better quality (predicted) ultra-rapid orbits from the IGS. If necessary, it also can download other information such as global ionospheric models, troposphere parameters and precise satellite clock information.

In the past few years many researchers have focused on fast network AR (see Odijk, 2002; Dai, 2002; Chen, 2001; Hu et al., 2005). These mainly focus on the estimation of atmospheric delay mathematically and/or stochastically to speed up the network AR. However, ambiguities need to be resolved again when any tracked satellites suffer from a cycle slip, or after the occurrence of data gaps, or problematic satellites at low elevation angles, and when satellites rise above, or set below, the station horizon.

Sun et al., (1999) suggests a sequential approach that takes advantage of the IF combination to eliminate the ionospheric effect. He also proposed network constraints to increase the ambiguity search speed and to enhance the reliability of the fixed ambiguities. More rigorous modelling of station-dependent errors, hardware and firmware improvements, more tracked satellites and the use of multi-frequency signals (such as the future L5 on GPS and Galileo), should provide better performance for fast network AR.

Generation of Network Residuals

Equation 5.1 can be rewritten by assuming that there are three reference stations, and the errors (correlated and uncorrelated) not explicitly included:

$$V_{1,3}^{i,j}(t) = \Delta\nabla L_{1,3}^{i,j}(t) - (\Delta\nabla p_{1,3}^{i,j}(t) + \lambda\Delta\nabla N_{1,3}^{i,j}(t)) \quad (5.4)$$

$$V_{2,3}^{i,j}(t) = \Delta\nabla L_{2,3}^{i,j}(t) - (\Delta\nabla p_{2,3}^{i,j}(t) + \lambda\Delta\nabla N_{2,3}^{i,j}(t)) \quad (5.5)$$

where $V_{1,3}$, $V_{2,3}$ are residuals between reference stations 1 to 3 and 2 to 3 with reference station 3 as a master station; i and j denote the satellite pair that form the DD measurements; and t is the specific epoch time. Equations 5.4-5.5 can be written for L1, L2 or for any other measurement combinations. For the sake of simplification in the following derivation, the satellites i and j are replaced by the symbol of other inter-frequency combinations (see Table 3.1) and the epoch time t is ignored. Thus, the network residuals can be written as:

for L1:

$$V_{1,3}^{L1} = \Delta\nabla L_{1,3}^{L1} - (\Delta\nabla p_{1,3}^{L1} + \lambda\Delta\nabla N_{1,3}^{L1}) \quad (5.6)$$

$$V_{2,3}^{L1} = \Delta\nabla L_{2,3}^{L1} - (\Delta\nabla p_{2,3}^{L1} + \lambda\Delta\nabla N_{2,3}^{L1}) \quad (5.7)$$

for L2:

$$V_{1,3}^{L2} = \Delta\nabla L_{1,3}^{L2} - (\Delta\nabla p_{1,3}^{L2} + \lambda\Delta\nabla N_{1,3}^{L2}) \quad (5.8)$$

$$V_{2,3}^{L2} = \Delta\nabla L_{2,3}^{L2} - (\Delta\nabla p_{2,3}^{L2} + \lambda\Delta\nabla N_{2,3}^{L2}) \quad (5.9)$$

for the WL:

$$V_{1,3}^{WL} = \Delta \nabla L_{1,3}^{WL} - (\Delta \nabla p_{1,3}^{WL} + \lambda \Delta \nabla N_{1,3}^{WL}) \quad (5.10)$$

$$V_{2,3}^{WL} = \Delta \nabla L_{2,3}^{WL} - (\Delta \nabla p_{2,3}^{WL} + \lambda \Delta \nabla N_{2,3}^{WL}) \quad (5.11)$$

for the IF (non-dispersive):

$$V_{1,3}^{IF} = \Delta \nabla L_{1,3}^{77,-60} - (\Delta \nabla p_{1,3}^{77,-60} + \lambda \Delta \nabla N_{1,3}^{77,-60}) \quad (5.12)$$

$$V_{2,3}^{IF} = \Delta \nabla L_{2,3}^{77,-60} - (\Delta \nabla p_{2,3}^{77,-60} + \lambda \Delta \nabla N_{2,3}^{77,-60}) \quad (5.13)$$

for the GF (dispersive):

$$V_{1,3}^{GF} = \Delta \nabla L_{1,3}^{GF} - (\lambda_{L2} \Delta \nabla N_{1,3}^{L2} - \lambda_{L1} \Delta \nabla N_{1,3}^{L1}) \quad (5.14)$$

$$V_{2,3}^{GF} = \Delta \nabla L_{2,3}^{GF} - (\lambda_{L2} \Delta \nabla p_{2,3}^{L2} - \lambda_{L1} \Delta \nabla N_{2,3}^{L1}) \quad (5.15)$$

Equations 5.6-5.11 indicate that the distance-dependent errors are lumped together into the residual vectors. However, Equations 5.12-5.13 isolate the non-dispersive error component, and Equations 5.14-5.15 isolate the dispersive error component.

ii) Generating Corrections

The residual vectors are used as input to generate the ‘network corrections’. The algorithm to generate the network corrections is based on the interpolation of these residual vectors, or more precisely a $n-1$ independent residual vector generated from a n reference station network. As a result, the estimate of the distance-dependent errors for the user station location can be obtained. The algorithm utilises the user’s approximate position for this purpose. In addition, the interpolation could be performed on an epoch-by-epoch and satellite-by-satellite basis.

A variety of interpolation algorithms has been developed over the past few years. Amongst them are the Linear Combination Model, the Distance-Based Linear Interpolation Method, the Linear Interpolation Method, the Low-order Surface Model, and the Least Squares Collocation Method. A mathematical review of these algorithms can be found in Dai (2002) and Fotopoulos & Cannon (2001).

It should be emphasised that the abovementioned algorithms specifically define network corrections and/or network coefficients, which could be applied in terms of coordinates (i.e. latitude, longitude and height) or in the measurement domain using different models (i.e. raw, SD or DD). Some of the algorithms first need the knowledge of user's approximate coordinates to calculate the network coefficients. In the case of the FKP algorithm (Section 5.1.2), it only requires the network coefficients when performing the calculation of the network corrections inside the user receiver itself (see Figure 5.3). Apart from this, one significant characteristic common to all of the methods is that it is necessary to first compute the $n-1$ coefficients and to form a $n-1$ linear combination with the $n-1$ residual vectors generated by the n reference station network (Dai, 2002):

$$\hat{V}_u = \bar{\alpha}\bar{V} = \alpha_1 V_{1,n} + \alpha_2 V_{2,n} + \dots + \alpha_{n-1} V_{n-1,n} \quad (5.16)$$

where \hat{V}_u is the estimate of the distance-dependent errors vector (or can be interpreted as the network corrections) at the user location, and α is the network coefficient. In this case, the coefficients are determined from the network adjustment of the station coordinates and remain constant if the user receiver is not in motion. They refer to one master reference station and one reference satellite, and therefore coefficients are dependent on the geometry between the user station and the reference station network (and the GPS satellite geometry). All of the abovementioned algorithms have been tested via Equation 5.16, and their performance were found to be at a very similar level (Ibid, 2002).

iii) Data Transmission & Format

This becomes critical for real-time applications. As in the case of the typical RTK technique, a radio link is typically used to transmit the appropriate data from a reference station. Other communication options for RTK data can be found at <http://www.network-rtk.info/wegener/communication.html>. Usually the data is formatted to comply with the industry standard format developed by the Radio Technical Commission for Maritime Services (RTCM). In RTCM v2.3 (RTCM, 2001), the appropriate data can be transmitted via Messages 18 and 19 (i.e. raw measurements), or 20 and 21 (i.e. measurement corrections).

In the case of network-RTK, the choice of RTCM format is dependent on the control centre (and the network-RTK method used) as shown in Figure 5.3. Both VRS and FKP use a special format via RTCM type 59 proprietary message (Euler et al., 2001). In a special case of FKP, a customised/compressed message type 59 has been developed to transmit the network coefficient parameters to multiple users (Wübenna et al. 1996). The use of a proprietary format for network RTK has caused a few problems (Euler et al., 2001; Brown et al., 2005), as such a non-standard format is biased towards a particular brand of receiver. The new release of RTCM ver3.0 (RTCM, 2004) is a good choice for a raw data format. Latest discussions indicate that the RTCM will include a supplementary message type 1014-1017 to standardise the network-RTK information (Wübenna et al., 2006), according to the proposal described in Euler et al. (2001).

It should be emphasised that the network-based technique can also be conducted in post-mission analysis mode using the same network-based RTK algorithm.

iv) User-side Processing

As already mentioned, the procedure to estimate the ambiguity float solution, and subsequently to obtain the ambiguity fixed solution in the network-based positioning, is no different from the procedure for single-base (baseline) positioning. The only difference is that the user-side processing is aided by the network corrections. According to Figure 5.3, the VRS method has a direct computation problem for user-side processing since the user is provided with the raw VRS measurements or measurement corrections already incorporating the network correction generated by the control centre. In the case of the FKP method, the user needs to interpolate the transmitted network coefficients using knowledge of their position, before applying the generated network corrections.

In the network-based technique, the process of AR and computation of the user position is currently conducted within the user receiver. This configuration does make the processing load heavier for the receiver. One concept is to shift the user-side processing to the control centre. This is highlighted in Figure 5.4 where the user observations are transmitted to a control centre, which runs the network-based and user-side processing algorithms.

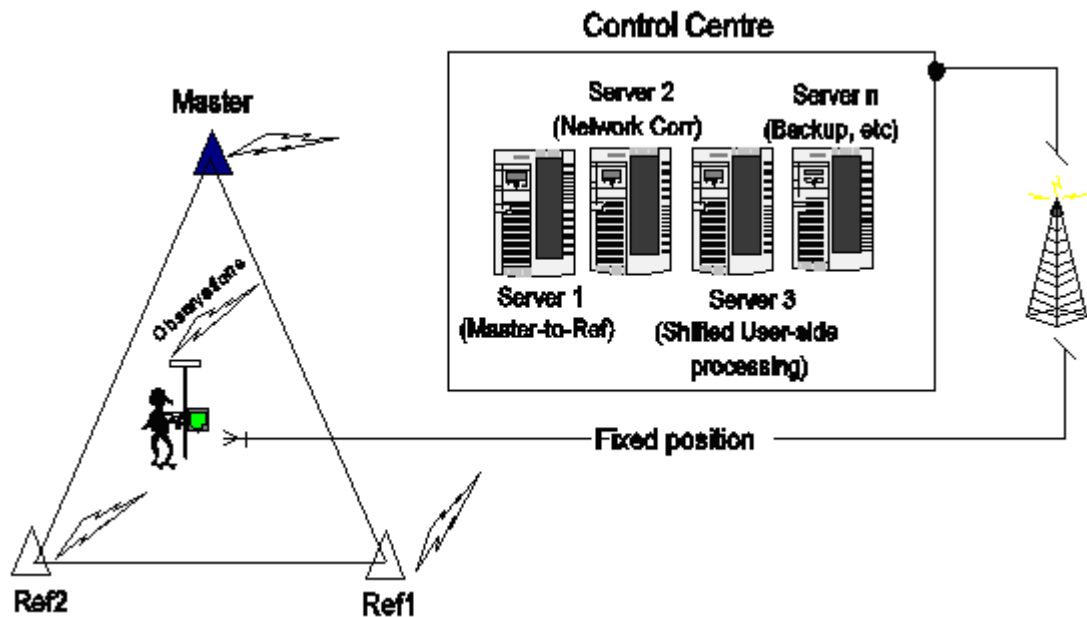


Figure 5.4 Network-based processing with ‘shifted’ user-side processing.

As a consequence the user only receives the final positioning report. The implementation of this “reverse RTK” concept is currently being considered by some manufacturers and network providers. In fact, a similar processing concept has been successfully implemented for post-mission analysis via the internet for static mode data, such as example the AUSPOS Online GPS Processing Service (via <http://www.ga.gov.au/bin/gps.pl>).

5.2 Network-Based Functional Model – Linear Combination Model

5.2.1 The Basic Model

The basic model for implementing the network-based technique in this study is the Linear Combination Method (LCM) (Wu, 1994). The early implementation of LCM was to average the spatially correlated orbital error using the code-based measurements within a network of reference stations. The use of this algorithm was extended by Han & Rizos (1996a) in order to reduce the effect of atmospheric delay using the carrier phase measurements. In the very first concept of LCM, the baseline vectors from the

multiple reference stations to the user station were estimated without the need to adjust the GPS orbit (Figure 5.5).

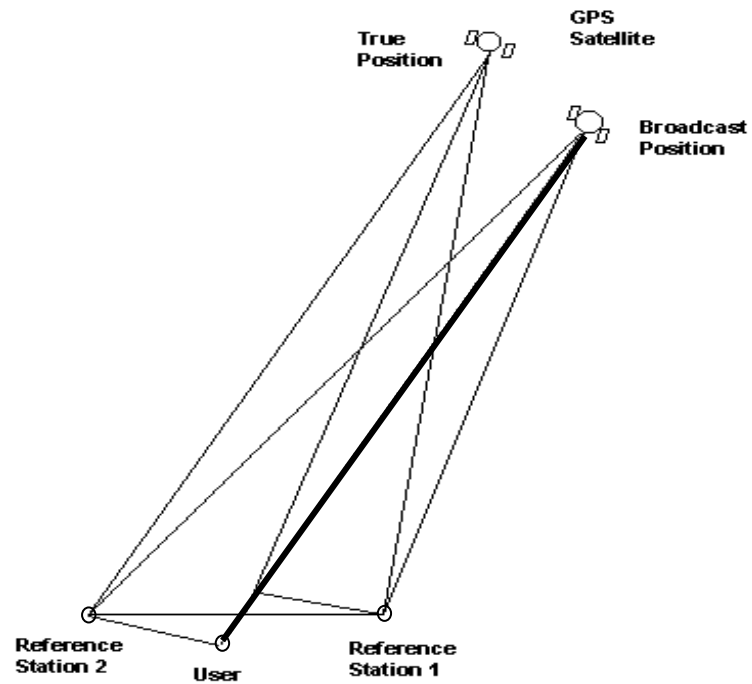


Figure 5.5 Geometric illustration of orbital error in SD measurements; the user station collinear with and located between two reference stations (Wu, 1994).

As illustrated in Figure 5.5, it is assumed that a user station is collinear with and located between two reference stations. The figure shows the effect of orbital error (in the SDs) that causes the baseline vector from reference 1 to user to move up, and from reference 2 to user to move down. The amount of vertical movements is approximately proportional to the baseline length. The errors can therefore be cancelled if the baseline vectors from the user to the i^{th} reference station, $\Delta\vec{X}_i$, are weighted inversely proportional to their baseline length.

The above concept is further generalised by assuming the orbital error can be partitioned into two components: in the direction of GPS satellite (S) to the user station, which is denoted as $\vec{\xi}$; and in the transverse direction $\vec{\eta}$, i.e., in the plane O that is perpendicular to the line-of-sight direction from the satellite to the user. The component $\vec{\eta}$ is further resolved into two mutually orthogonal components $\vec{\mu}$ (the along-track component) and \vec{v} (the cross-track component). The vector $\vec{\mu}$ represents the component

in the plane O, and \vec{v} represents the component perpendicular to that plane. Han (1997) described the geometric representation of these components, as indicated in Figure 5.6.

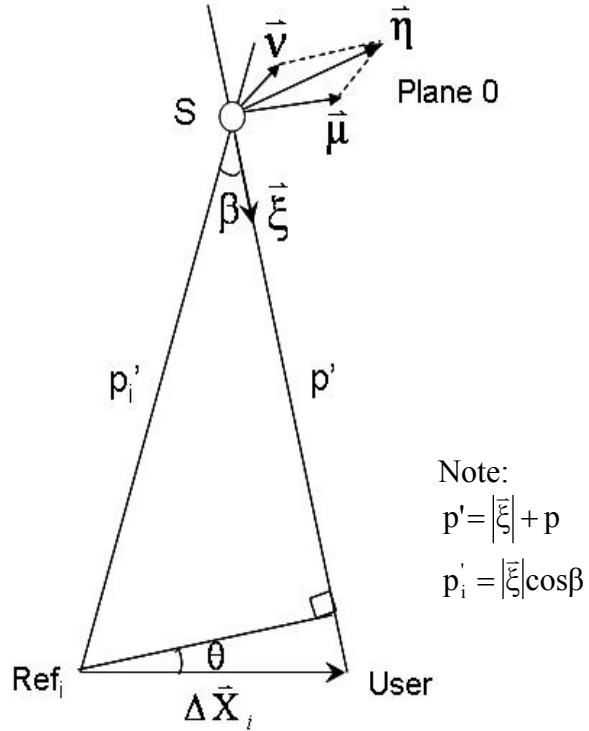


Figure 5.6 Representation of the orbital error components (Han, 1997).

Assuming the geometric ranges p (from satellite to user) and p_i (from satellite to Ref_i) is only affected by the orbital error, the vector $\vec{\xi}$ can be written as:

$$dp = p' - p = |\vec{\xi}| \quad (5.17)$$

and the relation with vector $\vec{\eta}$:

$$dp_i = p_i' - p_i = |\vec{\xi}| \cos \beta - |\vec{\eta}| \sin \beta \quad (5.18)$$

Taking the difference of Equations 5.17-5.18:

$$dp_i - dp = -|\vec{\xi}|(1 - \cos \beta) - |\vec{\eta}| \sin \beta \quad (5.19)$$

Since the baseline between the receivers is short compared to the geometric receiver-satellite range, and assuming that $P_i \approx p \approx 20,000\text{km}$, the first term on the right side of Equation 5.19 biases the SD range by less than 1mm if the orbital error is 20m and receivers' separation is less than 200km. Thus, this bias can be ignored. Using the vector dot products, Equation 5.19 can be rewritten as:

$$dp_i - dp = -(\bar{\mu} + \bar{v}) \cdot \frac{\Delta\bar{X}_i}{p} = -\bar{\eta} \cdot \frac{\Delta\bar{X}_i}{p} \quad (5.20)$$

Wu (1994) suggested if weights are chosen to be inversely proportional to the baseline lengths, then:

$$\sum_i \alpha_i \Delta\bar{X}_i = \vec{0} \quad (5.21)$$

i = number of reference stations

and requiring that the sum of weights be equal to 1:

$$\sum_i \alpha_i = 1 \quad (5.22)$$

Equation 5.22 ensures that:

$$\sum_i \alpha (dp_i - dp) = \sum_i \alpha_i \left(-\bar{\eta} \cdot \frac{\Delta\bar{X}_i}{p}\right) = 0 \quad (5.23)$$

where the SD linear combination using the pseudorange is free from the orbital error. The corresponding standard deviation of this linear combination is given by (Wu, 1994):

$$\sigma_e = \sigma_o \left(\sum_i \alpha_i^2 + 1 \right)^{\frac{1}{2}} \quad (5.24)$$

where σ_o is the standard deviation of the raw (one-way) pseudorange observations.

Equations 5.21-5.22 require two reference stations at a minimum if the user is on line joining the two reference stations, or three reference stations if a user station is on the plane defined by the three reference stations. More reference stations are obviously allowed, but their weights should be carefully selected. Thus, another constraint should be added:

$$\sum_i \alpha_i^2 = \min \quad (5.25)$$

which satisfies Equations 5.21-5.22. Equation 5.25 should be used to uniquely determine the weights or linear coefficient parameters. These can be determined by least squares estimation. Given the Gaussian coordinates of the reference stations and denoting X_m as the master station; X_u as the user station; and the other reference stations as $X_1 \dots X_n$; a set of α can be determined (Chen, 2001; Dai, 2002):

$$\alpha = \mathbf{B}^T (\mathbf{B}\mathbf{B}^T)^{-1} \mathbf{L} \quad (5.26)$$

where

$$\mathbf{B} = \begin{bmatrix} 1 & 1 & \dots & 1 & 1 \\ \Delta X_{1,m} & \Delta X_{2,m} & \dots & \Delta X_{n-1,m} & 0 \\ \Delta Y_{1,m} & \Delta Y_{2,m} & \dots & \Delta Y_{n-1,m} & 0 \end{bmatrix}, \quad \alpha = \begin{bmatrix} \alpha_1 \\ \alpha_2 \\ \cdot \\ \alpha_n \end{bmatrix}, \quad \mathbf{L} = \begin{bmatrix} 1 \\ \Delta X_{u,m} \\ \Delta Y_{u,m} \end{bmatrix}$$

and ΔX and ΔY are the coordinate differences of the stations (given by the subscripts). In this calculation, although a total of n network coefficients can be derived from Equation 5.26, only $n-1$ coefficients will be utilised to interpolate the network residuals (see Equation 5.16). The coefficient α_n is related to the master station. Dai (2002) has shown that if only three reference stations are used, the coefficients α_1 and α_2 are exactly the same for the Linear Interpolation Method (LIM) as used in the FKP method. However, they are different when the number of reference stations is greater than 3 because the linear combination model eliminates the orbit bias as well.

5.2.2 The Single-Differenced Model

Following Equation 5.21, assuming that there are three reference stations (by setting station 3 to be the master station), the complete LCM for carrier phase SD measurements can be written as (Han, 1997):

$$\begin{aligned} \sum_{i=1}^3 \alpha_i \Delta L_i = & \sum_{i=1}^3 \alpha_i \Delta p_i - c \sum_{i=1}^3 \alpha_i \Delta dt_i^R - \sum_{i=1}^3 \alpha_i \Delta \text{ion}_i + \sum_{i=1}^3 \alpha_i \Delta \text{trop}_i \\ & + \sum_{i=1}^3 \alpha_i \Delta \text{dmp}_i + \lambda \sum_{i=1}^3 \alpha_i \Delta N_i + \Delta E \sum_{i=1}^3 \alpha_i \Delta L_i \end{aligned} \quad (5.27)$$

where all terms have been previously defined (see also Equation 2.54-2.55, assuming the SD hardware delay is lumped in with the measurement noise). According to Equation 5.23, the above equation is free from orbital error (embedded within the geometric range). Ibid (1997) claims the above linear combination eliminates the ionospheric delay and reduces the residual tropospheric delay (i.e. after applying an a priori model).

Considering Equation 5.26, the ionospheric delay in Equation 5.27 can be written as:

$$\sum_{i=1}^3 \alpha_i \Delta \text{dion}_i = (\text{dion}_u - \text{dion}_3) - \begin{bmatrix} \alpha_1 \\ \alpha_2 \end{bmatrix}^T \begin{bmatrix} \text{dion}_1 - \text{dion}_3 \\ \text{dion}_2 - \text{dion}_3 \end{bmatrix} = 0 \quad (5.28)$$

because the effect of ionospheric delay is distance-dependent. In a similar manner, the residual tropospheric delay in Equation 5.27 can be represented as:

$$\sum_{i=1}^3 \alpha_i \Delta \text{dtrop}_i = (\text{dtrop}_u - \text{dtrop}_3) - \begin{bmatrix} \alpha_1 \\ \alpha_2 \end{bmatrix}^T \begin{bmatrix} \text{dtrop}_1 - \text{dtrop}_3 \\ \text{dtrop}_2 - \text{dtrop}_3 \end{bmatrix} \approx 0 \quad (5.29)$$

because the residual tropospheric delay is also distance-dependent, but shows strong variation with station height and location.

The station-dependent errors (see assumption 3 in sub-section 5.1.1) cannot be

rigorously modelled by the LCM. However, the linear combination term of station-dependent errors, i.e. multipath ($\sum_{i=1}^3 \alpha_i \Delta \text{mp}_i$) and measurement noise ($\Delta E_{\sum_{i=1}^3 \alpha_i \Delta L_i}$) represents the weighted mean value of these errors at the three reference stations for each satellite. Therefore, the model may reduce these errors to some extent (Ibid, 1997), and the residual part of distance-dependent errors will be ignored in the functional model.

The simplified SD LCM for carrier phase can be written as:

$$\sum_{i=1}^3 \alpha_i \Delta L_i = \sum_{i=1}^3 \alpha_i \Delta p_i - c \sum_{i=1}^3 \alpha_i \Delta t_i^R + \lambda \sum_{i=1}^3 \alpha_i \Delta N_i \quad (5.30)$$

5.2.3 The Double-Differenced Model

Using the measurements made from the reference stations and the user receiver, the SD LCM in Equation 5.30 can also be expressed as (Ibid, 1997):

$$\begin{aligned} \sum_{i=1}^3 \alpha_i \Delta L_i &= (L_u - L_3) - [\alpha_1 (L_1 - L_3) + \alpha_2 (L_2 - L_3)] \\ &= \Delta L_{u,3} - [\alpha_1 \Delta L_{1,3} + \alpha_2 \Delta L_{2,3}] \end{aligned} \quad (5.31)$$

However, the receiver clock errors still exist in Equation 5.31 and will cause serious problems if not properly estimated. The simplest way to handle such clock errors is to form the DD measurements. The DD combination for LCM measurements can be expressed as:

$$\begin{aligned} \Delta \nabla L_{u,3} - [\alpha_1 \Delta \nabla L_{1,3} + \alpha_2 \Delta \nabla L_{2,3}] &= \Delta \nabla p_{u,3} - \\ [\alpha_1 \Delta \nabla p_{1,3} + \alpha_2 \Delta \nabla p_{2,3}] + \lambda \Delta \nabla N_{u,3} &- [\alpha_1 \Delta \nabla N_{1,3} + \alpha_2 \Delta \nabla N_{2,3}] \end{aligned} \quad (5.32)$$

Rearranging Equations 5.4-5.5 and inserting them into Equation 5.32 gives:

$$\nabla \Delta L_{u,3} - [\alpha_1 \cdot V_{1,3} + \alpha_2 \cdot V_{2,3}] = \nabla \Delta \rho_{u,3} + \lambda \cdot \nabla \Delta N_{u,3} \quad (5.33)$$

where the terms in the bracket are identical to those in Equation 5.16, i.e. the network corrections. If the ‘fixed’ network residuals could be obtained on an epoch-by-epoch, satellite-by-satellite basis, the network corrections could also be generated in the same manner. In real-time mode, the network corrections vector together with the pseudorange and carrier phase data at reference station 3 can be transmitted to the user.

5.3 Proposed Network-Based Processing

In the post-mission approach, the network-based algorithm of LCM has been successfully implemented in static, fast-static and kinematic (relative) positioning (see Chen, 2001; Dai, 2002; Han, 1997; Hu et al., 2002; Janssen, 2003, Roberts, 2002) by assuming the network corrections and raw measurements are broadcast to the user. The algorithm has also tested using mixed-mode L1-only and dual-frequency receivers (Chen, 2001; Janssen, 2003; Roberts, 2002). In the real-time approach, i.e. the network-RTK mode, the LCM algorithm has also been utilised for DGPS positioning via the VRS method (see Figure 5.3) with some modification of Equation 5.26 (Hu et al., 2003). This real-time implementation was a joint research and development initiative between Satellite Navigation & Positioning Group of the University of New South Wales (UNSW), Australia; the Surveying & Mapping Laboratory of the Nanyang Technological University (NTU), Singapore; and the Singapore Land Authority (SLA) (Rizos, 2003).

Several improvements have been made to the above algorithm:

- a) Both the post-mission and the real-time approaches do not fully eliminate the ionospheric delay using dual-frequency receivers in the user-side processing.
- b) Both the post-mission and the real-time approaches do not isolate the dispersive and non-dispersive components of the network corrections. The current practice is to lump the network corrections into a single parameter (due to the process in sub-section 5.1.3 (i) Generation of the Network Residuals).
- c) The post-mission approach usually is assisted by independent software such as the BERNESE package to generate the network residuals.

The proposed network-based processing and network corrections generation methodology are described in the following sub-sections.

5.3.1 Proposed Network AR

All the options provided by the reference stations (Section 5.2.1 (i)) need to be used in order to assist the process of fast network AR. The IGS ultra-rapid orbit is utilised since its quality is much better than the broadcast one (see Section 3.4.2 (e)). The process takes advantage of several inter-frequency combinations of carrier phase and code measurements, as described in Section 3.2. The network AR process is summarised in four steps:

Step 1: Estimate the widelane ambiguity (with a combination of the narrowlane code-range or phase-range only). This process was discussed in Section 3.3.2.

Step 2: Estimate the L1 ambiguity with the IF combination along with the fixed widelane ambiguity. This process was discussed in Section 3.3.1.

Step 3: Ambiguity search, decorrelation and validation.

In Step 3, the well known LAMBDA method (Teunissen, 1994) is used for fast ambiguity search and decorrelation. The assurance criteria to determine the ‘best’ set of integer values are given in Section 2.4.3 (c). For the validation process the critical value is set to 3, as is often done in practice (Landau & Euler, 1992). However, it is not always guaranteed that the fixed ambiguities are correct since this statistical process has its own problems (see Verhagen, 2004). Therefore, step 4 is included.

Step 4: Adaptation.

Step 4 removes some low elevation satellites (and repeats Step 3) when the ambiguity validation test fails. If the validation test is passed, a further check is performed on the ‘fixed’ residuals against a ‘threshold’ value. The value can take the difference between the DD ionospheric delay scale on L1 and L2, which is set less than 5cm as suggested by Han (1997). Measurements beyond this threshold should be rejected. Hence, Step 4 can improve the reliability of the fixed ambiguities. Once the network ambiguities are resolved, they do not have to be resolved again, but need to be maintained (in a database) and checked on a continuous basis.

5.3.2 Dispersive and Non-Dispersive Corrections

Once network ambiguities are fixed, the residuals are used to approximate the distance-dependent errors within the area. The approach is to partition the residuals according to whether they are dispersive or non-dispersive. This partition is done via GF and IF combinations as discussed in sub-sections 3.2.2-3.2.3. Assuming there are three reference stations, a set of network coefficients ($\alpha_1, \alpha_2, \alpha_3$) can be calculated via Equation 5.26. According to the discussion in sub-section 5.2.1, only the coefficients α_1 and α_2 are utilised in the next step to generate the network corrections.

In order to generate the non-dispersive corrections, the fixed (DD) widelane and L1 network ambiguities, i.e. between reference station 1 to 3 and 2 to 3, are used to determine the IF ambiguity (see Equation 3.24). Once this ambiguity is obtained, it can be removed from Equations 5.12-5.13 to provide fixed IF residuals. Next, the non-dispersive correction can be written as (via Equation 5.16):

$$\text{Non_Disp_Corr} = [\alpha_1 \cdot V_{1,3}^{\text{IF}} + \alpha_2 \cdot V_{2,3}^{\text{IF}}] \quad (5.34)$$

In order to generate the dispersive corrections, the fixed (DD) L1 and L2 network ambiguities should be removed from Equations 5.14-5.15 to obtain the fixed GF residuals. However, it should be emphasised that in this work the residuals are scaled to the L1 frequency (see Equation 3.16) for the non-dispersive corrections to be applied to L1 measurements. Next, the dispersive correction can be written as (via Equation 5.16):

$$\text{Disp_Corr} = [\alpha_1 \cdot V_{1,3}^{\text{GF}} + \alpha_2 \cdot V_{2,3}^{\text{GF}}] \quad (5.35)$$

Due to the rapid variations of the ionosphere effect (see Section 3.4.2(a)), smoothing the dispersive component has to be performed as frequently as possible (e.g. on an epoch-by-epoch basis). On the other hand, non-dispersive components should change slowly and smoothly over time due to the behaviour of the tropospheric delay and orbit biases. Rapid variations in the non-dispersive component can be attributed to remaining noise in the IF measurements. For this reason it is suggested that non-dispersive errors should

not be smoothed on an epoch-by-epoch basis. In addition, a simple running average can be applied to smooth the non-dispersive corrections.

A simple smoothing function can be found in Weisstein (2002). After N epochs, Equation 5.34 can be given in a sequence as $\{\text{Non_Disp}_i\}_{i=1}^N$. A n-moving average is a new sequence as $\{S_i\}_{i=1}^{N-n+1}$ derived from the Non_Disp_i by taking the average of sub-sequences of n terms, which can be written as:

$$S_i = \frac{1}{n} \sum_{j=i}^{i+n-1} \text{Non_Disp}_j \quad (5.36)$$

The smoothing function (from a few seconds up to a few minutes, depending on the data rate) is useful to average the measurements noise because the non-dispersive corrections are generated via the IF combination.

5.3.3 Proposed User-Side Processing Strategies

Since the network corrections are now partitioned into dispersive and non-dispersive components, this fact can benefit the user-side processing. Performance analysis of the dispersive and non-dispersive corrections to user-side processing has recently become a major topic in network-based positioning research (Brown et al., 2005; Geisler, 2006; Alves et al., 2006). But how does this impact on user-side processing.

For user-side processing, the ability to resolve the master-to-user station carrier phase ambiguities is dependent on the quality of the dispersive network corrections. However, it is not guaranteed that good quality dispersive corrections are always available at each epoch and for each satellite pair. For example, there is a possibility of temporal failure of a reference station or unresolved network ambiguity for a certain satellite pair which results in a degradation of the network corrections. This problem will lead to less satellites being processed and an increased difficulty in resolving the ambiguity for master-to-user stations, especially if only the L1 or/and L2 observation is used in the network-based processing of the LCM (Equation 5.33).

Considering the above problems, the dispersive correction (Equation 5.35) is not used initially to reduce the dispersive effect to aid master-to-user AR. As an alternative, the LCM can be derived using the IF combination which eliminates the dispersive effect of the ionospheric delay. Following Equations 3.19, 5.33 and 5.34, the LCM for this strategy can be written as:

$$\nabla\Delta L_{u,3}^{IF} - [\alpha_1 \cdot V_{1,3}^{IF} + \alpha_2 \cdot V_{2,3}^{IF}] = \nabla\Delta\rho_{u,3} + \lambda \cdot \nabla\Delta N_{u,3}^{IF} \quad (5.37)$$

Note that the non-dispersive corrections are applied to the above equation in order to improve the IF measurement, and therefore to assist resolving the indirect ambiguity of L1. Thus, the strategy for master-to-user station AR is the same as described in Section 5.3.1, except that it is now aided by the non-dispersive corrections. The process is best conducted in the control centre as shown in Figure 5.4. Apart from reducing the user processing load, the process can also use the (predicted) IGS ultra-rapid orbit which is easily downloadable by the control centre computer.

Although Equation 5.37 maintains its geometric range, there is no intention to use this measurement for the user's position computation due to the large noise in the IF combination (see Table 3.1). The strategy is to calculate the user's position using the original carrier phase of DD L1 and/or DD L2 (see Equations 2.59-2.60). Since the DD L1 and DD L2 ambiguities have been 'indirectly' determined while processing Equation 5.37 (the previous step), they can be removed from the original carrier phase (i.e. fixed measurements). Thus, the least squares process in Equation 2.66 requires less parameters to be estimated.

The user positioning accuracy is now dependent on the satellite geometry, station-dependent and distance-dependent errors. The distance-dependent errors are dominant in that they are still present in these measurements. Both dispersive and non-dispersive corrections are now applied to each epoch and each satellite pair with an expectation that they reduce the effect of distance-dependent errors in the user's position computation. This can be described as follow:

$$\Delta\nabla L_{u,3}^{\text{fixed}} = \Delta\nabla p_{u,3} - \overbrace{[\Delta\nabla \text{dion}_{u,3} - \text{Disp_Corr}]}^{\text{Dispersive}} + \overbrace{[\Delta\nabla \text{dtrop}_{u,3} + \Delta\nabla O_{u,3} - \text{Non_Disp_Corr}]}^{\text{Non-Dispersive}} + \overbrace{(\Delta\nabla \text{mp}_{u,3} + \Delta\nabla E_{u,3})}^{\text{uncorrelated}} \quad (5.38)$$

Other residuals from Equation 5.38 will be taken into account for the stochastic model. Issues to do with the stochastic modelling for network-based positioning will be addressed in the next chapter.

5.3.4 Code Development – The Research Approach

To implement the proposed network-based processing technique, research-oriented programming code which was developed at UNSW has been modified. The original code was written in MATLAB for single-frequency static relative positioning. During the period of the study, this code has been upgraded to dual-frequency processing and five major modules have been developed (Figure 5.7):

1. Kinematic relative positioning module – the process uses all the available pseudorange and carrier phase measurements. The linear combinations and the differencing technique are utilised, and the float solution at each epoch is performed using least squares estimation, or indirect AR to obtain the float ambiguity. The LAMBDA method is used for ambiguity fixing at each epoch, and it should pass the validation criteria after some initialisation period.
2. Indirect AR module - the process is performed with various linear data combinations as discussed in Chapter 3.
3. Network-based functional module – the process utilises the network-based algorithm of the LCM as described in Section 5.2. Two different types of network corrections are obtained; the separated dispersive and non-dispersive corrections, and the ‘lump sum’ corrections.
4. Network-based stochastic modelling module – the original single-frequency code is corrected using the ‘lump sum’ network corrections. The stochastic modelling method based on variance-covariance estimation and residuals analysis can be performed (see Chapter 6).

5. IGS orbit module – this process decodes the ultra-rapid IGS orbit to determine the satellite positions with the aid of polynomial interpolation. This module is modified from Witchayangkoon (2000).

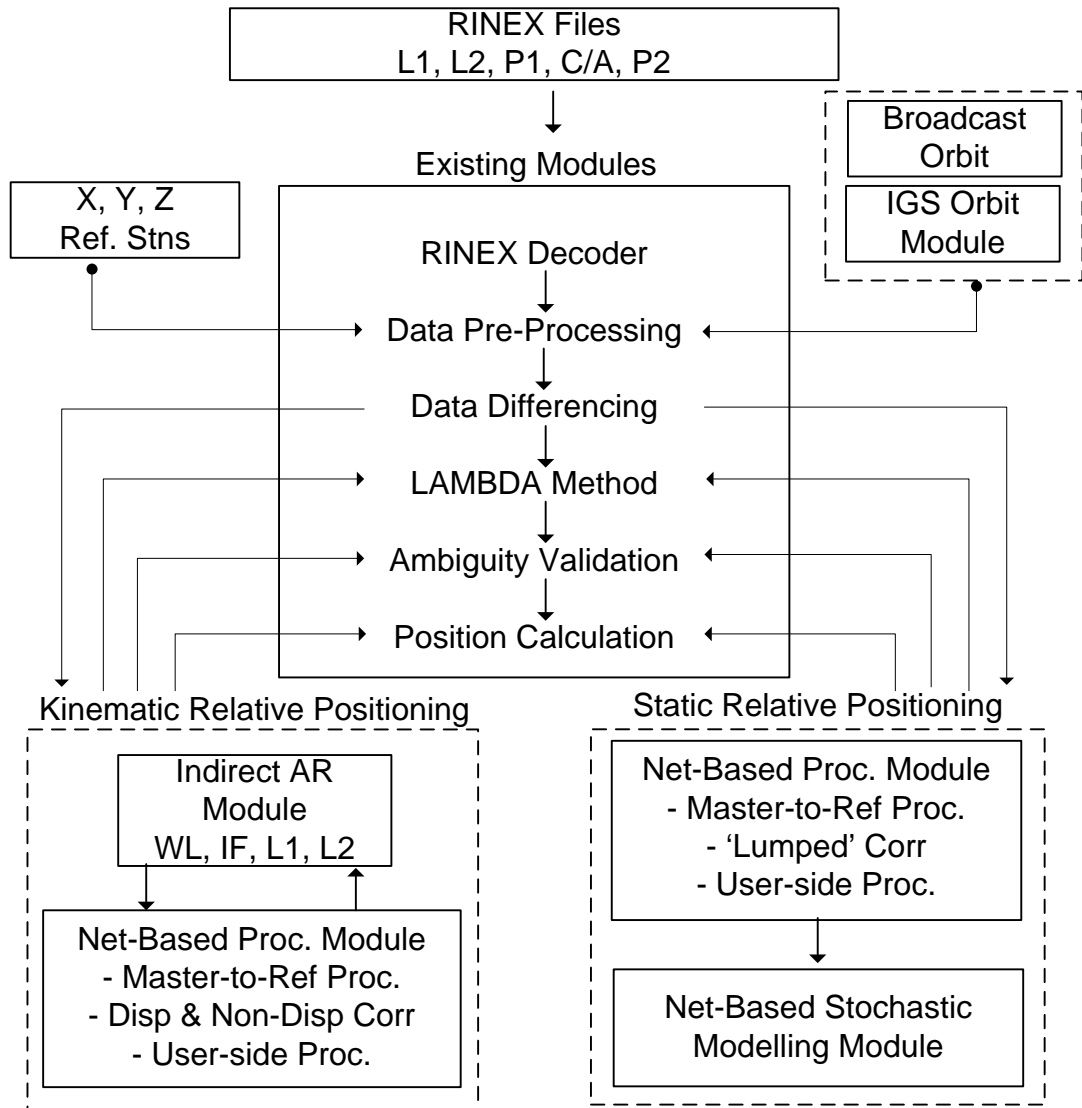


Figure 5.7 The UNSW (upgraded) GPS baseline processing modules for the proposed network-based positioning technique.

5.4 Tests for Local GPS Networks

5.4.1 Test Area

Two GPS networks in different geographical locations are used in this study. The first one is the Sydney Network (SYDNET) located in the mid-latitudes (latitude range $33^{\circ} 36' - 34^{\circ} 08'S$ and longitude range $150^{\circ} 34' - 151^{\circ} 12'E$), and the second is the small Singapore Integrated Multiple Reference Station Network (SIMRSN) located near the equator (latitude range $1^{\circ} 15' - 1^{\circ} 30'N$ and longitude range $103^{\circ} 40' - 103^{\circ} 59'E$). Figures 5.8-5.9 show the locations of the permanent reference stations within SYDNET and SIMRSN, respectively.

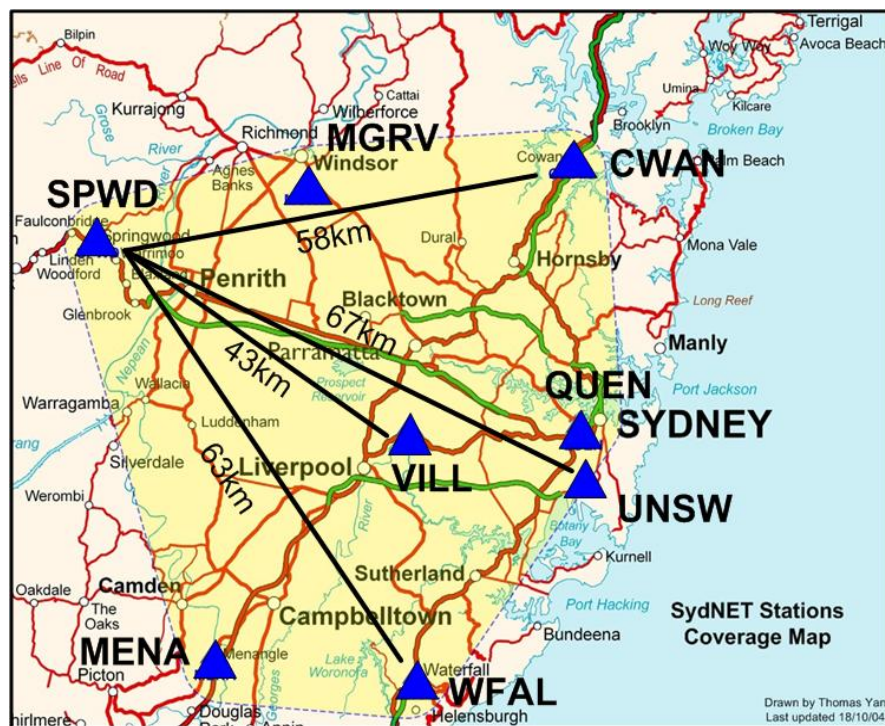


Figure 5.8 SYDNET Network: SPWD is the master station; VILL is the user station; UNSW, WFAL and CWAN are the other reference stations.

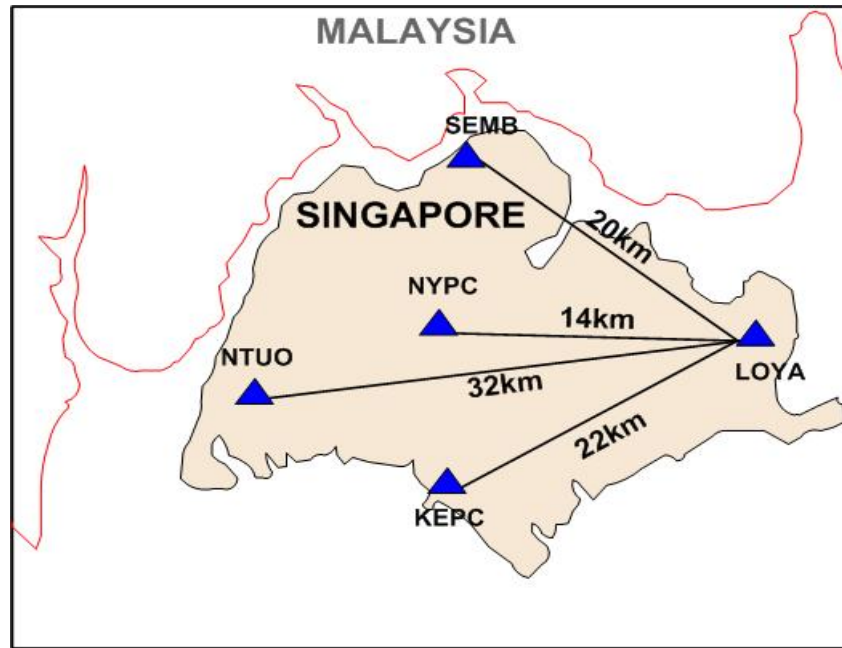


Figure 5.9 SIMRSN Network: LOYA is the master station; NYPC is the user station; SEMB, KEPC and NTUO are the other reference stations.

Stations SPWD of SYDNET and LOYA of SIMRSN were selected as the two master stations. Meanwhile station VILL of SYDNET and NYPC of SIMRSN were treated as user stations. Other stations are considered reference stations. The lengths of the master-to-user baselines are noted on Figures 5.8 and 5.9, i.e. ~43km for SYDNET and only ~14km SIMRSN. Although the baseline is short, it is expected that the atmospheric effects are more severe in the SIMRSN test. Tables 5.1-5.2 list the known coordinates of the stations for SYDNET and SIMRSN respectively. The station coordinates of SYDNET were obtained by submitting 6 days of data to the AUSPOS Online GPS Processing Service (<http://www.ga.gov.au/bin/gps.pl>), and the coordinates of SIMRSN were provided by the network centre. All station orthometric heights were calculated by first obtaining geoid heights from the EGM96 geoid calculator (<http://earth-info.nga.mil/GandG/wgs84/gravitymod/egm96/intpthel.html>).

Table 5.1 SYDNET reference station coordinates.

Reference Station ID	Latitude	Longitude	Ellipsoidal Hgt. (m)	Ortho. Hgt. (m)
WFAL	34° 08' 03.1633" S	150° 59' 41.8958" E	251.590	229.732
CWAN	33° 35' 37.3442" S	151° 10' 17.8835" E	218.037	194.546
UNSW	33° 55' 03.6148" S	151° 13' 54.6427" E	86.993	64.774
SPWD	33° 41' 54.7515" S	150° 33' 50.1808" E	399.452	375.690
VILL	33° 52' 50.2909" S	150° 58' 37.8007" E	42.617	19.920

Table 5.2 SIMRSN reference station coordinates.

Reference Station ID	Latitude	Longitude	Ellipsoidal Hgt. (m)	Ortho. Hgt. (m)
NTU0	1° 20' 44.8174" N	103° 40' 47.8260" E	76.257	69.167
SEMB	1° 28' 11.1081" N	103° 49' 10.3457" E	30.900	23.340
LOYA	1° 22' 21.5306" N	103° 58' 17.9294" E	51.153	42.913
KEPC	1° 16' 01.3266" N	103° 48' 25.7254" E	37.445	29.795
NYPC	1° 22' 44.8145" N	103° 50' 55.5085" E	55.645	47.895

5.4.2 Test Methodology & Data Description

To investigate the proposed network processing strategy, tests were conducted in post-mission mode, although they have ‘simulated’ the RTK mode. The method used here was rather conducted in the FKP mode, using the functional model of the LCM as discussed in Section 5.3. (Future code development will include VRS data generation as described in Equations 5.2-5.3.)

The process is performed on an epoch-by-epoch and satellite-by-satellite basis. In this work, the cycle-slips are not corrected but the affected observations are simply removed. All raw GPS measurements were corrected for the a priori tropospheric model and the IGS ultra-rapid orbit is used to determine the satellite positions. The dispersive correction, as suggested in sub-section 5.3.2, is generated at every epoch. In contrast, the non-dispersive is smoothed up to 3 epochs (45 seconds) using Equation 5.36. The network corrections (i.e. dispersive and non-dispersive) are generated by removing satellites in the master-to-reference combinations whose elevations are less than 10°. For master-to-user, there is a further varying of the satellite cut-off elevation angle for the various tests for 10°, 15° and 20°.

The focus is now on the master-to-user station processing. The process of analysing the results of the network-based technique is divided into two:

Internal: Single-base processing is conducted using the same stations and kinematic relative positioning algorithm. Therefore, a direct comparison of, for example, the ambiguity validation ratio value between the network-based and

single-base processing can be conducted. (Other comparisons can be conducted via external analysis.)

External: - The data are processed over an extended time to determine the most probable fixed ambiguity (this is the ‘known ambiguity’). This ‘known’ ambiguity will be used for comparisons of the fixed ambiguity results from network-based versus single-base processing.

- Since the user station is actually one of the reference stations, the precise coordinate of this station is known (the ‘true coordinates’; see Tables 5.1-5.2). This known coordinate will be used to compare the coordinates estimated using procedures with and without applying the network corrections.

In future work, the internal analysis should also cover the use of different network modelling methods (such as VRS) and variations in the correction generating algorithm. The above internal and external process analyses are shown in Figure 5.10.

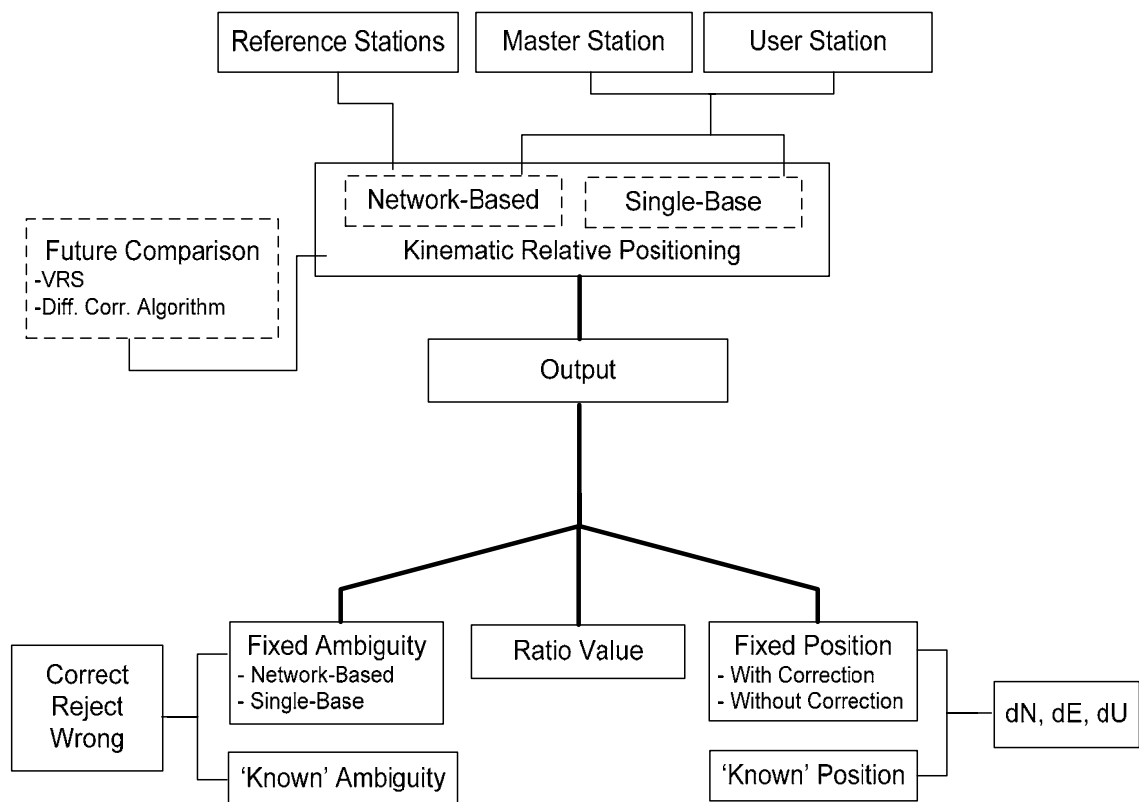


Figure 5.10 Methodology used to assess the performance of solutions using the network-based and single-base positioning techniques.

The test data were downloaded from the control centre for the DoY 131/05 (SYDNET) and DoY 166/03 (SIMRSN). The observation period was from 22:00-1:00 Sydney local time in the case of SYDNET, and 8:00-11:00 Singapore local time for the SIMRSN data, with 15s epoch interval. However, there is a delay of 10 minutes in the master-to-user station processing in order to generate and stabilise the network corrections. In total, there are 680 epochs of data being processed for both networks. Figures 5.11-5.12 indicate the number of satellites in view and the available corrections for the VILL and NYPC stations during the period of test. Figure 5.13 shows that the geometry of the satellites for both networks is good, with geometric dilution of precision (GDOP) less than 5.

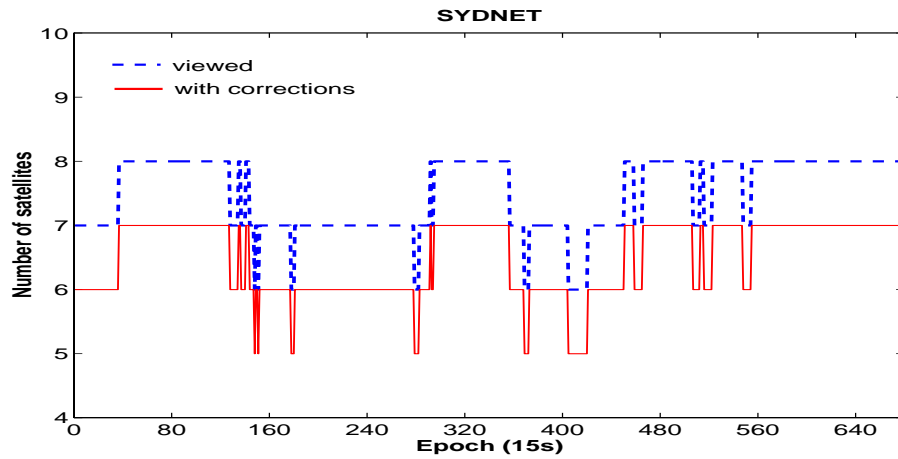


Figure 5.11 Number of satellites in view (at 10° elevation angle and above) and available corrections for the station VILL in SYDNET.

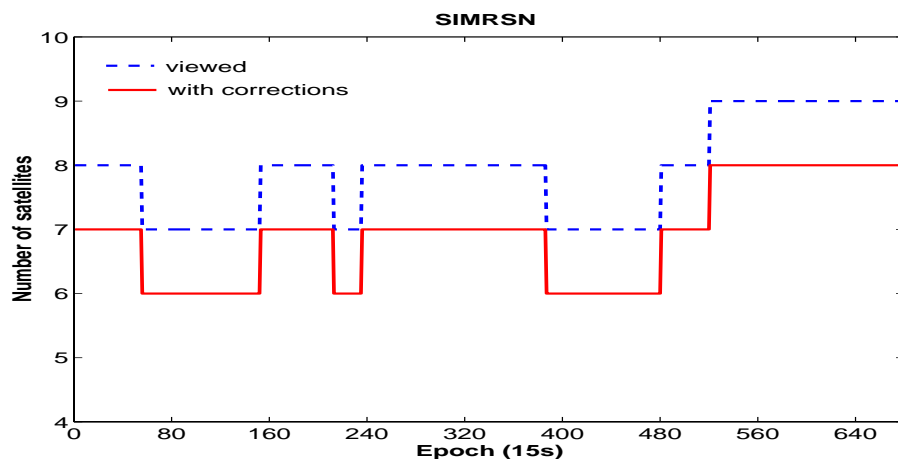


Figure 5.12 Number of satellites in view (at 10° elevation angle and above) and available corrections for the station NYPC in SIMRSN.

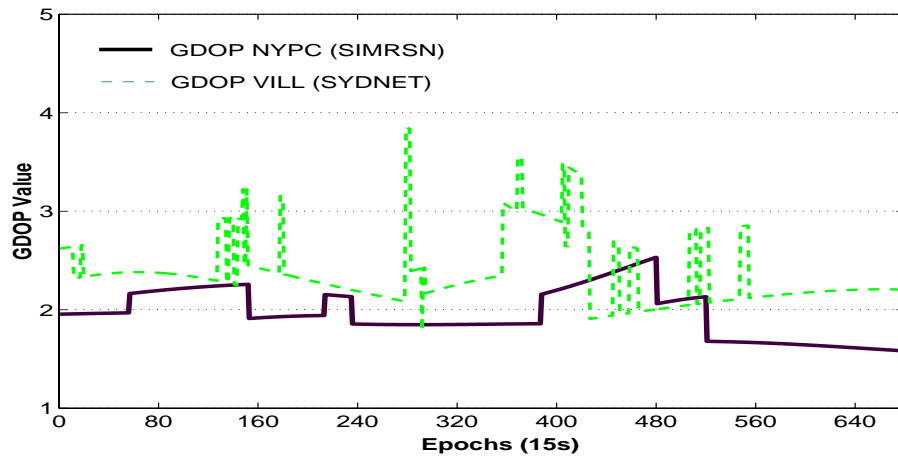


Figure 5.13 GDOP values for VILL (SYDNET) and NYPC (SIMRSN) during the tests.

5.4.3 Results & Discussion

The following results and discussion are restricted to the master-to-user station processing, for which the performance of the network-based technique could be assessed by the procedure described in Figure 5.10. In the case of master-to-reference station processing, although it is not explicitly addressed, the performance can be assessed via the generated dispersive and non-dispersive corrections as discussed in the next sub-section.

a) Performance Analysis of the Dispersive & Non-Dispersive Corrections

The Dispersive Corrections

Figures 5.14-5.15 show the ‘uncorrected’ residuals of the DD ionospheric delay on L1 (i.e. the dispersive effects) and the corresponding dispersive corrections for the master-to-user station, for all satellite combinations, both in the SYDNET and SIMRSN tests. Inspecting the residual patterns in these figures, it is obvious that the network corrections exhibit some trends. The magnitude of the corrections is approximately the same as the magnitude of the uncorrected residuals. However, it can be noticed that not all corrections exist for each satellite at certain epochs due to the unresolved network ambiguities (mostly those that refer to low elevation satellites).

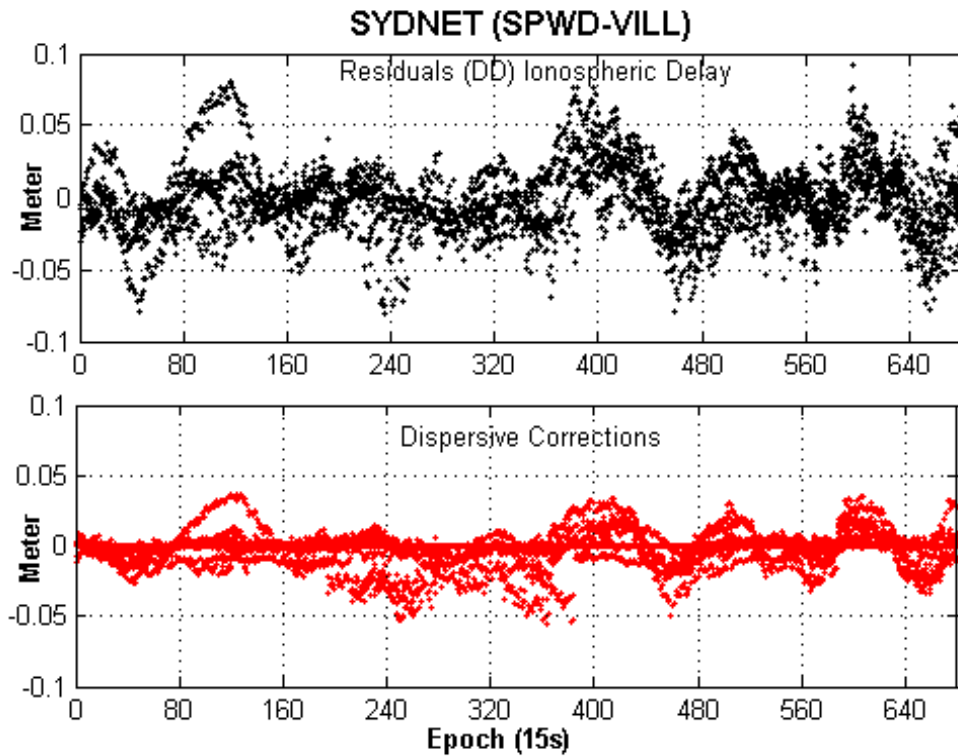


Figure 5.14 SYDNET, the mid-latitude experiment. **Top:** the ‘uncorrected’ DD ionospheric delay residuals (dispersive effects) and **Bottom:** the corresponding dispersive corrections (note the line at zero value indicates that no correction exists for some satellites); for all satellite combinations in the master-to-user station SPWD-VILL. The DoY is 131/05 during the year of low solar activity.

One can also compare the result of SIMRSN and SYDNET, where the magnitude of the residual ionospheric delay and dispersive corrections are almost the same even though the baseline lengths are different. This could be explained by the stronger atmospheric activity in the equatorial area, and due to the SIMRSN test being conducted during a year of high solar activity (see Figure 2.10).

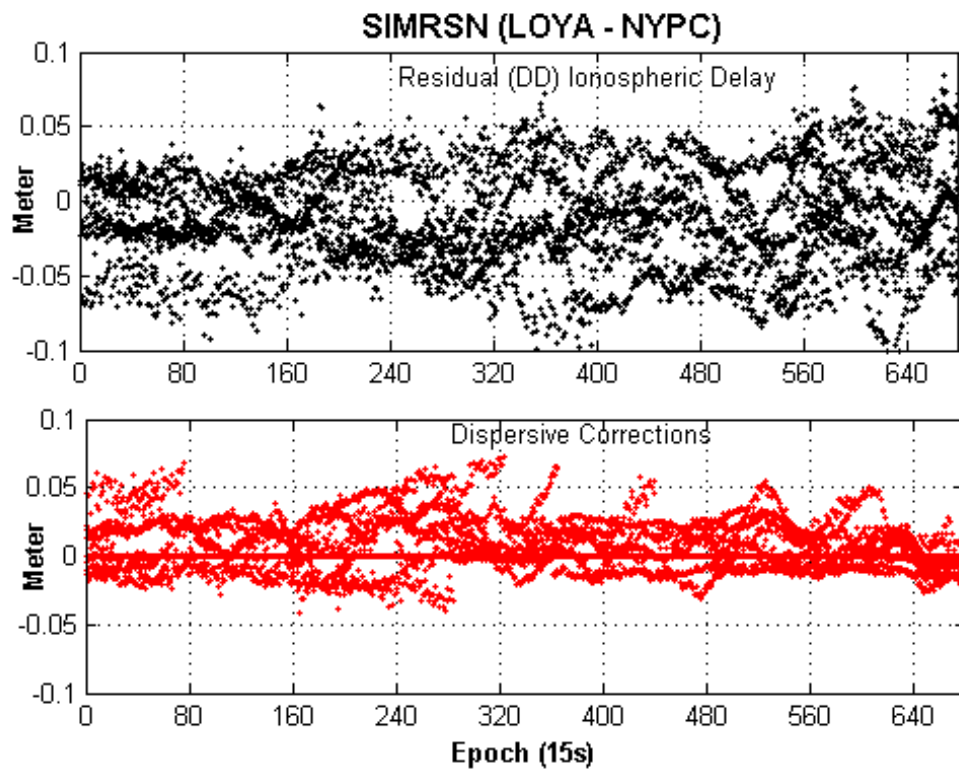


Figure 5.15 SIMRSN, the equatorial experiment. **Top:** The ‘uncorrected’ DD ionospheric delay residuals (dispersive effects) and **Bottom:** The corresponding dispersive corrections (note the line at zero value indicates no correction exists for some satellites); for all satellite combinations in the master-to-user station LOYA-NYPC. The DoY is 166/03 during a year of comparatively high solar activity.

Figure 5.16 shows the randomly selected residual ionospheric delay and the corresponding dispersive corrections for PRN21-22 in the case of SYDNET. Figure 5.17 shows the same quantities for PRN10-24 in the case of SIMRSN. These figures clearly show the generated network corrections, in the opposite directions, follow the trends and almost the magnitude of the residuals ionospheric delay. Therefore, it can be expected that the dispersive corrections should mitigate the residual ionospheric delay to some extent.

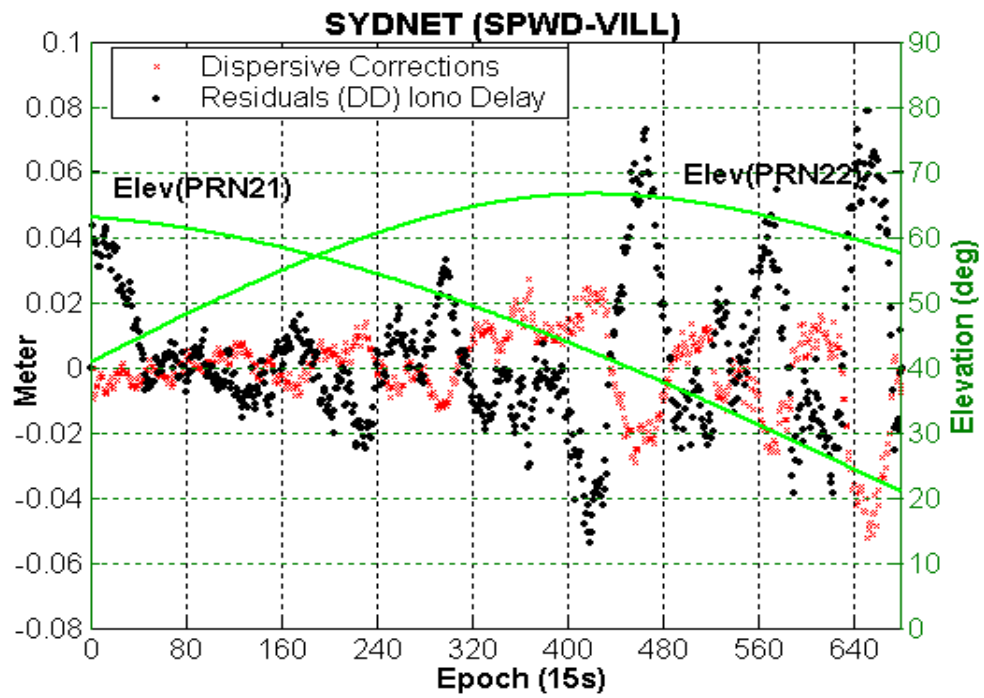


Figure 5.16 The SYDNET experiment: The ‘uncorrected’ DD ionospheric delay residuals on L1 and the corresponding dispersive corrections (vertical-axis on the left) for PRN21-22; the vertical-axis on the right indicates the satellite elevation angles.

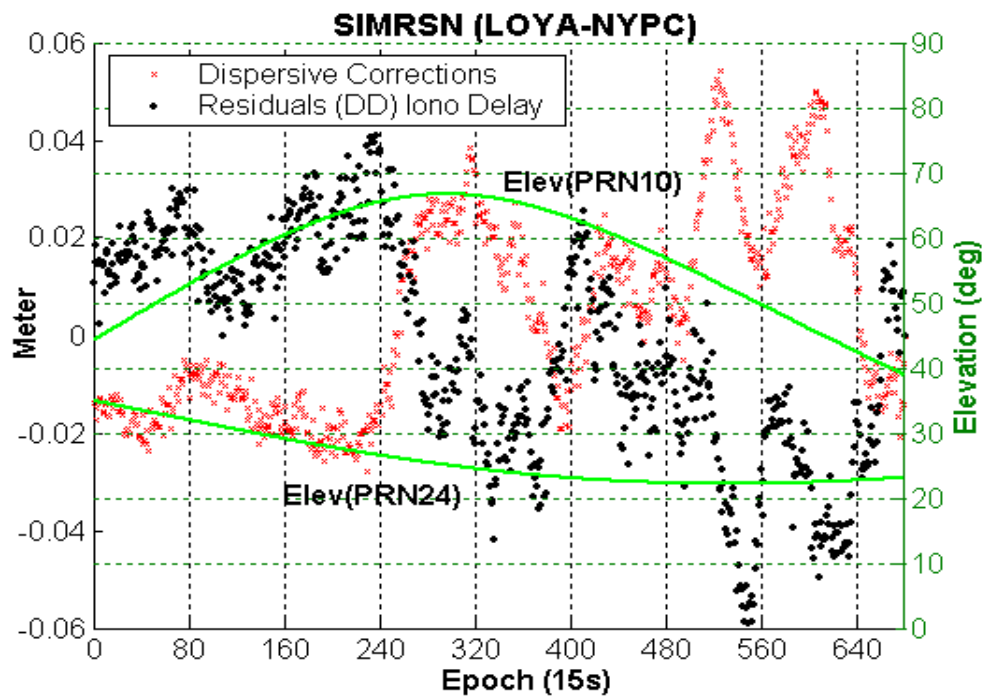


Figure 5.17 The SIMRSN experiment: The ‘uncorrected’ DD ionospheric delay residuals on L1 with the corresponding dispersive corrections (vertical-axis on the left) for PRN10-24. The vertical-axis on the right indicates the satellite elevation angles.

The Non-Dispersive Corrections

Figures 5.18-5.19 show the ‘uncorrected’ residuals of the DD IF (i.e. the non-dispersive effects) and the corresponding ‘original’ and smoothed non-dispersive corrections of master-to-user station, for all satellite combinations, for both the SYDNET and SIMRSN tests. The magnitudes and trends of these corrections are in the range of the uncorrected DD IF residuals, but the smoothed corrections exhibit less variation due to the application of Equation 5.36. In addition, both tests exhibit almost the same level of magnitude of DD IF residuals (and non-dispersive corrections), although the baseline lengths are different. Similar to the case of the ionospheric delay, this could be associated with the strong troposphere effect in the equatorial area and because the climate of Singapore is characterised as Tropical Rainforest (see also Chapter 4).

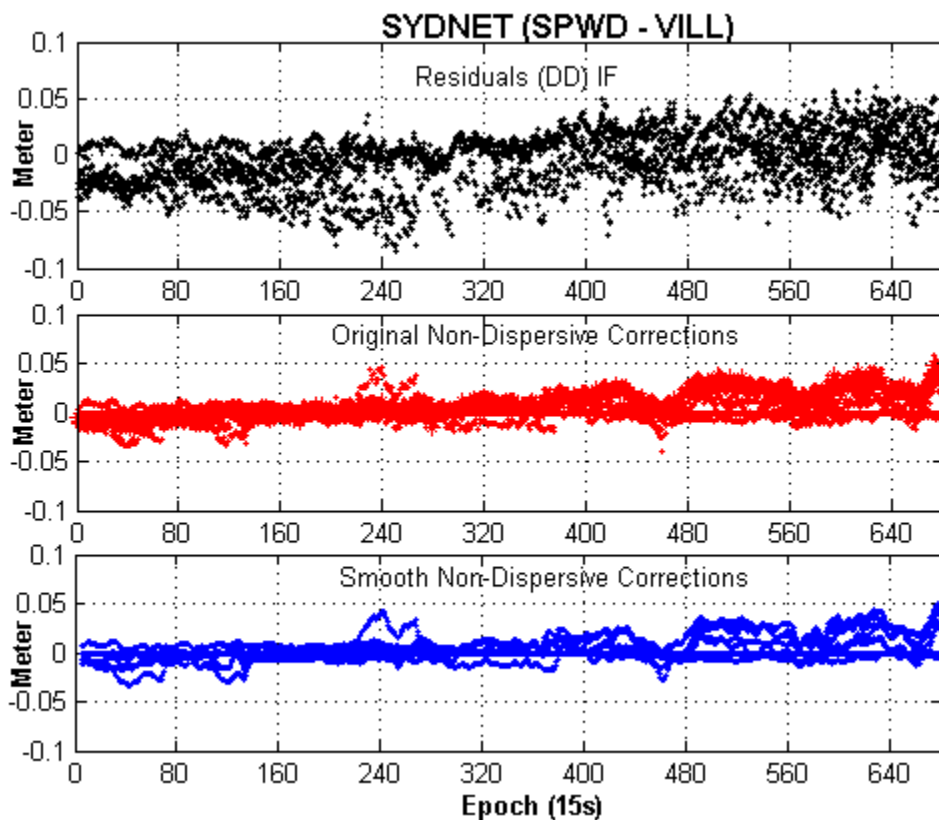


Figure 5.18 SYDNET, the mid-latitude experiment in DoY 166/03. **Top:** The ‘uncorrected’ DD IF residuals (dispersive effects); **Middle:** The original non-dispersive corrections; and **Bottom:** The smooth non-dispersive corrections (note the line at zero value indicates no correction exists for some satellites); for all satellite combinations in the master-to-user station SPWD-VILL.

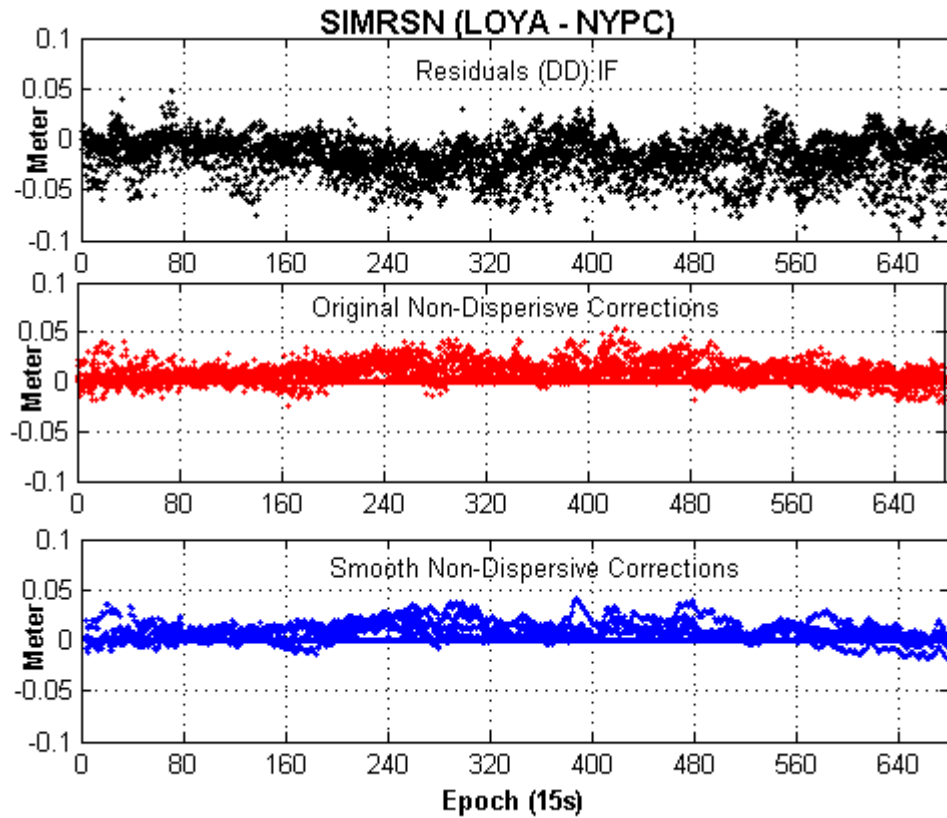


Figure 5.19 SIMRSN, the equatorial experiment in DoY 166/03. **Top:** The ‘uncorrected’ DD IF residuals (dispersive effects); **Middle:** The original non-dispersive corrections; and **Bottom:** The smooth non-dispersive corrections (note the line at zero value indicates no correction exists for some satellites); for all satellite combination in the master-to-user station LOYA-NYPC.

Figure 5.20 shows the selected DD IF residuals and the corresponding non-dispersive corrections for PRN21-26 in the case of SYDNET. Figure 5.21 shows the same quantities for PRN10-29 in the case of SIMRSN. These figures visually show that the generated non-dispersive corrections, in the opposite directions, follow the trends and almost the magnitude of the DD IF residuals.

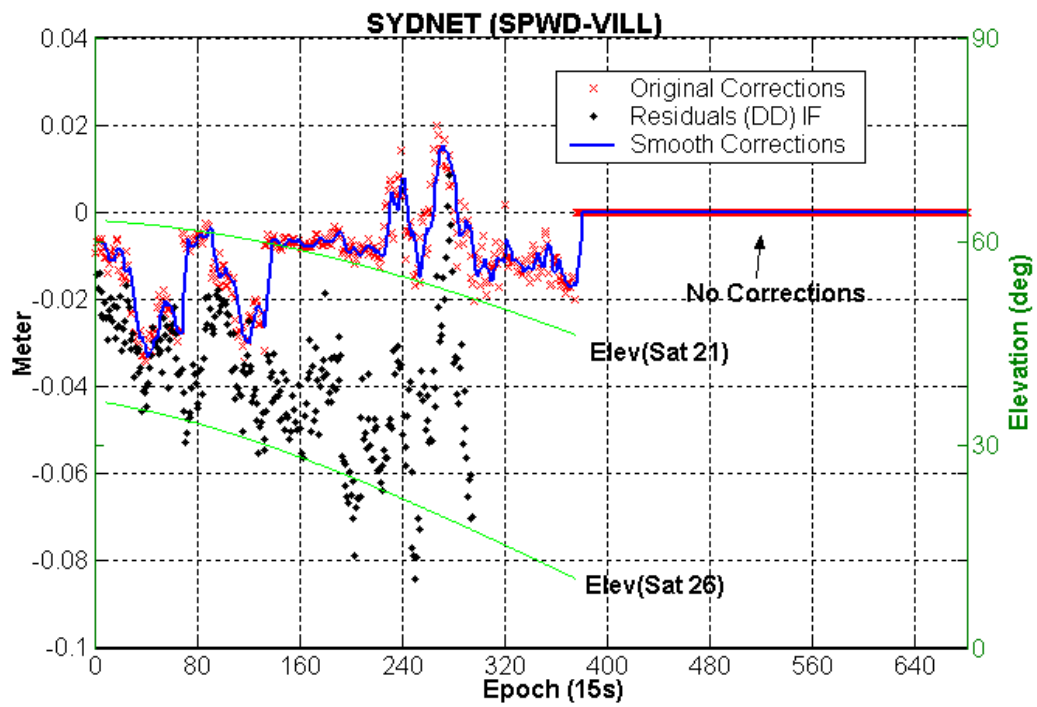


Figure 5.20 The SYDNET experiment: The ‘uncorrected’ DD IF residuals with the corresponding original and smooth corrections (vertical-axis on the left) for PRN21-26; the y-axis on the right indicates the satellite elevation angles.

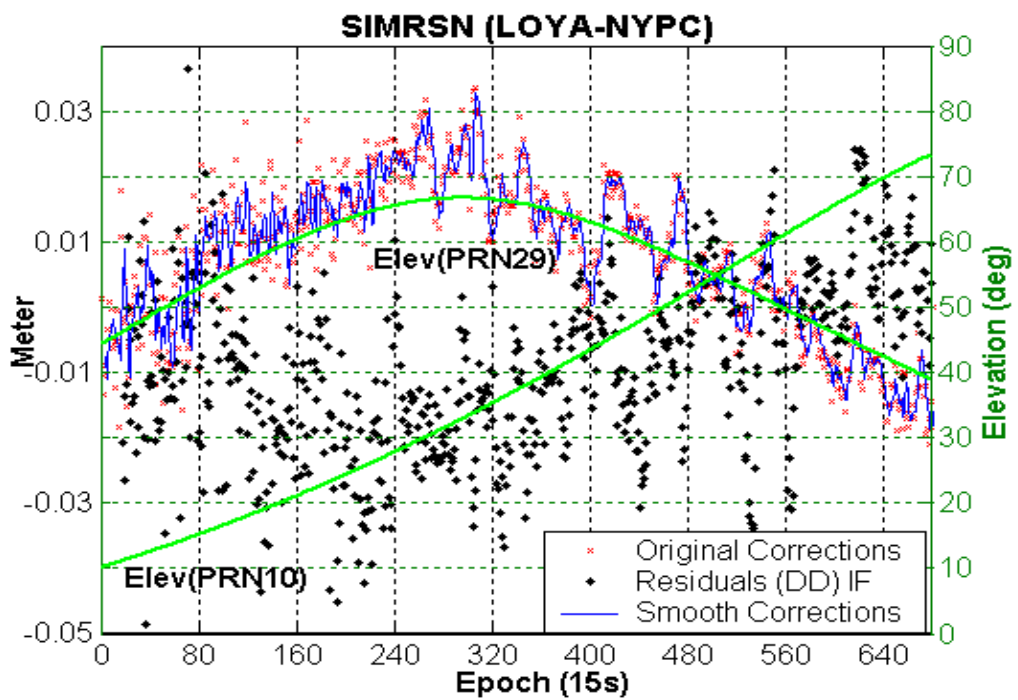


Figure 5.21 The SIMRSN experiment: The ‘uncorrected’ DD IF residuals with the corresponding original and smooth corrections (vertical-axis on the left) for PRN10-29; the y-axis on the right indicates the satellite elevation angles.

As described in Section 5.3.3, the non-dispersive corrections should improve the DD IF processing, which is critical for the next step - to determine the L1 ambiguity (via Equation 5.37). Figure 5.22 demonstrates the effectiveness of this non-dispersive correction in the case of SYDNET. In this figure, one can clearly notice that the corrected (i.e. network-based) residuals exhibit less magnitude than the uncorrected DD IF residuals. In addition, Figure 5.22 also indicates that the network-based technique can be processed for up to 375 epochs in contrast to only 295 epochs for the single-base technique. This visually shows that, no further processing is possible for PRN26 as it reaches a low elevation angle without the non-dispersive corrections. In contrast, an extra 20 minutes of observations can be used to determine the L1 ambiguity via the DD IF using the non-dispersive corrections. Figure 5.23 also shows the improvement in the DD IF residuals after applying the non-dispersive corrections in the case of SIMRSN. Thus, one can expect that the process of indirect L1 ambiguity resolution should perform better in the case of the network-based technique (see next sub-section).

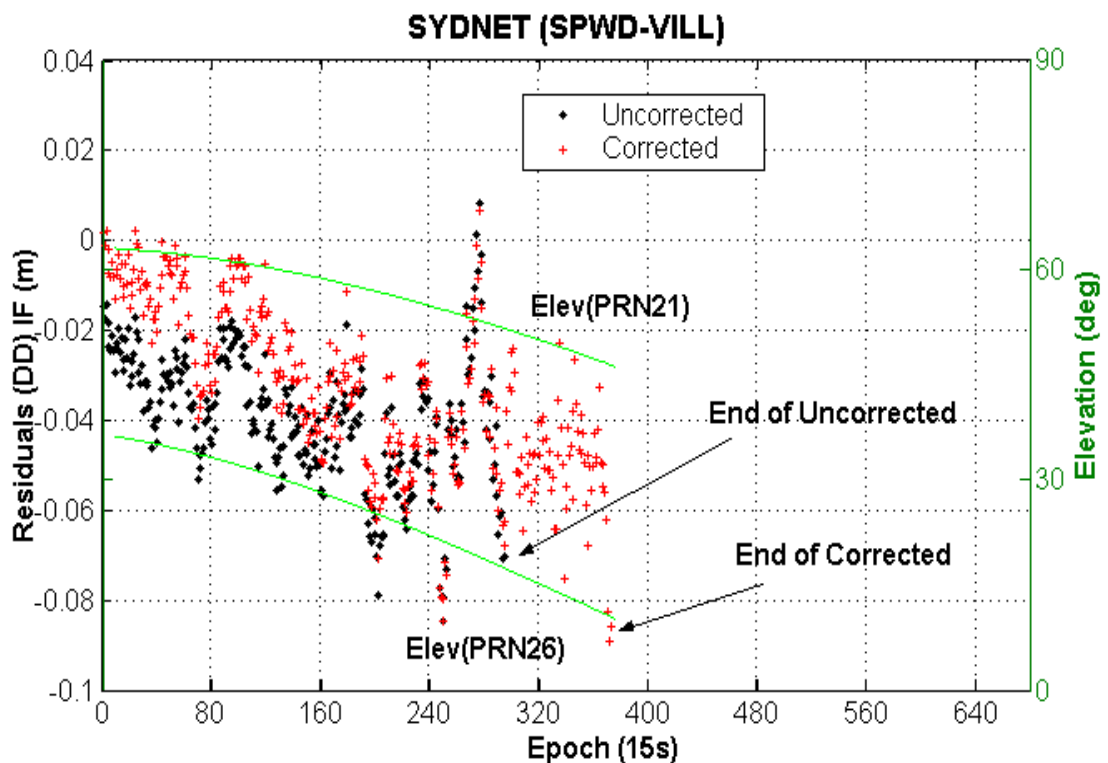


Figure 5.22 The SYDNET experiment: The ‘uncorrected’ and ‘corrected’ DD IF residuals for PRN21-26; the y-axis on the right indicates the satellite elevation angles.

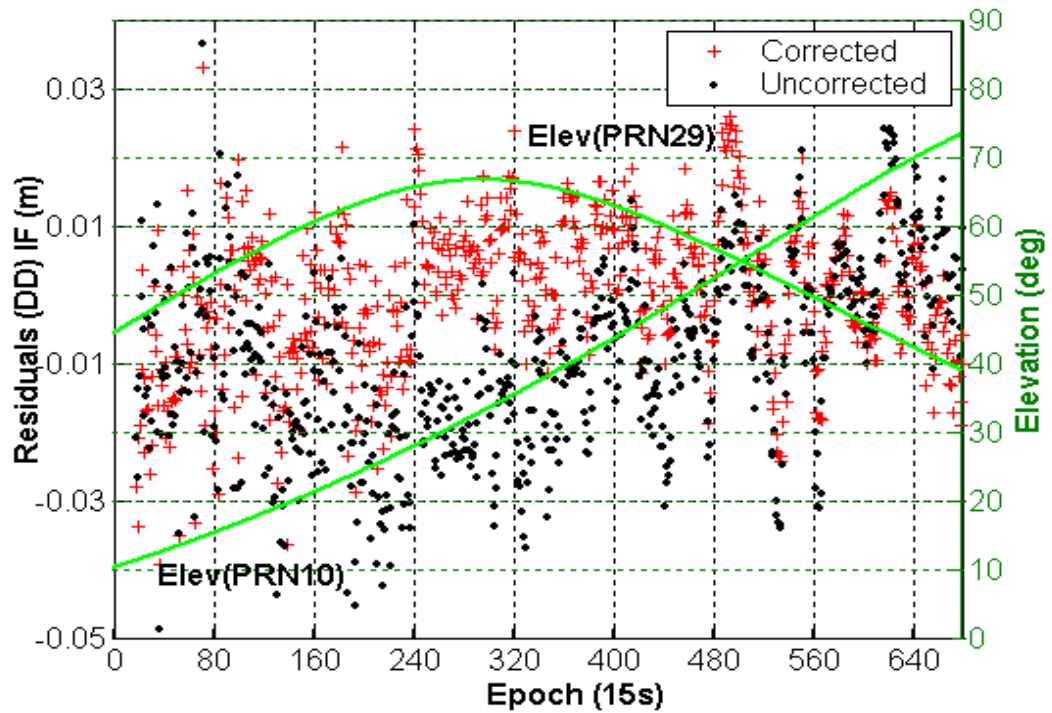


Figure 5.23 The SIMRSN experiment: The ‘uncorrected’ and ‘corrected’ DD IF residuals for PRN10-29; the vertical-axis on the right indicates the satellite elevation angles.

b) Ambiguity Analysis

During the period of the tests single epoch ‘indirect’ AR was attempted using both the single-base (via Equation 3.25) and network-based technique (via Equation 5.37). Following the methodology indicated in Figure 5.10, the result of the ambiguity analysis is summarised in Figure 5.24 and Table 5.3 (SYDNET), and Figure 5.25 and Table 5.4 (SIMRSN). In these tables, the first column indicates the satellite cut-off elevation angle. The second column is the number of DD L1 ambiguities which have been initialised epoch-by-epoch, satellite-by-satellite during the period of the tests. The other columns are the percentile AR statistics which indicate the percentage of correct ambiguity (compared to the ‘known’ ambiguity); the percentage of rejected ambiguity, i.e. the ambiguity that cannot be initialised (mostly due to low elevation satellite angle); and the percentage of wrong ambiguity, i.e. compared to the ‘known’ ambiguity.

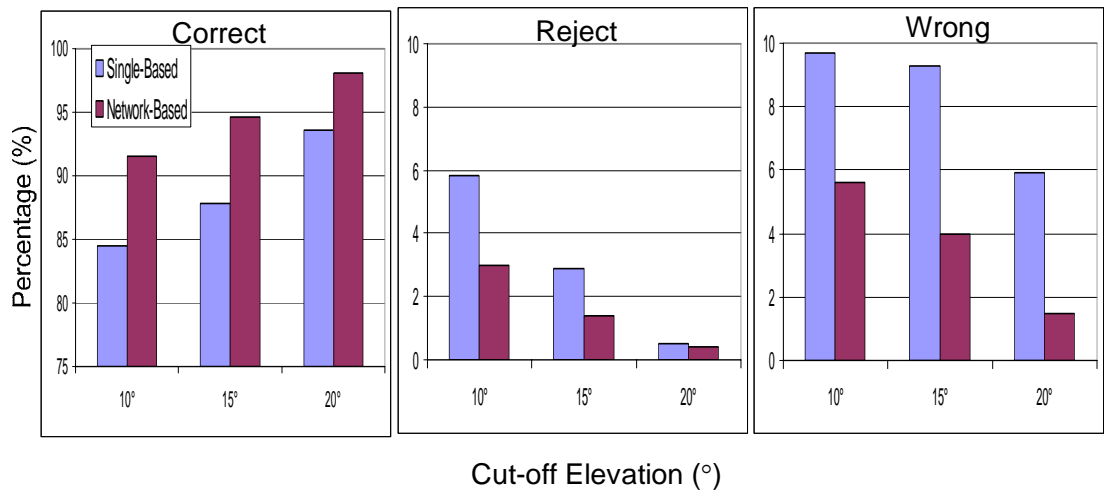


Figure 5.24 Statistical plots for single epoch AR for the SYDNET test.

Table 5.3 Statistical values for single epoch AR for the SYDNET test.

Cut-off Elevation	Case Initialize	Single-Base			Network-Based		
		Correct %	Reject %	Wrong %	Correct %	Reject %	Wrong %
10°	4103	84.5	5.8	9.7	91.5	3.0	5.6
15°	3916	87.8	2.9	9.3	94.6	1.4	4.0
20°	3345	93.6	0.5	5.9	98.1	0.4	1.5

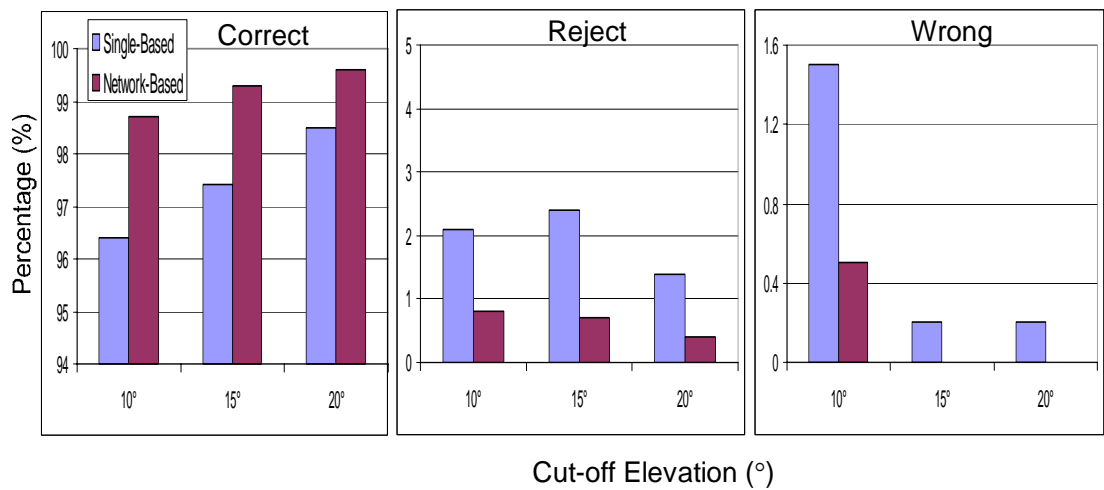


Figure 5.25 Statistical plots for single epoch AR for the SIMRSN test.

Table 5.4 Statistical values for single epoch AR for the SIMRSN test.

Cut-off Elevation	Case Initialize	Single-Base			Network-Based		
		Correct %	Reject %	Wrong %	Correct %	Reject %	Wrong %
10°	4665	96.4	2.1	1.5	98.7	0.8	0.5
15°	3584	97.4	2.4	0.2	99.3	0.7	0
20°	3033	98.5	1.4	0.2	99.6	0.4	0

The above results suggest that the network-based technique does perform better, i.e. higher percentage of correct fixes and lower percentage of rejected fixes, compared to the single-base mode. The more important fact is, however, that the network-based technique also results in less wrong ambiguity fixes. Compared to the single-base mode, the wrong ambiguity fix rates are reduced to 0.2% and 5.3% in the network-based technique for the SYDNET and SIMRSN tests, respectively. It also can be noted that the higher the cut-off elevation angle, the better the results for both techniques.

As indicated in Sections 2.4.3 and 5.3.1 (in Step 3), it is usual practice to validate the resolved ambiguity using the F-ratio test with a critical threshold value of 3. Figures 5.26-5.27 show the F-ratio validation values for both the SYDNET and SIMRSN tests. The figures clearly show that the network-based mode, in most cases, results in higher ratio values than the single-base technique.

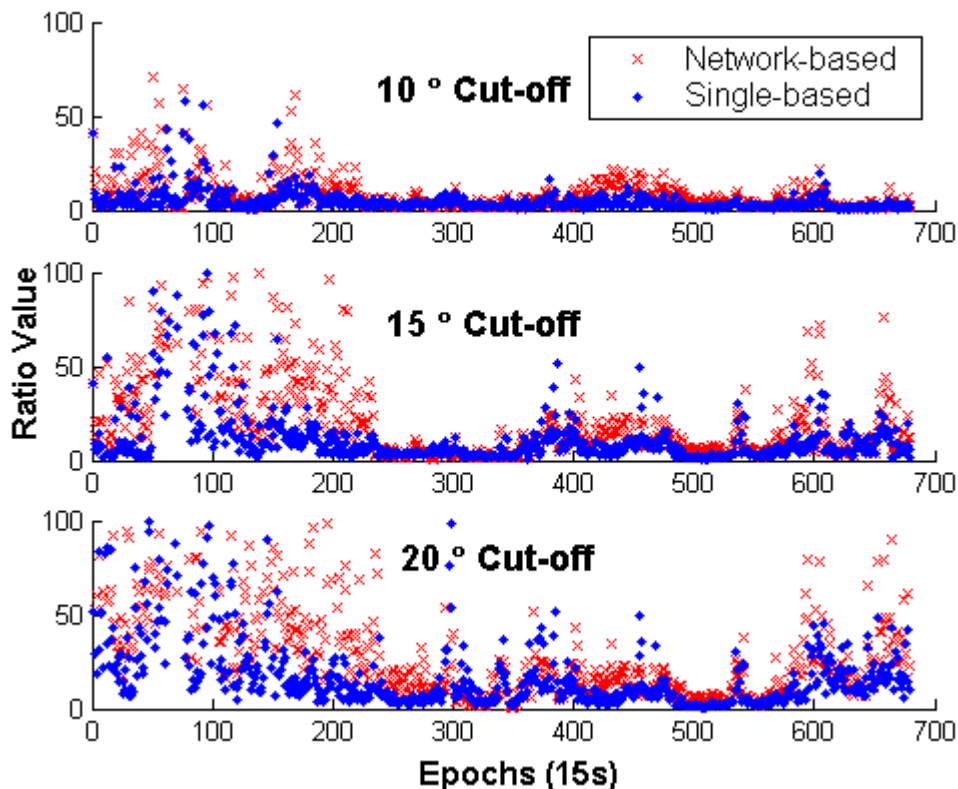


Figure 5.26 F-ratio values of single-base and network-based techniques using various elevation cut-off angles for the SIMRSN test.

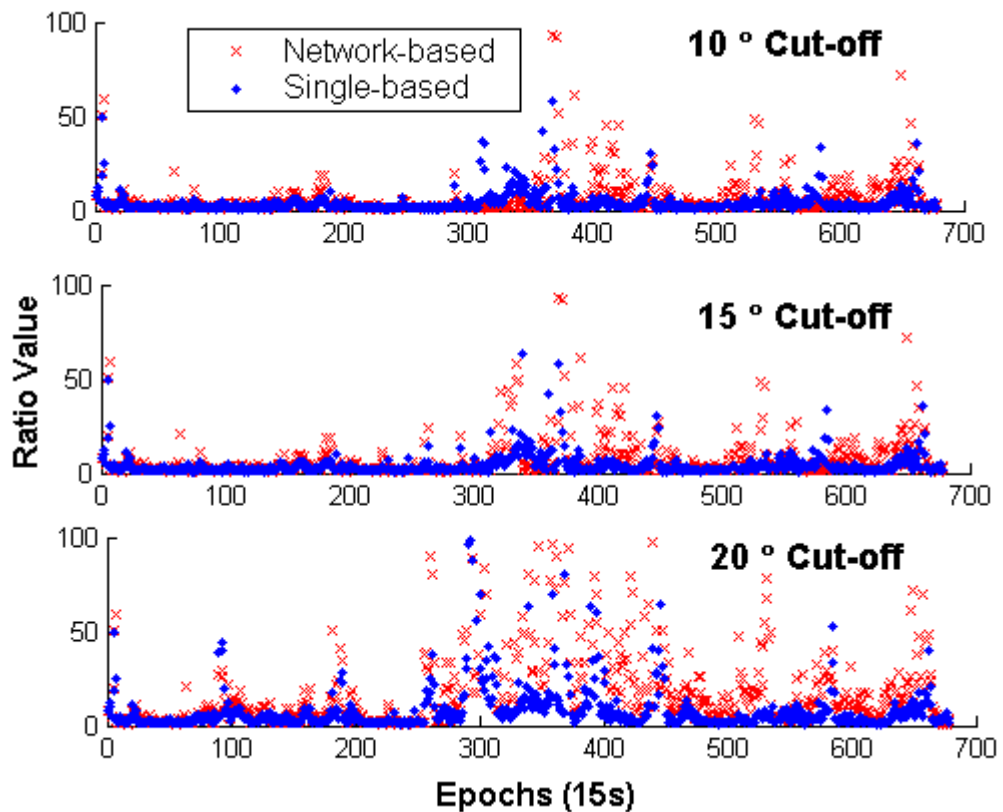


Figure 5.27 F-ratio values of single-base and network-based techniques using various elevation cut-off angles for the SYDNET test.

However, this does not mean that resolved ambiguities with F-ratio values above this critical value are always correct, or those with F-ratio values below this critical value are incorrect (Verhagen, 2004). It is interesting to analyse the performance of ambiguity validation, since the ambiguities are ‘known’, and determine whether the network-based technique can assist this validation technique or not.

Further analysis can be conducted by checking the critical F-ratio value of the correct and wrong ambiguity (Tables 5.3-5.4) against the ‘known’ ambiguity value on an epoch-by-epoch and satellite-by-satellite basis, for both the single-base and network-based techniques. The analyses can be categorised into four cases (the results are summarised in Tables 5.5-5.6 for the SYDNET and SIMRSN, respectively):

- a) The percentage of ambiguities which were passed and correctly accepted by the F-ratio test (first and the fourth columns of Tables 5.5-5.6);

- b) The percentage of ambiguities which were passed but incorrectly rejected (Type I error) by the F-ratio test (second and the sixth columns of Tables 5.5-5.6);
- c) The percentage of ambiguities which failed and correctly rejected by the F-ratio test (third and the seventh columns of Tables 5.5-5.6) and;
- d) The percentage of ambiguities which failed but incorrectly accepted (Type II error) by the F-ratio test (fourth and the eighth columns of Tables 5.5-5.6).

Table 5.5 Statistics of ambiguity validation for the SYDNET test.

Elevation	Single-Base				Network-Based			
	Passed %		Failed %		Passed %		Failed %	
	Accept	Reject	Accept	Reject	Accept	Reject	Accept	Reject
10°	47.8	52.2	18.3	81.7	58.7	41.3	29.4	70.6
15°	47.5	52.5	19.4	80.6	61.7	38.3	28.5	71.5
20°	66.6	33.4	13.9	86.1	85.1	14.9	20.0	80.0

Table 5.6 Statistics of ambiguity validation for the SIMRSN test.

Elevation	Single-Base				Network-Based			
	Passed %		Failed %		Passed %		Failed %	
	Accept	Reject	Accept	Reject	Accept	Reject	Accept	Reject
10°	55.6	44.4	5.0	95.0	74.6	25.4	4.5	95.5
15°	82.1	17.9	0	100	90.6	9.4	0	100
20°	90.3	9.7	0	100	96.6	3.4	Nil	Nil

Firstly, the above tables clearly indicate problems with the ratio test for both the single-base and network-based techniques. Secondly, the results of the network-based technique in both tables show higher percentages for correctly accepted (case a) and rejected (case b) ambiguities, but lower percentages of type I (case b) and type II (case d) errors. This result suggests that the network-based technique can assist the validation process. However, one must examine the results in Tables 5.5-5.6 ‘internally’ since the number of correct and wrong ambiguities for the single-base and network-based techniques are different (see also Tables 5.3-5.4). For example, in the case of SYDNET, although the percentage of Type II errors is larger in the network-based, the total wrong ambiguities is smaller than for the single-base mode (see Table 5.3). Since these tests differ only by applying the network correction or not, the overall result strongly suggests that applying the non-dispersive corrections (via Equation 5.37) strengthens the AR and the validation test.

c) Fixed L1 Residuals & Coordinates Analysis

As proposed in Equation 5.38 (i.e. after removing the ambiguity biases), the dispersive and non-dispersive corrections should be applied with the expectation that this reduces the remaining distance-dependent errors in the corrected measurements. It should be noted that the DD L1 measurements are also contaminated by residual station-dependent errors. However, based on the fact that the user is static (and the receiver is part of the station network), station-dependent errors are assumed to be at a minimum level. Figures 5.29-5.30 show all satellite combinations of the DD L1 residuals (for 10° cut-off elevation angle), with and without applying the corrections for the SYDNET and SIMRSN respectively.

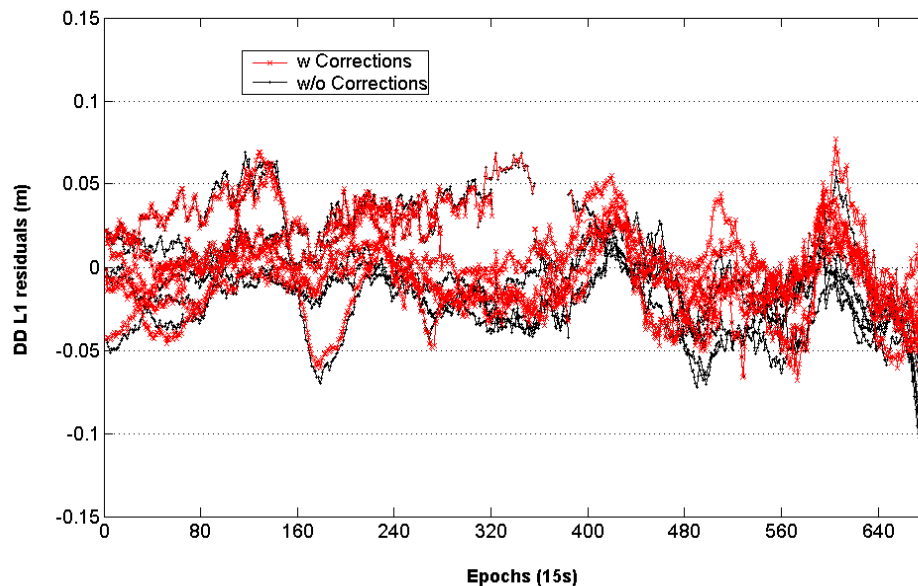


Figure 5.28 DD L1 residuals for SPWD-VILL (SYDNET), red is with correction and blue is without correction applied.

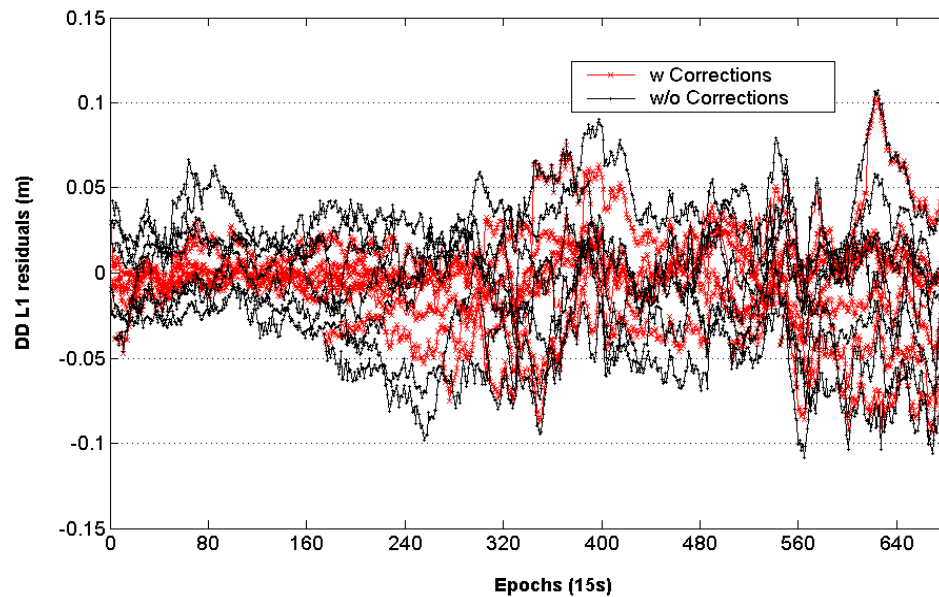


Figure 5.29 DD L1 residuals for LOYA-NYPC (SIMRSN), red is with correction and blue is without correction applied.

Figures 5.28-5.29 show, in general, that the dispersive and non-dispersive corrections have reduced the magnitude of the residuals compared with the results without applying the corrections. It can be seen that there are also residuals which are slightly increased after the corrections are applied. This problem could be explained by the fact that the dispersive and non-dispersive corrections are now being combined in Equation 5.38. This procedure in some sense generates the uncertainty of the ‘true’ corrections for some satellite pairs at a certain epoch. This, however, needs further investigation and should be the focus for future research into implementing this procedure.

Apart from the above problem, the user position is estimated for every epoch with and without applying the corrections. These estimated coordinates are compared with the ‘known’ coordinates of the user stations (VILL for SYDNET and NYPC for SIMRSN), and the difference (i.e. offset) is expressed in the three components dEast, dNorth and dUp. This is shown in Figures 5.31-5.32 (for 10° cut-off elevation angle) with their corresponding mean offset and variations. Tables 5.7-5.8 summarises this result, and for the other cut-off elevation angles used in the position calculations.

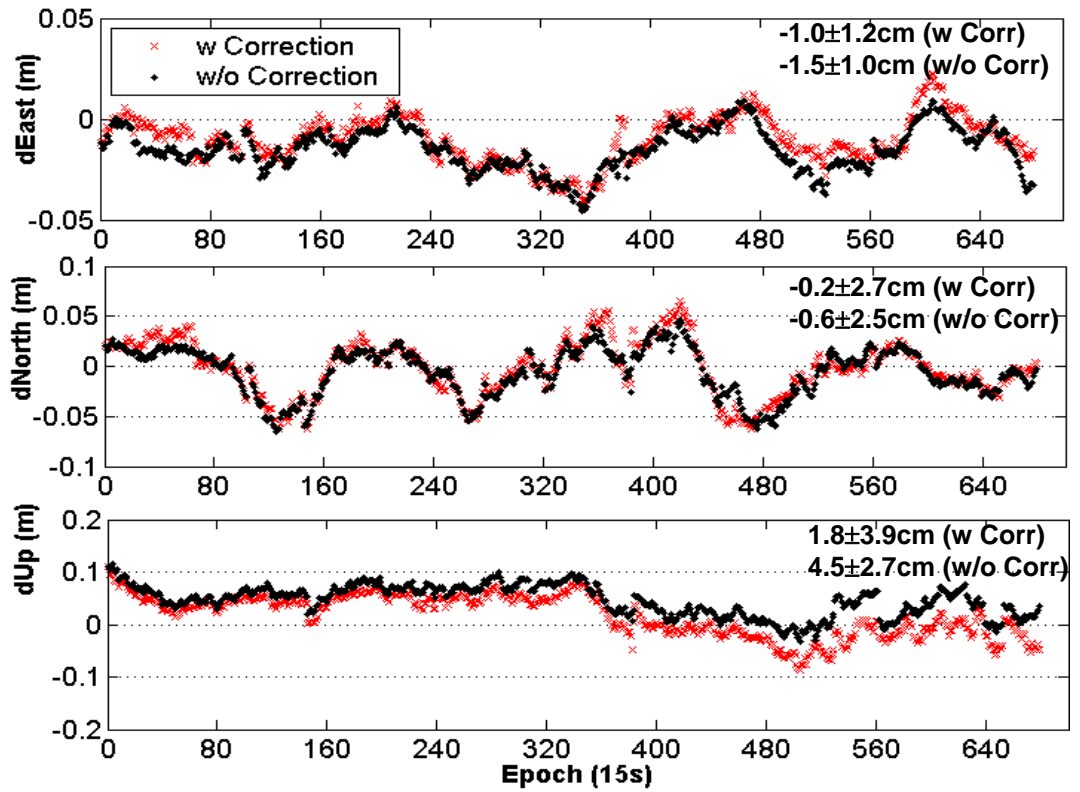


Figure 5.30 Offset of the estimated user positions (compared to the known position) of VILL (SYDNET). The estimated coordinates are obtained with and without correction applied.

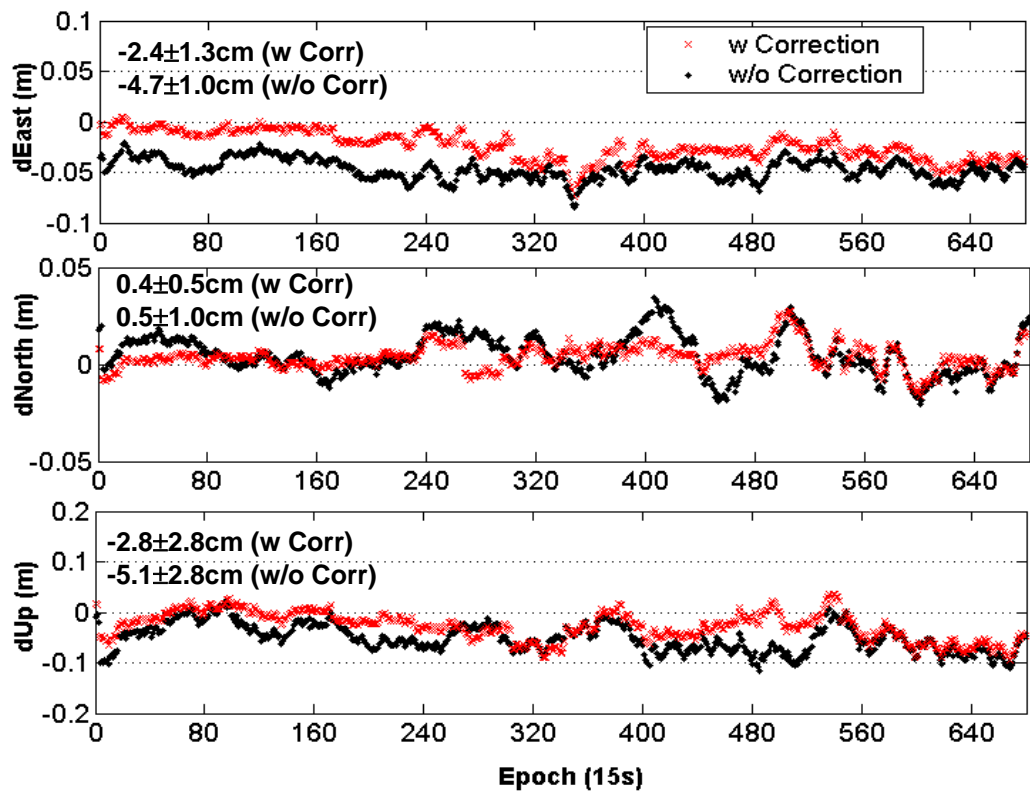


Figure 5.31 Offset of estimated user positions (compared to the known position) of NYPC (SIMRSN). The estimated coordinates are obtained with and without correction applied.

Table 5.7 Position statistics for VILL (SYDNET) with (single-base) and without (network-based) corrections applied compared to the known coordinate.

Cut-off Elevation	Single-Base			Network-Based		
	dEast (cm)	dNorth (cm)	dUp (cm)	dEast (cm)	dNorth (cm)	dUp (cm)
10°	-1.5±1.0	-0.6±2.5	4.5±2.7	-1.0±1.2	-0.2±2.7	1.8±3.9
15°	-1.5±1.0	-0.6±2.5	4.4±2.8	-1.0±1.1	-0.1±2.8	1.3±3.8
20°	-1.2±1.3	-0.8±3.5	2.9±3.4	-0.6±1.3	-0.6±3.7	-0.8±4.2

Table 5.8 Position statistics for NYPC (SIMRSN) with (single-base) and without (network-based) corrections compared to the known coordinate.

Cut-off Elevation	Single-Base			Network-Based		
	dEast (cm)	dNorth (cm)	dUp (cm)	dEast (cm)	dNorth (cm)	dUp (cm)
10°	-4.7±1.0	0.5±1.0	-5.1±2.8	-2.4±1.3	0.4±0.7	-2.8±2.8
15°	-4.5±1.5	0.4±1.1	-4.4±3.5	-2.1±1.8	0.5±0.8	-1.8±2.5
20°	-4.1±1.5	0.4±1.5	-5.4±5.9	-1.8±1.7	0.5±0.9	-1.8±3.2

From Figures 5.30-5.31 and Tables 5.7-5.8, it can be seen that the network corrections improve the coordinate accuracy when compared with the solution obtained without the network correction applied (except for a small increment of 0.1cm in dNorth component for 15° elevation angle test in Table 5.8). The mean offsets are reduced down to 0.5cm-2.4cm for the dEast component (except for the abovementioned case); 0.1-0.5cm for the dNorth component (except for the abovementioned case); and 2.3-3.7cm for the dUp component, for both the VILL and NYPC stations. The variations of these offset, however, does not show a discernible trend. In some cases the variation can increase after the correction is applied. Apart from this, some components in Tables 5.7-5.8 show improvement. This indicates that applying the combined correction (Equation 5.38) does not always guarantee less variability in the positioning results. This is also dependent on other residual biases that still exist, such as the station-dependent errors.

5.5 Concluding Remarks

Experiments with local GPS networks in mid-latitude and equatorial regions have been described. Some advantages of the network processing strategy were demonstrated. Test results and analyses have shown that the proposed strategy performs reasonably well in:

- a) generating the dispersive and non-dispersive corrections, and the smoothed non-dispersive corrections,
- b) resolving the ambiguities and assisting the ambiguity validation process, and
- c) computing the user's position.

Although the tests of the network-based processing strategy were conducted as single-epoch positioning, these are essentially “simulated” RTK results. In practice, when the user receiver is moving, it is difficult to mitigate station-dependent errors and this complicates the process of ambiguity resolution. Therefore, further tests are necessary to validate this new processing strategy with kinematic data. Additionally, future tests should consider the use of the VRS technique. The proposed network-based processing strategy discussed in this chapter is being implemented as part of the real-time processor of the SYDNET network.

INVESTIGATION INTO STOCHASTIC MODELLING FOR STATIC NETWORK-BASED GPS POSITIONING

6.0 Introduction

Although significant systematic errors can be modelled in network-based positioning, residual biases may still be present. In this case, not only the station-dependent terms but also the distance-dependent terms may affect the positioning process. It is difficult to define a functional model that can adequately deal with these residual biases, but their influence must be accounted for. The stochastic model, e.g. the variance-covariance (VCV) matrix, has been used to define the observation noise characteristics for this purpose.

To employ (weighted) least squares estimation, both the functional and stochastic models need to be defined. Unlike the functional model, research on the stochastic model of GPS measurements has not been as widespread (Bona, 2000; Teunissen et al., 1998; Teunissen, 2001; Tiberius et al., 1999). The common stochastic model assumes that raw GPS measurements are homoskedastic (i.e. their a priori variances are all the same) and statistically independent (Wang, 1998), while the constructed DD measurements are considered mathematically correlated. These assumptions are ‘unrealistic’ of course, since the GPS measurements exhibit different variances and are physically correlated with each other (spatially and/or temporally) in a sense that the atmospheric delay, orbital errors, and clock biases can be effectively cancelled out by the data differencing process. Moreover, the unique stochastic properties of the network must be taken into account since the original DD measurements from master-to-user station are corrected for by the network parameters.

In this chapter, the stochastic modelling of the GPS measurements will be assumed to be heteroskedastic (i.e. they have different a priori variance) and have temporal

correlations, which may be considered a more ‘realistic’ stochastic model. This realistic stochastic model will be adopted for static network-based positioning. In the course of investigating stochastic modelling, some questions should be answered. How to formulate the ‘realistic’ stochastic model for the network-based positioning technique? How to deal with the uncertainty of the network parameters in processing master-to-reference station data, e.g. in the Linear Combination Method (LCM)? What kind of improvement is expected in the positioning process by applying this ‘realistic’ stochastic model?

6.1 Formulation of the Stochastic Model

6.1.1 Quality Indicators

In the construction of the stochastic model for the DD measurements it is usually assumed that all raw measurements have the same a priori variance. Typically, the standard deviation of the GPS measurements are assumed to be 10-30cm for P-code and 0.02-0.03cm for carrier phase (Bona, 2000; Hoffmann-Wellenhof et al., 2001; Tiberius, 1999; see also Section 2.1.4), which could be derived by ‘perfect’ circumstances in the Monte Carlo simulations (Ward, 1996) or other heuristic methods.

As stated earlier, considering the GPS measurements to have the same level of variations is unrealistic. Moreover, if the threshold of the variations is too optimistic, one may have a wrong impression that the positioning result meets the quality requirement. On the other hand, applying different variance models to any group of measurements may require a very good criterion (Cross, 1983). In the case of GPS, one may use some quality indicators to obtain more reliable variances to support heteroskedastic modelling. Hence the following quality indicators are suggested.

Satellite Elevation

The basic assumption is that the signal which is transmitted from a low elevation angle satellite tends to be noisier than the signal coming from a high elevation angle satellite.

Using this criterion, the precision of one-way L1 GPS measurements for satellite j can be represented by an exponential function such as (Han, 1997):

$$\sigma^j = s.[a_0 + a_1.\exp(-e^j/e_0)] \quad (6.1)$$

where e^j is the elevation angle; a_0 , a_1 and e_0 are constants determined experimentally from different kinds of GPS receivers (e.g. Euler and Goad, 1991; Han, 1997); and s is a scale factor which will weigh the contribution of carrier phase measurements and is assumed to be constant over a short period of time (2-5 minute window of data) (Dai, 2002). As stated by Tiberius et al. (1999), the elevation dependence of measurement noises is induced mainly by the receiver antenna's gain pattern, with other factors such as atmospheric signal attenuation making a lesser contribution. Additionally, the use of satellite elevation angle as a quality indicator is dependent on the type of receiver used, as already indicated in Equation 6.1. For this reason, the use of satellite elevation angle does not always be a good indicator of the variation of measurement quality.

Signal to Noise Ratio (SNR)

It is common for GPS receivers to output the ratio of the power density of a received signal (S), and the total noise power density (N), measured at the same time and in the same place in a circuit (Langley, 1998b). The ratio S/N is often called the signal-to-noise ratio, or SNR. Usually, the carrier-to-noise power density ratio, C/N_0 , is preferred (Ibid, 1998b; Ward, 1996). The basic assumption is that the satellite signal which has a high C/N_0 value will be less noisy than the one with a low value of C/N_0 . Langley (1998b) suggested that the ratio is a key parameter in the analysis of GPS receiver performance and has a direct bearing on the precision of the receiver observations. For example, the precision of the phase lock loop (PLL) can be given as:

$$\sigma_{\text{PLL}} = \sqrt{\frac{B_p}{c/n_0} \frac{\lambda}{2\pi}} \quad (6.2)$$

where B_p is the carrier loop noise bandwidth (Hz); c/n_0 is the carrier-to-noise density expressed as a ratio ($=10^{(C/N_0)/10}$ for C/N_0 expressed in dB-Hz); and λ is the wavelength (m). Ward (1996) and Misra & Enge (2004) present more complex formulas for σ_{PLL} by

considering other factors such as the internal and external thermal noise, vibration-induced oscillator, and the presence of long and short delay multipath. Although SNR reflects the noise characteristics, Satirapod (2002) showed that there are variations in the SNR for the same receiver type, as well as for different receiver types.

Least Squares Residual

The satellite elevation angle and the SNR approaches have been the most popular means of defining the heteroskedastic model for GPS measurement quality. An alternative is to utilise the residual series of the DD measurements, which can be obtained from least squares estimation (see Equation 2.70). The basic assumption is that the least squares residuals contain sufficient information to reflect the presence of residual biases and measurement noises. An extended observation period is required to generate the redundant residuals in the positioning modes: static, fast static or even during the initialisation period of the kinematic mode. Several studies have reported that the residuals can be utilised to construct the heteroskedastic and correlated error model, so as to define the a priori VCV matrix of the DD measurements.

El-Rabbany (1994) and El-Rabbany & Kleusberg (2003) employed an empirical covariance function model, which can be determined from the residuals of the modified sequential least squares estimation procedure. In this way the effect of physical correlation can be taken into account. The studies found that neglecting the physical correlation can lead to unrealistically small standard deviations (i.e. a very optimistic VCV matrix) for the estimated parameters. Teunissen et al. (1998) exploited this residual to study the correlation between the two GPS frequencies. Their results seemed to prove that the residual-based non-diagonal VCV matrix can represent the noise characteristics better than the simple diagonal matrix does. They also claimed that if the L1 and L2 observations were assumed to be uncorrelated, less precise ambiguity estimates will be obtained. Dai (2002) suggested an integrated procedure for GPS/GLONASS processing that required the generation of an adaptive real-time VCV matrix. In fact, this real-time VCV matrix is iteratively estimated from the residual series (and the corresponding VCV matrix) of the least squares estimation procedure. Ibid (2002) claimed that the integrated procedure results in a success rate of 99.3% for single-epoch AR compared to 81.4% using the homoskedastic stochastic model. The

study also indicated that the residual-based stochastic model can produce better positioning results than the elevation-dependent empirical stochastic model does.

Based on the residual series and the corresponding VCV matrix of the residuals, a rigorous statistical method known as Minimum Norm Quadratic Unbiased Estimation (MINQUE) (Rao, 1971) can be employed to estimate the VCV matrix of the DD measurements (Wang et al., 1998). Moreover, a simplified MINQUE procedure has been developed by Satirapod (2002). Their studies claimed that the estimated VCV matrix with this method is capable of reducing the volume of the ambiguity search space while also increasing the reliability of the AR. This method will be discussed further in this Chapter.

6.1.2 VCV Matrix for Network-Based Positioning

In network-based positioning with an interpolation technique such as the LCM algorithm (see Chapter 5), the stochastic properties derived from the network (i.e. master-to-reference stations) parameters will affect the master-to-user estimates. That is, the uncertainty of components in the network correction will propagate into the master-to-user station solution. This propagation can be explained by using the VCV matrix (of the DD measurements).

a) Error Propagation Law

As in the case of the a priori variance of the measurements, the covariance itself can be estimated from simultaneous measurements (see Cross, 1983). However, the estimation is so difficult that it is often ignored (Ibid, 1983). As a result the VCV is a diagonal matrix. Meanwhile, the DD measurements are mathematically derived (by applying Equations 2.51 and 2.56), and the non-diagonal VCV components at a particular epoch (see Equation 2.65) are the result of applying the error propagation law (see Equation 2.63) and therefore, the VCV matrix of all the DD measurements is a block-diagonal matrix.

Similarly, the geometric correlation of network-based positioning can be defined using the error propagation law. The standard deviation for the single-differenced (SD) LCM measurements (Equations 5.30-5.31) is defined in Equation 5.24. Assuming a network

of three reference stations, the VCV matrix for this SD combination at a particular epoch is (Han, 1997):

$$\begin{aligned} \mathbf{VCV}_{\sum_{i=1}^3 \alpha_i \Delta \phi_i} &= \left(1 + \sum_{i=1}^3 \alpha_i^2 \right) \cdot \sigma_k^2 \\ &= (1 + \alpha_1^2 + \alpha_2^2 + \alpha_3^2) \begin{bmatrix} (\sigma^1)^2 & 0 & \dots & 0 \\ 0 & (\sigma^2)^2 & \dots & 0 \\ \vdots & \vdots & \ddots & \vdots \\ 0 & 0 & \dots & (\sigma^k)^2 \end{bmatrix} \end{aligned} \quad (6.3)$$

where k is the number of satellites, while the other parameters have been defined in Equations 5.21, 5.22 and 5.24. Equation 6.3 has specified that the SD of the LCM measurement is mathematically uncorrelated. Applying the double-differencing operator \mathbf{C} as defined in Equation 2.62, the VCV matrix for the DD of the LCM measurements at a particular epoch is:

$$\begin{aligned} \mathbf{VCV}_{\sum_{i=1}^3 \alpha_i \Delta \nabla \phi_i} &= \mathbf{C}_k \cdot \mathbf{VCV}_{\sum_{i=1}^3 \alpha_i \Delta \phi_i} \cdot \mathbf{C}_k^T \\ &= \frac{\left(1 + \sum_{i=1}^3 \alpha_i^2 \right)}{2} \cdot \mathbf{VCV}_{\Delta \nabla \phi_{u,3}} \end{aligned} \quad (6.4)$$

where u is the user station and the reference station 3 is considered to be the master station; and $\mathbf{VCV}_{\Delta \nabla \phi_{u,3}}$ is the VCV matrix for master-to-user station (which is similar to Equation 2.65). The first term of Equation 6.4 indicates that the geometric correlation of the network has been embedded within the VCV matrix. Han (1997) suggested that the variances (σ_k^2) should be estimated by the function described in Equation 6.1, at least for the heteroskedastic model of the raw measurements.

b) VCV Estimation by MINQUE

Similar to the functional model, the unknown parameters in the stochastic model can also be estimated. MINQUE is one of the modern statistical methods commonly used for this purpose (Koch & Kuche, 2002; Wang et. al., 1998; Xu et. al, 2006). The procedure is to directly estimate each component of the VCV matrix of the DD

measurements by utilising the least squares residual series. The estimation process is conducted without any assumptions (in contrast to the homoskedastic model) and without complex functional models (such as Equations 6.1-6.2).

In the case of the single-base technique, MINQUE has been successfully applied to estimating the VCV matrix of the DD measurements for static and fast static positioning (Wang, 1999; Satirapod, 2002). The same procedure could also be used to estimate the VCV matrix for the network-based technique. Since the DD measurements of master-to-user station are modified by the network correction (see Equation 5.33), the least squares residuals and the corresponding VCV matrix of residuals can be the input for MINQUE. While using the MINQUE for processing the master-to-user station baseline, the estimated VCV matrix should contain the unique stochastic properties of the network.

MINQUE Procedure

In this section, the MINQUE and the simplified MINQUE procedure as reported in Wang et al., (1998), Wang (1999) and Satirapod (2002) are reviewed. Suppose that m satellites are tracked at epoch i by two receivers (a master and user station), and subsequently the number of independent DD measurements is $r = m-1$. Without loss of generality, the VCV matrix of the DD measurements (Equation 2.65) can be parameterised as:

$$\mathbf{VCV} = \sigma^2 \mathbf{Q} \otimes \mathbf{I} = \sum_{j=1}^k \theta_j \mathbf{T}_{ji} \quad (6.5)$$

where \mathbf{Q} is the cofactor matrix; and $k = r(r+1)/2$ is the number of the unknown \mathbf{VCV} components; and

$$\begin{aligned} \boldsymbol{\theta} &= [\theta_1, \theta_2, \dots, \theta_k]^T \\ &= [\sigma_{11}^2, \sigma_{22}^2, \dots, \sigma_{rr}^2, \sigma_{12}, \sigma_{13}, \dots, \sigma_{1r}, \sigma_{23}, \dots, \sigma_{2r}, \dots, \sigma_{(r-1)r}]^T \end{aligned} \quad (6.6)$$

is the vector of the unknown VCV components; and \mathbf{T} is the accompanying matrix which is defined as follow (Wang, 1999):

$$\mathbf{T}_{1i} = \begin{bmatrix} 1 & 0 & \cdots & 0 \\ 0 & 0 & \cdots & 0 \\ \vdots & \vdots & \ddots & \vdots \\ 0 & 0 & \vdots & 0 \end{bmatrix}, \mathbf{T}_{2i} = \begin{bmatrix} 0 & 0 & \cdots & 0 \\ 0 & 1 & \cdots & 0 \\ \vdots & \vdots & \ddots & \vdots \\ 0 & 0 & \cdots & 0 \end{bmatrix}, \dots, \mathbf{T}_{ri} = \begin{bmatrix} 0 & 0 & \cdots & 0 \\ 0 & 0 & \cdots & 0 \\ \vdots & \vdots & \ddots & \vdots \\ 0 & 0 & \cdots & 1 \end{bmatrix}, \quad (6.7)$$

$$\mathbf{T}_{(r+1)i} = \begin{bmatrix} 0 & 1 & 0 & \cdots & 0 & 0 \\ 1 & 0 & 0 & \cdots & 0 & 0 \\ 0 & 0 & 0 & \cdots & 0 & 0 \\ \vdots & \vdots & \vdots & \ddots & \vdots & \vdots \\ 0 & 0 & 0 & \cdots & 0 & 0 \\ 0 & 0 & 0 & \cdots & 0 & 0 \end{bmatrix}, \mathbf{T}_{(r+2)i} = \begin{bmatrix} 0 & 0 & 1 & \cdots & 0 & 0 \\ 0 & 0 & 0 & \cdots & 0 & 0 \\ 1 & 0 & 0 & \cdots & 0 & 0 \\ \vdots & \vdots & \vdots & \ddots & \vdots & \vdots \\ 0 & 0 & 0 & \cdots & 0 & 0 \\ 0 & 0 & 0 & \cdots & 0 & 0 \end{bmatrix}, \dots, \quad (6.8)$$

$$\mathbf{T}_{ki} = \begin{bmatrix} 0 & 0 & 0 & \cdots & 0 & 0 \\ 0 & 0 & 0 & \cdots & 0 & 0 \\ 0 & 0 & 0 & \vdots & 0 & 0 \\ \vdots & \vdots & \vdots & \ddots & \vdots & \vdots \\ 0 & 0 & 0 & \cdots & 0 & 1 \\ 0 & 0 & 0 & \cdots & 1 & 0 \end{bmatrix}, \quad (6.9)$$

According to Rao (1970, 1971), a minimum norm quadratic unbiased estimation of the linear function of θ_i ($i= 1, 2, \dots, k$), i.e., $g_1\theta_1 + g_2\theta_2 + \dots + g_k\theta_k$, is the quadratic function $\mathbf{z}^T \mathbf{M} \mathbf{z}$ if the matrix \mathbf{M} is determined by solving the following matrix trace minimum problem (\mathbf{z} was defined in Equation 2.66):

$$\text{Tr}\{\mathbf{M.VCV.M.VCV}\} = \min \quad (6.10)$$

subject to

$$\mathbf{M}\mathbf{A} = \mathbf{0}, \quad (6.11)$$

$$\text{Tr}\{\mathbf{M}\mathbf{T}_i\} = g_i \quad (i = 1, 2, \dots, k) \quad (6.12)$$

where \mathbf{A} was defined in Equation 2.66; and $\text{Tr}\{\}$ is the trace operator of matrix. The MINQUE estimate of the VCV components is given as:

$$\hat{\boldsymbol{\theta}} = (\hat{\theta}_1, \hat{\theta}_2, \dots, \hat{\theta}_k)^T = \mathbf{S}^{-1} \mathbf{q} \quad (6.13)$$

where the matrix $\mathbf{S} = \{s_{ij}\}$ with

$$s_{ij} = \text{Tr}\{\mathbf{RT}_i\mathbf{RT}_j\} \quad (6.14)$$

and the vector $\mathbf{q} = \{q_i\}$ with

$$q_i = \mathbf{z}^T \mathbf{RT}_i \mathbf{Rz} \quad (6.15)$$

and

$$\mathbf{R} = \mathbf{WQ}_v\mathbf{W} \quad (6.16)$$

where \mathbf{W} was defined in Equation 2.66; and $\mathbf{Q}_v = [\mathbf{W}^{-1} - \mathbf{A}(\mathbf{A}^T\mathbf{P}\mathbf{A})^{-1}\mathbf{A}^T]$ is known as the residual cofactor matrix. Satirapod (2002) showed that \mathbf{R} can also be expressed by a partitioned matrix:

$$\mathbf{R} = \begin{bmatrix} \mathbf{R}_{11} & \mathbf{R}_{12} & \cdots & \mathbf{R}_{1r} \\ \mathbf{R}_{21} & \mathbf{R}_{22} & \cdots & \mathbf{R}_{2r} \\ \vdots & \vdots & \ddots & \vdots \\ \mathbf{R}_{r1} & \mathbf{R}_{r2} & \cdots & \mathbf{R}_{rr} \end{bmatrix} \quad (6.17)$$

The relationship between \mathbf{v} (i.e. the least squares residual; see Equation 2.66) and \mathbf{z} can be written as:

$$\mathbf{v} = -\mathbf{Q}_v\mathbf{Wz} \quad (6.18)$$

and

$$\mathbf{WQ}_v\mathbf{Wv} = -\mathbf{WQ}_v\mathbf{Wz} = \mathbf{Wv} \quad (6.19)$$

According to Equations 6.18 and 6.19, Equation 6.15 can be further written as:

$$q_i = \mathbf{z}^T \mathbf{RT}_i \mathbf{Rz} = \mathbf{v}^T \mathbf{RT}_i \mathbf{Rv} = \mathbf{v}^T \mathbf{WT}_i \mathbf{Wv} \quad (6.20)$$

It can be noticed from Equations 6.13-6.16 that elements of the **VCV** are implicitly defined. Therefore an iterative process must be performed to solve Equation 6.13

(Wang, 1999). Initially, an a priori value of θ_i is given by θ_i^0 , and the initial estimate of $\hat{\boldsymbol{\theta}}^1$ can be obtained by Equation 6.13. Using the previous estimate $\hat{\boldsymbol{\theta}}^j$ as the a priori value, the new estimate from the $(j+1)^{\text{th}}$ iteration is:

$$\hat{\boldsymbol{\theta}}^{j+1} = \mathbf{S}^{-1}(\hat{\boldsymbol{\theta}}^j) \mathbf{q}(\hat{\boldsymbol{\theta}}^j) \quad (j = 0, 1, 2, \dots) \quad (6.21)$$

This is called the iterated MINQUE. If $\hat{\boldsymbol{\theta}}$ converges, the converging value of $\hat{\boldsymbol{\theta}}$ will satisfy the following condition:

$$\mathbf{S}(\hat{\boldsymbol{\theta}}) \hat{\boldsymbol{\theta}} = \mathbf{q}(\hat{\boldsymbol{\theta}}) \quad (6.22)$$

which can be further expressed as (Rao, 1979):

$$\text{Tr}\{\mathbf{R}(\hat{\boldsymbol{\theta}}) \mathbf{T}_i\} = \mathbf{z}^T \mathbf{R}(\hat{\boldsymbol{\theta}}) \mathbf{T}_i \mathbf{R}(\hat{\boldsymbol{\theta}}) \mathbf{z} \quad (i = 1, 2, \dots, k) \quad (6.23)$$

For one session of observations, the computation of MINQUE is burdened with the requirement of computing the matrix \mathbf{R} . Satirapod (2002) showed that, for processing 6 satellites and 15 second sampling interval in a 60 minute session length, MINQUE requires 11250 kilobytes of computer memory. Ibid (2002) suggested that a simplified MINQUE procedure can be obtained by assuming that the matrix \mathbf{R} has a block-diagonal structure:

$$\mathbf{R}^* = \begin{bmatrix} \mathbf{R}_{11} & 0 & \dots & 0 \\ 0 & \mathbf{R}_{22} & \dots & 0 \\ \vdots & \vdots & \ddots & \vdots \\ 0 & 0 & \dots & \mathbf{R}_{rr} \end{bmatrix} \quad (6.24)$$

and subsequently, the matrix \mathbf{W} and the accompanying matrices \mathbf{T}_i have the following structures:

$$\mathbf{W} = \text{diag}(\mathbf{W}_n) \quad (n = 1, 2, \dots, r) \quad (6.25)$$

$$\mathbf{T}_i = \text{diag}(\mathbf{T}_{in}) \quad (n = 1, 2, \dots, r) \quad (6.26)$$

Then Equations 6.14 and 6.20 can be simplified as:

$$s_{ij} = \text{Tr}\{\mathbf{R}\mathbf{T}_i \mathbf{R}\mathbf{T}_j\} = \sum_{n=1}^r \text{Tr}\{\mathbf{R}_{nn} \mathbf{T}_{ik} \mathbf{R}_{nn} \mathbf{T}_{jk}\} \quad (6.27)$$

$$q_i = \mathbf{v}^T \mathbf{W}\mathbf{T}_i \mathbf{W}\mathbf{v} = \sum_{n=1}^r \text{Tr}\{\mathbf{v}_n^T \mathbf{W}_n \mathbf{T}_{in} \mathbf{W}_n \mathbf{v}_n\} \quad (6.28)$$

The results of the simplified MINQUE were shown to be very close to those from the original MINQUE, however the computational load is much less (Ibid, 2002). The simplified MINQUE (Equations 6.27 and 6.28) will be used as a heteroskedastic model in the next section.

6.2 Test of Stochastic Modelling

6.2.1 Experimental Data & Methods of Processing

To investigate the stochastic model described in the previous section, data from the Southern California Integrated GPS Network (SCIGN) has been used (<http://www.scign.org>). Figure 6.1 shows part of the geometry of this permanent network. Two sites FMTP and QHTP are considered as reference stations. The master station is assumed to be FXHS. Another two sites CSN1 and CMP9 are treated as user stations. These two baselines of master-to-user stations are referred to as FX-CM (i.e. FXHS to CMP9) and FX-CS (i.e. FXHS to CSN1).

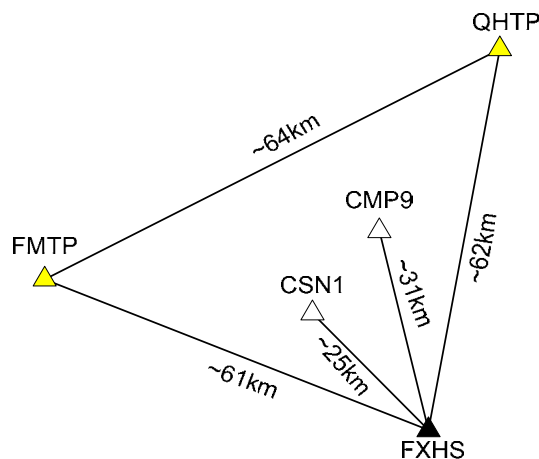


Figure 6.1 Geometric layout of the test network, part of SCIGN network.

Three different data sets for DoY221/00, DoY222/00 and DoY227/02, during periods of high solar activity, were tested. Each data set has a 30 second observation rate. The coordinates of all the stations (Table 6.1) were obtained using the Scripps Coordinates Update Tool (SCOUT) (<http://sopac.ucsd.edu/cgi-bin/SCOUT.cgi>). These coordinates will be considered to be ‘known’ coordinates in this experiment.

Table 6.1 Stations coordinates and baseline lengths from station FXHS.

SITE	X (m)	Y (m)	Z (m)	FXHS to: (m)
FXHS	-2511943.6388	-4653606.7722	3553873.9778	0
FMTP	-2545459.7204	-4612207.1586	3584252.1200	61319.550
QHTP	-2486712.3456	-4629002.0822	3604537.5090	61715.550
CSN1	-2520225.8551	-4637082.4402	3569875.3624	24447.760
CMP9	-2508505.9552	-4637175.0256	3579499.8619	30635.044

All master-to-reference and master-to-user station baselines were processed using the static positioning algorithm (i.e. a session solution) developed at UNSW (see Figure 5.7). Since this algorithm is single-frequency data based, long observation sessions were needed. All the data were processed with 15° cut-off elevation angle and the GPS broadcast orbits were utilised. The ambiguity-fixed residuals of the master-to-reference station baseline as defined in Equations 5.6-5.7 were used to generate the ‘lumped’ network correction (see Chapter 5) via Equation 5.16. The corresponding network coefficients were calculated using Equation 5.26 with the coordinates listed in Table 6.1. The network correction was then applied to each DD measurement for the master-to-user station baseline as defined in Equation 5.33.

In order to investigate the stochastic modelling, the data process of the master-to-user station baseline was conducted using two methods:

Method A: processing with a homoskedastic stochastic model and applying the error propagation law given by Equations 6.3 and 6.4.

Method B: processing with a heteroskedastic stochastic model estimated using the simplified MINQUE given by Equations 6.27 and 6.28.

The ambiguity-float position solution with the corresponding VCV matrix from each of the methods was the input to the LAMBDA processing (Teunissen, 1994). The next step was to validate the ambiguities obtained from LAMBDA. Subsequently, the baseline components were estimated and the least squares phase residuals were obtained. The results were analysed to assess the performance of Methods A and B.

6.2.2 Analysis of Test Results

As is usual the ambiguity candidates obtained by the LAMBDA processing can be validated by the F-ratio test. The F-ratio test with a critical threshold value larger than 2 is usually assumed to be a “pass” (Landau & Euler, 1992). The larger the ratio value, the higher the level of confidence in the ambiguity resolution (AR) results. The problem of this test with a critical value 3 was discussed in Section 5.4.3 (b). For this reason another well known ambiguity validation measure, the W-ratio (Wang, 1999), was used for the second test. For the W-ratio test, a critical value larger than 3 statistically represents a confidence level of 99.9%, for the discrimination between the best and the second best ambiguity candidates. More details on the W-Ratio test can be found in Ibid (1999) and the problem associated with this validation test was discussed in Verhagen (2004). Both the F-ratio and W-ratio tests were applied to Methods A and B. Figure 6.2 shows the results of the validation tests for baseline FX-CM and FX-CS.

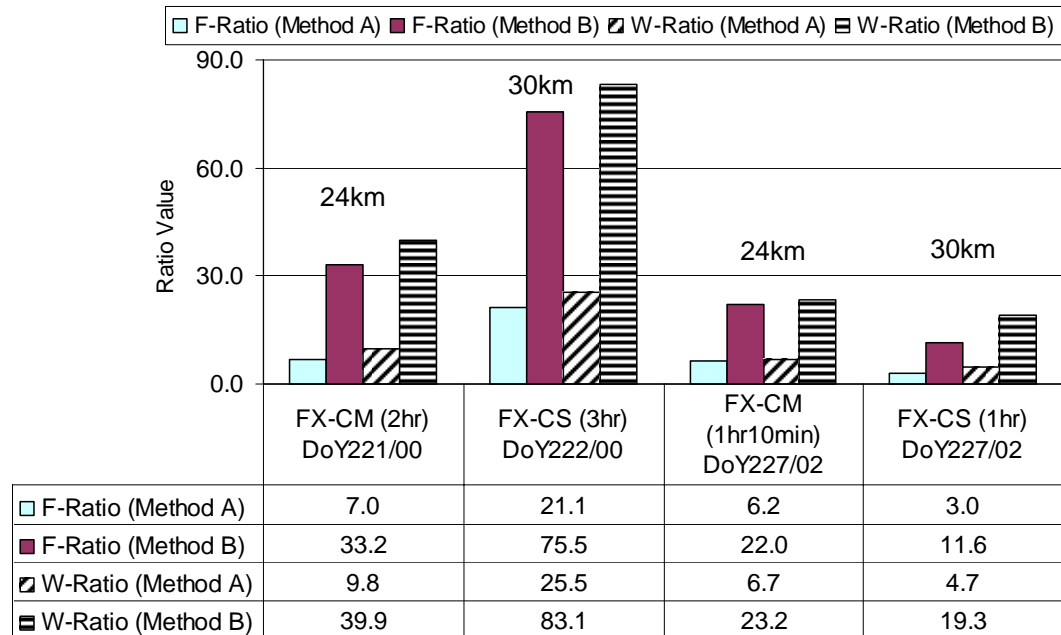


Figure 6.2 Result of ambiguity validation tests (F-ratio & W-ratio for processing Methods A and B, for baselines FX-CM and FX-CS, DoY 221/00, 222/00 and 227/02.

From Figure 6.2 it can be seen that both Methods A and B have passed the critical value for F-ratio and W-ratio tests. Baseline FX-CS in DoY 222/00 shows the highest ratio value for both tests, which could be the result of a long session of observations (3 hours). Both F- and W-ratio values obtained by Method B are consistently larger than those by Method A for all sessions. The result implies that Method B, with the heteroskedastic model as defined by the simplified MINQUE, performs better in both the ratio tests. Therefore, AR with Method B should have a higher level of confidence than for Method A.

Positioning results for the baselines FX-CM and FX-CS are summarised in Table 6.2. The estimated baseline lengths for Methods A and B differ by only one millimetre or less. In the case of FX-CS (DoY 222/00; 3hour session), the estimated baseline lengths for both methods are identical. These estimated values are very close to the ‘known’ baseline lengths for FX-CM and FX-CS given in Table 6.1. The estimated baseline vectors for Methods A and B in each session is almost the same, with the maximum difference being 4mm in the $\delta\hat{Y}$ component (see the 3hour session). In addition, the standard deviations of the estimated baseline vectors for Methods A and B is at the millimetre level. Overall, the results suggest that the difference between Methods A and

B is not significant in terms of estimated baseline lengths, baseline vectors and their standard deviations.

Table 6.2 Estimated baseline lengths, estimated baseline vectors and standard deviations of the baseline vectors for Methods A & B.

Baseline	Mthd	Estimated Length (m)	Estimated Baseline Vectors (m)			Standard Deviation (mm)		
			$\hat{\ell}$	$\delta\hat{X}$	$\delta\hat{Y}$	$\delta\hat{Z}$	$\sigma_{\delta\hat{x}}$	$\sigma_{\delta\hat{y}}$
FX-CM 221/00 (2hr session)	A	30635.049	3437.655	16431.671	25625.944	0.7	1.4	0.9
	B	30635.050	3437.654	16431.667	25625.947	0.8	1.1	0.7
FX-CS 222/00 (3hr session)	A	24447.743	-8282.216	16524.271	16001.420	0.5	0.9	0.6
	B	24447.743	-8282.221	16524.267	16001.423	0.5	0.9	0.6
FX-CM 227/02 (1hr 10min session)	A	30635.038	3437.701	16431.760	25625.867	0.7	0.8	1.2
	B	30635.037	3437.701	16431.760	25625.866	0.5	0.6	0.9
FX-CS 227/02 (1hr session)	A	24447.681	-8282.155	16524.291	16001.338	1.7	3.0	2.3
	B	24447.680	-8282.151	16524.290	16001.339	1.8	2.7	1.9

There are, however, differences of up to centimetre level in the estimated baseline length and vectors between the observation sessions. This is of course related to the different observation span lengths, different day of observations, different number of measurements, different satellite geometries and also different systematic errors that may exist in the measurements. The time series of the least squares phase residuals in Figure 6.3 show no significant difference between Methods A and B. However, the variation of the residuals in Method B is less than that for Method A.

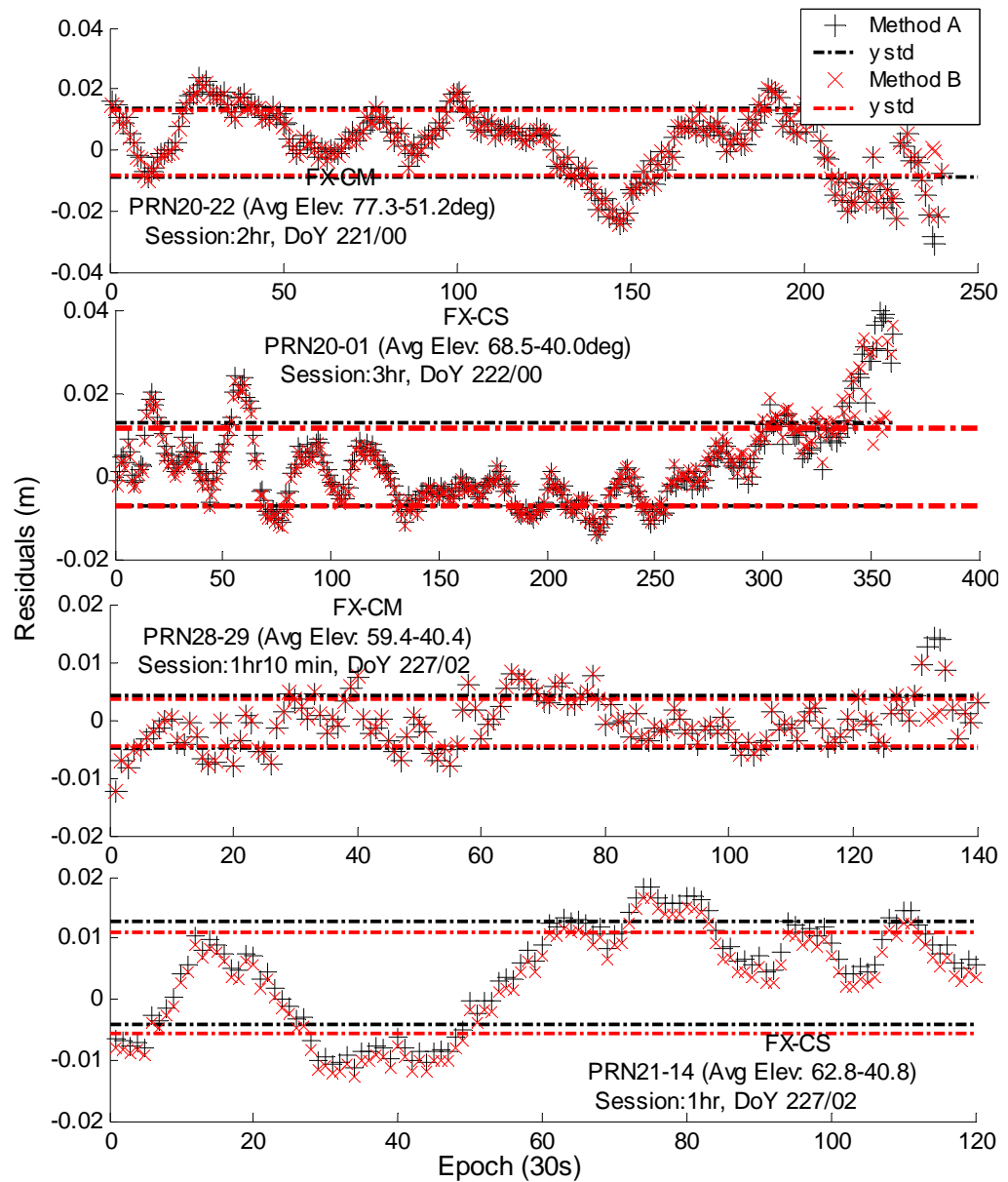


Figure 6.3 Time series of least squares phase residuals (metre) for selected satellite pairs in each session for Methods A and B. The cross-marker (black) and star-marker (red) represents the residual for Methods A and B respectively. The dash-dot line, black and red, represents the residual standard deviations for Methods A and B respectively.

6.3 Handling the Temporal Correlations

According to El-Rabbany & Klesuberg (2003) physical correlation may exist due to the improper modelling of the partially correlated measurement errors, and it can be of a

temporal and/or a spatial nature. Since the MINQUE (and simplified MINQUE) procedure described in Sections 6.1 and 6.2 are based on the assumption that the temporal correlation between epochs is absent, it could be advantageous to include them in the stochastic modelling.

Wang (1998) proposed a two-stage method to handle the temporal correlation. The basic idea is to transform the DD measurements into a set of new measurements which are assumed to be free of temporal correlation. According to Wang et al. (2002) and Satirapod (2002), the error vectors in Equation 2.66 can be replaced as:

$$\mathbf{v}(t) = \mathbf{R}.\mathbf{v}(t-1) + \mathbf{u}(t) \quad (6.29)$$

where the error terms (\mathbf{u}) are temporally independent with expectation (E):

$$\begin{aligned} E[\mathbf{u}(t).\mathbf{u}(r)^T] &= 0 \\ E[\mathbf{u}(t).\mathbf{u}(t)^T] &= \mathbf{\Omega} \quad t, r = 2, \dots, s \end{aligned} \quad (6.30)$$

and s is the number of observation epochs. Equation 6.29 is also called a first-order vector auto-regression model, as used by Sargan (1961). The whole VCV matrix for \mathbf{u} is:

$$E[\mathbf{u}.\mathbf{u}^T] = \mathbf{\Omega} \otimes \mathbf{I}_s \quad (6.31)$$

The matrix \mathbf{R} in Equation 6.29 is the correlation coefficient matrix:

$$\mathbf{R} = \begin{bmatrix} \rho_{11} & \rho_{12} & \cdots & \rho_{1n} \\ \rho_{21} & \rho_{22} & \cdots & \rho_{2n} \\ \vdots & \vdots & \ddots & \vdots \\ \rho_{n1} & \rho_{n2} & \cdots & \rho_{nn} \end{bmatrix} \quad (6.32)$$

which can be iteratively estimated via Equation 6.29 (see Wang et al, 2002). Following Equation 6.29, the error vectors in Equation 2.66 can be replaced by (Ibid, 2002):

$$\mathbf{G}\mathbf{v} = \mathbf{u} \quad (6.33)$$

where the structure of matrix \mathbf{G} contains the elements of the correlation coefficients of the matrix (see Ibid, 2002; Satirapod, 2002). The transformed measurements are obtained by inserting Equation 6.33 into Equation 2.66:

$$\bar{\mathbf{z}} = \bar{\mathbf{A}}\mathbf{x} + \mathbf{u} \quad (6.34)$$

where $\bar{\mathbf{z}} = \mathbf{G}\mathbf{z}$ and $\bar{\mathbf{A}} = \mathbf{G}\mathbf{A}$. The transformed measurements in matrix $\bar{\mathbf{z}}$ are temporally independent and have a simple stochastic model represented by Equation 6.30. MINQUE, as discussed in sub-section 6.1.2, could be used to estimate the unknown elements of the matrix $\mathbf{\Omega}$. As stated earlier, the new measurements in Equation 6.34 are assumed to be free of temporal correlation.

6.4 Testing of Temporal Correlation

6.4.1 Experimental Data, Methods of Processing and Assessments

In order to test the algorithms described in Section 6.3 for network-based positioning, three datasets were used.

Data Set 1: The data from the Singapore Integrated Multiple Reference Station (SIMRSN) on DoY166/03 with a 15 second interval for a 45 minute period. The geometry of this network is illustrated in Figure 6.4.

Data Set 2: The data from a part of the SCIGN on DoY166/03 with a 30 second interval for a 30 minute period. The geometry of this network is illustrated in Figure 6.5.

Data Set 3: The data from a part of the GPS Earth Observation Network (GEONET) in Japan on DoY041/03 with a 30 second interval for a 30 minute period. The geometry of this network is illustrated in Figure 6.6.

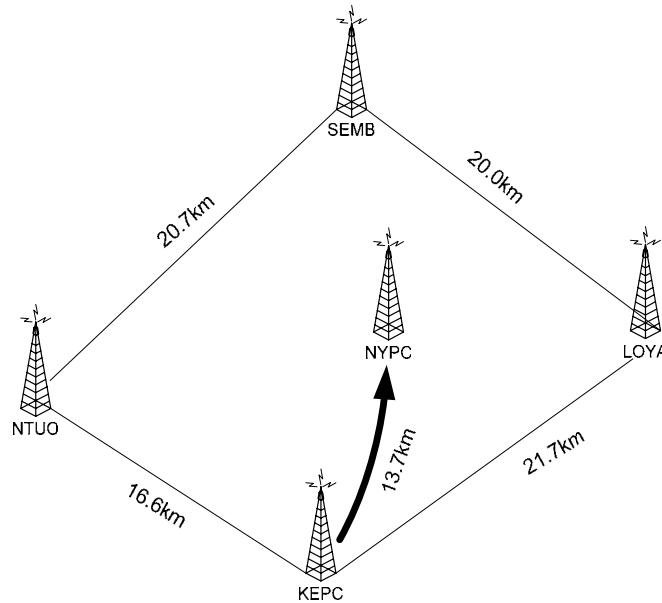


Figure 6.4 Data Set 1 (SIMRSN): KEPC is a master; NYPC is a user; NTUO, LOYA and SEMB are the reference stations.

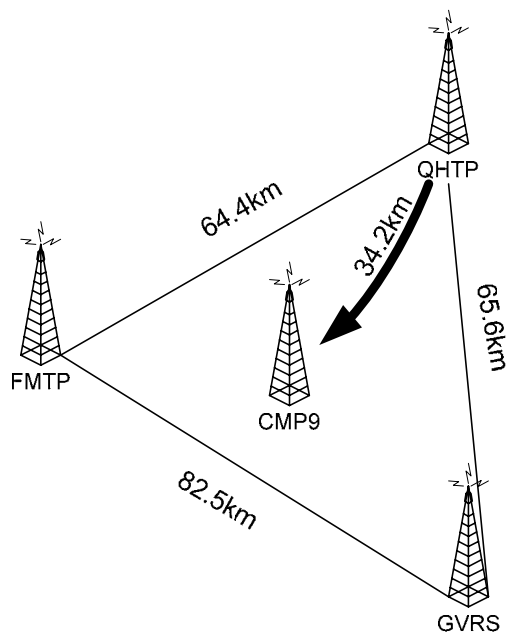


Figure 6.5 Data Set 2 (Part of SCIGN): QHTP is a master; CMP9 is a user; FMTP and GVRS are the reference stations.

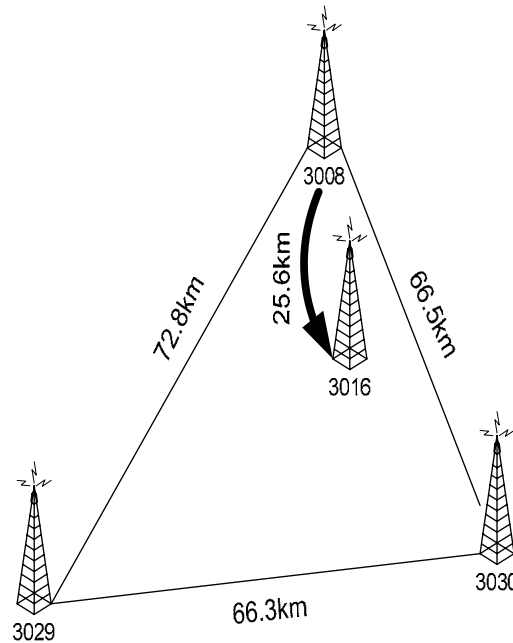


Figure 6.6 Data Set 3 (Part of GEONET): 3008 is a master; 3016 is a user; 3029 and 3030 are the reference stations.

Note, the master-to-user stations are KEPC-NYPC (Data Set 1), QHTP-CMP9 (Data Set 2) and 3008-3016 (Data Set 3). The other stations in these networks are the reference stations. All station coordinates were obtained from the network providers (Data Sets 1 and 2), or by processing several days of dual-frequency data (Data Set 3). All the data are processed using a 15° cut-off elevation angle and the GPS broadcast orbits. Unlike the previous experiment, the master-to-reference station baseline is processed using the BERNESSE software. Since all networks provide dual-frequency data, the Quasi Ionosphere Free (QIF) combination (see Section 3.3.3) is used for L1 ambiguity resolution for the master-to-reference station baseline. As previously explained, the ambiguity-fixed residuals of the master-to-reference station baseline were used to generate the ‘lumped’ network correction (see Chapter 5) and applied to each DD measurement of the master-to-user station baselines. Then, the master-to-user station baselines were processed using two different stochastic modelling methods.

Method A: processing with the homoskedastic stochastic model (without the temporal correlation).

Method B: processing with the heteroskedastic stochastic model estimated by MINQUE, and with the temporal correlation taken into account (Equation 6.34).

To assess the randomness of the residual series, the temporal correlation coefficient is calculated by applying the Durbin-Watson statistical test (Durbin & Watson, 1950) to the DD residuals. For a random series x_1, x_2, \dots, x_n , the correlation coefficient, ρ_x , is given by:

$$\rho_x = 1 - \frac{d}{2} \quad (6.35)$$

with

$$d = \frac{\sum_{i=2}^n (x_i - x_{i-1})^2}{\sum_{i=1}^n x_i^2} \quad (6.36)$$

The coefficient values range from -1 to +1, where a small value indicates that the measurements (i.e. the DD residuals) are statistically relatively uncorrelated. At this point it is expected that the residual series from Method B would be less correlated than those of Method A (due to Equation 6.34). Moreover, the autocorrelation can be used to examine the correlation characteristics of the time series. It is defined as the expected value of the product $x(t_1)x(t_2)$ (Bona, 2000):

$$\text{Corr}(t_1, t_2) = E\{(x(t_1))(x(t_2))\} \quad (6.37)$$

where $x(t_1)$ and $x(t_2)$ are the values of the residuals at time t_1 and t_2 , respectively. If the time series is stationary, the autocorrelation function depends only on the time difference or time lag ($\tau = t_2 - t_1$). For an ideal white noise process, $\text{Corr}_x(\tau) = 1$ if $\tau = 0$ and $\text{Corr}_x(\tau) = 0$ if $\tau \neq 0$ (Ibid, 2000). To demonstrate the use of Equations 6.36-6.37, a zero-baseline test was conducted. The data was collected on top of the Electrical Engineering Building, UNSW, on DoY 360/04 using two GPS receivers of the same type collecting data for 30 minutes. The L1 data was processed with 10s observation interval. The residual and the autocorrelation (or correlograms) plots are shown in Figures 6.7 and 6.8 respectively.

Since all systematic errors, including multipath, are assumed cancelled in the zero-baseline measurements, the residuals should represent just the receiver measurement

noise. Figure 6.7 explains why the homoskedastic model is not appropriate - all residual series from each satellite pair exhibit different standard deviations. In the case of PRN02 (average elevation of 54 deg), its standard deviation is larger than PRN27 (higher elevation). This shows that the satellite elevation angle does not always reflect the reality of the measurement noise.

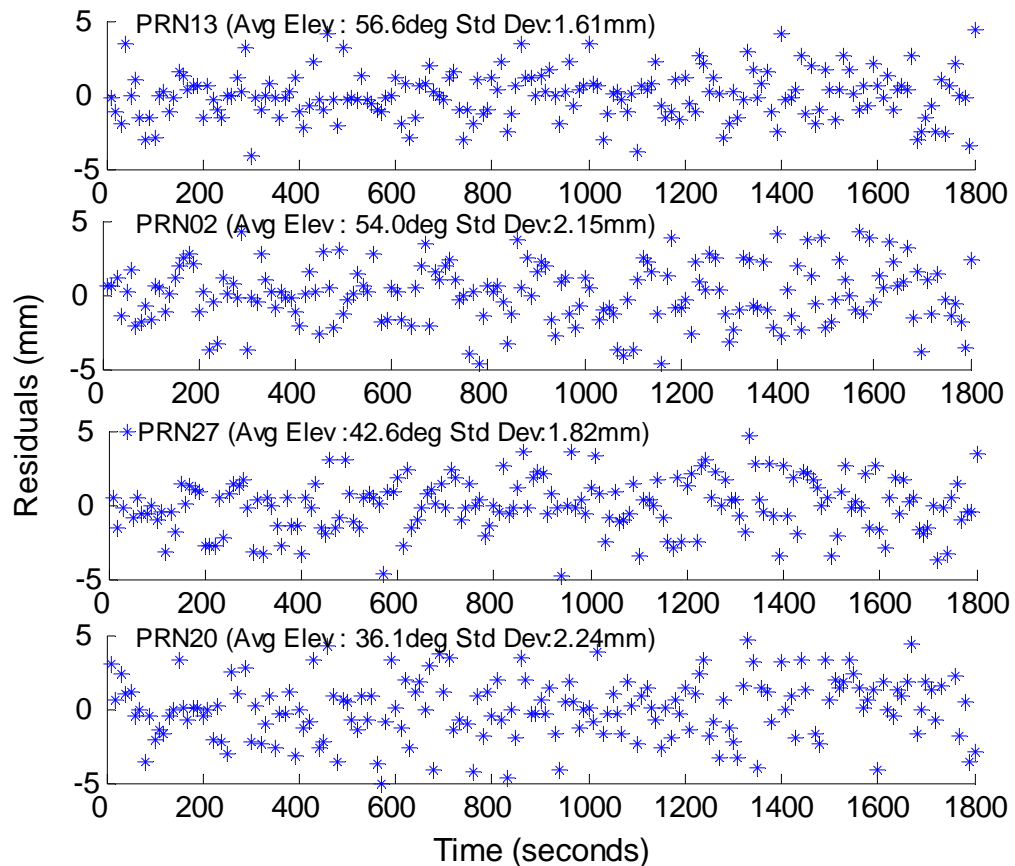


Figure 6.7 Residual plots for zero-baseline test. Base satellite is PRN01 at 66.4° (average) elevation angle with 10s observation rate.

As shown in Figure 6.8, the plots for autocorrelation on a satellite-by-satellite basis (as in Figure 6.7) shows a clear spike near the zero lag which is indicating the L1 measurement noise is more or less consistent with the assumption of white noise. Although there is a different correlation coefficient for each measurement, it is very small and similar in magnitude. Thus, less temporal correlation occurs for each measurement in this case. This is also indicated by the correlation coefficients calculated by Equation 6.35, where the value is 0.004 for PRN01-13; 0.003 for PRN01-02; 0.004 for PRN01-27; and 0.017 for PRN01-20. In the next section, the residual

analyses for all master-to-reference station baselines from Data Sets 1, 2 and 3 are discussed.

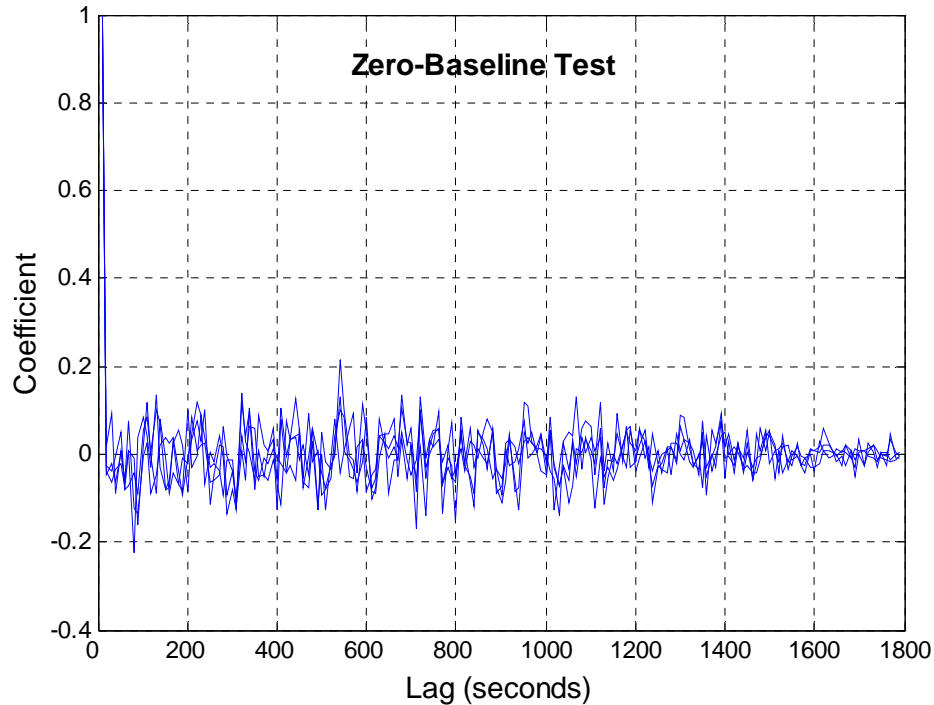


Figure 6.8 Autocorrelation plots (for the DD residuals in Figure 6.7) for the zero-baseline test.

6.4.2 Analysis of Results

Based on the stochastic modelling Methods A and B, the least squares time series and autocorrelation plots of the DD residuals for the master-to-user station baselines are presented in Figures 6.9a & 6.9b, 6.10a & 6.10b, and 6.11a & 6.11b for Data Sets 1, 2 and 3 respectively. The corresponding correlation coefficients are given in Tables 6.3, 6.4 and 6.5 for the DD residuals of each satellite pair.

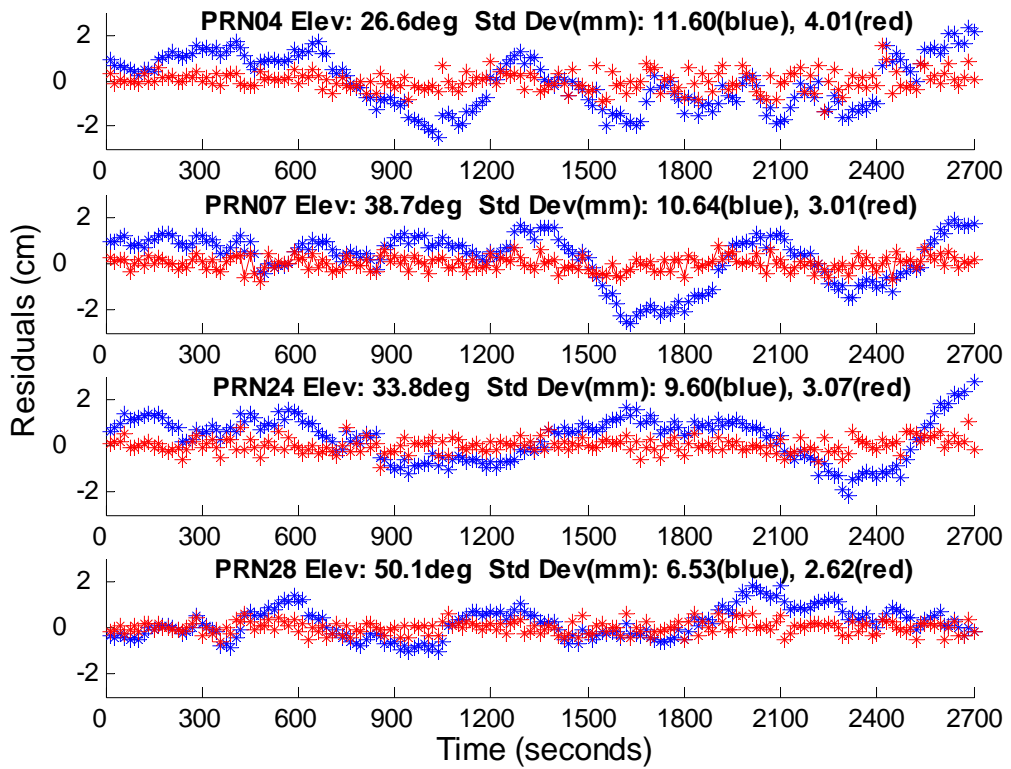


Figure 6.9a Residual plots of Methods A (blue-star) and B (red-star) for Data Set 1, with 15s representing 1epoch. Base satellite is PRN10 at 46.1° (average) elevation angle.

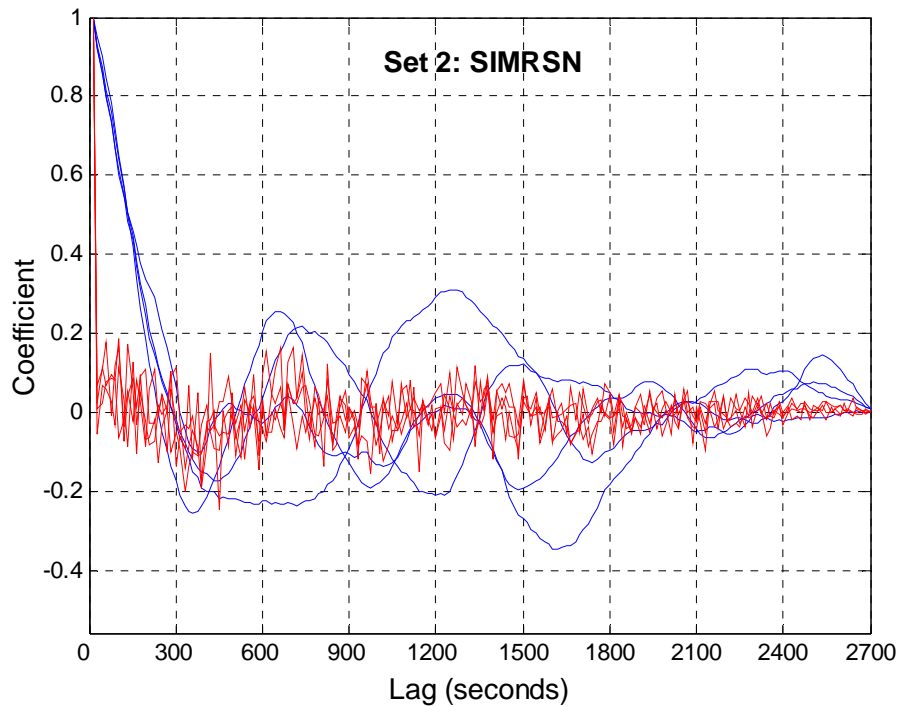


Figure 6.9b Autocorrelation plots (for the DD residuals in Figure 6.9a) for Methods A (blue-line) and B (red-line) for Data Set 1.

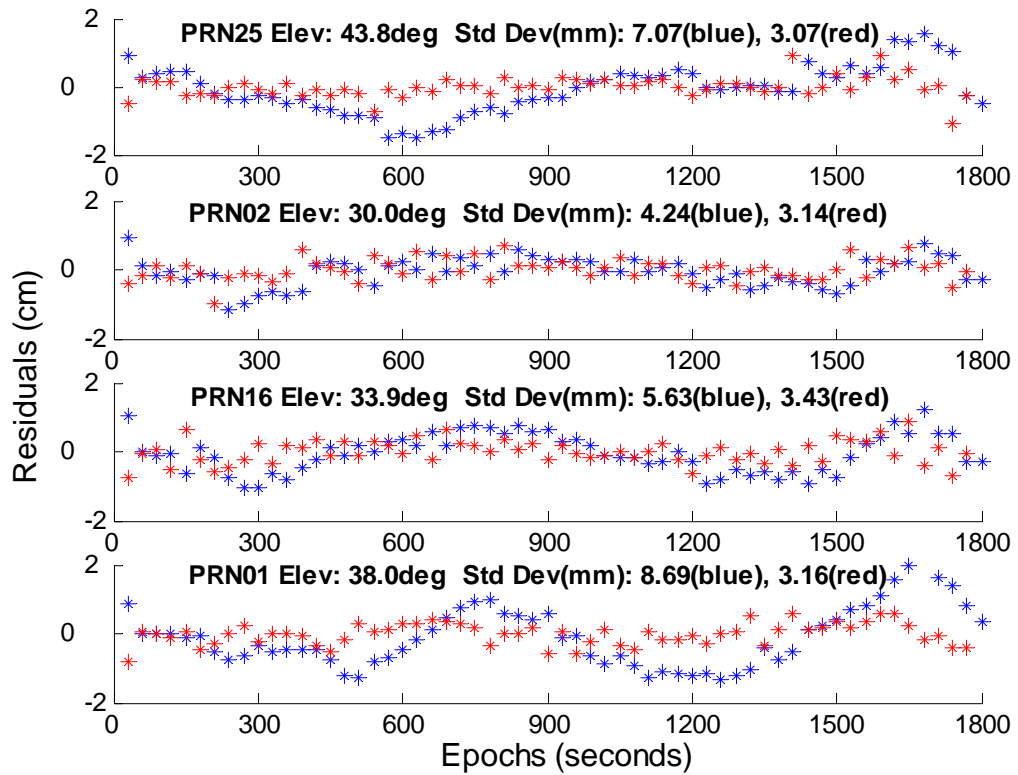


Figure 6.10a Residual plots of Methods A (blue-star) and B (red-star) for Data Set 2, with 30s representing 1epoch. Base satellite is PRN06 at 61.9° (average) elevation angle.

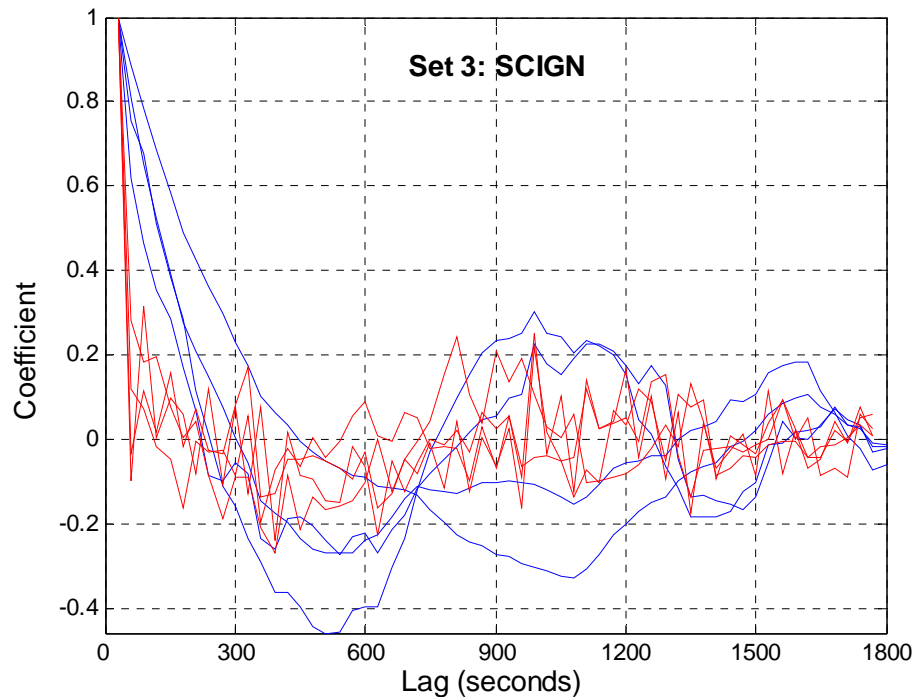


Figure 6.10b Autocorrelation plots (for the DD residuals in Figure 6.10a) for Methods A (blue-line) and B (red-line) for Data Set 2.

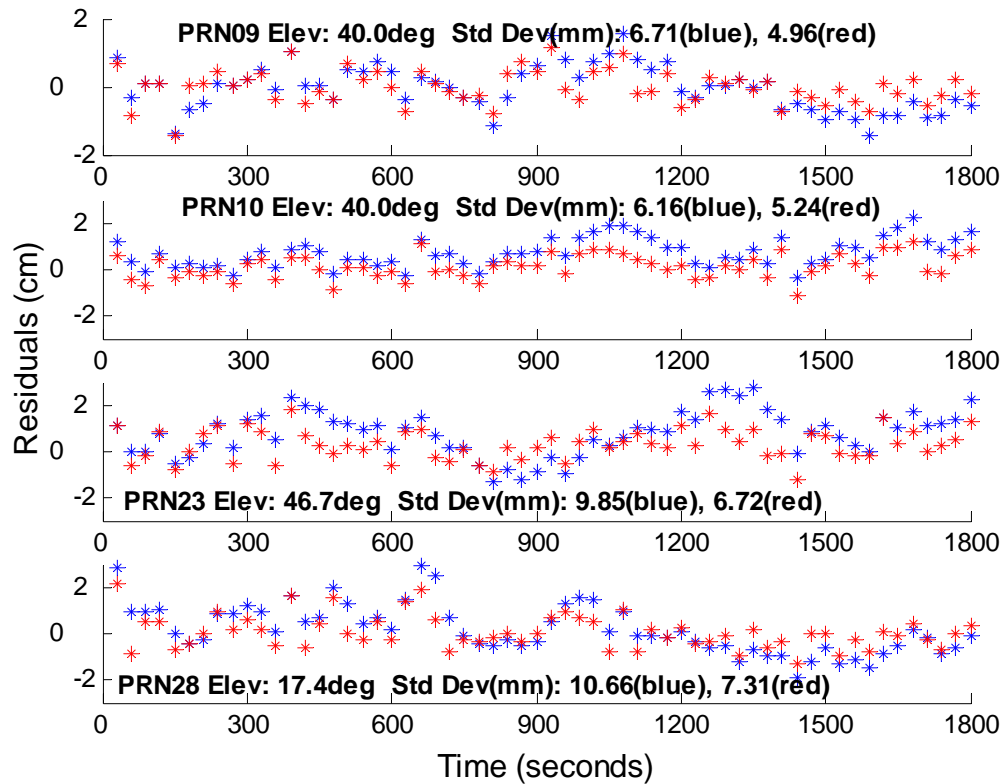


Figure 6.11a Residual plots of Methods A (blue-star) and B (red-star) for Data Set 3, with 30s representing 1epoch. Base satellite is PRN29 at 56.5° (average) elevation angle.

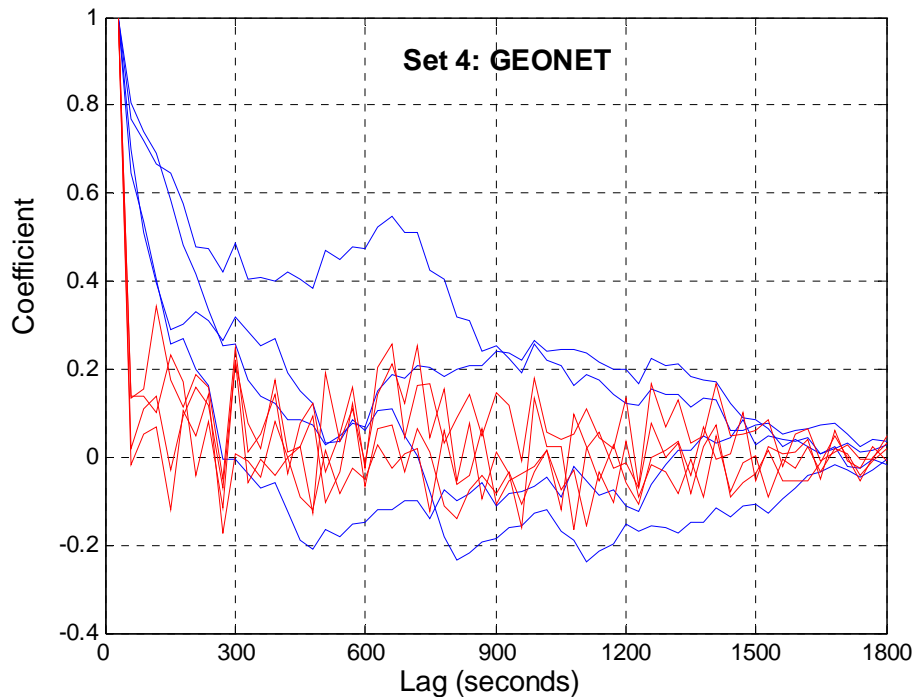


Figure 6.11b Autocorrelation plots (for the DD residuals in Figure 6.11a) for Methods A (blue-line) and B (red-line) for Data Set 3.

Table 6.3 Estimated correlation coefficients for the DD residuals of Data Set 1.

Method	PRN10-04	PRN10-07	PRN10-24	PRN10-28
A	0.94	0.97	0.97	0.92
B	0.01	0.07	0.02	-0.06

Note: All value rounded to 2 decimal digits

Table 6.4 Estimated correlation coefficients for the DD residuals of Data Set 2.

Method	PRN20-25	PRN20-02	PRN20-16	PRN20-01
A	0.88	0.62	0.76	0.92
B	-0.03	-0.06	-0.04	-0.08

Note: All value rounded to 2 decimal digits

Table 6.5 Estimated correlation coefficients for the DD residuals of Data Set 3.

Method	PRN29-09	PRN29-10	PRN29-23	PRN29-28
A	0.65	0.77	0.80	0.70
B	0.02	0.14	0.13	0.02

Note: All value rounded to 2 decimal digits

From Figures 6.9a, 6.10a and 6.11a, it is noticeable that the DD residuals in Data Sets 1, 2, and 3 have a smaller standard deviation for Method B, and the residuals are also closer to a zero mean if compared to Method A. Examining the residual plots in Data Set 1 (Figure 6.9a), the standard deviation of Method A is much smaller than that of Method B, compared to the other data sets (Figure 6.10a and 6.11a). This can be explained by the higher data rate of 15 seconds in Data Set 1. Therefore, it is expected that stronger correlations still exist (i.e. between the same satellite pairs) in this data, which can be modelled quite well for Method B. In Data Sets 2 and 3, the data rate was 30 seconds. It is expected that they are already less correlated. Thus, this explains the smaller standard deviation in Method A. El-Rabbany & Kleusberg (2003) have also indicated that the resulting standard deviation of the estimate is a function of the data interval. They also concluded that the standard deviations without physical correlation approach the ones with physical correlation as the data interval increases.

The autocorrelation plots in Figures 6.9b, 6.10b and 6.11b suggest that the existing correlations have been taken into account in Method B. This can be examined from those figures where all of the autocorrelation results from Method B show a spike near zero lag, but no spike in Method A. Moreover, the time lag of zero autocorrelation is

also smaller in Method B. This result suggests that there exist strong correlations in the DD residuals of Method A. The estimated correlation coefficients (Equation 6.35) in Tables 6.4, 6.5 and 6.6 also indicate a large coefficient range from 0.62 to 0.97 for Method A, but smaller coefficient values for Method B. But Method B still exhibits strong correlations. In the case of Data Set 3 in Table 6.6, PRN29-10 and PRN29-23 show large coefficient values compared to other results. This might indicate that a strong correlation still exists, which cannot be modelled by either method. However, the coefficients are still smaller in the case of Method B. Overall, the result suggests that Method B is less correlated and the residuals are more random.

The positioning results of Methods A and B were calculated for the static session for Data Sets 1, 2 and 3. There are, however, only differences of a few millimetres in the estimated baseline vectors using Methods A and B. Thus, it can be interpreted that applying different stochastic models, such as Methods A and B, will not dramatically improve the quality of the estimated baseline components, which is similar to the previous finding in Section 6.2.

6.5 Concluding Remarks

There is limited research on the stochastic modelling of GPS measurements even for single-base (baseline) positioning. In the case of network-based positioning there is almost no discussion except for the network-based algorithm that was developed by Racquet (1998). The basis of his algorithm exploits the elevation dependence of DD measurements and covariance analysis of the network measurement errors.

This chapter investigated the ‘realistic’ stochastic model of the static network-based positioning technique. The least squares residuals can be used to define the heteroskedastic model of the DD measurements. Using MINQUE (or its simplified version), the estimated VCV matrix should include the uncertainty from the network estimates. Test results of this ‘realistic’ stochastic model suggest that the performance of the ambiguity validation tests is improved, which can therefore provide better confidence in the AR process. Based on autocorrelation plots and the estimated

correlation coefficients, it is suggested that strong temporal correlations exist in the homoskedastic model. Residual analysis of the heteroskedastic model shows that this temporal correlation can be effectively modelled using transformed measurements. Therefore the VCV matrix estimated by MINQUE can be represented as a block-diagonal matrix. Nevertheless, the estimated baseline components do not change very much regardless of the stochastic model that is used.

CONCLUSIONS AND RECOMMENDATIONS

7.0 Summary and Conclusions

Residual Analysis of Distance-Dependent Errors in the Low Latitude Region

A comprehensive analysis of the effect on GPS positioning of the residual atmospheric delay and the residual orbit errors has been conducted upon applying an a priori tropospheric model and the double-differencing (DD) technique to data from a network of continuously operating reference stations (CORS) in a low latitude region. The analysis confirms the fact that these residual errors do exhibit the characteristic of being distance-dependent (i.e. a function of the separation of the pair of GPS receivers considered in the DD).

As expected, the residual ionospheric delay is the largest among the various GPS error sources, having a peak magnitude about 4 hours after midnight (local time). At this peak the magnitude reaches up to 130 cm for a long baseline, 100 cm for a medium length baseline, and 30 cm for a short baseline. These values are equivalent to 6.3 cycles, 5.3 cycles and 1.6 cycles of L1; 8.8 cycles, 6.7 cycles and 2.0 cycles of L2; 2.5 cycles, 2 cycles and 0.57 cycles of widelane; respectively. Variations of these residuals during a 24 hour period are summarised in Figure 7.1 (see 'Iono on L1'). Since the data are observed near the solar maximum year in 2003, these residual values are relatively high. However the ionospheric delay is assumed to be practically eliminated by the Ionosphere-Free (IF) combination, and long observation sessions enable the ambiguities to be correctly resolved.

Although the data is processed with the precise orbit and the IF combination, there exists residual errors in the DD measurements due to the tropospheric delay. If no a

priori model is applied, the amount of the tropospheric effect is so large that the residual is comparable with the residual ionospheric delay. This unusual characteristic can be explained by the unique condition of the troposphere in the low latitude region. The magnitude of the residual tropospheric delay is about 120 cm for a long baseline, 60 cm for a medium length baseline, and 20 cm for a short baseline. Variations of the tropospheric delay during a 24 hour period are summarised in Figure 7.1 (see ‘Tropo w/o Model’). Once the Saastamoinen tropospheric delay model is applied, their magnitude reduces to about 80% for the long baseline, 60% for the medium length baseline, and about 20% for the short baseline. Although the Saastamoinen model in general is adequate, there still exist residual effects that can not be ignored for a long baseline as its magnitude is about 20 cm. Medium and short baselines exhibit rather small residuals (at the few centimetre level). Their variations during a 24 hour period are summarised in Figure 7.1 (see ‘Tropo+Model’). The residuals are still a problem, especially for the indirect ambiguity resolution (AR) by the IF combination, and for the precise determination of the vertical coordinate components of the GPS receiver stations.

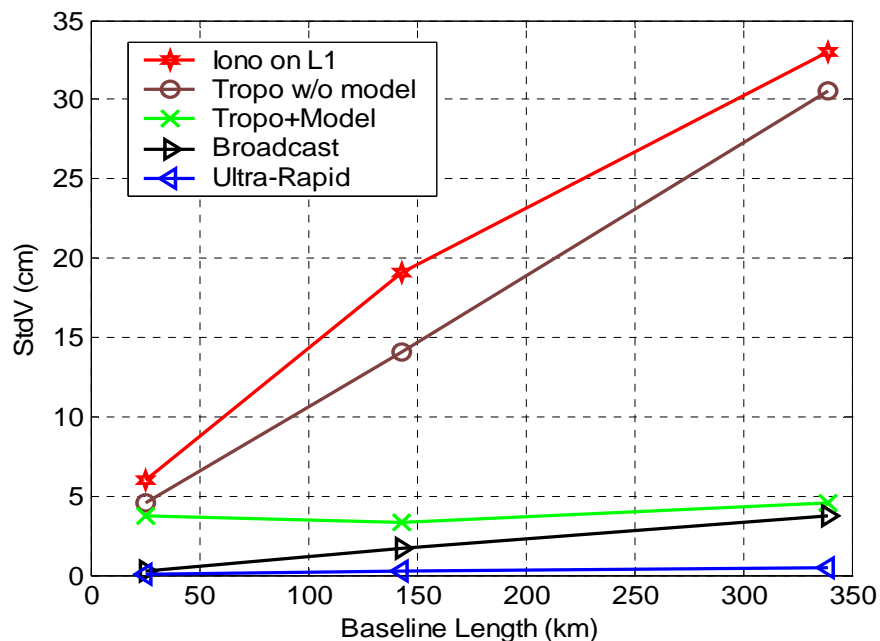


Figure 7.1 Variations of distance-dependent residuals against baseline length.

Unlike the atmospheric delay, the residual orbital errors are in fact very small. The magnitude of residual orbital errors for the broadcast orbits is about 12 cm for the long baseline, 5 cm for the medium length baseline, and 0.7 cm for the short baseline. Variations of these residuals during a 24 hour period are summarised in Figure 7.1 (see ‘Broadcast’). However, the magnitude of the residual orbital errors becomes even less significant if ultra-rapid IGS orbits are used, i.e. 2.5 cm for the long baseline, 1cm for the medium length baseline, and 0.1 cm for the short baseline. Variations of these residuals during a 24 hour period are summarised in Figure 7.1 (see ‘Ultra-Rapid’).

In conclusion, the residual analysis suggests that GPS carrier phase-based positioning in a low latitude region can experience severe problems due to the residual atmospheric delay. The residual can complicate the long range AR, especially if single-frequency measurements are used, making it difficult to achieve cm-level accuracy. Moreover, during the peak period of residual ionospheric delay, single-frequency AR becomes almost impossible even for a short baseline. Although the ionospheric delay can be effectively eliminated using dual-frequency measurements, the challenging problem is the residual tropospheric delay.

Investigation of Residual Tropospheric Delay in the Low Latitude Region

This investigation has focussed on the CORS network in South-East Asia, particularly on Malaysian Peninsula, and where the International GNSS Services (IGS) stations in Indonesia, Philippines, India and Singapore, together with the Malaysian Active Surveying Stations (MASS) stations, are considered to form a ‘regional network’. The IGS station in Singapore (NTUS) and the MASS stations together are considered to be a ‘local network’ for the purpose of this investigation. One-day length observations (from most MASS stations) and monsoon observations (for 3 month data analysis at selected MASS stations) were analysed. It was found that the IF measurements show a large residual tropospheric delay magnitude during the North-East and South-West monsoon periods. The peak occurs during the North-East monsoon, which corresponds to the meteorological reports of hot and wet conditions in the Malaysian Peninsula during this period.

The data analysis indicates that the dry Saastamoinen and dry modified Hopfield models are able to remove up to 89% of the tropospheric delay in this region. However, no more than 4% improvement over the dry troposphere models can be achieved even if the total (dry and wet) Saastamoinen and modified Hopfield models are applied. Nevertheless, the Saastamoinen and modified Hopfield models perform at the same level of effectiveness in terms of modelling the tropospheric delay in this area. This means that the wet tropospheric delay is still difficult to deal with using either model.

The investigation has found that the residual tropospheric delay can be further reduced by introducing additional (tropospheric) parameters in the least squares estimation process. Although a few millimetres of improvement for the coordinate precision were achieved in the horizontal direction, the height component was noticeably improved, by up to 12-36mm during the two monsoon periods. In conclusion, the estimation of tropospheric parameters is necessary for high accuracy GPS positioning in the low latitude area.

The absolute zenith path delay (ZPD) during the two monsoon periods shows short term variations with a large magnitude. The trends of absolute ZPD estimates in both the local and regional networks are close to the values derived by the IGS, but a better accuracy of absolute ZPD can be achieved from the regional network. On the other hand, the investigation has found that there is no significant difference in the estimation of relative ZPD from the regional network compared to the local network. In summary, high quality absolute ZPD estimates are difficult to obtain, most likely due to the use of too simple a mapping function. However, the fact that there is no difference in the estimation of relative ZPD from the regional or local networks is good news for positioning activities in this area, where further attempts to model the residual tropospheric delay by using local networks would be necessary.

Development of Processing Strategy for Network-Based Positioning

Based on the Linear Combination Method (LCM), a new processing strategy has been developed. Firstly, the 'network corrections' were partitioned into *dispersive* (ionosphere-related) and *non-dispersive* (troposphere and orbit-related) components.

The non-dispersive components change slowly and smoothly over time due to the behaviour of the tropospheric delay and orbit biases. Rapid variations in the non-dispersive components can be regarded as being due to remaining multipath and noise. A simple running average was useful for smoothing the non-dispersive correction. Secondly, the 'smooth' non-dispersive correction was applied in the LCM of processing IF measurements (i.e. from master-to-user station) in order to reduce the residual tropospheric delay. In this way the 'indirect' L1 ambiguity resolution with various linear data combinations is possible. Once the indirect L1 ambiguity is resolved, the ambiguity can be removed from the original DD L1 measurements. Finally, the dispersive and non-dispersive corrections are applied at the final positioning step.

This processing strategy was tested in post-mission analysis that "simulates" real-time kinematic (RTK). Two local networks were used in this test: (1) Singapore Integrated Multiple Reference Station Network (SIMRSN), and (2) Sydney Network (SYDNET). For comparison purposes, the processing of master-to-user stations were conducted using the network-based and the single-base reference positioning techniques. Both utilised IF measurements. The smooth non-dispersive corrections applied in the network-based technique performed better than for the single-base reference technique, in terms of improving the IF measurements, in resolving the indirect ambiguities, in assisting the ambiguity validation process, and, together with the dispersive corrections, has improved the estimation of the test receiver's position.

In summary, a new processing strategy has been proposed augmenting existing network-based positioning algorithms, in particular via the LCM, which uses the 'lumped' (i.e. dispersive + non-dispersive) network corrections. This new processing strategy is being implemented as part of the real-time software of the new SYDNET network processor 'engine'.

Investigation of the Stochastic Modelling for Static Network-Based Positioning

The basis of this investigation was to use the least squares residuals as the quality indicators, assuming that they adequately reflect the presence of the residual biases and measurement noise due to the imperfect functional model in the network-based

positioning. The least squares residuals have been used to formulate the ‘realistic’ stochastic model via the variance-covariance (VCV) matrix, which takes account of the heteroscedastic and correlated errors in the DD measurements.

The simplified Minimum Norm Quadratic Unbiased Estimation (MINQUE) was employed to estimate the VCV matrix. Test results for some stations of the Southern California Integrated Network (SCIGN) have shown that this more realistic stochastic model improves the ambiguity validation tests. Additionally, a two-stage procedure was implemented to handle the temporal correlation in the data for the case of static network-based positioning. The basis of the two-stage procedure is to transform the DD measurements into a set of new measurements which are assumed to be free of temporal correlation. The procedure has been tested in three networks; SIMRSN, part of SCIGN and the GPS Earth Observation Network (GEONET) in Japan. Test results suggest that this two-stage procedure can account for the temporal correlation, at least to some extent.

In conclusion, applying the realistic stochastic model for static network-based positioning has improved the ambiguity validation test and the handling of the temporal correlation. Nevertheless, the estimated baseline vector components (whether using the realistic stochastic model or the standard stochastic model) are close to each other no matter what form the stochastic model takes.

7.1 Recommendations

It is recommended that research on tropospheric delay for meteorology applications in the low latitude region be extended, especially now that GPS CORS networks such as the MASS network are now fully operational. The research effort should focus on how to derive precise absolute ZPD values that could be input into Numerical Weather Prediction (NWP) models.

Extensive research should be conducted on mitigating station-dependent errors, both for master-to-reference stations and master-to-user stations. The former baselines have an

advantage due to them being static (reference stations). The latter is still a challenge since user receivers may be operating in kinematic mode. Proper handling of the station-dependent errors can improve AR and positioning results.

It is recommended that a method for monitoring the quality of the dispersive and non-dispersive corrections generated by CORS networks be developed. For example, investigating the appropriate characteristics of the ‘sliding time window’ could optimise the smoothing function of the non-dispersive corrections.

In this investigation some research has been conducted into the stochastic modelling of network-based positioning. Although the methodology proposed works reasonably well, there remains room for improvement. Thus, refining the stochastic model can improve carrier phase AR. For kinematic positioning, it is expected that some type of signal-to-noise ratio (SNR) formulation and/or an appropriate sliding residual window can be incorporated into the improved stochastic model.

REFERENCES

- Abdul K.T., Hua, T.C., Azhari, M., Rahim, M.S. Hua, C.L., et al. (2000): *The Realization of GDM2000*. Downloadable via (<http://www.jupem.gov.my/GDM/pdf/GDM2000Realization.pdf>).
- Abidin, H.Z. (1993): *Computational and Geometrical Aspects of On-The-Fly Ambiguity Resolution*. Dept. of Geodesy & Geomatic Eng., University of New Brunswick, Canada, Tech. Report, no. 164, 290pp.
- Allison, T. (1991): *Multi-Observable Processing Techniques for Precise Relative Positioning*. Proc. of 4th Int. Tech. Meeting of the Satellite Division of the Inst. of Navigation, Albuquerque, New Mexico, 11-13 September, 715–726.
- Alves, P., Kotthoff, H., Geisler, I., Zelzer, O. and Euler, H.J. (2006): *Rover Processing with Network RTK and Quality Indicators*. U.S. Institute of Navigation National Tech. Meeting, January 18-20, Monterey, California. Downloadable via (<http://www.leica-geosystems.com/s-e/en/downloads>).
- Bauersima, I. (1983): *NAVSTAR/Global Positioning System II*. Mitteilungen der Satelliten-Beobachtungsstation Zimmerwald, No. 10, Astronomical Inst., University of Berne.
- Bassiri, S. and Hajj, G. (1993): *Higher-Order Ionospheric Effects on the Global Positioning System Observables and Means of Modeling Them*. Manuscripta Geodaetica, 18:280-289.
- Beutler, G., Bauersima, I., Gurtner, W., Rothacher, M., Schildknecht, T., et al. (1988): *Atmospheric Refraction and Other Important Biases in GPS Carrier Phase Observation*. In: Atmospheric Effects on Geodetic Space Measurements, Monograph 12, School of Surveying, UNSW, Australia, 15-43.
- Beutler, G., Weber, R., Hugentobler, U., Rothacher, M. and Verdun., A. (1998a): *GPS Satellite Orbits*. In: GPS for Geodesy, 2nd Edition, Springer-Verlag, Berlin Heidelberg New York, 43-111.
- Beutler, G., Weber, R., Brockmann, E., Rothacher, M. and Verdun., A. (1998b): *The GPS as a Tool in Global Geodynamics*. In: GPS for Geodesy, 2nd Edition, Springer-Verlag, Berlin Heidelberg New York, 569-598.
- Beutler, G., Rothacher, M., Springer, T., Kouba, J. and Neilan, R.E. (1998c): *The Int. GPS Service (IGS): An interdisciplinary Service in Support of Earth Sciences*. 32nd COSPAR Scientific Assembly, Nagoya, Japan, 12-19 July, 1-23.

- Bevis, M., Businger, S., Herring, T. A., C. Rocken., Anthes, R. A., et al. (1992): *GPS Meteorology: Remote Sensing of Atmospheric Water Vapor Using the Global Positioning System*. Journal of Geophysical Research, 97(14):787-801.
- Bevis, M., Businger, S., Chiswell, S., Herring, T.A., Anthes, R. A., et al. (1994): *GPS Meteorology: Mapping Zenith Wet Delays onto Precipitable Water*. Journal of Applied Meteorology, 33:379-386.
- Blewitt, G. (1997): *Basics of the GPS Technique: Observation Equations*. In: Geodetic Applications of GPS, Nordic Geodetic Commission, Sweden, 10-54.
- Blewitt, G. (1998): *GPS Data Processing Methodology*. In: GPS for Geodesy, 2nd Edition, Springer-Verlag, Berlin Heidelberg New York, 231-268.
- Bona, P. (2000): *Precision, Cross Correlation, and Time Correlation of GPS Phase and Code Observations*. GPS Solutions, 4(2):3-13.
- Broecker, W.S. (2006): 'Breathing Easy, Et tu O₂'. Downloadable via (<http://www.columbia.edu/cu/21stC/issue-2.1/broecker.htm>).
- Brown, N., Geisler, I. and Troyer, L. (2005): *RTK Rover Performance using the Master-Auxiliary Concept*. Int. Symposium on GPS/GNSS 2005, 8-10 December, Hong Kong. Downloadable via (<http://www.leica-geosystems.com/s-e/en/downloads>).
- Brunner, F.K. and Tregoning, P. (1994): *Tropospheric Propagation Effects in GPS Height Results Using Meteorological Observations*. Australian Journal of Geodesy, Photogrammetry, and Surveying, 60: 49-65.
- Brunner, F.K. and McCluskey, S. (1991): *Tropospheric Zenith Delay Parameters: How Many Should be Estimated in GPS Processing?* Australian Journal of Geodesy, Photogrammetry, and Surveying, 55: 67-75.
- Businger, S., Chiswell, S., Bevis, M., Duan, J., Anthes, A. R., et al. (1996): *The Promise of Atmospheric Monitoring*. Journal of Applied Meteorology, 77(1):5-18.
- Chang, C.C. and Tseng, C.L. (1999): *Testing on Tropospheric Modelling for GPS Tracking Stations in Taiwan*. Geomatics Research Australasia, 70: 77-94.
- Chen, X., Han, S., Rizos, C. and Goh, P.C. (2000): *Improving Real-Time Positioning Efficiency Using the Singapore Integrated Multiple Reference Station Network (SIMRSN)*. Proc. of 13th Int. Tech. Meeting of the Satellite Division of the Inst. of Navigation, Salt Lake City, Utah, 19-22 September, 9-18.
- Chen, H.Y. (2001): *A Study on Real-Time Medium-Range Carrier Phase-Based GPS Multiple Reference Stations*. PhD Thesis, School of Surveying & Spatial Info. Sys., The University of New South Wales, Australia.
- CODE (2006): *Center for Orbit Determination in Europe*, via (<http://www.cx.unibe.ch/aiub/ionosphere.html#cgim>).

- Collins, J.P. (1999): *An Overview of GPS Interfrequency Carrier Phase Combinations*. Downloadable via (http://gauss.gge.unb.ca/papers.pdf/L1L2combinations_collins.pdf).
- Coster, A., Foster, J. and Erickson, P. (2003): *Space Weather – Monitoring the Ionosphere with GPS*. GPS World, 5(1). Internet version, via (<http://www.gpsworld.com/gpsworld/>).
- Cross, P.A. (1983): *Advanced Least Squares Applied to Position-Fixing*. The Department of Land Surveying, North East London Polytechnic, London, England, Working Paper, no. 6, 39-41.
- Dai, L. (2002): *Augmentation of GPS with GLONASS and Pseudolite Signals for Carrier Phase-Based Kinematic Positioning*. PhD Thesis, School of Surveying & Spatial Info. Sys., The University of New South Wales, Australia.
- Davis, J.L., Herring, T.A., Shapiro, I.I., Rogers, A.E.E. and Elgered, G. (1985): *Geodesy by Radio Frequency: Effects of Atmospheric Modeling Errors on Estimates of Baseline Length*. Radio Science, 20(6): 1593-1607.
- Dierendonck, A.J.V. (1996): *GPS Receivers*. In: Global Positioning System: Theory and Applications, Volume I, American Inst. of Aeronautics and Astronautics, Inc., 329-405.
- Dodson, A.H., Shardlow, P.J., Hubbard, L.C.M., Elgered, G. and Jarlemark, P.O.J. (1996): *Wet Tropospheric Effects on Precise Relative GPS Height Determination*. Journal of Geodesy, 70(4):188-202.
- Duan, J., Bevis, M., Fang, P., Bock, Y., Chiswell, S., et al. (1996): *GPS Meteorology: Direct Estimation of the Absolute Value of Precipitable Water*. Journal of Applied Meteorology, 35(6): 830-838.
- Durbin, J. and Watson, G.S. (1950): *Testing for Serial Correlation in Least Squares Regression I*. Biometrika, 37:409-428.
- Elgered, G., Davis, J., Herring, T. and Shapiro, I. (1991): *Geodesy by Radio Interferometry: Water Vapor Radiometry for Estimation of the Wet Delay*. Journal Geophysical Research, 96: 6541-6555.
- El-Rabbany, A.E.S. (1994): *The Effect of Physical Correlations on the Ambiguity Resolution and Accuracy Estimation in GPS Differential Positioning*. PhD Thesis, Dept. of Geodesy and Geomatics Engineering Tech. Report No. 170, University of New Brunswick, Fredericton, New Brunswick, Canada, 161pp.
- El-Rabbany, A.E.S. and Kleusberg, A. (2003): *Effect of Temporal Physical Correlation on Accuracy in GPS Relative Positioning*. Journal of Surveying Engineering, 129(1):28-32.
- Eresmaa, R. and Jarvinen, H. (2006): *An Observation Operator for Ground-Based GPS Slant Delays*. Tellus, 58A: 131-140.

- Euler, H.J. and Goad, C.C. (1991): *On optimal filtering of GPS dual-frequency observations without using orbit information*. Bulletin Geodesique, 65:130-143.
- Euler, H.J., Keenan, C.R., Zebhauser, B. E. and Wubbena, G. (2001): *Study of a Simplified Approach in Utilizing Information from Permanent Reference Station Arrays*. Proc. of 14th Int. Tech. Meeting of the Satellite Division of the Inst. of Navigation, Salt Lake City, Utah, 11-14 September, 379-391.
- Fontana, D.R., Cheung, W. and Stansell, T. (2001): *The Modernized L2 Civil Signal: Leaping Forward in the 21st Century*. GPS World, 9(1): 28-34.
- Fortes, L.P. (2002): *Optimizing the Use of GPS Multi-Reference Stations for Kinematic Positioning*. Proc. of 15th Int. Tech. Meeting of the Satellite Division of the Inst. of Navigation, Portland, Oregon, 24-27 September, 2359–2372.
- Fotopoulos, G. and Cannon, M.E. (2001): *An Overview of Multi-Reference Stations Methods for Cm-Level Positioning*. GPS Solutions, 4(3): 1-10.
- Frei, E. and Beutler, G. (1990): *Rapid static positioning based on the fast ambiguity resolution approach FARA: theory and first results*. Manuscripta Geodaetica, 15 (4): 325-356.
- Gao, Y. and Chen, K. (2004): *Performance Analysis of Precise Point Positioning Using Real-Time Orbit and Clock Products*. Journal of Global Positioning Systems, 3(1-2): 95-100.
- Geisler, I. (2006): *Performance Improvement of Network RTK Positioning*. U.S. Institute of Navigation National Tech. Meeting, January 18-20, Monterey, California. Downloadable via (<http://www.leica-geosystems.com/s-e/en/downloads>).
- Gendt, G. (1998): *IGS Combination of Tropospheric Estimates*, via (http://igscb.jpl.nasa.gov/projects/tropo_est.html).
- Georgiadou, Y. and Kleusberg, A. (1988): *On the Effect of Ionospheric Delay on Geodetic Relative GPS Positioning*. Manuscripta Geodaetica, 13:1-8.
- Gold, R. (1967): *Optimal Binary Sequence for Spread Spectrum Multiplexing*. IEE Transactions Info. Theory, 33(3): 619-621.
- Guidry, M. (2002): *Computer Science Education Project*. Department of Physics and Astronomy, University of Tennessee, via (<http://csep10.phys.utk.edu/astr161/lect/earth/atmosphere.html>).
- Gustafsson, N., Berre, L., Hornquist, S., Huang, X.Y., Lindspong, M., et al. (2001): *Three-Dimensional Variational Data Assimilation for a Limited Area Model, Part I: General Formulation and the Background Error Constraint*. Tellus, 53A: 425-426.

- HAARP (2003): *High Frequency Active Auroral Research Program*, via (<http://www.haarp.alaska.edu/haarp/ion4.html>).
- Han, S. and Rizos, C. (1996a): *GPS Network Design and Error Mitigation for Real-Time Continuous Array Monitoring System*. Proc. of 9th Int. Tech. Meeting of the Satellite Division of the Inst. of Navigation, Kansas City, Missouri, September 17-20, 1827-1836.
- Han, S. and Rizos, C. (1996b): *Improving the Computational Efficiency of the Ambiguity Function Algorithm*. Journal of Geodesy, 71(6):330-341.
- Han, S. (1997): *Carrier Phase-Based Long-Range GPS Kinematic Positioning*. PhD Thesis, School of Geomatic Engineering, The University of New South Wales, Australia.
- Hasegawa, S. and Stokesbury, D.P. (1975): *Automatic Digital Micro-Wave Hygrometer*. Review of Scientific Instruments, 46:867-873.
- Ho, Y.H., Ahmad Faisal, M. Z., Mardina, A., Abdul Ghafar, R. and Wan Salwa, W. H. (2002): *Equatorial TEC variations during geomagnetic storm of July 15-17, 2000*. Proc. of the Int. Union of Radio Science, Maastricht, The Netherlands, 17-24 August, paper 820.
- Hoffmann-Wellenhof, B., Lichtenegger, H. and Collins, J. (2001): *Global Positioning System: Theory and Practice*. 5th edition, Springer, Berlin, Germany.
- Hopfield, H.S. (1969): *Two-Quartic Tropospheric Refractivity Profile for Correcting Satellite Data*. Journal of Geophysical Research, 74(17): 4487-4499.
- Hu, G.R., Khoo, H.S., Goh, P.C. and Law, C.L. (2002): *Testing of Singapore Integrated Multiple Reference Station Network (SIMRSN) for precise fast static positioning*. Proc. of the European Navigation Conference-GNSS2002, 27-30 May, Copenhagen, Denmark, CD-ROM.
- Hu, G.R., Khoo, H.S., Goh, P.C. and Law, C.L. (2003): *Development and Assessment of GPS Virtual Reference Station for RTK Positioning*. Journal of Geodesy, 77(5-6):292-302.
- Hu, G., Abbey, D.A., Castleden, N., Featherstone, W.E., Earls, C., et al. (2005): *An Approach for Instantaneous Ambiguity Resolution for Medium- to Long-Range Multiple Reference Station Networks*. GPS Solutions, 9(1): 1-11.
- Hudnut, K.W (2005): *Future Navigation Needs Your Input*. GPS World, 11(1). Internet version, via (<http://www.gpsworld.com/gpsworld/>).
- ICD-GPS-200C (2003): *Interface Control Document GPS 200C*. Downloadable via ([http://www.navcen.uscg.gov/gps/geninfo/ICD-GPS-200C with IRNs 12345.pdf](http://www.navcen.uscg.gov/gps/geninfo/ICD-GPS-200C%20with%20IRNs%2012345.pdf)).
- ICD-GPS-705 (2002): *Interface Control Document GPS 705*. Downloadable via (<http://www.navcen.uscg.gov/gps/modernization/number.pdf>).

- Ifadis, I.M. (2000): *A New Approach to Mapping the Atmospheric Effect for GPS Observations*. Earth Planets Space, 52:703-708.
- IGS (2005): *Int. GNSS Service*. IGS Central Bureau, Pasadena, via (<http://igs.cb.jpl.nasa.gov>).
- Janes, H.W., Langley, B. and Newby, S.P. (1989): *A Comparison of Several Models for the Prediction of Tropospheric Propagation Delay*. Proc. Of the 5th International Geodetic Symposium on Satellite Positioning, Las Cruces, NM, 777-788.
- Janssen, V. (2003): *A Mixed-Mode GPS Network Processing Approach for Volcano Deformation Monitoring*. PhD Thesis, School of Surveying & Spatial Info. Sys., The University of New South Wales, Australia.
- Jonge, D.P.J., Tiberius, C.C.J.M. and Teunissen, P.J.G. (1996): *Computational Aspect of the LAMBDA Method for GPS Ambiguity Resolution*. Proc. of 9th Int. Tech. Meeting of the Satellite Division of the Inst. of Navigation, Kansas City, Missouri, September 17-20, 935-944.
- Joosten, P. and Tiberius, C.C.J.M. (2002): *LAMBDA: FAQ*. GPS Solutions, 6(1-2): 109-114.
- Kim, D. and Langley, R.B. (2000): *GPS Ambiguity Resolution and Validation: Methodologies, Trends and Issues*. Int. Symposium on GPS/GNSS, Seoul, Korea, November 30-December 2.
- Kleusberg, A. (1998): *Atmosphere Models from GPS*. In: GPS for Geodesy, 2nd Edition, Springer-Verlag, Berlin Heidelberg New York, 599-622.
- Klobuchar, J.A. (1986): *Design and Characteristics of the GPS Ionospheric Time Delay Algorithm for Single Frequency Users*. Proc. of the PLANS'86 Conference, Las Vegas, Nevada, 4-7 November, 280-286.
- Klobuchar, J.A. (1996): *Ionospheric Effects on GPS*. In: Global Positioning System: Theory and Applications, Volume I, American Inst. of Aeronautics and Astronautics, Inc., 485-515.
- Koch, K.R. and Kusche, J. (2002): *Regularization of Geopotential Determination from Satellite Data by Variance Components*. Journal of Geodesy, 76:259-268.
- Kouba J. and Heroux, P. (2001): *Precise Point Positioning Using IGS Orbit and Clock Products*. GPS Solutions, 5(2): 12-28.
- Lachapelle, G., Alves, P., Fortes, L.P., Cannon, M.E. and Townsend, B. (2000): *DGPS RTK Positioning Using a Reference Network*. Proc. of 13th Int. Tech. Meeting of the Satellite Division of the Inst. of Navigation, Salt Lake City, Utah, 19-22 September, 1165-1171.

- Landau, H. and Euler, H.J. (1992): *On-the-Fly Ambiguity Resolution for Precise Differential Positioning*. Proc. of 5th Int. Tech. Meeting of the Satellite Division of the Inst. of Navigation, Albuquerque, New Mexico, 16-18 September, 607-613.
- Landau, H., Vollath, U. and Chen, X. (2003): *Virtual Reference Stations versus Broadcast Solutions in Network RTK – Advantages and Limitations*. Proc. of GNSS2003, the European Navigation Conference, Graz, Austria, 22-25 April. Downloadable via (http://trl.trimble.com/docushare/dsweb/Get/Document-83158/VRSvsFKP/GNSS_2003.pdf).
- Langley, R. (1998a): *Propagations of the GPS Signals*. In: GPS for Geodesy, 2nd Edition, Springer-Verlag, Berlin Heidelberg New York, 111-151.
- Langley, R. (1998b): *GPS Receivers and Observables*. In: GPS for Geodesy, 2nd Edition, Springer-Verlag, Berlin Heidelberg New York, 151-183.
- Langley, R. (1999): *Dilution of Precision*. GPS World, 5(1): 52-59.
- Leick, A. (2004): *GPS Satellite Surveying*. 2nd Edition, John Wiley and Sons, New York.
- Lewis, S. (1996): *GPS Market and Applications*. In: Understanding GPS, Principles and Applications, Artech House, Boston, London, 487-516.
- Lindlohr, W. and Wells, D.E. (1985): *GPS Design Using Undifferenced Carrier Beat Phase observations*. Manuscripta Geodaetica, 10:255-295.
- Lynn, W. and Anil, T. (1995): *DGPS architecture based on separating error components, virtual reference stations and FM sub-carrier broadcast*. Proc. of 8th Int. Tech. Meeting of the Satellite Division of the Inst. of Navigation, Nashville, Tennessee, 12-15 September, 128-139.
- MacDonald, D. (2002): *Broadcast Ionospheric Model Accuracy and the Effect of Neglecting Ionospheric Effects on C/A Code Measurements on a 500 km Baseline*. Waypoint Consulting, unpublished report. Downloadable via (<http://www.novatel.com/Documents/Waypoint/Reports/iono.pdf>).
- Marel, H. V. D. (1998): *Active GPS Control Stations*. In: GPS for Geodesy, 2nd Edition, Springer-Verlag, Berlin Heidelberg New York, 389-433.
- Meindl, M., Schaer, S., Hugentobler, U. and Beutler, G. (2003): *Tropospheric Gradient Estimation at CODE: Results from Global Solutions*. Int. Workshop on GPS Meteorology, “GPS Meteorology: Ground-Based and Space-Borne Applications”, Tsukuba, Japan, 14-17 January.
- Mendes, V.B. and Langley, R.B. (1994): *A Comprehensive Analysis of Mapping Functions Used in Modelling Tropospheric Propagation Delay in Space Geodetic Data*. KIS 94, Int. Symposium on Kinematic Systems in Geodesy, Banff, Canada, August 30-September 2.

- Merigan, J.M., Swift, E.R., Wong, R.F. and Saffel, J.T. (2002): *A Refinement to the World Geodetic System 1984 Reference Frame*. Proc. of 15th Int. Tech. Meeting of the Satellite Division of the Inst. of Navigation, Portland, Oregon, 24-27 September, 1519–1529.
- Mervart, L. (1995): *Ambiguity Resolution Techniques in Geodetic and Geodynamic Applications of the Global Positioning System*. PhD Thesis, University of Bern, 76-80.
- Misra, P. and Enge, P (2004): *Global Positioning System: Signals, Measurements and Performance*. Ganga-Jamuna Press, Lincoln, Massachusetts.
- MMS (2003): *Malaysian Meteorological Service*. Ministry of Science, Technology and Innovation, via (<http://www.kjc.gov.my>).
- Mockler, S.B. (1995): *Water Vapor in the Climate System*. Special Report, AGU, Washington, D.C., via (http://www.agu.org/sci_soc/mockler.html).
- NASA (2006): *National Aeronautics and Space Administration – Solar Physics*, via (<http://science.msfc.nasa.gov/ssl/pad/solar/sunspots.htm>).
- Niell, A. (1996): *Global Mapping Functions for the Atmosphere Delay at Radio Wavelengths*. Journal of Geophysical Research, 101(B2):3227-3246.
- Niell, A. (2000): *Improved Atmospheric Mapping Functions for VLBI and GPS*. Earth Planets Space, 52:699-702.
- Niell, A. (2003): *Information from a Numerical Weather Model for Improving Atmosphere Delay Estimation in Geodesy*. Int. Workshop on GPS Meteorology, “GPS Meteorology: Ground-Based and Space-Borne Applications”, Tsukuba, Japan, 14-17 January.
- Odiijk, D. (2002): *Fast Precise GPS Positioning in the Presence of Ionospheric Delays*. PhD Thesis, Delft University of Technology, Delft, The Netherlands, 69-102.
- Owens, J.C. (1967): *Optical Refractive Index of Air: Dependence on Pressure, Temperature and Composition*. Applied Optics, 6:51-58.
- Pacione, R. and Vespe, F. (2003): *GPS Zenith Total Delay Estimation in the Mediterranean Area for Climatological and Meteorological Applications*. Journal of Atmospheric and Oceanic Technology, 20:1034-1042.
- Park, K.-D., Nerem, R.S., Schenewerk, M.S. and Davis, J.L. (2004): *Site-Specific Characteristics of Global IGS and CORS GPS Sites*. Journal of Geodesy, 77:799-803.
- Racquet, J.F. (1998): *Development of a Method for Kinematic GPS Carrier-Phase Ambiguity Resolution Using Multiple Reference Receivers*. PhD Thesis, Dept. of Geomatic Eng., The University of Calgary, 47-50.

- Rao, C.R. (1970): *Estimation of Heteroscedastic Variances in Linear Models*. Journal of American Statistical Association, 65:161-172.
- Rao, C.R. (1971): *Estimation of Variance and Covariance Components – MINQUE*. Journal of Multivariate Analysis, 1:257-275.
- Rao, C.R. (1979): *MINQUE theory and its relation to ML and MML estimation of variance components*. Sankhya, 41(B):138-153.
- Rizos, C. (1997): *Principles and Practice of GPS Surveying*. Monograph 17, School of Geomatic Engineering, The University of New South Wales, Sydney, Australia, 101-382.
- Rizos, C. (2003): *Network RTK Research and Implementation – A Geodetic Perspective*. Journal of Global Positioning Systems, 1(2):144-150.
- Roberts, C. (2002): *A Continuous Low-Cost GPS-Based Volcano Deformation Monitoring System in Indonesia*. PhD Thesis, School of Surveying & Spatial Info. Sys., The University of New South Wales, Australia, 206-212.
- Rocken, C., Ware, R., Van Hove, T., Solheim, F., Alber, C., et al. (1993): *Sensing Atmospheric Water Vapor with the Global Positioning System*. Geophysical Research Letters, 20(23):2631-2634.
- Rocken, C., Van Hove, T., Johnson, J., Solheim, F. and Ware, R. W. (1995): *GPS/STORM-GPS Sensing of Atmospheric Water Vapor for Meteorology*. Journal of Atmospheric and Oceanic Technology, 12: 468-478.
- Rocken, C., Sokolovskiy, S., Johnson, J.M. and Hunt, D. (2001): *Improved Mapping of Tropospheric Delays*. Journal of Applied Meteorology, 18:1205-1213.
- Rothacher, M. and Mervart, L. (1996): *Manual of Bernese GPS Software*. Version 4.0, Astronomical Inst., University of Berne.
- RTCM (2001): *RTCM Recommended Standards for Differential GNSS Service*. RTCM Special Committee no. 104, Version 2.3, 136-2001/SC104-STD.
- RTCM (2004) : *RTCM Recommended Standards for Differential GNSS Service*. RTCM Special Committee no. 104, Version 3.0, 30-2004/SC104-STD.
- Sargan, J.D. (1961): *The Maximum Likelihood Estimation of Econometric Relationships with Autoregressive Residuals*. Econometrica, 29:414-426.
- Satirapod, C. (2002): *Improving the GPS Data Processing Algorithm for Precise Static Relative Positioning*. PhD Thesis, School of Surveying & Spatial Info. Sys., The University of New South Wales, Australia.
- Saastamoinen, J. (1972): *Atmospheric Correction for the Troposphere and Stratosphere in Radio Ranging of Satellites, the Use of Artificial Satellites for Geodesy*. Geophysics Monograph Series, 15: 247-251.

- Saastamoinen, J. (1973): *Contribution to the theory of atmospheric refraction*. Bulletin Geodesique, 107:13-34.
- Schuler, T. (2001): *On Ground-Based GPS Tropospheric Delay Estimation*. PhD Thesis, Universität der Bundeswehr, München.
- Seeber, G. (1993): *Satellite Geodesy*. De Gruyter, Berlin, Germany, 531pp.
- Skone, S. and Hoyle, V. (2005): *Troposphere Modeling in a Regional GPS Network*. Journal of Global Positioning Systems, 4(1-2): 230-239.
- Smith, E.K. and Weintraub, S. (1953): *The Constants in the Equation of Atmospheric Refractive Index at Radio Frequencies*. Proc. of the Inst. of Radio Engineers, 41(8): 1035-1037.
- Spilker, J.J. (1996a): *GPS Signal Structure and Theoretical Performance*. In: Global Positioning System: Theory and Applications, Volume I, American Inst. of Aeronautics and Astronautics, Inc., 57-119.
- Spilker, J.J. (1996b): *GPS Navigation Data*. In: Global Positioning System: Theory and Applications, Volume I, American Inst. of Aeronautics and Astronautics, Inc., 121-175.
- Spilker, J.J. (1996c): *Tropospheric Effects on GPS*. In: Global Positioning System: Theory and Applications, Volume I, American Inst. of Aeronautics and Astronautics, Inc., 517-546.
- Sunil, B.B., Mendes, V.B. and Langley, R.B. (1997): *Effect of Tropospheric Mapping Functions on Space Geodetic Data*. IGS Analysis Center Workshop, Pasadena, CA, 2-14 March.
- Sun, H., Melgard, T. and Cannon, M.E. (1999) *Real-time GPS Reference Network Carrier Phase Ambiguity Resolution*. U.S. Institute of Navigation National Tech. Meeting, San Diego, California, 25-27 January, 193-199.
- Teunissen, P.J.G. (1994): *A New Method for Fast Carrier Phase Ambiguity Estimation*. Proc IEE PLANS'94, Las Vegas, Nevada, 11-15 April, 562-573.
- Teunissen, P.J.G. and Kleusberg, A. (1998): *Quality Control and GPS*. In: GPS for Geodesy, 2nd Edition, Springer-Verlag, Berlin Heidelberg New York, 231-268.
- Teunissen, P.J.G., Jonkman, N.F. and Tiberius, C. (1998): *Weighting GPS Dual Frequency Observations: Bearing the Cross of Cross-Correlation*. GPS Solutions, 2(2):28-37.
- Teunissen, P.J.G. (2001): *Proper Weighting of Your GPS Data is Important*. GIM International, 15(12):73pp.
- Thayer, G.D. (1974): *An Improved Equation for the Radio Refractive Index of Air*. Radio Science, 9(10): 803-807.

- Tiberius, C., Jonkman, N. and Kenselaar, F. (1999): *The Stochastic of GPS Observables*. GPS World, 10(2): 49-54.
- Tregoning, P., Boers, R., O'Brien, D. and Hendy, M. (1998): *Accuracy of Absolute Precipitable Water Vapor Estimates from GPS Observations*. Journal of Geophysical Research, 103:701-719.
- Verhagen, S. (2004): *Integer Ambiguity Validation: an Open Problem?* GPS Solutions, 8(1): 36-43.
- Vollath, U., Buecherl, A., Landau, H., Pagels, C. and Wagner, B. (2000): *Multi-Base RTK Positioning Using Virtual Reference Stations*. Proc. of 13th Int. Tech. Meeting of the Satellite Division of the Inst. of Navigation, Salt Lake City, Utah, 19-22 September, 123-131.
- Vollath, U., Landau, H. and Chen, X. (2002): *Network RTK Concept and Performance*. Proc. of the GNSS Symposium, Wuhan, China, 6-8 November. Downloadable via (<http://www.gpsnet.dk/showing-php?ID=371>).
- Vollath, U., Brockmann, E. and Chen, X. (2003): *Troposphere: Signal or Noise?* Proc. of 16th Int. Tech. Meeting of the Satellite Division of the Inst. of Navigation, Portland, Oregon, 9-12 September, 1709-1717.
- Wan Salwa, W.H., Ahmad Faisal, M.Z., Abdul Ghafar, R. and Ho, Y.H. (2002): *Studies on Equatorial Total Electron Content Near Solar Maximum Activity from 1998-2000*. Proc. of the Int. Union of Radio Science, Maastricht, The Netherlands, 17-24 August, paper 1029.
- Wang, J. (1998): *Stochastic Assessment of the GPS Measurements for Precise Positioning*. Proc. of 11th Int. Tech. Meeting of the Satellite Division of the Inst. of Navigation, Nashville, Tennessee, 15-18 September, 81-89.
- Wang, J., Stewart, M.P. and Tsakiri, M. (1998): *Stochastic Modelling for Static GPS Baseline Data Processing*. Journal of Surveying Engineering, 121(4):171-181.
- Wang J. (1999): *Modelling and Quality Control for Precise GPS and GLONASS Satellite Positioning*. PhD Thesis, School of Spatial Sciences, Curtin University of Technology, Perth, Australia, 55-113.
- Wang, J., Satirapod, C. and Rizos, C. (2002): *Stochastic Assessment of GPS Carrier Phase Measurements for Precise Static Relative Positioning*. Journal of Geodesy, 76:95-104.
- Wanninger, L. (1993): *Effects of the Equatorial Ionosphere on GPS*. GPS World, 7(1): 49-54.
- Wanninger, L. (1995): *Improved ambiguity resolution by regional differential modeling of the ionosphere*. Proc. of 8th Int. Tech. Meeting of the Satellite Division of the Inst. of Navigation, Nashville, Tennessee, 12-15 September, 55-62.

- Wanninger, L. (1999): *The performance of Virtual Reference Stations in Active Geodetic GPS-Networks under Solar Maximum Conditions*. Proc. of 12th Int. Tech. Meeting of the Satellite Division of the Inst. of Navigation, Nashville, Tennessee, 14-17 September, 1419–1427.
- Wanninger, L. and May, M. (2001): *Carrier Phase Multipath Calibration of GPS Reference Stations*. Journal of the Inst. of Navigation, 48(2):113-124.
- Wanninger, L. (2003): Virtual Reference Stations (VRS). GPS Solutions, 7:143-144.
- Ward, P. (1996): *GPS Satellite Signal Characteristics*. In: Understanding GPS, Principles and Applications, Artech House, Boston, London, 83-116.
- Warnant, R. (2002): *Atmospheric Perturbations on GNSS Signals and their Influence on Time Transfer*. XXIIth General Assembly of the Int. Union of Radio Science, Maastricht, The Netherlands, 17-24 August, paper 572.
- Weisstein, W.E. (2002): *Moving Average*. From Mathworld—A Wolfram Web Resource (via <http://mathworld.wolfram.com/MovingAverage.html>).
- Wiederholt L.F. and Kaplan, E.D. (1996): *GPS System Segments*. In: Understanding GPS, Principles and Applications, Artech House, Boston, London, 59-81.
- Witchayangkoon, B. (2000): *Elements of GPS Precise Point Positioning*. PhD Thesis, The University of Maine, Orono, Maine, 11-34.
- Wormley, S.J. (2006): *Educational Observatory Inst., Inc.*, via (http://www.edu-observatory.org/gps/gps_accuracy.html).
- Wu, J.T. (1994): *Weighted Differential GPS Method for Reducing Ephemeris Error*. Manuscripta Geodaetica, 20: 1-7.
- Wübenna, G., Bagge, A., Seeber, G., Boder, V. and Hankemeier, P. (1996): *Reducing Distance Dependent Errors for Real-Time DGPS Applications by Establishing Reference Stations Networks*. Proc. of 9th Int. Tech. Meeting of the Satellite Division of the Inst. of Navigation, Kansas City, Missouri, 17-20 September, 1845–1852.
- Wübenna, G., Bagge, A. and Schmitz, M. (2001a): *RTK Networks Based on Geo++® GNSMART- Concept, Implementation, Results*. Proc. of 14th Int. Tech. Meeting of the Satellite Division of the Inst. of Navigation, Salt Lake City, Utah, 11-14 September, 368 - 378.
- Wübenna, G., Bagge, A. and Schmitz, M. (2001b): *Network-Based Techniques for RTK Applications*. Proc. of GPS Symposium, Japan Inst. of Navigation, Tokyo, 14-16 November, 53-65.
- Wübenna, G., Schmitz, M. and Bagge, A. (2006): *Real-Time GNSS Data Transmission Standard RTCM 3.0*. IGS Workshop 2006, “Perspective and Visions for 2010 and Beyond”, Darmstadt, Germany, 18-20 May.

- Xu, G. (2003): *GPS: Theory, Algorithms and Applications*. Springer-Verlag, Berlin Heidelberg, Germany.
- Xu, P., Shen, Y., Fukuda, Y. and Liu, Y. (2006): *Variance Component Estimation in Linear Inverse ill-Posed Models*. Journal of Geodesy, 80:69-81.
- Zain, A.F.M., Ho, Y.H. and Abdullah, M. (2002): *Enabling GPS Technology on Equatorial Ionosphere Monitoring During Geomagnetic Storm of July 15-17, 2000*. Proc. of 15th Int. Tech. Meeting of the Satellite Division of the Inst. of Navigation, Portland, Oregon, 24-27 September, 1341-1344.
- Zhang, J. and Lachapelle, G. (2001): *Precise Estimation of Residual Tropospheric Delays Using a Regional GPS Network for RTK Applications*. Journal of Geodesy, 75 (5-6): 255-266.

BIBLIOGRAPHY

- Boder, V., Menge, F., Seeber, G., Wübenna, G. and Schmitz, M. (2001): *How to Deal with Station-Dependent Errors- New Development of the Absolute Field Calibration of PCV and Phase-Multipath with a Precise Robot*. Proc. of 14th Int. Tech. Meeting of the Satellite Division of the Inst. of Navigation, Salt Lake City, Utah, 11-14 September, 2166-2176.
- Boehm, J. and Schuh, H. (2004): *Vienna Mapping Functions in VLBI Analyses*. IVS 2004 General Meeting Proceedings, Ottawa, Canada, 9-11 February 9-11, 277-281.
- Camargo, P.E., Monico, F.G. and Ferreira, D.D. (2000): *Application of Ionospheric Corrections in the Equatorial Region for L1 GPS Users*. Earth Planets Space, 52: 1083-1089.
- Fedrizzi, M., Langley, R.B., Komjathy, A., Santos, M.C., De, Paula, E.R., et al. (2001): *The Low-latitude Ionosphere: Monitoring its Behaviour with GPS*. Proc. of 14th Int. Tech. Meeting of the Satellite Division of the Inst. of Navigation, Salt Lake City, Utah, 11-14 September, 2468-2475.
- Rizos, C., Han, S. and Chen, H.Y. (2000): *Regional-Scale Multiple Reference Stations for Carrier Phase-Based GPS Positioning: A Correction Generation Algorithm*. Earth Planets Space, 52:795-800.
- Willgalis, S., Seeber, G., Krueger, C.P. and Romao, V.M.C. (2002): *A Real Time Reference Network for Recife, Brazil, Enabling Precise and Reliable Cadastral Surveys*. FIG XXII Int. Congress, Washington D.C., 19-26 April.

ACADEMIC ACTIVITY

LIST OF PUBLICATIONS

(2003-Current):

Musa, T.A., Wang, J., Rizos, C. (2003): *Stochastic modelling for network-based GPS positioning*. Proc. of 6th Int. Symp. on Satellite Navigation Technology Including Mobile Positioning & Location Services, Melbourne, Australia, 22-25 July, *paper reviewed conference*.

Rizos, C., Kinlyside, D., Yan, T., Omar, S., & **Musa, T.A.** (2003): *Implementing network RTK: The SydNET CORS infrastructure*. Proc. of 6th Int. Symp. on Satellite Navigation Technology Including Mobile Positioning & Location Services, Melbourne, Australia, 22-25 July, *paper reviewed conference*.

Musa, T.A. (2003): *Stochastic Modelling for Network-Based Positioning*. Geomatics Research Australasia, 79: 97pp.

Musa, T.A., Wang, J., Rizos, C. (2004): *A stochastic modelling method for network-based GPS positioning*. GNSS2004, Rotterdam, The Netherlands, 16-19 May.

Musa, T.A., Wang, J., Rizos, C., Lee, Y.J., Mohamed, A. (2004): *Mitigating residual tropospheric delay to improve users network-based positioning*. Int. Symp. on GPS/GNSS, Sydney, Australia, 6-8 December.

Wang, J., Lee, H.K., Lee, Y.J., **Musa, T.A.**, Rizos, C. (2004): *Online stochastic modelling for network-based GPS real-time kinematic positioning*. Int. Symp. on GPS/GNSS, Sydney, Australia, 6-8 December.

Musa, T.A., Wang, J., Rizos, C., Lee, Y.J., & Mohamed, A. (2004): *Mitigating residual tropospheric delay to improve users network-based positioning*. Journal of GPS, 3(1-2), 322-330.

Musa, T.A., Lim, S., Rizos, C. (2005): *Low latitude troposphere: A preliminary study using GPS CORS data in South East Asia*. U.S. Institute of Navigation National Tech. Meeting, San Diego, California, 24-26 January, 685-693.

Wang, J., Lee, H.K., Lee, Y.J., **Musa, T.A.**, Rizos, C. (2005): *Online stochastic modelling for network-based GPS real-time kinematic positioning*. Journal of GPS, 4(1-2), 113-119.

Musa, T.A., Lim, S., Rizos, C. (2005): *GPS network-based approach to mitigate residual tropospheric delay in low latitude area*. Proc. of 18th Int. Tech. Meeting of

the Satellite Division of the Inst. of Navigation, Long Beach, California, 13-15 September, 2606-2613.

- Musa, T.A.**, Lim, S., Rizos, C. (2005): *Modelling of Dispersive and Non-dispersive Effects on Network-Based Positioning*. Dynamic Planet 2005, Cairns, Australia, 22-26 August.
- Musa, T.A.**, Lim, S., Yan, T, Rizos, C. (2006). Mitigation of Distance-Dependent Errors for GPS Network Positioning. *International Global Navigation Satellite Systems Society*, Holiday Inn Surfers Paradise, Australia, 17-21 July.
- ***Musa, T.A.**, Lim, S., Rizos, C. (2006). Network-based RTK Positioning: Impact of Separating Dispersive and Non-dispersive Components on User-side Processing Strategy. *Submitted to *GPS Solutions*.

LIST OF PRESENTATIONS

By author (2003-Current):

- Musa, T.A.** (2003): *Stochastic modelling for network-based GPS positioning*. SNAP seminar, UNSW, Sydney, 20 June. *Oral Presentation*.
- Musa, T.A.**, Wang, J., Rizos, C. (2003): *Stochastic modelling for network-based GPS positioning*. The 6th Int. Symp. on Satellite Navigation Technology Including Mobile Positioning & Location Services, Melbourne, 22-25 July. *Oral Presentation*.
- Musa, T.A.** (2003): *Stochastic Modelling for Network-Based Positioning*. The 30th Annual Research Seminars, School of Surveying & SIS, UNSW, Sydney, 10-11 November. *Oral Presentation*.
- Musa, T.A.** (2004): *A stochastic modelling method for network-based GPS positioning*. SNAP seminar, UNSW, Sydney, 18 June. *Oral Presentation*.
- Musa, T.A.**, Wang, J., Rizos, C., Lee, Y.J., Mohamed, A. (2004): *Mitigating residual tropospheric delay to improve users network-based positioning*. The Int. Symp. on GPS/GNSS, Sydney, 6-8 Dec. *Oral & Poster Presentation*.
- Musa, T.A.** (2005): *Modelling of Non-dispersive Effects on Network-Based Positioning*. Staff-Student Development Seminars (SSDS), UNSW, Sydney, 7 July. *Oral Presentation*.
- Musa, T.A.** (2005): *GPS Network-Based Approach to Mitigate Residual Tropospheric Delay in Low Latitude Area*. Staff-Student Development Seminars (SSDS), UNSW, Sydney, 28 September. *Oral Presentation*.
- Musa T.A.** (2005): *Modelling of dispersive and non-dispersive effects on network-based positioning - user processing perspective*. The 32nd Annual Research

Seminars, School of Surveying & SIS, UNSW, Sydney, 7-8 November. *Oral Presentation.*

By co-author:

Musa, T.A., **Wang, J.**, Rizos, C. (2004): *A stochastic modelling method for network-based GPS positioning.* GNSS2004, Rotterdam, The Netherlands, 16-19 May. *Oral Presentation.*

Musa, T.A., **Lim, S.**, Rizos, C. (2005): *Modelling of Dispersive and Non-dispersive Effects on Network-Based Positioning.* Dynamic Planet 2005, Cairns, Australia, 22-26 August. *Poster Presentation.*

Musa, T.A., Lim, S., **Rizos, C.** (2005): *Low latitude troposphere: A preliminary study using GPS CORS data in South East Asia.* U.S. Institute of Navigation National Tech. Meeting, San Diego, California, 24-26 January. *Oral Presentation.*

Musa, T.A., **Lim, S.**, Rizos, C. (2005): *Network-Based Approach to Mitigate Residual Tropospheric Delay In Low Latitude Area.* Research Seminar, School of Mechanical & Aerospace Engineering, Seoul National University, Korea, 30 March. *Oral Presentation.*

Musa, T.A., Lim, S., & Rizos, C. (2005). Presented by : **Andrew G. Dempster:** *GPS network-based approach to mitigate residual tropospheric delay in low latitude area.* 18th Int. Tech. Meeting of the Satellite Division of the U.S. Institute of Navigation, Long Beach, California, 13-16 September. *Oral Presentation.*

Musa, T.A., Lim, S., Yan, T, **Rizos, C.** (2006). *Mitigation of Distance-Dependent Errors for GPS Network Positioning.* *International Global Navigation Satellite Systems Society*, Holiday Inn Surfers Paradise, Australia, 17-21 July.

LIST OF COURSE & WORKSHOP ATTENDED

Workshop: ***Research Devp. Program Induction Workshop & Group Presentation***

Presenter: Dianne Wiley (UNSW)

Location & date: UNSW, NSW, Australia, 23 - 24 June 2003.

Workshop: ***Real-Time Kinematic Positioning***

Presenter: Prof. Will Featherstone, Western Australian Center for Geodesy, Curtin University

Location & date: UNSW, NSW, Australia, 5 December 2004.

Workshop: ***GNSS Developments and the Land Surveyor***

Presenter: Prof. C. Rizos, Craig Roberts, Thomas Yan, School of Surveying & SIS, UNSW

Location & date: UNSW, NSW, Australia, 6 - 10 December 2004.

Short Course: ***An Introduction to Precise Point Positioning***

Presenter: Prof. Yang Gao, Dept of Geomatics Eng, The University of Calgary, Canada

Location & date: UNSW, NSW, Australia, 15 December 2004.

Short Course: ***Advanced RTK-GPS: Concepts & Operations***

Presenter: Prof. C. Rizos, Dr Craig Roberts, Thomas Yan, School of Surveying & SIS,
UNSW

Location & date: UNSW, NSW, Australia, 7 - 8 February 2005.